PhD-FSTM-2022-020
The Faculty of Sciences, Technology and Medicine

DISSERTATION

Defence held on 23/03/2022 in Esch-sur-Alzette

to obtain the degree of

DOCTEUR DE L´UNIVERSITÉ DU LUXEMBOURG EN BIOLOGIE

by

Sònia SABATÉ SOLER

Born on 24 May 1993 in Barcelona (Spain)

INCREASING THE COMPLEXITY OF MIDBRAIN ORGANOID SYSTEMS FOR DEVELOPMENTAL STUDIES AND DISEASE MODELLING

Dissertation defence committee

Prof. Dr Jens C. Schwamborn, dissertation supervisor
Professor, Université du Luxembourg

Dr Sally Cowley
Head, James and Lillian Martin Centre for Stem Cell Research, University of Oxford

Prof. Dr Michel Mittelbronn
Professor, Université du Luxembourg

Prof. Dr Adrian Ranga
Professor, KU Leuven

Prof. Dr Malte Spielmann
Professor, Universität zu Lübeck

UNIVERSITY OF LUXEMBOURG

DOCTORAL THESIS

INCREASING THE COMPLEXITY OF MIDBRAIN ORGANOID SYSTEMS FOR DEVELOPMENTAL STUDIES AND DISEASE MODELLING

by

Sònia Sabaté Soler

Developmental and Cellular Biology Group

Luxembourg Centre for Systems Biomedicine

Dissertation defence committee

Prof. Dr. Jens C. Schwamborn, Dissertation supervisor
Dr Sally Cowley
Prof. Dr. Michel Mittelbronn
Prof. Dr. Adrian Ranga
Prof. Dr. Malte Spielmann

March 23, 2022

Affidavit

I hereby declare that the PhD thesis “Increasing the complexity of midbrain organoid systems for developmental studies and disease modelling” has been written independently and without any other sources than cited.

Sònia Sabaté Soler

Luxembourg, 23.03.2022

If the human brain was so simple
That we could understand it,
We would be so simple
That we couldn't.

Emerson M. Pugh

Acknowledgements

This PhD thesis is the result of four years of efforts and hard work, which I could achieve thanks to the support and contributions of many people. Therefore, I would like to thank all those for their help and guidance.

First, I would like to thank my thesis supervisor Prof. Dr. Jens Schwamborn, who gave me the opportunity to board on this journey of scientific knowledge and personal growth. My PhD experience in the Developmental and Cellular Biology group made me grow not only as a scientist, but also as a person, where I learned about positivism, patience, resilience and teamwork. I want to thank Prof. Schwamborn for his enthusiasm, optimism and trust, which motivated me to keep a critical thinking and obtain good results.

My sincere gratitude goes to my committee members. I am deeply grateful to Dr. Sally Cowley, who not only supported me with her guidance and advices, but also was kind enough to host me in her group and personally teach me one of the most important techniques for the development of my thesis. Big thanks go to Prof. Dr. Michel Mittelbronn for sharing his knowledge and expertise with me, and guide me after my CET presentations. I would like to express my gratitude to Prof. Dr. Adrian Ranga and Prof. Dr. Malte Spielman for agreeing to be part of my thesis committee and for taking their time to read and evaluate my PhD thesis.

I gratefully acknowledge the Centre-PD, which provided with funding for my trip to the James and Lillian Martin Centre for Stem Cell Research in Oxford to learn the microglia differentiation protocol.

Special thanks go to my colleagues from the DVB group and alumni, who helped and supported me during these four years. I am very grateful to Dr. Emanuel Berger for his patience and training when I had just arrived in the group, the year he spent supervising me was extremely helpful for the rest of my PhD time. Big thanks go to Dr. Cláudia Saraiva, who was a wonderful mentor, and had the endless patience and motivation to guide and support me every time I reached for advice. Cláudia and Matthieu were kind enough to revise my thesis and give me their feedback; for that I also say big thanks to you. I am very grateful to the rest of my DVB members, which made my PhD years an unforgettable experience; Isabel, Kiki, Jennifer, Gemma, Matthieu, Nathasia, Silvia, Javi, Alise, Sarah, Graham, Michele, Elisa, Daniela, Henry and Semra. Thank you all for our scientific discussions, our chats over lunch, our coffee breaks together and for letting me draw you all on the whiteboard!

I am deeply thankful to my colleagues from the LCSB. Special thanks go to Thea, Myrto and Vyron for making me smile every time we crossed paths in the centre. This PhD experience not only brought me knowledge and personal growth, but also new friends from the DVB and the LCSB that I hope will stay in my life for many more years.

Lastly, I would like to express my gratitude to my family and friends, who gave me the strength and courage to undertake this adventure. To my parents, to whom I always looked up to and who always comforted and supported me in the good and bad moments, and to my brother, who always listened to me and made me laugh even when my mood was not in its best, I say; sense vosaltres no hauria sigut possible. Moltes gràcies per haver estat al meu costat i haver cregut en mi des del primer moment. Gracias por vuestro incondicional soporte, cariño y apoyo. To my friends, I say thank you for always being by my side, for supporting me and for cheering my mood up with good conversations and laughs. Finally, I want to thank my fiancé, who has encouraged me every day of this journey, and had the patience to listen to the most specific scientific speeches I gave at home. I want to thank him for his unconditional support and the endless smiles.

Abstract

Increasing the complexity of midbrain organoid systems for developmental studies and disease modelling

The discovery of iPSC technology revolutionized the biomedical field, allowing the development of translatable and complex 2D and 3D cell culture systems. Organoids are 3D models containing multiple cell types that mimic complex microenvironments. This is highly advantageous to understand human development, physiology and disease, especially in inaccessible areas such as the brain. Human midbrain-specific organoids have been developed to study the midbrain (abundant in dopaminergic neurons). In Parkinson's Disease (PD), dopaminergic neurons in the *substantia nigra* of the midbrain degenerate, causing a broad spectrum of clinical features. Midbrain organoids (MO) are rich in dopaminergic neurons, and contain spatially organized groups of neural cells and progenitors. MO generated from PD patients' cells recapitulate dopaminergic neuron degeneration. In this thesis, we first demonstrated that dopaminergic neuron PD phenotypes and drug rescue effects were similar between MO and mice. After, we identified different neuronal clusters, progenitor cells, radial glia and mesenchymal cells in MO by scRNA-Seq. As expected, due to the neuro-ectodermal patterning of the MO' starting cell population, we confirmed the absence of mesoderm-derived cell types, such as microglia and endothelial cells. This represents a limitation for the system in terms of cellular and molecular complexity. Microglia in the human brain perform surveillance, defence and homeostasis functions; they phagocytose metabolic waste products and cell debris. We successfully developed a novel protocol to integrate functional microglia into our MO model. SnRNA-Seq analysis and electrophysiological results suggested a reduction of stress levels and higher maturation of neurons in the presence of microglia, respectively. We then aimed to vascularise MO, which would better recapitulate the brain environment and improve oxygen and nutrient supply into the organoid core (a common 3D culture limitation). We integrated an endothelial network into MO by fusion with vascular organoids, and observed the presence of blood vessel components like pericytes and basal lamina. Furthermore, vascularized assembloids showed decreased levels of cell death and hypoxia. Finally, by co-culturing microglia with vascularized assembloids, we modelled the neurovascular unit in 3D. Altogether, this work contributes to the development of advanced 3D region-specific organoids, which better recapitulate the complexity of the human brain. These novel MO systems represent one step further into modelling neuroinflammation and blood brain barrier disruption, typical from neurodegenerative disorders such as PD, which might lead to more reliable and personalized medical approaches.

Dissemination

The work carried out during the course of this PhD project resulted in two first-author and two contributing-author manuscripts. Two of them have been published, one is under revision and one is in preparation. They explain in detail the results obtained to fulfil the objectives of my PhD project.

Published

Javier Jarazo, Kyriaki Barmpa, Jennifer Modamio, Claudia Saraiva, Sònia Sabaté-Soler, Isabel Rosety, Anne Griesbeck, Florian Skwirblies, Gaia Zaffaroni, Lisa M. Smits, Jihui Su, Jonathan Arias-Fuenzalida, Jonas Walter, Gemma Gomez-Giro, Anna S. Monzel, Xiaobing Qing, Armelle Vitali, Gerald Cruciani, Ibrahim Boussaad, Francesco Brunelli, Christian Jäger, Aleksandar Rakovic, Wen Li, Lin Yuan, Emanuel Berger, Giuseppe Arena, Silvia Bolognin, Ronny Schmidt, Christoph Schröder, Paul M.A. Antony, Christine Klein, Rejko Krüger, 2 Philip Seibler and Jens C. Schwamborn (September 2021). 'Parkinson's Disease Phenotypes in Patient Neuronal Cultures and Brain Organoids Improved by 2-Hydroxypropyl-β-Cyclodextrin Treatment'. In: Movement Disorders, pp. 1–16. Doi: 10.1002/mds.28810.

Lisa M. Smits, Stefano Magni, Kaoru Kinugawa, Kamil Grzyb, Joachim Luginbühl, Sonia Sabate-Soler, Silvia Bolognin, Jay W. Shin, Eiichiro Mori, Alexander Skupin, Jens C. Schwamborn (July 2020). Single-cell transcriptomics reveals multiple neuronal cell types in human midbrain-specific organoids. Cell Tissue Res. *382*, 463. Doi: 10.1007/s00441-020-03249-y.

Submitted

Sonia Sabate-Soler, Sarah Louise Nickels, Cláudia Saraiva, Emanuel Berger, Ugne Dubonyte, Kyriaki Barmpa, Yan Jun Lan, Tsukasa Kouno, Javier Jarazo, Graham Robertson, Jafar Sharif, Haruhiko Koseki, Christian Thome, Jay W. Shin, Sally A. Cowley, Jens C. Schwamborn (2022). 'Microglia integration into human midbrain organoids leads to increased neuronal maturation and functionality'. In: GLIA (under review). Doi: https://doi.org/10.1101/2022.01.21.477192.

In preparation

Sonia Sabate-Soler, Alise Zagare, Kyriaki Barmpa, Kristian Haendler, Malte Spielman, Cláudia Saraiva, Jens Schwamborn (*in preparation*). 'Vascularization of human midbrain organoids leads to reduced hypoxia and a complex microglia morphology'.

Abbreviations

2D	Two-dimensional
3D	Three-dimensional
ActA	Activin A
ADP	Adenosine diphosphate
ATF3	Activating transcription factor 3
ATP	Adenosine triphosphate
BBB	Blood-brain barrier
BDNF	Brain-Derived Neurotrophic Factor
BMP	Bone Morphogenetic Protein
BMP4	Bone Morphogenetic Protein 4
BSA	Bovine serum albumin
CD31	Cluster of differentiation 31
CD34	cluster of differentiation 34
CD45	cluster of differentiation 45
CD68	cluster of differentiation 68
cDNA	Complementary DNA
CHIR	CHIR-99021
CNS	Central nervous system
DA	Dopamine
DAPT	N-(N-(3, 5-diuorophenacetyl-L-alanyl))-S-phenylglycinet-butyl ester
dbcAMP	Dibutyryladenosine cyclic monophosphate
DEGs	Differentially expressed genes
DMEM	Modified Dulbecco's Eagle's medium
DMSO	Dimethylsulfoxide
DNA	Deoxiribonucleic acid
Drop-Seq	Droplet-sequencing
EBs	Embryoid bodies
ECM	Extracellular matrix
FACS	Fluorescence-activated cell sorting

FDR	False discovery rate
FGF-2/8	Fibroblast growth factor 2/8
FOXA2	Forkhead box protein A2
GABA	γ-aminobutyric acid
GBA	Glucocerebrosidase
GDNF	Glial cell-derived neurotrophic factor
GFAP	Glial fibrillary acidic protein
GM-CSF	Granulocyte-macrophage colony-stimulating factor
gRNA	Guide RNA
hMOs	Human midbrain organoids
HP-β-CD	2-Hydroxypropyl-β-Cyclodextrin
IBA1	Ionized calcium binding adaptor molecule 1
IL-34	Interleukin 34
iPSCs	Induced pluripotent stem cells
KOSR	Knockout serum replacement
LAMP1/2	Lysosomal-associated membrane protein 1/2
LC3	Microtubule-associated protein 1A/1B-light chain 3
LDH	Lactate dehydrogenase
LDN	LDN-193189
LMX1A	LIM Homeobox Transcription Factor 1 Alpha
LPS	Lipopolysaccharide
LRRK2	Leucine rich repeat kinase 2
MAP2	Microtubule associated protein 2
MAPT	Microtubule-Associated Protein Tau
MEA	Multi-electrode array
mfNPCs	Midbrain floor plate neural precursor cell
MGL	Microglia
MHC-II	Major histocompatibility complex
MRI	Magnetic resonance imaging
mRNA	Messenger RNA
MTT	3-[4,5-dimethylthiazol-2-yl]-2,5-diphenyltetrazolium bromide

NEAA	Non-essential amino acids
NESC	Neuro-epithelial stem cells
OCT4	Octamer-binding transcription factor 4
P2RY12	Purinergic receptor P2Y12
PARK7	Parkinsonism associated deglycase
PAX6	Paired box protein 6
PBS	Phosphate-buffered saline
PD	Parkinson's Disease
PDGF-BB	Platelet-derived growth factor-BB
PDGFRβ	Platelet derived growth factor receptor beta
Pen/Strep	Penicillin/Streptomycin
PFA	Paraformaldehyde
PINK1	PTEN-induced kinase 1
PMA	Purmorphamine
PNVP	Peri-neural vascular plexus
PRKN	Parkin RBR E3 Ubiquitin Protein Ligase
PSD95	Postsynaptic density protein 95
RA	Retinoic Acid
RGL	Radial glia
RIPA	Radioimmunoprecipitation
RNA	Ribonucleic acid
RPL37A	Ribosomal Protein L37a
RT	Room temperature
S100b	S100 calcium-binding protein B
SAG	Smoothened agonist
SB	SB-431542
scRNA-Seq	Single-cell RNA sequencing
Shh	Sonic hedgehog
SNCA	Alpha-synuclein
snRNA-Seq	Single-nuclei RNA sequencing
SOX1/2	Sex determining region Y-box 1/2

SSEA-4	Stage-specific embryonic antigen-4
SYP	Synaptophysin
TCA	Tricarboxylic acid
TEM	Transmission electron microscopy
TGF-β	Transforming growth factor _
TH	Tyrosine hydroxylase
TMEM119	Transmembrane protein 199
TUBB3	Class III βTubulin
TUJ1	Class III βTubulin
ULA	Ultra-low attachment
VE-Cadherin	Vascular-endothelial cadherin
VEGF-A	Vascular endothelial growth factor A
VEGFR	Vascular endothelial growth factor receptor

List of figures

TABLE OF CONTENTS

CHAPTER 1

INTRODUCTION

1.1. Development of the human brain

The brain is one of the most complex organs in the human body. The adult brain has a volume of around 1300 cm^3 (Ball et al., 2012) and an approximate weight of 1.4 kg, with slight differences between genders (Parent and Carpenter, 1996). Even though it represents around 2% of the body weight (Parent and Carpenter, 1996), its energy needs are high. It accounts for, at least, 20% of the energy consumption in the human body (Magistretti and Allaman, 2015). Its developments starts in early embryonic ages, after fertilization and cleavage, following the gastrulation process (Gilbert and Barresi, 2017).

1.1.1. Neurulation and brain region specification

During vertebrate development, three germ layers cover the late-stage gastrula: endoderm, mesoderm and ectoderm (Gilbert and Barresi, 2017). The endoderm gives rise to the pharynx, digestive organs and associated glands; the mesoderm generates the heart, muscles, bone marrow, circulatory system and skeleton. The ectoderm, which is the outer layer on the gastrula, gives rise to the epidermis and nervous system – depending on molecular gradients of BMP, which acts as a neural inhibitor (Gilbert and Barresi, 2017). In the third week of human gestation, around embryonic day 20-27, following neural induction, a part of the ectoderm – the neuroectoderm – forms the neural plate. Molecular signalling from the paraxial mesoderm, induce the neural plate

border formation, separating neuroectoderm from non-neural ectoderm (Gammill and Bronner-Fraser, 2003). The neuroectoderm folds inwards during the neurulation process, giving rise to the neural tube (Figure 1.1, Stiles and Jernigan, 2010) The cells from the former neural plate border develop into neural crest cells, which will differentiate into sensory neurons situated in ganglia along the side of the spinal cord (Gammill and Bronner-Fraser, 2003). Neuroepithelial stem cells in the neural tube will give rise to the neural cells from the central nervous system (Gilbert and Barresi, 2017).

In order for the neurulation process to successfully develop, mesodermal structures communicate with the neuroepithelium. The paraxial mesoderm develops into somites, transient structures that play an important role on neural crest cell migration. Somites will develop into vertebrae and ribs, skin and skeletal muscles (Gilbert, 2000). The notochord – a transient mesenchymal tissue – plays a crucial role on the patterning on the neural tube through signalling molecules called hedgehog proteins, such as Sonic hedgehog or Shh (Ramesh et al., 2017).

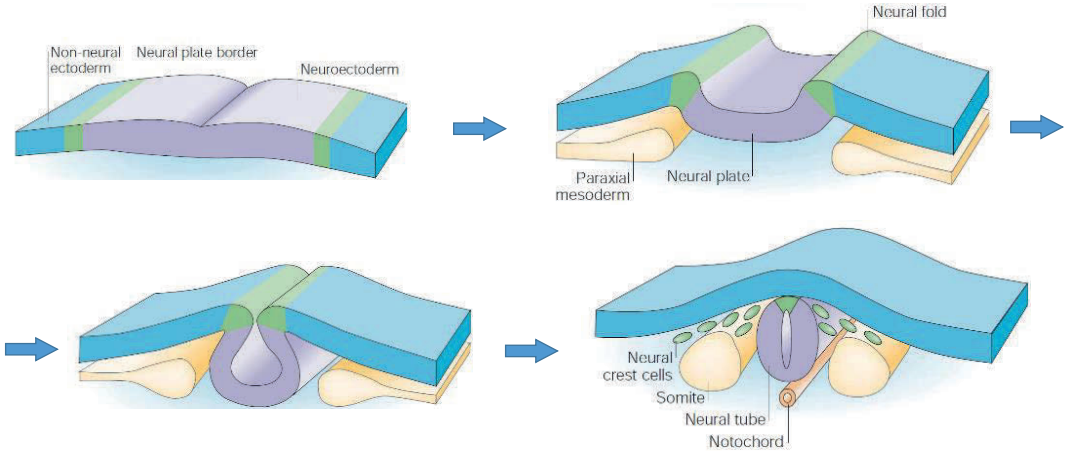

FIGURE 1. 1. **Neurulation process in vertebrates**. The ectoderm is divided into neuroectoderm (purple), which will give rise to the nervous system and non-neural ectoderm (blue), which will develop into the epidermis. During neurulation, the neuroectoderm invaginates, folding in the neural plate border (green). The last stage is the closing of the neural tube, which precedes its regionalization and development into brain regions (adapted from Gammill and Bronner-Fraser, 2003).

1.1.2. Development and cellular diversity of the midbrain

The polarization of the neural tube through the dorso-ventral axis will define the different types of regions and neurons that will differentiate in the human brain. Before its complete closure, the anterior region of the neural tube will give rise to the forebrain (prosencephalon), the midbrain (mesencephalon) and the hindbrain (rhombencephalon). The three initial vesicles that will give rise to the different regions of the mature brain. The posterior region of the neural tube will give rise to the spinal cord (Figure 1.2, Gilbert and Barresi, 2017). The midbrain will constitute, together with the medulla and pons, the brainstem (Figure 1.2, Jacobson and Marcus, 2008).

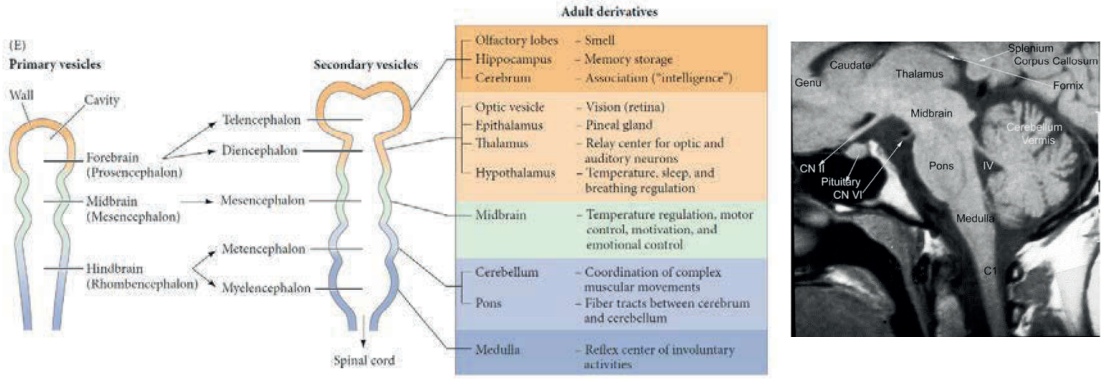

FIGURE 1. 2. **From neural tube patterning to brainstem formation**. Development and formation of the different human brain regions from the primary vesicles in the anterior neural tube (left, Gilbert and Barresi, 2017). MRI image of the brainstem in the human brain (right, Jacobson and Marcus, 2008).

With the development of the neural tube, the forebrain or prosencephalon will develop into telencephalon and diencephalon. Cells from the telencephalon will differentiate into basal ganglia, composed by cell nuclei situated in the inner layers of the neocortex. The basal ganglia will give rise to several structures: corpus striatum, subthalamic nucleus and substantia nigra, which will communicate with each other thanks to neuronal projections to control, amongst other functions, motor movement (Young et al., 2021). Neuronal nuclei from the substantia nigra are situated in the ventral region of the midbrain (ventral tegmental area), while axonal projections are directed towards forebrain regions, such as the striatum (Loughlin and Fallon, 1984). The substantia nigra receives its name due to the accumulation of neuromelanin pigment – synthesized in the dopamine synthesis pathway – giving them a dark appearance. Two different structures compose the substantia nigra; the pars reticulate (inhibitory) and the pars compacta (dopaminergic, Young et al., 2021).

Midbrain dopaminergic neurons constitute different systems including the nigrostriatal system. It originates in the *substantia nigra pars compacta* and extends into the dorsal striatum, where these neurons project their axons. This pathway is related to control of voluntary motor movement. However, other dopaminergic systems in the midbrain – such as mesolimbic and mesocortical dopaminergic systems, which start in the ventral tegmental area– participate in emotion-based behaviour (Chinta and Andersen, 2005).

1.1.2.1. Differentiation of neurons and macroglia

During neural development in humans, the floor plate – ventral area of the neural tube – and the notochord participate in the development of multiple neuronal cell types (Hynes et al., 1995a). These areas induce dopaminergic neuron differentiation in the developing midbrain via Shh signalling (Hynes et al., 1995b). The midbrain-hindbrain boundary locally produces FGF8, which together with Shh, promotes dopaminergic neuron differentiation in the midbrain (Ye et al., 1998). Shh induces the expression of genes such as *FOXA2* – which induces *NGN2* upregulation – and *LMX1A* – which induces *MSX1* expression. The expression of these genes is crucial for the development of ventral midbrain dopaminergic neurons (Andersson et al., 2006; Arenas, 2008; Kele et al., 2006).

Neuro-epithelial stem cells from the neural tube will not only give rise to neurons, but also macroglia (astrocytes and oligodendrocytes). Astrocytes develop in a first differentiation wave, prior to oligodendrocyte differentiation (Figure 1.3, Skoff, 1990). Neuro-epithelial stem cells in the neural tube give rise to radial glia that, once neurogenesis is over, will differentiate into astrocytes, or into intermediate cells that will eventually give rise to astrocytes (Reemst et al., 2016). This process driven by the expression of transcription factors such as *ATF3* and *NFIA*. Later, the expression of *RUNX2* will promote astrocyte maturation (Tiwari et al., 2018). Once developed, astrocytes are one of the biggest cell populations in the brain, and will divide into different subtypes depending on the location (Reemst et al., 2016). In a second wave of differentiation, in the ventricular zone of the neural tube, neuro-epithelial stem cells will differeniate into oligodendrocyte precursor cells (Bergles and Richardson, 2016), which will differentiate into oligodendrocytes. These precursors will stay in the brain and generate oligodendrocytes also in adult ages, and therefore being one of the most represented cell clusters in the adult brain (Bergles and Richardson, 2016). A subset of neural stem cells will remain undifferentiated and self-renew in the adult brain. Interactions between neural

stem cells, astroglia, ependymal cells, vascular cells and mature neurons can lead to adult neurogenesis, while a subset of neural precursor cells will remain undifferentiated in the adult human brain (Kuhn et al., 1996; Ma et al., 2009; Palmer et al., 1995).

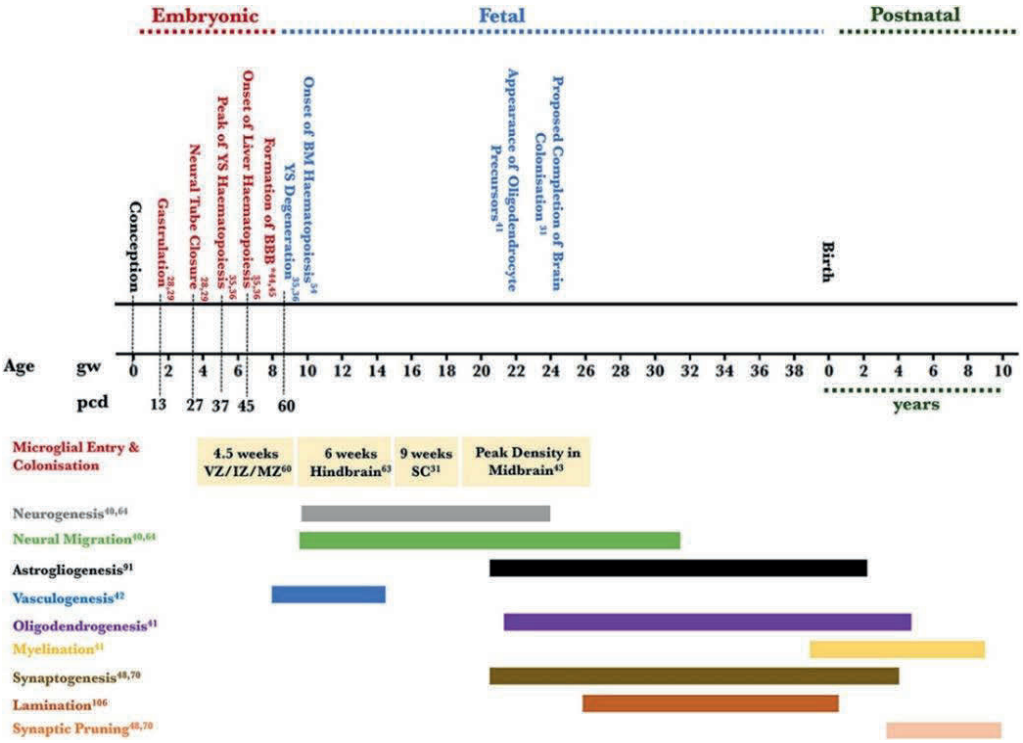

FIGURE 1. 3. **Timeline of the development and invasion of human brain cells.** Microglial (red) entry and colonisation in the brain happens at early embryonic age, before vasculogenesis (blue). Astrogliogenesis (black) and Oligodendrogenesis (purple) occur later during foetal and early postnatal development (Menassa and Gomez-Nicola, 2018).

1.1.2.2. Immune system development

Microglia, unlike macroglia and neurons, do not have a neuro-ectodermal origin, but arise from mesodermal extra-embryonic tissue and invade the developing brain at early embryonic stages (Figure 1.3). After gastrulation, extra-embryonic mesoderm develops in the yolk sac (Lacaud and Kouskoff, 2017) where, during the third week of human gestational age, primitive haematopoiesis begins. Stem cells have a myeloid and erythroid commitment (Ginhoux et al., 2013) and they will give rise to primitive erythrocytes, megakaryocytes and macrophages. Later on, the rest of the erythroid-myeloid lineage, as well as lymphoid cells, will develop during definitive haematopoiesis in the yolk sac, foetal embryo and in the bone marrow, being the latest persistent during post-natal age (Lacaud and

Kouskoff, 2017; Tavian and Péault, 2005). Myeloid stem cells – expressing IBA1, CD68, CD45 and MHC-II – will develop into macrophage precursor through the expression of transcription factors such as PU.1 (Chan et al., 2007). Around week 4.5 of gestational age in humans, these precursor cells migrate from the yolk sac to the developing brain through blood vessels (Ginhoux et al., 2010), and enter through the telencephalon in the forebrain (Ginhoux et al., 2013; Menassa and Gomez-Nicola, 2018). After this, they colonize the developing brain regions, reaching the midbrain region by week 22 of human gestation (Menassa and Gomez-Nicola, 2018). This invasion process occurs prior to the blood-brain barrier formation and, therefore, the developing central nervous system is easily accessible by microglia precursor cells. Single-cell RNA sequencing studies showed that, between the 6^{th} and 11^{th} gestational week, microglia represent around 1.1% of the ventral midbrain cells (La Manno et al., 2016).

Once microglia enter the central nervous system, they subsequently distribute through different developing regions. Microglia expand until they reach different proportions depending on the brain region, which will stay stable during adulthood. Immunohistochemistry studies have showed that, in adult age, microglia represent around 10% of the cells in the *substantia nigra* of the midbrain (Mittelbronn et al., 2001). The formation and closure of the blood-brain shortly after the microglia precursor invasion makes the access to the central nervous system by external cells difficult and rare. Microglia have self-renewal ability, which ensures their preservation and long-lasting presence in the brain. Studies showed the re-arrangement of microglia in the post-natal brain, and the ability to re-populate the brain regions via self-renewal after a substantial cell number loss (Bennett et al., 2016; Eyo et al., 2018). Analysis in the human brain cortex showed that microglia have a yearly turnover of 28%. Most of the microglia cells will have a relatively short lifespan; on average, they have an age of 4.2 years. Despite the fact that the majority of microglia are renewed, a small subset – constituted by less than 4% of the total cells – can live up to 20 years (Réu et al., 2017). Around 1.4% of microglia are proliferating at any given time in the developed brain (Askew et al., 2017).

After birth, circulating blood monocytes can enter the central nervous system through the blood-brain barrier following infection or inflammation and differentiate into resident microglia. However, this process has rarely been observed (Ginhoux et al., 2013).

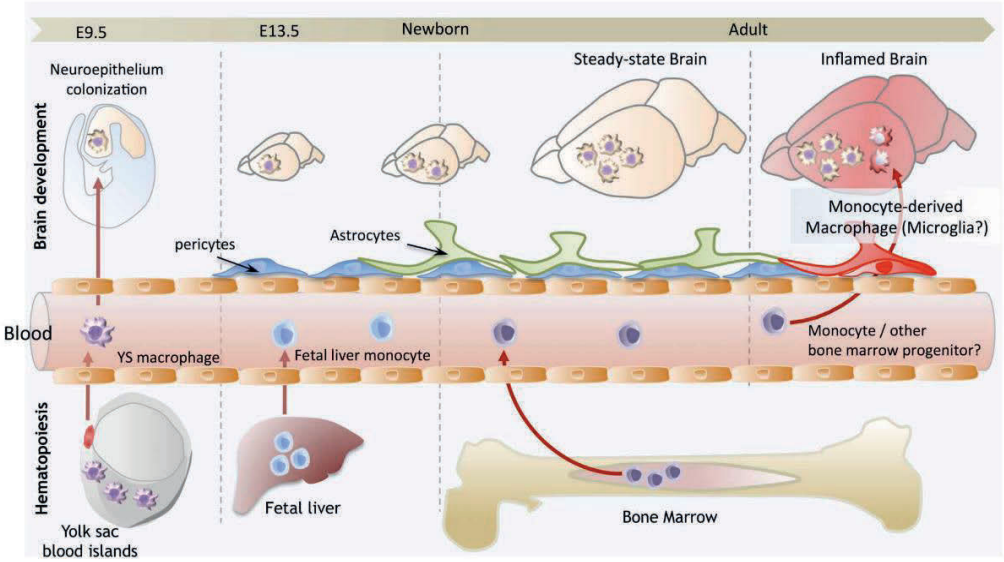

FIGURE 1. 4. **Microglia colonization of the neuro-epithelium and invasion of the developing brain in mice.** Primitive macrophages emerge from the yolk sac onto the circulation system around mouse embryonic day 9.5 (E9.5), which corresponds to gestational week 4.5 in humans. Macrophage precursor cells then reach the developing brain before the blood-brain barrier closure. In rare occasions, upon infection or bone barrow transplantation, circulating blood monocytes can be recruited into the CNS and travel through the BBB onto the brain parenchyma (Ginhoux et al., 2013).

1.1.2.3. Vasculature system development

During neurulation in humans and rodents, when the neural tube is in the process of closure, endothelial cell precursors from the somites (called angioblasts, Figure 1.1) establish a vascular network around the neural tube, called peri-neural vascular plexus (PNVP). Cells form the PNVP following pro-angiogenic molecular queues – mainly VEGF-A – produced by the developing neural cells in the neural tube (Bautch and James, 2009a; Hogan et al., 2004; Peguera et al., 2021). Simultaneously to the PNVP formation, radial glia cells differentiate from neuro-epithelial stem cells in the neural tube (Peguera et al., 2021). During the progression of angiogenesis in the developing CNS, endothelial cells will form capillaries and venules with the help of pericytes, embedded in a basal lamina rich in extracellular matrix proteins. These endothelial cells will form close contacts via tight and *adherens* junctions, forming a protective network called the Blood-brain barrier (BBB, Tata et al., 2015). The BBB in the developed brain will contain arteries and arterioles that form a dense network with high resistance and low permeability. Arterioles,

capillaries and venules will penetrate the brain parenchyma, forming tree-like shapes and often called the ‘Cerebrovascular tree’ (Iadecola, 2017).

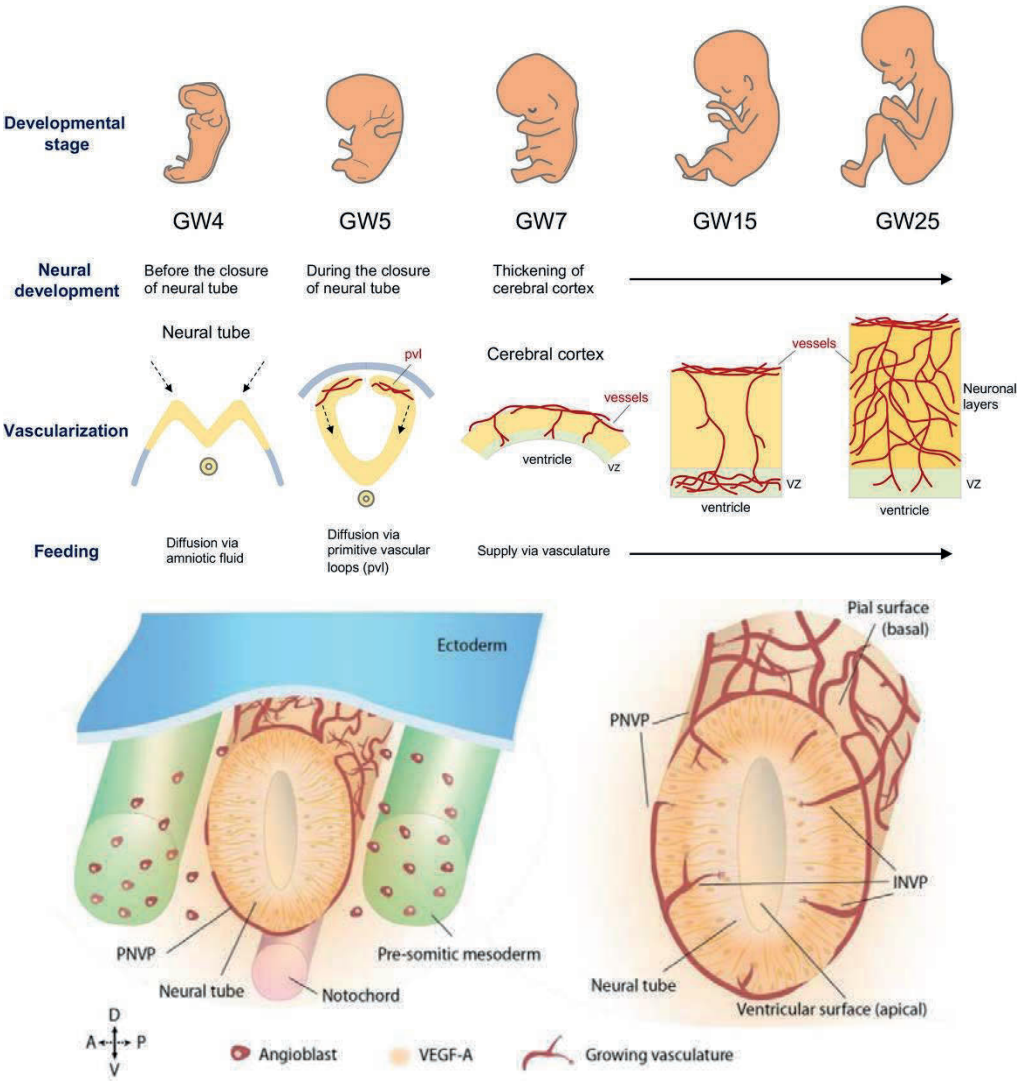

FIGURE 1. 5. **Development of human brain vasculature**. During the closure of the neural tube, the peri-neural vascular plexus (pvl, PNVP, red) forms around it. Around gestational week (GW) 7, blood vessels start growing into the cerebral cortex following pro-angiogenic signals (upper panel, Matsui et al., 2021). Angioblasts in the presomitic mesoderm are recruited by the neural tube. Blood vessels grow inwards shortly after the establishment of the PNVP, entering the pial surface (basal) and growing into the ventricular surface (Peguera et al., 2021).

While the mesodermal origin of endothelial cells forming the brain vasculature is clear, researchers have been exploring the origin of brain pericytes in the last decades. Pericytes are support cells – also called mural cells – that provide endothelial cells with structural support and molecular signalling (Tata et al., 2015). Pericytes in the brain can have a mesodermal or neuro-ectodermal

origin. Forebrain pericytes raise from neuro-ectodermal cells in the neural tube and neural crest cells, while pericytes in the brainstem and spinal cord seem to derive from mesodermal tissue (Couly et al., 1992, 1993; Etchevers et al., 2001; Korn et al., 2002). Besides the mesodermal and neuro-ectodermal origin of pericytes, researchers also observed that cells derived from embryonic haematopoiesis sites – such as the yolk sac – can be recruited from the blood flow into the developing brain, where they would initially derive to CD31-positive F4/80-positive macrophages and eventually give rise to cerebrovascular pericytes (Yamamoto et al., 2017).

1.2. Cellular interactions and communication in the human brain

Brain cells are in continuous communication with one another via direct contacts, as well as molecular and electrical signalling. Neurons connect with each other through synapses, where the axon end of a neuron communicates with other neurons' dendrite tip. They exchange information through neurotransmitter release (chemical synapse) or electrical impulses (electrical synapse), inducing a response in the receiving neuron (Lovinger, 2008; Pereda, 2014). In the midbrain, the major source of dopamine in the CNS, we can find 90% of the dopaminergic neurons in the brain. Dopaminergic neurons in the *substantia nigra pars compacta* project their axons to the dorsal striatum, communicating with different neuronal populations through the *nigro-striatal* pathway (Chinta and Andersen, 2005; Young et al., 2021).

Neurons not only communicate with each other, but also with other neural and non-neural cell types in the brain. Astrocytes closely interact with neurons and are involved in synaptic function, thus giving rise to the concept of 'tripartite synapse'. They provide the neurons with metabolic and structural support, and participate in the brain homeostasis maintenance. Although they are not electrically excitable cells, astrocytes respond to neurotransmitter release via neurotransmitter receptors, signalling cascades and intracellular calcium variations. Astrocytes have receptors for most neurotransmitters, and respond to signalling through the release of molecules that affect synaptic activity, often called gliotransmitters (Araque et al., 2014; Durkee and Araque, 2019; Min and Nevian, 2012).

Oligodendrocytes also interact with neurons, since they are responsible for myelination of axons in myelinated neurons. Oligodendrocyte damage and demyelination of axons leads to inflammation and loss of axonal protection, followed by a neurodegeneration, causing a broad range of neurological disorders (Kang et al., 2013; Kassmann et al., 2007). Communication between neurons and oligodendrocytes can occur through vesicular release. Neurons release

vesicles at axon-glial junctions that promote myelin sheath growth and stability (Hughes and Appel, 2019; Mensch et al., 2015). Oligodendrocytes not only communicate with neurons through the physical process of myelination, but also represent a source of potassium and metabolites for neurons (Duncan et al., 2021).

Apart from interacting with macroglia, neurons constantly communicate with microglia in the brain. Resting microglia develop surveying functions in the brain to ensure the correct physiology of neurons and other cell types. Microglia inspect their environment thanks to their motile processes and clear the brain parenchyma from cell debris, tissue components and metabolic waste products (Nimmerjahn et al., 2005). They recognize apoptotic neurons through complex surface signalling (Witting et al., 2000). During development, microglia regulate cell death and proliferation in the neurogenic niche via phagocytosis. Microglia physically interact with neurons through contacts between microglial processes and neuronal soma, where they establish signalling pathways through purinergic receptors. Researchers observed that activity of neuronal mitochondria induces the formation of junctions between microglia and neuronal soma, and inhibition of purinergic receptors prevented these contacts (Cserép et al., 2020). There is a bidirectional communication between microglia and neural precursors in the developing brain (Arnò et al., 2014). Recent studies showed that, in mice deficient for the P2RY12 and MERTK/Axl phagocytosis pathways, neurogenesis was disrupted. Therefore, the phagocytosis ability of microglia is important not only to clear cell debris and waste products, but also for neurogenesis in the developing brain (Diaz-Aparicio et al., 2020).

Cellular contacts and cell-cell communication are not restricted to two cell types, but multi-cellular interactive networks form in the developing brain for their correct functioning. An example of these multi-cellular interactions is the one formed by brain vasculature and neural cells. The cellular architecture of blood vessels in the brain is not restricted to endothelial and mural cells forming the BBB. While blood vessels in the brain surface are in contact with a thick layer of smooth muscle cells, penetrating vessels interact with pericytes, neurons, astrocytes and microglia, and a smaller proportion of smooth muscle cells, forming the neurovascular unit (Figure 1.6, McConnell et al., 2017). The main function of the neurovascular unit is regulating blood flow in the brain in order to maintain its changing metabolic needs (Bautch and James, 2009a). One of the main signalling molecule between blood vessels and neurons cells is VEGF-A and its receptor (VEGFR, present on endothelial cells). VEGF is a key factor on the development of the neurovascular unit. Lower production of this factor by neural progenitor cells dramatically affects vascular development, leading to neuronal cell death in the developing cortex (Haigh et al., 2003). Astrocytes support the barrier functions of blood vessels in the neurovascular unit through release of molecules such as Wnts, norrin, sonic hedgehog

(Shh), retinoic acid (RA) and angiopoietin-1 (Ang-1, Liebner et al., 2018). Concerning microglia, although their role in the neurovascular unit is still unknown, they participate in the support of vascular growth through signalling molecules such as Wnts.

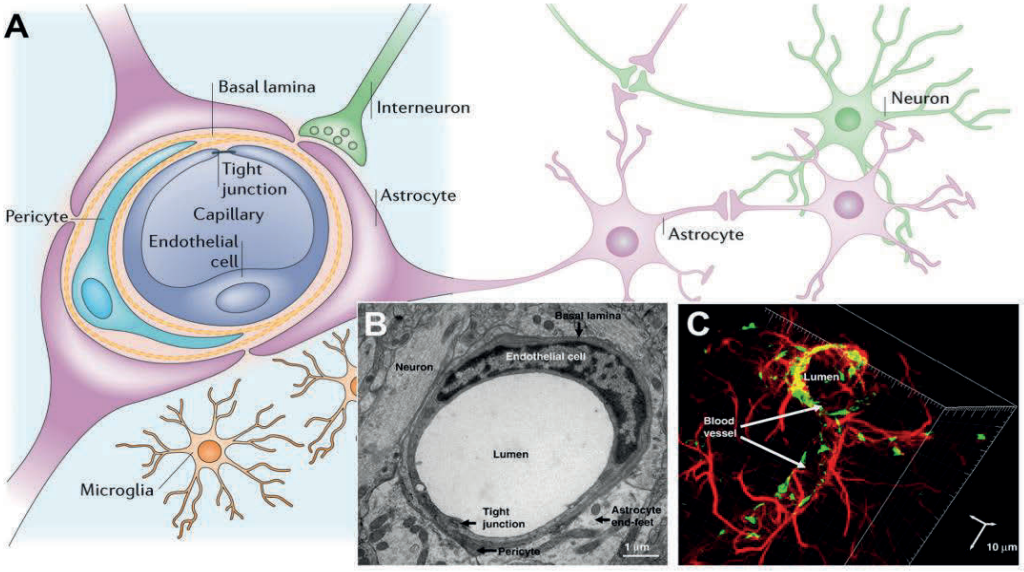

FIGURE 1. 6. **The neurovascular unit**. **A.** Diagram showing blood vessels, composed by endothelial cells (dark blue), pericytes (light blue) and a basal lamina (dashed orange) interacting with neurons (green), astrocyte feet (purple) and microglia (orange) in the brain. **B**. Electron microscopy image of the neurovascular unit in the rat brain. **C**. 3D visualization of an immunofluorescence staining showing GFAP-positive astrocytes (red) surrounding von-Willebrand factor-positive endothelial cells (green) (McConnell et al., 2017; Weiss et al., 2009).

1.2.1. Neurodegeneration

In neurodegenerative diseases, there is a progressive loss of specific neuronal cell populations in the brain, with neuronal death as the common factor amongst them. Neurodegenerative disorders can be classified by their clinical features – being movement disorders and behavioural alterations the most common. They can also be classified by the anatomic location of neuronal loss or main molecular alterations, especially accumulations of specific proteins (Dugger and Dickson, 2017). Accumulation of proteins can, in most cases, be detected before the appearance of clinical symptoms (Gibb and Lees, 1988; Schmitt et al., 2000), and it often leads to dysregulations of proteasome and autophagosomal/lysosomal systems, oxidative stress, apoptosis, and neuroinflammation (Dugger and Dickson, 2017).

1.2.1.1. Parkinson's Disease

Alzheimer's disease is the most common neurodegenerative disorder worldwide. It is characterized by accumulation of two products; in the extracellular space, neuritic plaques of 42-amino-acid amyloid-beta ($A\beta_{1-42}$) accumulate and, intracellularly, neurofibrillary tangles composed of hyper-phosphorylated MAPT protein (Erkkinen et al., 2018). Parkinson's disease (PD) is the second most common neurodegenerative disease after Alzheimer's, with age being the main risk factor to develop PD (it has a prevalence around 1% in people over 60 years, and 3% in people over 80 years). Clinical features of PD can be classified in motor and non-motor symptoms. Motor symptoms include bradykinesia, resting tremor, rigidity and postural instability. Amongst non-motor symptoms are dysautonomia, sleep disturbances, mood disorders and cognitive disturbances. The progression of the disease correlates with the appearance of dementia. (Erkkinen et al., 2018). The main hallmarks of PD are the degeneration of dopaminergic neurons in the *substantia nigra* of the midbrain and in basal ganglia, and the accumulation of misfolded or aggregated protein in neuronal cytoplasm and axons, called Lewy bodies and Lewy neurites. These protein inclusions contain mainly α-synuclein and, in a lower amount, other insoluble proteins and lipids (Inamdar et al., 2007). Around 80% of PD cases are idiopathic, while 20% are genetic (Bhat et al., 2018; Inamdar et al., 2007). Genetic PD is caused by mutations in genes such as *SNCA* (alpha-synuclein), *PINK1* (PTEN induced putative kinase 1), *LRRK2* (leucine-rich repeat kinase 2) *PARK7* (Parkinsonism Associated Deglycase) and *PRKN*. Mutations in genes such as *GBA* (glucocerebrosidase) and *UCHL1* (Ubiquitin C-Terminal Hydrolase L1) can increase the risk of PD development (Blauwendraat et al., 2020). Interactions between gene variants (Nalls et al., 2019), as well as interactions between environmental factors and gene mutations can also increase the risk of PD (Bhat et al., 2018). Despite its onset being normally at late stages of life, researchers have hypothesized that changes during brain development could determine the disease onset and progression, speculating that PD could be considered a developmental disorder (Huntley and Benson, 2020; Von Linstow et al., 2020; Schwamborn, 2018).

One of the most known processes that accompany neurodegeneration is neuroinflammation. During neuroinflammation, immune brain cells develop a self-protective response to injury or infection. Microglia belong to the group of innate immune system cells, which respond rapidly to injury through a short-

term response. Microglia, together with astrocytes, are the main cell types responsible for neuroinflammation (Troncoso-Escudero et al., 2018). Necrosis signals (in the case of PD, secreted by dopaminergic neurons) can be recognized by microglia and astrocyte receptors – e.g. Toll-like receptors (TLRs) and nucleotide oligomerization domain receptors (NLRs). Furthermore, endogenous molecules like α-synuclein can be recognized by microglia and astrocytes and trigger an immune response (Roodveldt et al., 2010; Troncoso-Escudero et al., 2018). Microglial activation upon neuronal damage and protein accumulation in PD leads to a morphological change, where microglia processes retract and cells acquire an amoeboid morphology. These morphology changes are accompanied by a molecular response cascade, including the production of cytokines and chemokines, activation of inflammatory pathways (such as Nuclear Factor kappa B (NF-κB) pathway) and oxidative stress in the substantia nigra (Członkowska et al., 1996; Hirsch and Hunot, 2009; McGeer et al., 1988). In PD and neuroinflammation, microglial activation upon recognition of molecules – such as α-synuclein or necrosis signals from neurons – leads to a response cascade where microglia release pro-inflammatory molecules and neurotoxic factors that contribute to neuronal damage. This further supports microglial activation, creating a pro-inflammatory positive-feedback loop called reactive microgliosis (Figure 1.7, Block et al., 2007; Castaño et al., 1998; Couch et al., 2011; Tansey and Goldberg, 2010).

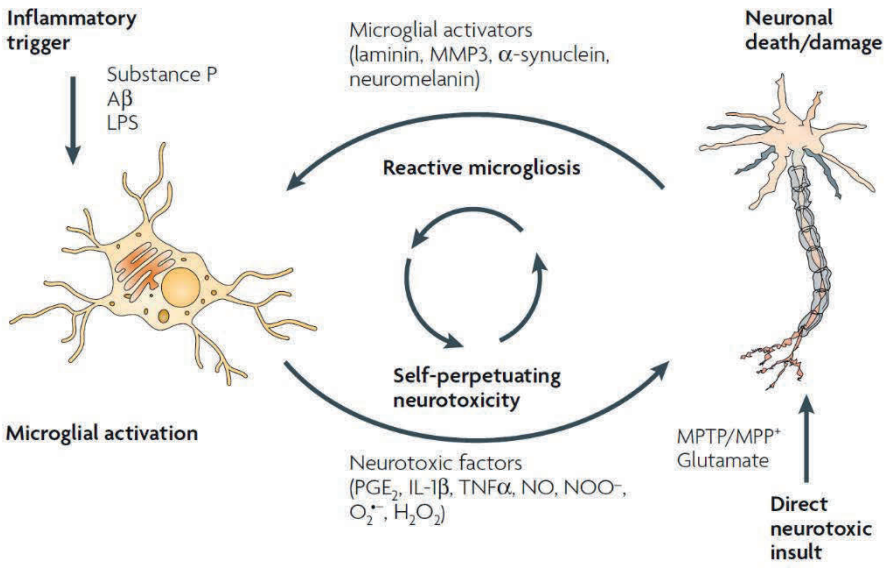

FIGURE 1. 7. **Reactive microgliosis.** Microglial activators can be recognized by receptors in microglia, and trigger an immune response by production of potentially neurotoxic molecules. In response to neuronal damage and neurodegeneration, microglia become overactivated and further release neurotoxic factors, sustaining the inflammation and neuronal damage cycle. In the diagram, reactive microgliosis between microglia and a myelinated neuron. Reactive microgliosis is a hallmark of the neuroinflammatory process in PD, perpetuating the (non-myelinated) dopaminergic neuron degeneration (Block et al., 2007).

Neuroinflammation has been linked not only to neurodegeneration, but also to vasculature and BBB damage and disruption (Daneman et al., 2010; Liebner et al., 2018). Induction of neuroinflammation by LPS administration leads to microglial activation and increase of BBB permeability via Tumour Necrosis Factor-α (Nishioku et al., 2010). On the other hand, in PD, α-synuclein induces BBB dysfunction via impairment of tight junction protein expression, and activation of brain pericytes, which release inflammatory molecules leading to changes in barrier permeability (Dohgu et al., 2019; Gray and Woulfe, 2015; Kuan et al., 2016). Increases in BBB permeability can lead to microglia activation and neuroinflammation (Ju et al., 2018). Overall, PD is not restricted to neurodegeneration, but it implies a machinery of processes where neurons, glia and vasculature undergo interconnected pathways that promote the disease progression (Takata et al., 2021).

1.3. Human brain models to study development and disease

Classical studies of the human brain were restricted to *post-mortem* brain observations. The work of Camillo Golgi, who developed in 1870 a staining technique with silver nitrate that would allow the observation of nerve cells to study their complex organization and interconnections, led to an expansion of the neuroscience field (Ghosh, 2020). Basing his studies on the staining technique development by Golgi, Santiago Ramón y Cajal was able to visualize single neurons and, later on, astrocytes in the human brain. Their ground-breaking findings in the neuroscience field made Golgi and Ramón y Cajal awarded with the Nobel Prize in physiology and medicine in 1906. Later on, Pío del Río-Hortega was able to identify the “third element”, a missing cell type in the brain that Ramón y Cajal was unable to determine. This “third element” was named microglia and oligodendrocytes (Boullerne and Feinstein, 2020). With the progression of the 20th century, the field of neuroscience experienced an expansion along with the development of new methods and techniques. Since then, *post-mortem* human brain samples, animal models, and *in vitro* cell culture systems have been explored to further

understand brain structure and functionality in health and disease. In the case of PD and neurodegeneration studies, *post-mortem* human samples – human midbrain and *substantia nigra* – represent a precise way to study cellular and molecular phenotypes and pathology mechanisms. However, the low availability of such samples represents a limitation. The availability of animal models is higher, but they not always reproduce human brain processes, and their use raises ethical concerns. These disadvantages often make animal models unsuitable to study the human brain (Jagmag et al., 2015; Vijayanathan et al., 2021).

1.3.1. 2D cell culture systems and iPSCs

2-dimensional (2D) cell culture systems are monolayer cell systems, often composed by a single cell type, that allow for studying cellular and molecular mechanisms in that specific cell type in health and disease. Studies have used 2D dopaminergic neuron cultures to study neurodegeneration and PD (Klucken et al., 2012; Outeiro et al., 2008; Xicoy et al., 2017). The source of cells in those studies was either *post-mortem* human tissue or immortalized tumour-derived cell lines (such as neuroglioma and neuroblastoma). The discovery of pluripotent stem cell induction in 2006 by Takahashi and Yamanaka (Takahashi and Yamanaka, 2006) represented the start of modern cell culture, which awarded Yamanaka with the Nobel Prize in physiology and medicine in 2012. They discovered that adult fibroblasts could be re-programmed into stem cells, called induced pluripotent stem cells (iPSCs) via overexpression of *Oct3/4, Sox2, Klf4* and *c-Myc.* IPSCs can then be differentiated into most cell types in the human body. Their findings opened the door to a different approach of cell culture studies, overcoming the limitations of human cell availability and making a step forward into personalized medicine (Takahashi and Yamanaka, 2006).

The iPSC technology allowed researchers to study cellular and molecular aspects of brain physiology and disease. Differentiation of iPSCs into neurons from healthy individuals and PD patients has been achieved to study PD cellular and molecular pathology (Lang et al., 2019; Panagiotakopoulou et al., 2020; Schweitzer et al., 2020). Furthermore, glial cells have been successfully differentiated from iPSCs to study cellular (patho)physiology. Astrocytes (di Domenico et al., 2019; Leventoux et al., 2020; Tsunemi et al., 2020), oligodendrocytes (Czepiel et al., 2011; Djelloul et al., 2015; Livesey et al., 2016) and microglia (Badanjak et al., 2021; Haenseler et al., 2017a; Panagiotakopoulou et al., 2020) can be efficiently derived from iPSCs to investigate PD. Furthermore, endothelial cells (Hollmann et al., 2017; Jamieson et al., 2019) and pericytes (Jamieson et al., 2019) have been differentiated from iPSCs as a cell culture model of the BBB.

The complexity of cell culture models increased with the establishment of co-culture systems. Unlike mono-cellular 2D culture systems, co-cultures allow for the understanding of contacts and molecular interactions between cell types. Researchers have applied co-culture systems of neurons with microglia to study inflammatory response (Haenseler et al., 2017a). Astrocytes have been successfully co-cultured with neurons to study astrocyte contribution to neurodegeneration (di Domenico et al., 2019; Russo et al., 2018). Besides neurons and glia, interactions between endothelial cells and pericytes and their implications in BBB stability have been investigated via co-culture (Jamieson et al., 2019).

1.3.2. Lab-on-a-chip

The combination of monoculture or co-culture systems with engineered microfluidic devices gave rise to “organ-on-a-chip” or “lab-on-a-chip” technologies. In those systems, cells in 2D, layers of different cell types (often referred as 2.5D) and 3-dimensional (3D) structures are cultured in microfluidic chips. Chips contain microchannel that control microscale fluids (10^{-9} to 10^{-18} litres) driven by passive transport – such as hydrostatic pressure – or active pumping – perfusable systems. This makes them not only suitable to study interactions between multiple cells, but also their physiological, mechanical and biochemical environment, closer to that of the human body (Wu et al., 2020). The fact that cell environment and inter-tissue interactions cannot be modelled accurately by 2D culture systems often creates the need of validation with *in vivo* models. However, animal models do not always mimic human physiological environments. Scientists suggested that organ-on-a-chip technologies could represent a step forward into independence of cell culture systems and towards the end of reliability on animal models (Van Der Meer and Van Den Berg, 2012; Wu et al., 2020).

Organ-on-a-chip technologies have been applied for biomarker detection using sensors and drug testing (Harpaz et al., 2020; Sung and Shuler, 2009). The interaction of neuron layers through axonal bundles has been assessed with these methods (Kilic et al., 2016). Tissue slices have been cultured on-chip to study tissue interactions between liver, bone marrow and cerebral cortex (Sonntag et al., 2010). BBB models have been assessed using this method in healthy (Musafargani et al., 2020; Park et al., 2019) and pathological conditions (Vatine et al., 2019). Furthermore, physiological (Dong et al., 2022; Lee et al., 2022) and disease (Alcendor et al., 2013; Lyu et al., 2021) aspects of the neurovascular unit have been investigated on-chip. Despite the fact that lab-on-a-chip technologies have an increased complexity and bring more information

to researchers in comparison to 2D cultures, 2D and 2.5D systems often fail to recapitulate the 3D microenvironment of human tissue (Moysidou and Owens, 2021).

1.3.3. 3D models and midbrain-specific organoids

The first 3D tissue culture models were composed by tissue-specific cell types (often co-cultured and layered) embedded in an extracellular matrix gel, which allowed for the study of (patho)physiological processes. However, the number of different cell types is limited in those systems, and the 3D environment is not always accurately represented. With the rise stem cell-derived organoid systems, the limitation of mimicking 3D tissue microenvironment was overcome. The initial population of pluripotent stem differentiates into to multiple cell types in 3D, giving rise to spheroids and organoids with different types of cells that interact with each other in a microenvironment that resembles the one in human tissue and organs (Figure 1.8, Caddeo et al., 2017; Gjorevski et al., 2014; Lancaster and Knoblich, 2014).

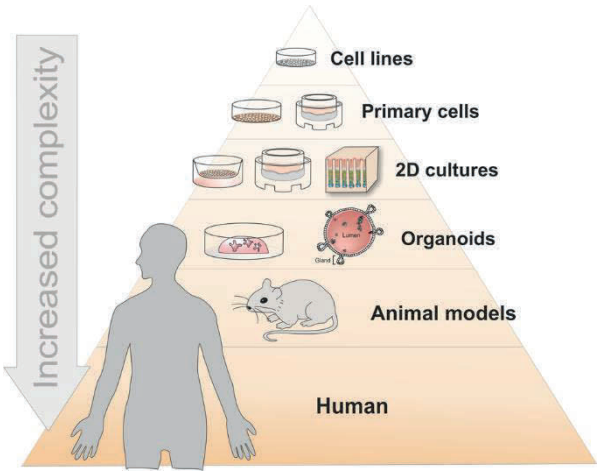

FIGURE 1. 8. **Complexity of cell culture systems.** Cell line and primary cell culture complexity can be increased in 2D culture by on-chip systems. Organoid models allow for further study of 3D microenvironments, which can be further advanced using organ-on-chip and assembloid technologies (Aguilar et al., 2021).

Organoid models have a cellular heterogeneity, with multiple cell types that connect and communicate with each other in a tissue-like manner. Brain organoids have been developed during the last decade to study neural development and neurological disorders (Lancaster et al., 2013; Lindborg et al., 2016). To specifically target brain processes in discrete brain regions - such as forebrain and midbrain - region-specific brain organoids have been engineered (Birey et al., 2017; Jo et al., 2016; Monzel et al., 2017; Qian et al., 2016). Midbrain-specific organoids are rich in dopaminergic neurons, and contain astrocytes and oligodendrocytes. Neurons in midbrain organoids

communicate through neurotransmitter release and electrical impulses (Smits et al., 2019). Furthermore, monogenetic PD, where patient-specific organoids carry the LRRK2-G2019S mutation can be studied using this model (Monzel et al., 2017; Nickels et al., 2020).

1.3.4. Advanced 3D models: assembloids and organoids on-chip

The brain is a highly dynamic tissue, where neurons project their axons to different regions, establishing communications from a brain area to another. Region-specific organoids are suitable to study mechanisms restricted to a brain area; however, interactions between brain regions cannot be effectively recapitulated with discrete-region organoids. Furthermore, single organoids are not suitable to study cell migration between regions and circuit assembly (such as the nigro-striatal pathway). The generation of assembloids overcame this limitation. Brain assembloids consist in multiple region-specific organoids in contact with each other (Pasca, 2018).

An effective method to generate assembloids is direct organoid fusion (Bagley et al., 2017; Xiang et al., 2017). In order to study cellular and molecular interactions between cells from different brain regions, efforts have focused on fusing region-specific organoids. Cortical organoids, rich in glutamatergic neurons and astrocytes, have been successfully fused with ventral forebrain organoids, abundant in GABAergic interneurons. Researchers observed that GABAergic neurons migrate and make contacts with glutamatergic neurons from the cortical region of assembloids, modelling, thus, cortical interneuron migration (Bagley et al., 2017; Birey et al., 2017; Xiang et al., 2017). Organoid fusion has been hypothesized to be a suitable method to study interactions in the *nigrostriatal* pathway in physiological conditions and PD. The study of axonal projections of midbrain dopaminergic neurons towards basal ganglia and striatum would be of high valuable for PD modelling (Pasca, 2019). Another inter-organ interactive assembloid system could be developed to studying the interactions between brain and intestine. Connecting brain and gut organoids would be of great value for the scientific community, since evidence indicates that the brain and gut are in constant communication via molecular signalling through the enteric nervous system. In PD, α-synuclein has been found in the gastrointestinal tract (Braak et al., 2006). Furthermore, it potentially can spread to the brain through the vagal nerve via microtubule-associated transport (Holmqvist et al., 2014). Gut-brain interactive models are, thus, of high value to study α-synuclein spread and inter-organ communication in PD (Reiner et al., 2020). Gut-specific organoids have been assembled with neural crest cells to study the enteric nervous system *in vitro* (Workman et al., 2017). Assembly of organoids with other cell

types by addition or mixing is an effective way to increase the complexity organoid systems. Since starting cell populations used for organoid generation are often limited to a cell lineage, external incorporation of cells is necessary to complete the model with all cell compartments. In the case of the brain, microglia – yolk-sac derived – and endothelial cells – mesoderm-derived – are often absent in 3D cell culture systems (Pasca, 2019). Microglia-like cells have been successfully assembled into cortical organoids to study Alzheimer's disease (Lin et al., 2018). Schizophrenia has also been modelled in brain organoids where primary microglia were integrated (Sekar et al., 2016).

In order to assemble specific cell types into assembloids, cell-encapsulated bioprinting has also been assessed. Hydrogel materials, which mimic the extracellular matrix, are a suitable environment where cell types can be included prior to co-culture and assembly with organoids (Unagolla and Jayasuriya, 2020). Vascularization of brain organoids is an example of this method. The use of hydrogels that contain and support endothelial cells, alone or in combination with pericytes, has been applied to vascularize brain organoids (Grebenyuk and Ranga, 2019; Kinoshita et al., 2016; Roudsari et al., 2016; Xu et al., 2012; Zhang et al., 2016).

Assembly of organoids represents the future perspectives towards inter-connected multi-organoid systems, modelling the human body in a complex fashion. The increasing complexity of cell culture systems where organoids and assembloids are inter-connected led to the introduction of the term "body-on-chip" in the scientific community (Williamson et al., 2013).

CHAPTER 2

MOTIVATION AND AIMS

The rise of 3D cell culture models allowed for a more accurate recapitulation of multi-cellular interactions and 3D microenvironments from human organs than 2D systems. Recent efforts have focused on the development of midbrain-specific organoids, rich in dopaminergic neurons. One of the final goals of midbrain organoids is PD modelling. Reduced number and morphological complexity of TH-positive dopaminergic neurons in midbrain organoids carrying the G2019S LRRK2 mutation have been observed. While the applicability of midbrain organoids for PD modelling has been proven, studies where phenotypes are compared to *in vivo* systems have not yet been assessed. Apart from dopaminergic neurons, midbrain organoids contain neural precursor cells, astrocytes and oligodendrocytes. Neurons in midbrain organoids make contacts and communicate via synaptic contacts, neurotransmitter release and electrical activity. However, not all cell types of the midbrain are represented in organoids. Microglia, the immune cell compartment in the brain, and a vasculature system, have not been identified in midbrain organoids via immunodetection. In order to confirm the absence of mesoderm-derived cell types, and to better investigate the present and absent cellular populations in organoids, an extensive analysis assessing cell types should be performed.

The absence of microglia in midbrain organoids means that phagocytosis of cell debris and communication with other cell types to maintain homeostasis do not occur. This could lead to high oxidative stress and cell death in the inner core of the tissue. In 3D culture systems, the oxygen and nutrient supply in the inner centre is often restricted, which leads to high levels of hypoxia and cell death in the centre. By integrating microglia into midbrain organoids, we hypothesize we could reduce oxidative stress and the amount of apoptotic bodies in the core. Furthermore, without microglia neuroinflammation-related processes cannot be modelled in the system. Besides microglia, a vasculature system is absent in midbrain organoids. Microglia interact with endothelial cells, pericytes, neuron projections and astrocytes in the brain forming the neurovascular unit. We speculate that a vasculature system in midbrain organoids would be highly beneficial in terms of oxygen and nutrient supply – further reducing the cell death levels in the core, cell communication and signalling. We hypothesize that endothelial cells would make contacts with neurons and microglia in midbrain organoids, representing the neurovascular unit in 3D. These observations and speculations led us to the main hypothesis of this PhD thesis:

“The integration of microglia and a vasculature system into midbrain organoids increases the complexity of the models and thus mimics closely the human brain environment, and reduces cell culture-related issues such as necrosis, hypoxia or stress”

The aims of the thesis are:

- Validate midbrain organoid PD phenotypes *in vivo* to confirm the translatability of the system.
- Explore and characterize cell populations in midbrain organoids.
- Integrate microglia into midbrain organoids and characterize the advanced system.
- Incorporate a vasculature system in midbrain organoid, and assess the possible effects it has on cell death and hypoxia.
- Advance the model by simultaneously integrating vasculature and microglia, mimicking the neurovascular unit in 3D.

CHAPTER 3

MATERIALS AND METHODS

All comprehensive information concerning materials and methods are included in each corresponding original article listed in chapter 4 – Results. In the following section, the main experimental procedures I conducted myself are listed and linked to the corresponding article.

Methods

hiPSC culture

see Manuscript III (Sabate-Soler et al. 2022)

see Manuscript IV (Sabate-Soler et al. *in preparation*)

Derivation and culture of human neuro-epithelial stem cells

see Manuscript III (Sabate-Soler et al. 2022)

see Manuscript IV (Sabate-Soler et al. *in preparation*)

Generation of midbrain organoids

see Manuscript III (Sabate-Soler et al. 2022)

see Manuscript IV (Sabate-Soler et al. *in preparation*)

Macrophage precursor derivation and microglia differentiation

see Manuscript III (Sabate-Soler et al. 2022)

see Manuscript IV (Sabate-Soler et al. *in preparation*)

Co-culture of midbrain organoids with macrophage precursors and 3D microglia differentiation

see Manuscript III (Sabate-Soler et al. 2022)

see Manuscript IV (Sabate-Soler et al. *in preparation*)

Vascular organoid derivation and co-culture with midbrain organoids

see Manuscript IV (Sabate-Soler et al. *in preparation*)

Immunofluorescence staining

see Manuscript II (Smits et al. 2020)

see Manuscript III (Sabate-Soler et al. 2022)

see Manuscript IV (Sabate-Soler et al. *in preparation*)

Confocal microscopy

see Manuscript II (Smits et al. 2020)

see Manuscript III (Sabate-Soler et al. 2022)

see Manuscript IV (Sabate-Soler et al. *in preparation*)

High-Content Imaging and image analysis in MATLAB

see Manuscript III (Sabate-Soler et al. 2022)

Statistical analysis in Graphad

see Manuscript III (Sabate-Soler et al. 2022)

see Manuscript IV (Sabate-Soler et al. in preparation)

Multi-electrode array (MEA)

see Manuscript III (Sabate-Soler et al. 2022)

RT-PCR

see Manuscript III (Sabate-Soler et al. 2022)

Western Blot assay and analysis

see Manuscript I (Jarazo et al. 2021)

see Manuscript III (Sabate-Soler et al. 2022)

see Manuscript IV (Sabate-Soler et al. *in preparation*)

LDH assay

see Manuscript IV (Sabate-Soler et al. *in preparation*)

Hypoxyprobe assay and analysis

see Manuscript IV (Sabate-Soler et al. 2022)

3D reconstruction and image analysis with IMARIS

see Manuscript IV (Sabate-Soler et al. 2022)

CHAPTER 4

RESULTS

4.1. MANUSCRIPT I

Parkinson's Disease Phenotypes in Patient Neuronal Cultures and Brain Organoids Improved by 2-Hydroxypropyl-β-cyclodextrin Treatment

---

This article has been published in *Movement Disorders.*

4.1.1. Preface

PD is the second most common neurodegenerative disorder worldwide, after Alzheimer's disease. Mutations in the *PINK1* gene lead to the development of the disease, with cellular phenotypes such as Lewy Body formation (Nybø et al., 2020). *PINK1* is involved in mitochondrial homeostasis and mitophagy, as well as membrane trafficking and autophagy (Ashrafi and Schwarz, 2012; Brás et al., 2015). Effects of *PINK1* loss of function in dopaminergic neurons has been studied *in vitro.* However, no studies where *PINK1* mutations are studied using organoid systems have been done until now. Furthermore, drug treatments targeting autophagy and mitopagy to rescue dopaminergic neuron phenotypes in *PINK1*-induced PD are scarce.

In this article, we study in detail neuronal phenotypes associated with *PINK1* mutations *in vitro*. We used patient-derived iPSCs and neurons to assess *PINK1*-associated phenotypes. We observed changes in energetic profile, imbalanced proliferation, apoptosis, mitophagy, differentiation efficiency of dopaminergic neurons and astrocyte levels in patient-derived cells compared to controls. Because of the higher cellular complexity and interactions, we validated neuronal phenotypes with midbrain organoids and *in vivo*. We studied the gene correction of a *PINK1* point mutation, and observed a rescue of metabolic processes and electrophysiological rates. Gene-correction ameliorated the differentiation efficiency of dopaminergic neurons and restored astrocyte levels. Apart from PD phenotyping in 2D and 3D, treatment with 2-hydroxypropyl-β-cyclodextrin was applied to patient-derived neurons, midbrain organoids and mice. Rescue of phenotypes such as autophagy, mitophagy, neuron differentiation and neuronal degeneration were observed after treatment. Mice models not only validated the neuronal phenotypes observed in midbrain organoids, but also the rescue of dopaminergic neuron loss upon Cyclodextrin treatment. The fact that the neuronal phenotype observed in 3D was validated in animal models proved the translatability from midbrain organoids to *in vivo* systems.

In this article, I supported the first author by studying the effects of *PINK1* mutations on autophagy in neuronal cell cultures. I performed and analysed western blot assays, which showed significant decrease in the LC3-II/LC3-I ration in patient-derived neurons. These experiments supported other results that showed reduced autophagy in mutant lines. Figure S6A and S6B show the results of my participation in the manuscript.

RESEARCH ARTICLE

Parkinson's Disease Phenotypes in Patient Neuronal Cultures and Brain Organoids Improved by 2-Hydroxypropyl-β-Cyclodextrin Treatment

Javier Jarazo, PhD,[1,2] Kyriaki Barmpa, MSc,[1] Jennifer Modamio, PhD,[1] Cláudia Saraiva, PhD,[1] Sònia Sabaté-Soler, MSc,[1] Isabel Rosety, MSc,[1] Anne Griesbeck, PhD,[3] Florian Skwirblies, BSc,[3] Gaia Zaffaroni, PhD,[4] Lisa M. Smits, PhD,[1] Jihui Su, BSc,[5] Jonathan Arias-Fuenzalida, PhD,[1] Jonas Walter, PhD,[1] Gemma Gomez-Giro, PhD,[1] Anna S. Monzel, PhD,[1] Xiaobing Qing, PhD,[1] Armelle Vitali, MSc,[6] Gerald Cruciani, MSc,[6,7] Ibrahim Boussaad, PhD,[6,7] Francesco Brunelli, PhD,[8] Christian Jäger, PhD,[9] Aleksandar Rakovic, PhD,[10] Wen Li, PhD,[5] Lin Yuan, PhD,[5] Emanuel Berger, PhD,[1] Giuseppe Arena, PhD,[6] Silvia Bolognin, PhD,[1] Ronny Schmidt, PhD,[3] Christoph Schröder, PhD,[3] Paul M.A. Antony, PhD,[6] Christine Klein, MD,[10] Rejko Krüger, MD,[6,11,12] Philip Seibler, PhD,[10] and Jens C. Schwamborn, PhD[1*]

[1]*Developmental and Cellular Biology, Luxembourg Centre for Systems Biomedicine University of Luxembourg, Esch-sur-Alzette, Luxembourg*
[2]*OrganoTherapeutics société à responsabilité limitée simplifiée (SARL-S), Esch-sur-Alzette, Luxembourg*
[3]*Sciomics GmbH, Heidelberg, Germany*
[4]*Institute for Globally Distributed Open Research and Education, Gothenburg, Sweden*
[5]*Institute of Health Sciences, China Medical University, Shenyang, China*
[6]*Translational Neuroscience, Luxembourg Centre for Systems Biomedicine University of Luxembourg, Esch-sur-Alzette, Luxembourg*
[7]*Disease Modeling and Screening Platform, Luxembourg Institute of Systems Biomedicine, University of Luxembourg and Luxembourg Institute of Health, Belvaux, Luxembourg*
[8]*Department of Molecular Medicine, University of Pavia, Pavia, Italy*
[9]*Metabolomics Platform, Enzymology and Metabolism, Luxembourg Centre for Systems Biomedicine University of Luxembourg, Esch-sur-Alzette, Luxembourg*
[10]*Institute of Neurogenetics, University of Lübeck, Lübeck, Germany*
[11]*Centre Hospitalier de Luxembourg, Parkinson Research Clinic, Luxembourg, Luxembourg*
[12]*Transversal Translational Medicine, Luxembourg Institute of Health, Strassen, Luxembourg*

ABSTRACT: Background: The etiology of Parkinson's disease (PD) is only partially understood despite the fact that environmental causes, risk factors, and specific gene mutations are contributors to the disease. Biallelic mutations in the phosphatase and tensin homolog (PTEN)-induced putative kinase 1 (*PINK1*) gene involved in mitochondrial homeostasis, vesicle trafficking, and autophagy are sufficient to cause PD.
Objectives: We sought to evaluate the difference between controls' and *PINK1* patients' derived neurons in their transition from neuroepithelial stem cells to neurons, allowing us to identify potential pathways to target with repurposed compounds.
Methods: Using two-dimensional and three-dimensional models of patients' derived neurons we recapitulated PD-related phenotypes. We introduced the usage of midbrain organoids for testing compounds. Using Clustered Regularly Interspaced Short Palindromic Repeats (CRISPR)/CRISPR-associated protein 9 (Cas9), we corrected the point mutations of three patients' derived

*__Correspondence to:__ Dr. Jens C. Schwamborn, Luxembourg Centre for Systems Biomedicine University of Luxembourg, 7 avenue des Hauts-Fourneaux, L-4362, Esch-sur-Alzette, Luxembourg; E-mail: jens.schwamborn@uni.lu

Relevant conflicts of interest/financial disclosures: J.J., S.B., and J.C.S. are cofounders and shareholders of OrganoTherapeutics société à responsabilité limitée simplifiée (SARL-S). C.S. is founder of Sciomics GmbH.

Funding agencies: This project was funded by the Fonds National de la Recherche (FNR) Luxembourg (CORE, C13/BM/5791363). This is a European Union Joint Program–Neurodegenerative Disease Research (JPND) project (INTER/JPND/14/02; INTER/JPND/15/11092422). This project is also supported by the European Union's Horizon 2020 research and innovation program under grant agreement no. 668738, Systems Medicine of Mitochondrial Parkinson's Disease (SysMedPD). The automated screening platform was supported by a PEARL grant of the FNR to R.K. (FNR/P13/6682797). G.A. is supported by the FNR Mitochondrial Risk factors in Parkinson's Disease (MiRisk-PD) (C17/BM/11676395). J.J. is supported by a Pelican award from the Fondation du Pelican de Mie et Pierre Hippert-Faber. J.J., L.M.S., A.S.M., J.W., and X.Q. were supported by FNR Aides à la Formation-Recherche. G.G.G. was funded by the Neuronal ceroid lipofuscinosis (NCL)-Stiftung (Hamburg, Germany). A.R., C.K., and P.S. are supported by the Deutsche Forschungs Gemeinschaft (DFG) (FOR2488).

Received: 4 May 2021; **Revised:** 7 September 2021; **Accepted:** 10 September 2021

Published online in Wiley Online Library (wileyonlinelibrary.com). DOI: 10.1002/mds.28810

cells. We evaluated the effect of the selected compound in a mouse model.

Results: PD patient-derived cells presented differences in their energetic profile, imbalanced proliferation, apoptosis, mitophagy, and a reduced differentiation efficiency to tyrosine hydroxylase positive (TH+) neurons compared to controls' cells. Correction of a patient's point mutation ameliorated the metabolic properties and neuronal firing rates as well as reversing the differentiation phenotype, and reducing the increased astrocytic levels. Treatment with 2-hydroxypropyl-β-cyclodextrin increased the autophagy and mitophagy capacity of neurons concomitant with an improved dopaminergic differentiation of patient-specific neurons in midbrain organoids and ameliorated neurotoxicity in a mouse model.

Conclusion: We show that treatment with a repurposed compound is sufficient for restoring the impaired dopaminergic differentiation of PD patient-derived cells.

Key Words: Parkinson's disease; *PINK1*; isogenics; cyclodextrin; organoids

Neurodegenerative diseases pose a great threat to aging populations.[1] Due to the lack of disease-modifying therapies, patients suffering from Parkinson's disease (PD) have to rely on symptomatic treatments.[2] Affected genes, reported as risk or causative factors of PD, control major cellular processes such as cell proliferation, membrane trafficking, mitochondrial homeostasis, and autophagy.[3] Among these, *PINK1* is involved in regulating mitochondrial function and morphology by quarantining damaged mitochondria before their degradation as well as triggering the process of mitophagy.[4] The fact that individuals with biallelic pathogenic variants in *PINK1* develop PD shows that an altered mitochondrial function, morphology, and degradation are linked to its pathogenesis.[5]

One of the hallmarks of PD is the loss of dopaminergic neurons in the substantia nigra pars compacta, but other regions are also affected.[6] Reports of postmortem neuropathological studies of patients having mutations in *PINK1* show that Lewy bodies, mainly composed of synuclein alpha (SNCA), are present in several brain regions of some of these patients.[7] Work in the zebrafish and organoid models previously suggested that a loss of function of *PINK1* might lead to a developmental reduction in the number of dopaminergic neurons.[8,9] However, implications of *PINK1* and its PD-associated mutations during the transition from neural precursor cells to differentiated neurons were not studied in depth in a human cell model. Techniques for recapitulating disease phenotypes in culture had a recent breakthrough with the introduction of organoid cultures.[10] These organ-like structures contain different cell types in a spatially organized fashion, recapitulating at least some of the main functions of the respective organ. Importantly, they have been proven valid models for human diseases.[10-12]

In this study, the induced pluripotent stem cells (iPSCs) of patients with PD with *PINK1* mutations and healthy individuals were differentiated into a neuroepithelial stem cell (NESC) state and later into dopaminergic neurons. Different features such as proliferation capacity, apoptosis, and differentiation efficiency were analyzed using computational algorithms for pattern recognition through high-content image analysis. We demonstrated that the differentiation efficiency of patient-derived NESCs is reduced while maintaining an increased proliferative activity on neuronal differentiation and exhibiting increased apoptosis of tyrosine hydroxylase positive (TH+) neurons. We performed an immuno-based protein-profiling analysis of organoids at different stages of development confirming that proteins involved in cell cycle, differentiation, apoptosis, and autophagy pathways were differentially abundant in the case of the patient. Using extracellular flux analysis and microelectrode array, we assessed the energetic profile of NESCs and the firing activity of differentiated neurons, which were altered in patient-derived cells. Moreover, using a pH-sensitive reporter tagging a mitochondrial protein, we observed a reduced autophagy and mitophagy capacity. Gene correcting the patients' mutation with the clustered regularly interspaced short palindrome repeats (CRISPR)/CRISPR-associated protein 9 (CRISPR/Cas9) system improved the mitochondrial activity, firing rate, and differentiation efficiency. Treatment with the compound 2-hydroxypropyl-β-cyclodextrin (HP-β-CD) resolved the mitophagy impairment and improved the dopaminergic differentiation in patient-derived cells by modifying the levels of proteins involved in dopaminergic differentiation, autophagy, apoptosis, and neuroinflammation.

Materials and Methods

Reagents and Resources Information

Detailed information about the reagents and resources used in this article are summarized in Table S7.

Detailed Description of Protocols

A summary is given of the different procedures. A detailed explanation can be found in the Supplementary Information, Extended Material and Methods.

Information About Cell Lines

Healthy controls 1 and 2 gave written informed consent at the University of Tübingen. Healthy control 3 was provided by Bill Skarnes. Patient *PINK1* 1 and patient *PINK1* 2 gave written informed consent at the University of Lübeck. Patient *PINK1* 3 and patient parkin samples were obtained from Coriell Institute, now held by the National Institute of Neurological Disorders and Stroke human cell and data repository. From each donor, one clone per iPSC line was derived and used in this study.

NESC Derivation and Neuron Differentiation

Human NESCs were generated as described elsewhere.[13] Neuronal differentiation was induced by culturing NESCs in N2B27 supplemented with 10 ng/mL human Brain Derived Neurotrophic Factor (hBDNF) (Peprotech, 450-02), 10 ng/mL human Glial cell line-derived Neurotrophic Factor (hGDNF) (Peprotech [East Windsor, NJ], 450-10), 500 μM Dibutyryl Cyclic Adenosine Monophosphate (dbcAMP) (Sigma [St. Louis, MO], D0627), 200 μM ascorbic acid, 1 ng/mL Transforming growth factor beta 3 (TGF-β3) (Peprotech, 100-36E), and 1 μM purmorphamine (PMA) (differentiation media 1) for 6 days. Afterward, the same media without PMA (differentiation media 2) was used for the duration of the correspondent experiment.

Immunocytochemistry

Fixation was done using 4% Paraformaldehyde (PFA) for 15 minutes at Room Temperature (RT). After 3× 1 × phosphate-buffered saline (PBS) washing steps, cells were permeabilized using 0.5% Triton X-100 in 1 × PBS for 15 minutes at RT. Blocking was performed for 1 hour at RT. Incubation with the first antibodies was done overnight at 4°C in blocking buffer. Incubation with the secondary antibodies was for 2 hours at RT in blocking buffer.

Immunohistochemistry

Processing of organoids was performed as previously described.[14]

Western Blotting

Pellets of neurons differentiated for 21 days coming from a confluent well of a 6-well plate were lysed. Lysates were then centrifuged, quantified, resolved, and transferred from the gel to polyvinylidene fluoride membranes in an iBlot2 device (Thermo Fisher [Waltham, MA], IB24001). Membranes were blocked for 60 minutes at RT. Primary antibodies were incubated at 4°C overnight. Secondary antibodies were incubated for 60 minutes at RT. Membranes were revealed using the SuperSignal West Pico Chemiluminescent Substrate (Thermo Fisher [Waltham, MA]).

Extracellular Flux Analysis (SeaHorse Measurements)

Human NESCs were seeded in a Matrigel-coated XF 96-well plate (Agilent Technologies [Santa Clara, CA], 102416-100) at a density of 65,000 cells per well. Three baseline measures and three measurements after each compound injection were performed.

Microelectrode Array Measurements

The Maestro microelectrode array (MEA; Axion BioSystems [Atlanta, GA]) system was used to measure the spontaneous activity of neurons. Axion Integrated Studio was used to process the raw data as previously described.[14]

Rosella Mitophagy Reporter

The pH sensor fluorescent protein pH-sensitive green fluorescent protein (pHluorin) was fused to red fluorescent protein from Discosoma (DsRed) and the entire open reading frame of adenosine triphosphate (ATP) Synthase F1 Subunit Gamma (ATP5C1) or Microtubule-associated protein 1A/1B-light chain 3 (LC3) as described in Sargsyan et al[15] and Arias-Fuenzalida et al.[16]

Gene Editing

Gene correction of patient's point mutation was performed as previously described.[17,18] Briefly, donor constructs with a positive selection module (PSM) and designed guide RNAs (gRNAs) targeting *PINK1* were transfected into human induced pluripotent stem cells (hiPSCs). Fluorescent selection was done by cell sorting; removal of the PSM was performed with transposase piggyBac excision-only mRNA, and selection was done via cell sorting.

RNA Isolation, Reverse-Transcription Polymerase Chain Reaction, and Quantitative Polymerase Chain Reaction

Total RNA was isolated using miRNeasy Mini Kit (Qiagen, Hilden, Germany) and treated with the RNase-Free DNase Set (Qiagen). cDNA was reverse transcribed using the High-Capacity RNA-to-cDNA Kit (Invitrogen, Waltham, MA). Quantification of gene expression was performed using the LightCycler 480 Probes software (Roche, Basel, Switzerland).

Compound Treatment

HP-β-CD dissolved in water (Sigma, H-107) was added on every media change at the different concentrations

tested and kept throughout the entire differentiation process. Untreated conditions are regular differentiation media.

Image Acquisition

Cell carrier Ultra plates were imaged in an automated manner using an Opera Quadruple Enhanced High

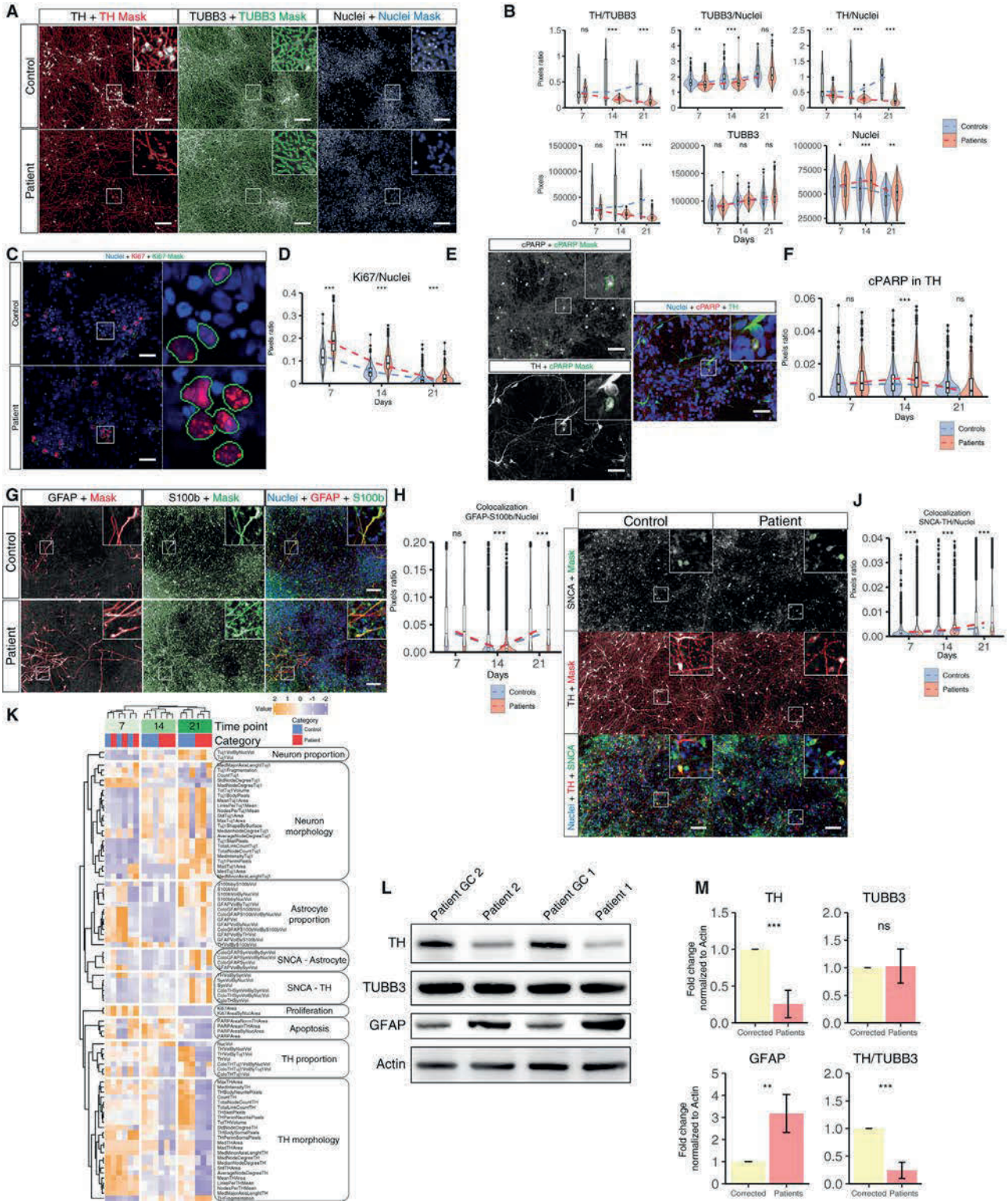

FIG. 1. Legend on next page.

Sensitivity (QEHS) spinning disk microscope (PerkinElmer, Waltham, MA).

Image Analysis

The image analysis was performed using MatLab (MathWorks, Natick, MA) as previously described.[16,19]

Microfluidics Culture

Neuroepithelial stem cells (NESCs) were seeded in an OrganoPlate (Mimetas [Leiden, the Netherlands], 9603-400-B) as explained elsewhere.[20]

Immuno-Based Protein-Profiling Sample Incubation, Data Acquisition, and Analysis

Organoids from control and patient-derived NESCs were treated with HP-β-CD in a 96-well ultra-low attachment (ULA) plate format for 30 days of differentiation at a concentration of 5 μM. The samples were analyzed on scioDiscover antibody microarrays (Sciomics, Baden-Wuerttemberg, Germany) targeting 1360 different proteins with 1830 antibodies. Differences in protein abundance or phosphorylation levels between different samples or sample groups are presented as log-fold changes (logFC) calculated for the basis two.

Animal Experiments

A total of 15 male, 2-month-old C57bl/6 mice were used in the study. MPTP at 30 mg/kg was intraperitoneally injected for 5 days to generate the subacute PD mouse model. Model verification was performed using both behavioral analysis and pathological assessment. TH staining was used to evaluate the dopaminergic neuronal loss in substantia nigra. HP-β-CD was injected every second day in the dose of 4000 mg/kg subcutaneously for 15 days.

Statistical Analysis and Graphical Representation

Statistical analysis performed on each assay is mentioned in each figure legend. All of the statistical analyses were performed in R (R Foundation for Statistical Computing, Vienna, Austria). Clustering and heatmaps were produced using the complexheatmap package of R.[21]

Results

Reduced TH+ Neuron Differentiation, Increased Proliferation, Astrocyte Activation, and Apoptosis in Patient-Specific Cells

To evaluate whether impaired mitochondrial function could affect dopaminergic differentiation, hiPSCs were derived from three patients carrying a mutation in

FIG. 1. Impaired differentiation of neural stem cells of patient carrying *PINK1* mutations. (**A**) Images representing the median values of a 14-day differentiation neuronal two-dimensional culture of controls and patients groups. Raw images of the markers tyrosine hydroxylase (TH), Tubulin Beta 3 Class III (TUBB3), and Hoechst are presented with its respective perimeter mask and a zoomed region (scale bar = 100 μm). (**B**) Quantification of TH, TUBB3, and Hoechst at time points 7, 14, and 21 after the induction of differentiation. Pixel quantification (lower panel) with their respective ratios (upper panel). Acquisition was performed at 20× sampling randomly 15 fields per well. Five wells of controls and five wells of patients were acquired per replicate. Total fields of controls (fc) and fields of patients (fp) analyzed time points 7 (fc = 219; fp = 215), 14 (fc = 209; fp = 219), and 21 (fc = 207; fp = 220) were collected over three independent replicates using all the lines. (**C**) Images representing the median values of proliferation marker Ki67 and Hoechst of control and patient-derived cells at day 7 of differentiation in a two-dimensional culture with their respective zoomed region and perimeter mask (scale bar = 50 μm). (**D**) Quantification of Ki67 at time points 7, 14, and 21 after the induction of differentiation in a two-dimensional culture, normalized to the nuclear area. Acquisition was performed at 20× sampling randomly 15 fields per well. Ten wells of controls and 10 wells of patients were acquired per replicate per time point. Images analyzed per time point: 7 (fc = 425; fp = 421), 14 (fc = 411; fp = 424), and 21 (fc = 416; fp = 432) were collected over three independent replicates using all the lines. (**E**) Representative images of apoptotic marker cleaved poly adenosin phosphate (ADP)-ribose polymerase (cPARP), dopaminergic marker TH, and Hoechst at day 14 of differentiation in a two-dimensional culture with their respective zoomed region and perimeter mask (scale bar = 50 μm). (**F**) Quantification of cPARP within the TH area at time points 7, 14, and 21 after the induction of differentiation in a two-dimensional culture, normalized to the TH area. Acquisition was performed at 20× sampling randomly 15 fields per well. Ten wells of controls and 10 wells of patients were acquired per replicate per time point. Images analyzed per time point: 7 (fc = 219; fp = 215), 14 (fc = 209; fp = 219), and 21 (fc = 207; fp = 220) were collected over three independent replicates using all of the lines. (**G**) Images representing the median values of a 21-day differentiation neuronal two-dimensional culture of control and patient groups. Raw images of the markers glial fibrillary acidic protein (GFAP) and S100 calcium binding protein B (S100b) are presented with their respective perimeter masks and zoomed regions (scale bar = 100 μm). (**H**) Quantification of colocalization between GFAP, S100B, and TH normalized to nuclear area at time points 7, 14, and 21 after the induction of differentiation in a two-dimensional culture. (**I**) Images representing the median values of a 21-day differentiation neuronal two-dimensional culture of control and patient groups. Raw images of the markers synuclein alpha (SNCA) and TH are presented with their respective perimeter masks and zoomed regions (scale bar = 100 μm). (**J**) Quantification of colocalization between SNCA and TH normalized to nuclear area at time points 7, 14, and 21 after the induction of differentiation in a two-dimensional culture. (**K**) Heatmap clustering different phenotypes during the process of differentiation between control and patient-derived neurons in a two-dimensional culture. Normalized scale within category of phenotype. (**L**) Western blot analysis of TH, TUBB3, and GFAP proteins extracted from two patient-derived *PINK1* p.Q456X-mutant neurons (patients 1 and 2) and their respective isogenic gene-corrected (GC) controls (patient 1 GC and patient 2 GC) after 30 days of differentiation (two-dimensional cultures). β-actin was used as loading control. (**M**) Quantitative immunoblot analysis of data presented in **C**. Histogram bars represent the mean values (± standard deviation) of TH, TUBB3, and GFAP signals in at least three independent experiments using the two isogenic pairs. Data were normalized against β-actin levels and expressed as fold change. Except for panels **L** and **M**, all control and patient lines were used. Statistical analysis was performed using Kruskal–Wallis and Dunn's tests for multiple comparisons. Adjustment of the *P*-value for multiple tests was performed using Benjamini-Hochberg. $^{*}P < 0.05$, $^{**}P < 0.01$, $^{***}P < 0.001$; ns, not significant. [Color figure can be viewed at wileyonlinelibrary.com]

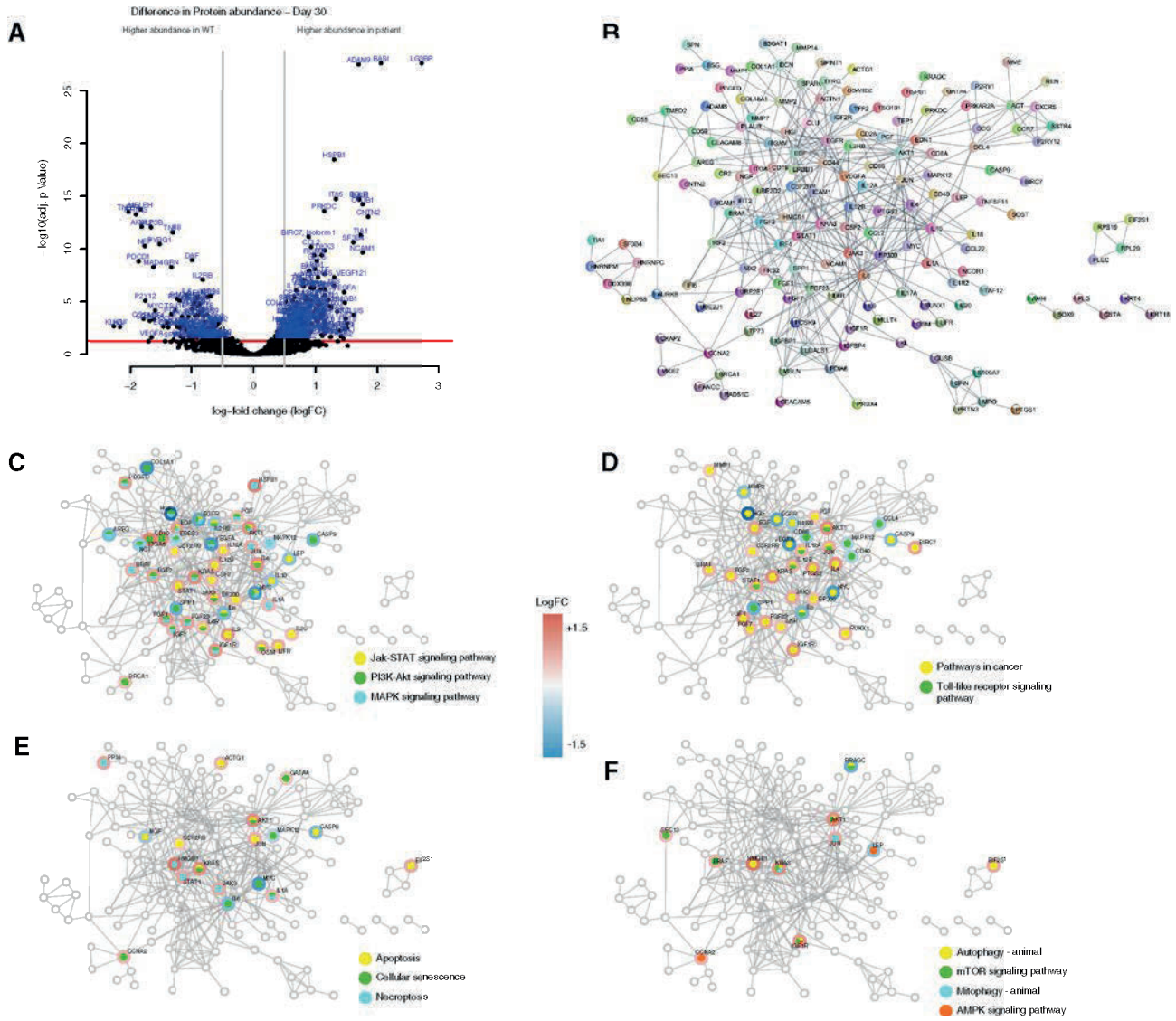

FIG. 2. Differential abundance of proteins between control and patient-derived organoids at day 30 of neuronal differentiation. (**A**) Volcano plot of proteomics data. The *x* axis represents the log fold change (logFC) between patient-derived and control organoids, with positive logFC indicating that the protein is more abundant in patient data than in control data, and the opposite for negative logFC. The *y* axis represents the *P*-value of the comparison adjusted for multiple testing using Benjamini-Hochberg. Proteins with adjusted *P*-value <0.05 and absolute logFC >0.5 were considered differential. (**B**) Network of the protein–protein interactions among the differential proteins obtained from the Search Tool for the Retrieval of Interacting Genes/Proteins (STRING) database. Interactions obtained from all data sources and with a confidence score >0.9 (high) were considered. Differential proteins that are not reported to interact with other differential proteins are not represented. (**C**–**F**) Mapping of significantly enriched Kyoto Encyclopedia of Genes and Genomes (KEGG) pathways on the protein–protein interaction network. KEGG pathways were tested for enrichment in proteins present in the network compared to the human genome and were considered significantly enriched if their *P*-value adjusted by Benjamini-Hochberg was <0.05. Nodes corresponding to proteins that belong to a selection of significantly enriched pathways are highlighted with different colors on the STRING network. The border of the nodes depicts the logFC of the pathway proteins in the comparison of control and patient-derived organoids. Control line 1 and patient line 1 were used for the proteomics experiments. Jak-STAT, janus kinase and signal transducer and activator of transcription; PI3K-Akt, phosphatidylinositol 3-kinase and Akt (protein kinase B); MAPK, mitogen-activated protein kinase; mTOR, mechanistic target of rapamycin; AMPK, AMP-activated protein kinase [Color figure can be viewed at wileyonlinelibrary.com]

PINK1: two carrying p.Q456X (rs45539432)[22] and one carrying p.I368N (rs774647122) and three age-matched and sex-matched controls (Fig. S1A). Human iPSCs were further differentiated into a stable neural precursor state (NESCs) following a previous report[13] and used as a starting population for studying dopaminergic neuron differentiation efficiency (Fig. S1B). Using an automated image analysis algorithm, the proportion of Tubulin Beta 3 Class III (TUBB3)–positive signal that colocalizes with TH was quantified. Patient-derived NESCs showed a reduced capacity to differentiate into TH+ neurons (worsened at later time points) while maintaining the same level of overall neuronal differentiation compared with controls (Fig. 1A,B, Table S8). To confirm the impaired dopaminergic differentiation, we differentiated NESCs in a three-dimensional microfluidic environment observing the same pattern (Fig. S1C,D). Assessment of the proliferation marker

Ki67 after 7, 14, and 21 days of differentiation (Fig. 1C–F) showed that patient-derived cells maintained a higher proliferative capacity after induction of differentiation. The apoptotic marker cleaved poly adenosin phosphate (ADP)-ribose polymerase (cPARP) showed an increased signal in patient-derived TH+ neurons at time point 14 (Fig. 1E,F). The amount of glial fibrillary acidic protein (GFAP) and S100 calcium binding protein B (S100b)–positive cells (markers of activated astrocytes) was significantly higher at day

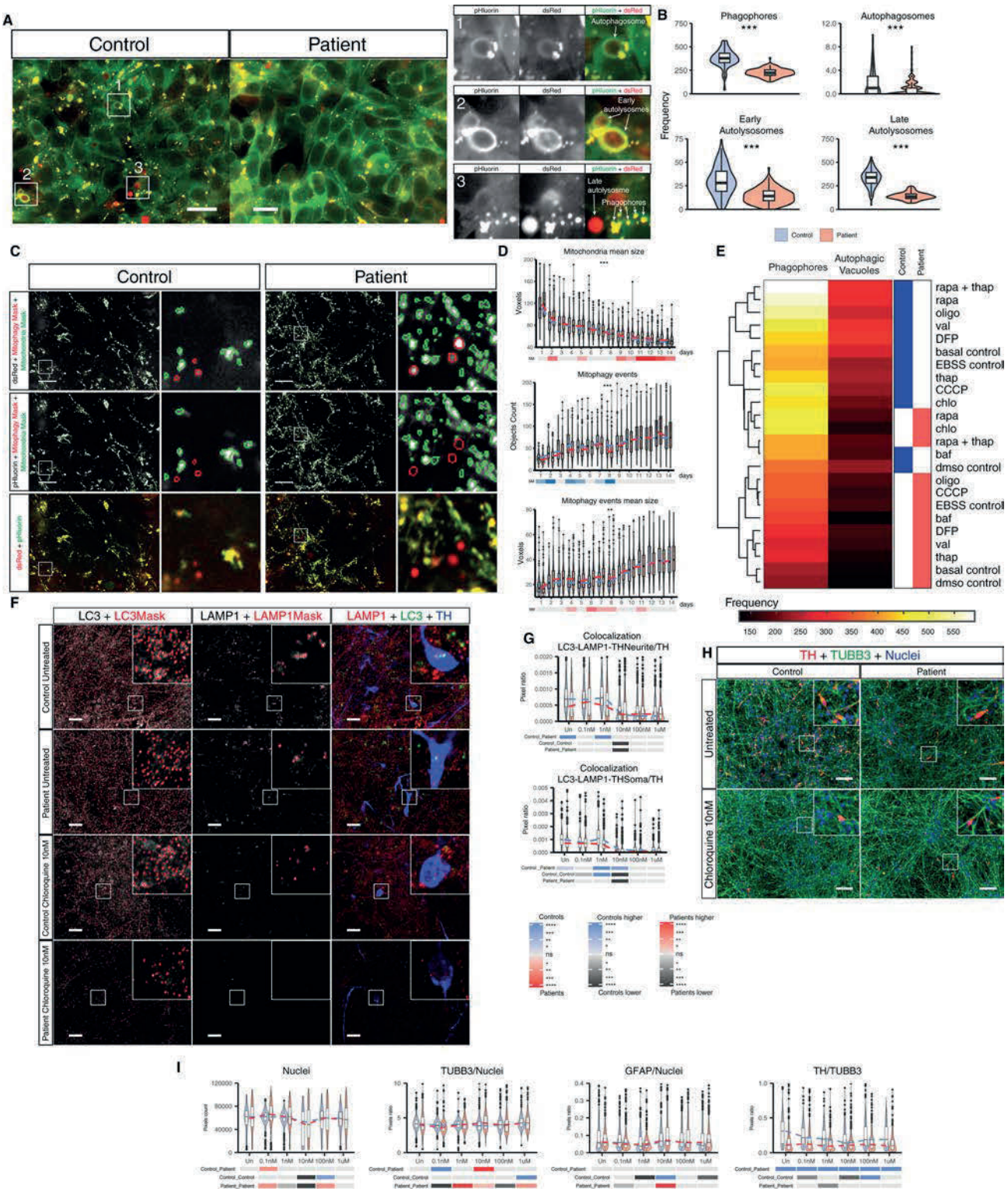

FIG. 3. Legend on next page.

21 of differentiation (Fig. 1G,H), the time point with the lowest TH levels in patients. During differentiation, there is a reduction of the GFAP marker at day 14 (controls being higher) followed by an increase at day 21 (higher increase in patient cells). An increase in astrocytic markers have been previously linked to oxidative stress.[23] Total levels of SNCA colocalizing with TH significantly increased in the patients through the different stages of differentiation (Fig. 1I,G). A cluster analysis considering all the different phenotypic features analyzed through the different time points of differentiation showed a discerning pattern in TH proportion and morphology at later time points, days 14 and 21 of differentiation (Fig. 1K).

Gene Correction–Restored Energetic Profile and Differentiation Efficiency

To evaluate the effect of the point mutation in cells derived from patients with PD, homozygous correction of the g.20655C>T (p.Gln456Ter) mutation in *PINK1* was performed in two patient lines and homozygous correction of the c.1103T>A (p.Ile368Asn) in one patient line using Fluorescence-activated cell sorting (FACS)-assisted CRIPSR/Cas9 editing.[17,18] After gene correction, the reduced TH levels were improved, and the increased levels of astrocytes were reduced in neurons cultured in two-dimensional conditions (Fig. 1L,M). The increased levels of TH after gene correction were also confirmed by immunofluorescence (Fig. S2A,B). Extracellular flux analysis (Seahorse, Agilent Technologies [Santa Clara, CA]) showed that gene correction reduced significantly the higher glycolytic activity of patient-derived NESCs (Fig. S2C–E,F). MEA measurements showed that the firing activity and the network burst firing in neurons cultured in two-dimensional were increased after gene correction (Fig. S2F–H). To assess the gene correction of *PINK1* not only at the genomic level but also at a functional level, we analyzed the expression of *PINK1*-regulated mitophagy markers in differentiated neurons cultured in two-dimensional. Mono-ubiquitination of Voltage Dependent Anion Channel 1 (VDAC1), performed by parkin in a *PINK1*-dependent manner,[24] was restored in the two gene-corrected lines tested. This was accompanied by decreased parkin levels in Carbonyl cyanide m-chlorophenyl hydrazone (CCCP)-treated neurons after *PINK1* gene correction as a result of mitophagy-induced parkin degradation[25] (Fig. S2I,J).

Proteomics Analysis in Organoids Confirm Dysregulated Pathways at Different Time Points

We performed an immuno-based protein analysis of three-dimensional midbrain organoids derived from control and patient cells at different time points of differentiation. Differentially abundant proteins were detected at days 10 (182 proteins), 20 (302), and 30 (267) of differentiation (Fig. 2A, Fig. S3–S5, and Supplemental Datasets 1–3). Selected protein–protein interaction analysis using the Search Tool for the Retrieval of Interacting Genes/Proteins (STRING) database[26] and Cytoscape[27] revealed several direct as well as indirect interactions of the differential proteins corresponding with pathways involved in apoptosis, necroptosis, protein synthesis, metabolism, and cell cycle (Fig. 2B–F). Also, proteins

FIG. 3. Modulation of autophagy alters neuronal differentiation. (**A**) Representative images of human induced pluripotent stem cells (hiPSCs) carrying the Rosella construct targeting microtubule-associated proteins 1A/1B light chain 3B (LC3) for control and patient-derived cells and zoomed images with representative identification of the different stages of the autophagy process detected with the Rosella reporter (scale bar = 20 μm). (**B**) Absolute quantification of phagophores, autophagosomes, early autolysosomes, and late autolysosomes for controls and patient-derived hiPSCs. All structures were measured under basal conditions. Acquisition was performed at 60× sampling randomly. Images analyzed: fields of controls (fc) = 131 and fields of patients (fp) = 131 were collected over three independent replicates using control line 1 and patient line 3. (**C**) Images representing the median values of neurons in a two-dimensional culture tagged with the Rosella construct for depicting mitophagy events at day 8 of differentiation showing the red fluorescent protein from Discosoma (dsRed) and pH-sensitive green fluorescent protein (pHluorin) raw signal (with their corresponding masks). A merged image of both channels is shown at the bottom of the panel and zoomed images in the right panel of each line (scale bar = 20 μm). (**D**) Time series quantification of the mitophagy capacity during neuronal differentiation for 14 days in a two-dimensional culture. Different properties of mitochondria and mitophagy events were assessed. Measurements were performed once a day during the entire differentiation protocol. Images analyzed: fc = 97–219 and fp =126–224 range measured per day for 14 days. Acquisition was performed at 60× sampling randomly 15 fields per well. Five wells of control 1 and 5 wells of patient 3 were acquired per replicate over three independent replicates. (**E**) Heatmap clustering for control and patient-derived cells across all mitophagy and autophagy modulating treatments in control line 1 and patient line 3 hiPSCs. Scale in absolute event frequency of phagophores or autophagic vacuoles detected. (**F**) Images representing the median values of neurons in a two-dimensional culture stained for LC3, lysosomal associated membrane protein 1 (LAMP1), and tyrosine hydroxylase (TH) after treatment with different concentrations of chloroquine with their respective zoomed areas (scale bar = 20 μm). (**G**) Quantification of immunostaining for LC3, LAMP1, and TH+ and their respective colocalizations, normalized to nuclear area at different chloroquine concentrations. (**H**) Images representing the median values of neurons in a two-dimensional culture stained for Tubulin Beta 3 Class III (TUBB3), glial fibrillary acidic protein (GFAP), and TH after treatment with different concentrations of chloroquine, with their respective zoomed areas (scale bar = 50 μm). (**I**) Quantification of immunostaining for GFAP, TUBB3, and TH+ and their respective colocalizations, normalized to nuclear area at different chloroquine concentrations. Except for panels **A** to **E**, all control and patient lines were used. Statistical analyses for panels **B**, **G,** and **I** were performed using Kruskal–Wallis and Dunn's tests for multiple comparisons. Statistical analysis for panel **D** was performed using a nonparametric test for repeated measures in factorial design (nparLD). Adjustment of the *P*-value for multiple tests was performed using Benjamini-Hochberg. **P* < 0.05, ***P* < 0.01, ****P* < 0.001, *****P* < 0.0001; ns, not significant. baf, bafilomycin; CCCP, carbonyl cyanide m-chlorophenyl hydrazone; chlo, chloroquine; DFP, deferiprone; dmso, Dimethyl sulfoxide; EBSS, Earle's Balanced Salt Solution; oligo, oligomycin; rapa, rapamycin; thap, thapsigargin; val, valinomycin. [Color figure can be viewed at wileyonlinelibrary.com]

involved in inflammation and autophagy showed dysregulation between controls and patients during the process of differentiation (Fig. 2E,F and Fig. S3).

PINK1 *Patient-Specific Neurons Present a Reduced Mitophagy Capacity*

To understand the mitochondrial dynamics in these cells, we generated lines expressing the Rosella

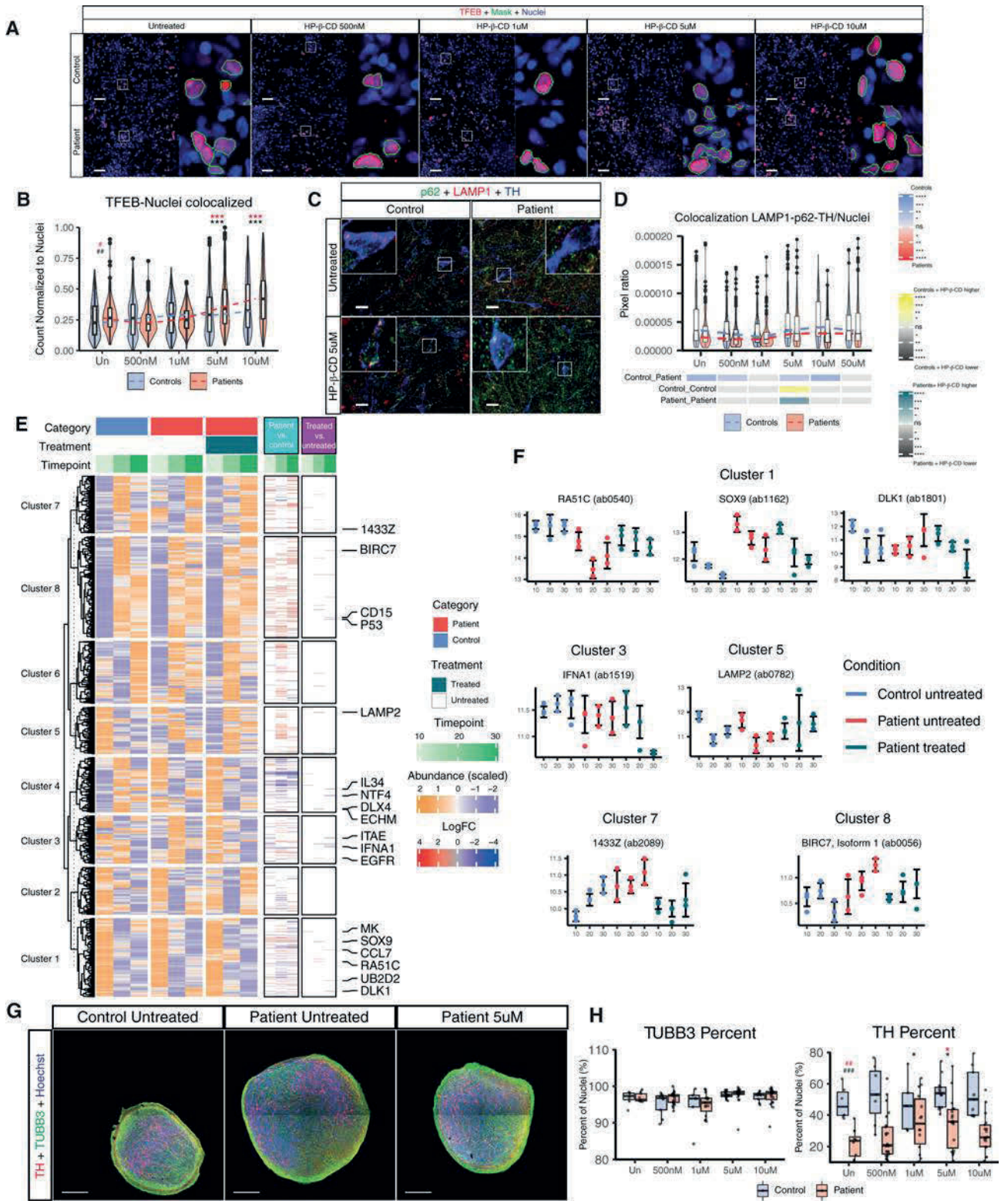

FIG. 4. Legend on next page.

construct bound to microtubule-associated proteins 1A/1B light chain 3B (LC3) or to adenosine triphosphate (ATP) synthase F1 subunit gamma (ATP5C1) to evaluate the autophagy status and mitochondrial degradation by mitophagy (Fig. 3). Already at the hiPSC level, classification of the different stages of autophagy[16] showed that autophagy was reduced in patient-derived cells (*PINK1*, p.I368N) compared with a control line (Fig. 3A,B). To confirm with a different assay, we analyzed the ratio of LC3 membrane-bound form/LC3 cytosolic form (LC3-II/LC3-I) by Western blot, which was reduced in 21-day differentiated neurons in two-dimensional cultures derived from patients (Fig. S6A,B). Measurements throughout differentiation revealed significantly fewer mitophagy events in patients' neurons carrying the Rosella construct (Fig. 3C,D and Fig. S6C). The mitophagy events observed in *PINK1* patient-derived cells might be mediated by *PINK1*-parkin independent mitophagy pathways.[28] Rapamycin inhibits the mammalian target of rapamycin (mTOR), which modulates autophagy by reducing transcription factor EB (TFEB)'s nuclear translocation.[29] Patient-derived cells treated with rapamycin showed an increase in the frequency of phagophores and autophagic vacuoles to similar levels as those observed in controls, which presented a similar response to the rapamycin treatment (Fig. 3E and Fig. S6D). In this study, one patient and control line were genetically modified to stably carry the Rosella construct, hence caution is needed in interpreting the mitophagy results detected with the reporter. We then assessed the effect of chloroquine, a known blocker of the autophagic flux by reducing the fusion between autophagosomes and autolysosomes,[30] during the neuronal differentiation process. The total levels of LC3 were increased in the patient-untreated group and reduced after treatment with chloroquine (Fig. S6E). No difference was observed in the total levels of lysosomal associated membrane protein 1 (LAMP1) in untreated samples. When evaluating the levels of colocalization of LC3 and LAMP1, no difference in the overall colocalization was observed, but when considering the colocalization with TH as well, control TH+ neurons presented a higher level of colocalized LC3-LAMP1 in the soma as well as in the neurites in untreated conditions (Fig. 3F,G). This occurred concomitantly with a significant reduction in the levels of TH+ cells at a concentration of 10 nM of chloroquine and increased GFAP particularly in controls (Fig. 3H,I and Fig. S6F). Higher concentrations of chloroquine showed an increase of the TH+ levels compared with the treatment with 10 nM chloroquine, which could be explained by the reported increase of transforming growth factor beta (TGFβ) superfamily receptors in the plasma membrane after chloroquine treatment.[31] TGFβ plays an important role in the specification of dopaminergic neurons.[32-34]

Treatment with HP-β-CD Increased TFEB Nuclear Translocation in Neurons, Modified the Abundance of Proteins Related to Dopaminergic Neurons Differentiation, and Increased Dopaminergic Neuron Differentiation Efficiency of Brain Organoids

Due to the observed altered autophagy and mitophagy pattern, we explored ways for modulating autophagy with repurposed compounds. Treatment with the

FIG. 4. Treatment with HP-β-CD improves neuronal differentiation by increasing autophagy. (**A**) Representative images of differentiated neurons in a two-dimensional culture stained for TFEB, with their respective zoomed images (scale bar = 50 μm). (**B**) Quantification of the colocalization between TFEB and Nuclei signal with the different treatment concentrations. Images analyzed: 540 fields per category (control or patient) per condition, acquired over three independent replicates using all lines. (**C**) Images representing the median values of neurons in a two-dimensional culture stained for p62, lysosomal associated membrane protein 1 (LAMP1), and tyrosine hydroxylase (TH) after treatment with different concentrations of HP-β-CD, with their respective zoomed areas (scale bar = 20 μm). (**D**) Quantification of immunostaining for the colocalization of sequestosome 1 (SQSTM1 or p62), LAMP1 and TH+, normalized to nuclear area at different HP-β-CD treatment concentrations. (**E**) Protein abundance measured in control-derived, patient-derived, and HP-β-CD-treated patient-derived organoids at time 10, 20 and 30 days of the neuronal differentiation was scaled for each protein separately. A k-means partitioning (k = 8) was performed in order to obtain clusters of proteins with similar expression dynamics. The proteins differentially abundant between control and patient-derived organoids, and between patient and treated patient-derived organoids are also shown (Benjamini-Hochberg, BH-adjusted *P*-value<0.05 and absolute logFC>0.5). (**F**) Normalized expression of selected proteins that show differential expression between patient and treated patient-derived organoids is reported. Three data points were collected for each condition and time point. Whiskers represent one standard deviation from the median of the measurements. (**G**) Representative images of control, patient and patient treated derived organoids at 30 days of differentiation (scale bar = 200 μm). (**H**) Quantification of the markers TH, Tubulin Beta 3 Class III (TUBB3) and Hoechst. Each dot represents one section analyzed. Sections analyzed: control (7, 9, 5, 14, and 9) and patient (9, 25, 15, 18, and 19) respectively for the different treatments (Un, 500 nM, 1 μM, 5 μM, and 10 μM) collected over three independent replicates. Control 1, patient 1, and patient 3 lines were used. For panels **A** to **D**, all control and patient lines were used. For panels **E** and **F**, control line 1 and patient line 1 were used. For panels **B**, **D,** and **H**, statistical analyses were performed using Kruskal–Wallis and Dunn's tests for multiple comparisons. Adjustment of the *P*-value for multiple tests was performed using Benjamini-Hochberg (BH). The adjusted significance are represented in red. Comparisons between control untreated and patient untreated are presented with #. Comparison between the patient-untreated condition and the different treatment concentrations are represented with *. *$P < 0.05$, **$P < 0.01$, ***$P < 0.001$, ****$P < 0.0001$; ns, not significant. Significance hashtag represent: #$P < 0.05$, ##$P < 0.01$, ###$P < 0.001$; ns stands for not significant. Un, untreated. 1433Z, tyrosine 3-monooxygenase/tryptophan 5-monooxygenase; BIRC7, baculoviral inhibitor of apoptosis protein (IAP) repeat containing 7; CCL7, C-C motif chemokine ligand 7; CD15, fucosyltransferase 4; DLK1, Delta like non-canonical notch ligand 1; DLX4, distal-less homeobox 4; ECHM, enoyl coenzyme a hydratase short chain 1 mitochondrial; EGFR, epidermal growth factor receptor; IFNA1, interferon alpha 1; IL34, interleukin 34; ITAE, integrin subunit alpha E; LAMP2, lysosomal associated membrane protein 2; MK, midkine; NTF4, neurotrophin 4; P53, tumor protein 53; RADC, RAD51 paralog C; SOX9, sex-determining region Y (SRY)-box transcription factor 9; UB2D2, ubiquitin conjugating enzyme E2 D2 [Color figure can be viewed at wileyonlinelibrary.com]

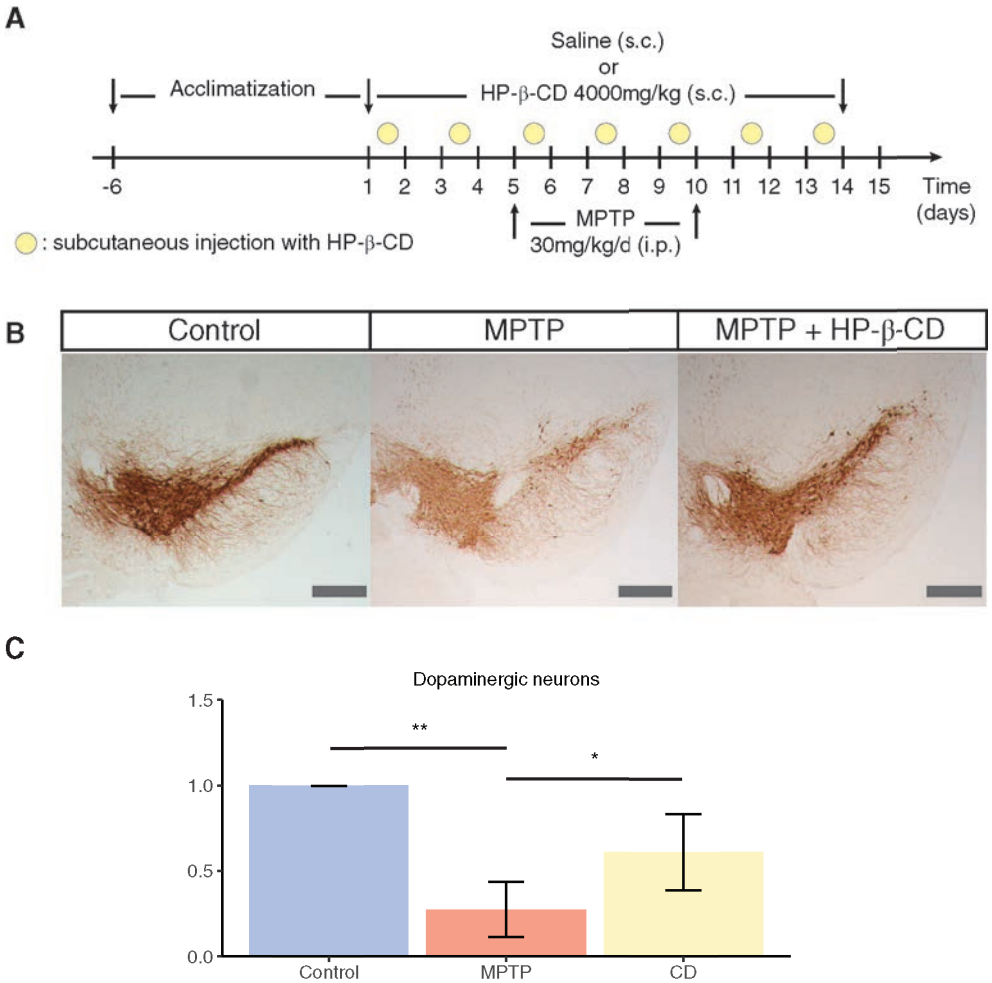

FIG. 5. Treatment with 2-hydroxypropyl-β-cyclodextrin (HP-β-CD) protects against toxicity of MPTP. (**A**) Treatment scheme for the generation of MPTP-induced subacute Parkinson's disease mice model and treatment with HP-β-CD. (**B**) Representative mouse midbrain sections stained for tyrosine hydroxylase (TH) in control, MPTP, or HP-β-CD-treated mice (scale bar = 400 μm). (**C**) Stereological quantification of the TH levels in mouse sections normalized to control levels. Statistical analysis was performed using Kruskal–Wallis and Dunn's tests for selected comparisons. *$P < 0.05$, **$P < 0.01$. [Color figure can be viewed at wileyonlinelibrary.com]

compound HP-β-CD was reported to modulate autophagy by increasing TFEB nuclear translocation in human neuroglioma cells.[29,35,36] Treatment with HP-β-CD during the entire differentiation process was able to increase the proportion of nuclei that colocalized with TFEB in a two-dimensional neuronal culture at 21 days of differentiation (Fig. 4A,B). Moreover, HP-β-CD upregulated the gene expression of FK506 binding protein 8 (*FKBP8*) and FUN14 domain-containing protein 1 (*FUNDC1*), outer mitochondrial membrane–anchored proteins that present the LC3 interacting region motif mediating mitophagy (Fig. S7A). Treatment with HP-β-CD led to an increase in mitophagy and in overall autophagy assessed with the Rosella construct (Fig. S7B, C). We also observed that this increased autophagy occurs in TH+ neurons by assessing the colocalization of sequestosome 1 (SQSTM1 or p62), LAMP1, and TH at concentrations above 5 μM reaching a plateau (Fig. 4C,D).

The effect of HP-β-CD during neuronal differentiation was assessed at three different time points in a three-dimensional environment using midbrain organoids. Protein abundance analysis (Fig. 4E,F, Fig. S7D, Supplemental Datasets 1–6) showed differentially abundant proteins between untreated and treated patient-derived organoids involved in the differentiation of dopaminergic neurons (SRY-box transcription factor 9 [SOX9] and delta like non-canonical notch ligand 1 [DLK1]), mitochondrial metabolism and mtDNA integrity (interferon alpha 1 [IFNA1] and RAD51 paralog C [RA51C]), and autophagy (lysosomal associated membrane protein 2 [LAMP2], tyrosine 3-monooxygenase/tryptophan 5-monooxygenase activation protein zeta [14-3-3ζ], and baculoviral IAP repeat containing 7 [BIRC7]) (Fig. 4F). The reduced proportion of dopaminergic neurons in patient-derived brain organoids was increased after treatment with HP-β-CD increased the proportion of TH+ cells without

changing the amount of TUBB3+ neurons (Fig. 4G,H, Fig. S8A, Table S8). HP-β-CD treatment in patient-specific neurons, carrying the homozygous p.R275W (rs34424986) parkin RBR E3 ubiquitin protein ligase (*PRKN*) mutation, increased the amount of dopaminergic neurons (Fig. S8B) concomitant with an increase in nuclei pixels. Parkin is known to be a downstream effector of *PINK1* induction of mitophagy, and alterations can lead to mitochondrial alterations and TH+ neuronal loss.[37] Because HP-β-CD composition is a mixture of cyclodextrin rings substituted with different degrees of hydroxypropyl,[38] we further characterized the composition of the used HP-β-CD mixture in these experiments and determined that the most frequent isomer is one with six degrees of substitution (Fig. S9A–C). Knowledge of the cyclodextrin composition will leverage application in future clinical trials and facilitate comparisons of treatment results between different neurodegenerative diseases.[38]

Treatment with HP-β-CD Reduces the Toxicity Generated by -Methyl-4-Phenyl-1,2,3,6-Tetrahydropyridine (MPTP) Treatment in Mice

To assess the effect of HP-β-CD in in vivo conditions, 1-methyl-4-phenyl-1,2,3,6-tetrahydropyridine (MPTP) induced subacute PD mice models were generated by intraperitoneal injection for 5 days of 30 mg/kg MPTP. A preventive treatment with HP-β-CD (Fig. 5A) was applied subcutaneously for 15 days. This treatment scheme showed a positive effect of HP-β-CD in reducing the loss of TH+ neurons in the midbrain of mice caused by MPTP (Fig. 5B,C).

Discussion

Our findings suggest that a loss-of-function mutation in *PINK1*[39] affects the transition between a neural precursor state and a differentiated TH+ neuron (Fig. 1). Previous reports showed no difference between a patient line carrying the p.Q456X mutation and control lines; however, these differences could be explained by the different differentiation protocol[22] and/or the low number of patient lines used in these studies.[40] Patient-derived cells remained highly proliferative upon induction of differentiation (Fig. 1C,D). This matches previous reports showing that the loss of *PINK1* activity triggers an increase in glycolysis via a reactive oxygen species–mediated stabilization of hypoxia-inducible factor-1α (HIF1α), associated with the Warburg effect.[41,42] Cells that manage to differentiate into TH+ neurons presented higher levels of apoptosis as previously reported.[43-45] Patients' derived neurons also presented an increased proportion of activated astrocytes (Fig. 1G,H) as well as of total SNCA in TH+ cells (Fig. 1I,J). Gene correction of *PINK1* allowed neural precursor cells to reduce their dependence on glycolysis and increase the firing activity in differentiated neurons as well as increase the proportion of TH+ neurons upon differentiation (Fig. 1L,M, Fig. S2). Gene correction seems to trigger a metabolic change that allows the switch from stem cells to differentiated cells.[46]

Proteomics analysis of control and patient-derived organoids at different stages of differentiation confirmed that the altered cell cycle, increased apoptosis, and reduced differentiation capacity observed coincided with dysregulation of these pathways (Fig. 2C–F, and Fig. S3A–D). It also showed dysregulation of the autophagy pathway, a common process impaired in PD as well as in other neurodegenerative diseases.[47,48]

Impaired mitochondrial turnover, due to reduced mitophagy activity, was observed in patient cells (Fig. 3C,D) in accordance with a previous report.[49] This altered mitophagy balance occurred simultaneously with an overall impaired autophagy (Fig. 3A,B, G). Regulation of autophagy with rapamycin led to a clustering of patient's together with control's cells (Fig. 3E), matching previously reported effects.[50] Modulating autophagy with chloroquine showed that a reduced colocalization of LC3 and LAMP1 led to a reduction TH+ neurons without altering the overall amount of neurons and increased the amount of GFAP levels (Fig. 3H,I). Treatment with different concentrations of HP-β-CD increased the presence of TFEB in the nuclei of patient-derived neurons (Fig. 4A,B). Further studies need to be performed to establish the indirect link between TFEB nuclear translocation and the upregulation of *PINK1* independent mitophagy pathways. HP-β-CD treatment increased the amount of autophagy events as well as the colocalization of LAMP1-p62 in TH+ neurons at concentrations above 5 μM, plateauing at 10 and 50 μM, concomitantly to the increase of TFEB nuclear translocation increase (Fig. 4C,D). Using cells edited with the Rosella construct tagging LC3, we observed similar effects (Fig. S7).

Differentially abundant protein analysis between untreated and treated patient organoids showed that the HP-β-CD has an effect not only in autophagy but also in proteins regulating dopaminergic neuronal differentiation (Fig. 4E,F). Levels of SOX9 and DLK1 were significantly reduced after treatment. SOX9 maintains the multipotency characteristics of neural precursor cells, reducing neuronal differentiation as well as increasing astrogliogenesis and astrocyte differentiation.[51-53] Downregulation of DLK1 through paired like homeodomain 3 (PITX3) has been shown to be necessary for the differentiation of A9/substantia nigra pars compacta dopaminergic neurons.[54-56] Levels of DLK1 increased over time in untreated patient organoids and were reduced after HP-β-CD treatment (Fig. 4F). Increased levels of RA51C, reported to help mtDNA replication and integrity, were seen after treatment.

This coincided with reduced levels of IFNA1, known to reduce the autophagy clearance of mtDNA.[57,58] Reduced levels of LAMP2 in untreated patient organoids match previous reports in cerebrospinal fluid concentrations in patients with PD.[59,60] Similar results were reported in the brain extracts of patients with PD.[61] LAMP2 is known to increase autophagic flux, reduce SNCA levels, and reduce the degeneration of dopaminergic neurons.[62,63] Treatment with HP-β-CD significantly increased the levels of LAMP2 in patient-derived organoids (Fig. 4E,F). Moreover, HP-β-CD significantly reduced the levels of BIRC7, a protein known for inhibiting autophagy by reducing the levels of LC3II, autophagy related 5 (ATG5), and beclin 1 (BECN1).[64] Levels of another autophagy-related protein, 14-3-3ζ, were increased in untreated patient organoids (Fig. 4F). 14-3-3ζ negatively regulates the early stages of autophagy.[65] Plus, 14-3-3 proteins are known regulators of the localization of TFEB between the nucleus and the cytoplasm, maintaining TFEB in the cytoplasm when it is phosphorylated.[66] A significant reduction of 14-3-3ζ was observed after HP-β-CD treatment of patient organoids (Fig. 4F), suggesting that its downregulation facilitates the translocation of TFEB to the nucleus. Furthermore, treatment with HP-β-CD improved the impaired dopaminergic differentiation observed in the patient organoids (Fig. 4G, H). The induction of the translocation of TFEB is significant at concentrations of 5 and 10 μM (Fig. 4B), whereas the effect of HP-β-CD in the differentiation of the organoids was observed only at 5 μM. This would lead one to think that the beneficial aspects of the TFEB translocation when treating organoids with HP-β-CD for 30 consecutive days occur in a narrow concentration window.

Interestingly, it has been reported that increasing autophagy via expression of TFEB has positive effects in other neurodegenerative diseases, such as Alzheimer's disease, Niemann Pick disease, and Gaucher disease by improving the degradation of protein aggregates.[67-69] Moreover, treatment with HP-β-CD is currently in a phase 2b/3 clinical trial for treating Niemann Pick disease (NPD, NCT02534844). Although the permeability of HP-β-CD to the blood–brain barrier is low (≈0.2% of blood circulating HP-β-CD),[70-72] previous reports have shown a positive effect in reducing neurodegeneration in mice treated only systemically.[70] We observed protection against the toxicity generated by MPTP after intraperitoneal treatment with HP-β-CD (Fig. 5). It has been reported that MPTP treatment increases brain-barrier permeability,[73] and this could have boosted the beneficial effects observed by HP-β-CD treatment. It is also possible that the pretreatment with HP-β-CD blocked MPTP-induced dysfunction of the blood–brain barrier as it has been reported for other treatments.[74]

The present work demonstrates that HP-β-CD ameliorates the dopaminergic neuronal loss phenotype, confirming the therapeutic potential of modulating the autophagy/lysosomal pathway in the context of PD. ■

Acknowledgments: We thank Prof. Dr. Hans R. Schöler of the Max Planck Institute, Dr. Jared Sterneckert of the Center for Regenerative Therapies Dresden, Prof. Dr. Thomas Gasser of the Hertie Institute in Tübingen, William Skarnes of the Jackson Laboratory, the Coriell Institute for providing cell lines, and Prof. T. Graham and A. Sargsyan from the University of Utah for kindly providing us with the Rosella construct. Gene editing was supported by the flow cytometry core of the Luxembourg Centre for Systems Biomedicine (LCSB) bioimaging platform. Zdenka Hodak of the LCSB Metabolomics Platform for providing technical and analytical support. We thank the Disease Modeling Screening Platform from LCSB and Luxembourg Institute of Health (LIH) for their help with performing automated and high-throughput procedures. Finally, we also thank the private donors who support our work at the LCSB.

Data Availability Statement

All original and processed data including the scripts used in this work are publicly available at this doi: https://doi.org/10.17881/c80y-2k58

References

1. Gammon K. Neurodegenerative disease: brain windfall. Nature 2014;515(7526):299–300.
2. Lozano CS, Tam J, Lozano AM. The changing landscape of surgery for Parkinson's disease. Mov Disord 2018;33(1):36–47.
3. Brás J, Guerreiro R, Hardy J. SnapShot: genetics of Parkinson's disease. Cell 2015;160(3):570.
4. Ashrafi G, Schwarz TL. The pathways of mitophagy for quality control and clearance of mitochondria. Cell Death Differ 2012;20(1):31–42.
5. Larsen SB, Hanss Z, Krüger R. The genetic architecture of mitochondrial dysfunction in Parkinson's disease. Cell Tissue Res 2018;373(1):21–37.
6. Goedert M, Spillantini M, Tredici K, Braak H. 100 years of Lewy pathology. Nat Rev Neurol 2012;9(1):13–24.
7. Nybø CJ, Gustavsson EK, Farrer MJ, Aasly JO. Neuropathological findings in PINK1-associated Parkinson's disease. Parkinsonism Relat Disord 2020;78:105–108.
8. Anichtchik O, Diekmann H, Fleming A, Roach A, Goldsmith P, Rubinsztein DC. Loss of PINK1 function affects development and results in neurodegeneration in zebrafish. J Neurosci 2008;28(33):8199–8207.
9. Brown SJ, Boussaad I, Jarazo J, et al. PINK1 deficiency impairs adult neurogenesis of dopaminergic neurons. Sci Rep 2021;11(1):6617.
10. Lancaster MA, Renner M, Martin C-A, et al. Cerebral organoids model human brain development and microcephaly. Nature 2013;501(7467):373–379.
11. Smits LM, Reinhardt L, Reinhardt P, et al. Modeling Parkinson's disease in midbrain-like organoids. NPJ Parkinsons Dis 2019;5(1):1–8.
12. Clevers H. Modeling development and disease with organoids. Cell 2016;165(7):1586–1597.
13. Reinhardt P, Glatza M, Hemmer K, et al. Derivation and expansion using only small molecules of human neural progenitors for neurodegenerative disease modeling. PLoS One 2013;8(3):e59252.
14. Monzel AS, Smits LM, Hemmer K, et al. Derivation of human midbrain-specific organoids from neuroepithelial stem cells. Stem Cell Reports 2017;8(5):1144–1154.
15. Sargsyan A, Cai J, Fandino LB, et al. Rapid parallel measurements of macroautophagy and mitophagy in mammalian cells using a single fluorescent biosensor. Sci Rep 2015;5:12397.
16. Arias-Fuenzalida J, Jarazo J, Walter J, et al. Automated high-throughput high-content autophagy and mitophagy analysis platform. Sci Rep 2019;9(1):9455.

17. Jarazo J, Qing X, Schwamborn JC. Guidelines for fluorescent guided biallelic HDR targeting selection with PiggyBac system removal for gene editing. Front Genet 2019;10(190):190.

18. Arias-Fuenzalida J, Jarazo J, Qing X, et al. FACS-assisted CRISPR-Cas9 genome editing facilitates Parkinson's disease modeling. Stem Cell Reports 2017;9(5):1423–1431.

19. Bolognin S, Fossépré M, Qing X, et al. 3D cultures of Parkinson's disease-specific dopaminergic neurons for high content phenotyping and drug testing. Adv Sci (Weinh) 2018;6(1):1800927.

20. Moreno EL, Hachi S, Hemmer K, et al. Differentiation of neuroepithelial stem cells into functional dopaminergic neurons in 3D microfluidic cell culture. Lab Chip 2015;15(11):2419–2428.

21. Gu Z, Eils R, Schlesner M. Complex heatmaps reveal patterns and correlations in multidimensional genomic data. Bioinformatics 2016;32(18):2847–2849.

22. Seibler P, Graziotto J, Jeong H, Simunovic F, Klein C, Krainc D. Mitochondrial Parkin recruitment is impaired in neurons derived from mutant PINK1 induced pluripotent stem cells. J Neurosci 2011;31(16):5970–5976.

23. Chen Y, Qin C, Huang J, et al. The role of astrocytes in oxidative stress of central nervous system: a mixed blessing. Cell Prolif 2020; 53(3):e12781.

24. Geisler S, Holmström K, Skujat D, et al. PINK1/Parkin-mediated mitophagy is dependent on VDAC1 and p62/SQSTM1. Nat Cell Biol 2010;12(2):119–131.

25. Kovalchuke L, Mosharov EV, Levy OA, Greene LA. Stress-induced phospho-ubiquitin formation causes parkin degradation. Sci Rep 2019;9(1):11682.

26. Szklarczyk D, Gable AL, Lyon D, et al. STRING v11: protein-protein association networks with increased coverage, supporting functional discovery in genome-wide experimental datasets. Nucleic Acids Res 2019;47(D1):D607–D613.

27. Shannon P, Markiel A, Ozier O, et al. Cytoscape: a software environment for integrated models of biomolecular interaction networks. Genome Res 2003;13(11):2498–2504.

28. McWilliams TG, Prescott AR, Montava-Garriga L, et al. Basal mitophagy occurs independently of PINK1 in mouse tissues of high metabolic demand. Cell Metab 2018;27(2):439–449.

29. Martini-Stoica H, Xu Y, Ballabio A, Zheng H. The autophagy–lysosomal pathway in neurodegeneration: a TFEB perspective. Trends Neurosci 2016;39(4):221–234.

30. Klionsky DJ, Abdelmohsen K, Abe A, et al. Guidelines for the use and interpretation of assays for monitoring autophagy (3rd edition). Autophagy 2016;12(1):1–222.

31. Dunmore BJ, Drake KM, Upton PD, Toshner MR, Aldred MA, Morrell NW. The lysosomal inhibitor, chloroquine, increases cell surface BMPR-II levels and restores BMP9 signalling in endothelial cells harbouring BMPR-II mutations. Hum Mol Genet 2013;22(18): 3667–3679.

32. Farkas LM, Dünker N, Roussa E, Unsicker K, Krieglstein K. Transforming growth factor-beta(s) are essential for the development of midbrain dopaminergic neurons in vitro and in vivo. J Neurosci 2003;23(12):5178–5186.

33. Luo SX, Timbang L, Kim JI, et al. TGF-β signaling in dopaminergic neurons regulates dendritic growth, excitatory-inhibitory synaptic balance, and reversal learning. Cell Rep 2016;17(12):3233–3245.

34. Tesseur I, Nguyen A, Chang B, et al. Deficiency in neuronal TGF-β signaling leads to nigrostriatal degeneration and activation of TGF-β signaling protects against MPTP neurotoxicity in mice. J Neurosci 2017;37(17):4584–4592.

35. Song W, Wang F, Lotfi P, Sardiello M, Segatori L. 2-Hydroxypropyl-β-cyclodextrin promotes transcription factor EB-mediated activation of autophagy. J Biol Chem 2014;289(14):10211–10222.

36. Kilpatrick K, Zeng Y, Hancock T, Segatori L. Genetic and chemical activation of TFEB mediates clearance of aggregated α-synuclein. PLoS One 2015;10(3):e0120819.

37. Shaltouki A, Sivapatham R, Pei Y, et al. Mitochondrial alterations by PARKIN in dopaminergic neurons using PARK2 patient-specific and PARK2 knockout isogenic iPSC lines. Stem Cell Reports 2015;4(5): 847–859.

38. Yergey AL, Blank PS, Cologna SM, Backlund PS, Porter FD, Darling AJ. Characterization of hydroxypropyl-beta-cyclodextrins used in the treatment of Niemann-Pick Disease type C1. PLoS One 2017;12(4):e0175478.

39. Grünewald A, Breedveld GJ, Lohmann-Hedrich K, et al. Biological effects of the PINK1 c.1366C>T mutation: implications in Parkinson disease pathogenesis. Neurogenetics 2007;8(2):103–109.

40. Chung S, Kishinevsky S, Mazzulli JR, et al. Parkin and PINK1 patient iPSC-derived midbrain dopamine neurons exhibit mitochondrial dysfunction and α-synuclein accumulation. Stem Cell Reports 2016;7(4):664–677.

41. Requejo-Aguilar R, Lopez-Fabuel I, Fernandez E, Martins LM, Almeida A, Bolaños JP. PINK1 deficiency sustains cell proliferation by reprogramming glucose metabolism through HIF1. Nat Commun 2014;5(4514):5514.

42. Agnihotri S, Golbourn B, Huang X, et al. PINK1 is a negative regulator of growth and the Warburg effect in glioblastoma. Cancer Res 2016;76(16):4708–4719.

43. Michel PP, Hirsch EC, Hunot S. Understanding dopaminergic cell death pathways in Parkinson disease. Neuron 2016;90(4):675–691.

44. Zhang S, Tang M-B, Luo H-Y, Shi C-H, Xu Y-M. Necroptosis in neurodegenerative diseases: a potential therapeutic target. Cell Death Dis 2017;8(6):e2905.

45. Iannielli A, Bido S, Folladori L, et al. Pharmacological inhibition of necroptosis protects from dopaminergic neuronal cell death in Parkinson's disease models. Cell Rep 2018;22(8):2066–2079.

46. Zhang J, Nuebel E, Daley GQ, Koehler CM, Teitell MA. Metabolic regulation in pluripotent stem cells during reprogramming and self-renewal. Cell Stem Cell 2012;11(5):589–595.

47. Nixon RA. The role of autophagy in neurodegenerative disease. Nat Med 2013;19(8):983–997.

48. Guo F, Liu X, Cai H, Le W. Autophagy in neurodegenerative diseases: pathogenesis and therapy. Brain Pathol 2018;28(1):3–13.

49. Liu W, Acín-Peréz R, Geghman KD, Manfredi G, Lu B, Li C. Pink1 regulates the oxidative phosphorylation machinery via mitochondrial fission. Proc Natl Acad Sci U S A 2011;108(31):12920–12924.

50. Li J, Kim S, Blenis J. Rapamycin: one drug, many effects. Cell Metab 2014;19(3):373–379.

51. Cheung M, Briscoe J. Neural crest development is regulated by the transcription factor Sox9. Development 2003;130(23):5681.

52. Selvaraj P, Xiao L, Lee C, et al. Neurotrophic factor-α1: a key Wnt-β-catenin dependent anti-proliferation factor and ERK-Sox9 activated inducer of embryonic neural stem cell differentiation to astrocytes in neurodevelopment. Stem Cells 2017;35(3):557–571.

53. Scott CE, Wynn SL, Sesay A, et al. SOX9 induces and maintains neural stem cells. Nat Neurosci 2010;13(10):1181–1189.

54. Jacobs FMJ, Veenvliet JV, Almirza WH, et al. Retinoic acid-dependent and -independent gene-regulatory pathways of Pitx3 in mesodiencephalic dopaminergic neurons. Development 2011;138(23):5213.

55. Jacobs FMJ, van der Linden AJA, Wang Y, et al. Identification of Dlk1, Ptpru; and Klhl1 as novel Nurr1 target genes in mesodiencephalic dopamine neurons. Development 2009;136(14):2363.

56. Oliveira MAP, Balling R, Smidt MP, Fleming RMT. Embryonic development of selectively vulnerable neurons in Parkinson's disease. NPJ Parkinsons Dis 2017;3(1):21.

57. Donega V, Burm SM, van Strien ME, et al. Transcriptome and proteome profiling of neural stem cells from the human subventricular zone in Parkinson's disease. Acta Neuropathol Commun 2019;7(1):84.

58. Mishra A, Saxena S, Kaushal A, Nagaraju G. RAD51C/XRCC3 facilitates mitochondrial DNA replication and maintains integrity of the mitochondrial genome. Mol Cell Biol 2018;38(3):e00489.

59. Klaver AC, Coffey MP, Aasly JO, Loeffler DA. CSF lamp2 concentrations are decreased in female Parkinson's disease patients with LRRK2 mutations. Brain Res 2018;1683:12–16.

60. Youn J, Lee S-B, Lee HS, et al. Cerebrospinal fluid levels of autophagy-related proteins represent potentially novel biomarkers of early-stage Parkinson's disease. Sci Rep 2018;8(1):16866.

61. Murphy KE, Gysbers AM, Abbott SK, et al. Lysosomal-associated membrane protein 2 isoforms are differentially affected in early Parkinson's disease. Mov Disord 2015;30(12):1639–1647.

62. Issa A-R, Sun J, Petitgas C, et al. The lysosomal membrane protein LAMP2A promotes autophagic flux and prevents SNCA-induced Parkinson disease-like symptoms in the Drosophila brain. Autophagy 2018;14(11):1898–1910.

63. Xilouri M, Brekk OR, Landeck N, et al. Boosting chaperone-mediated autophagy in vivo mitigates α-synuclein-induced neurodegeneration. Brain 2013;136(Pt 7):2130–2146.

64. Liu K, Yu Q, Li H, et al. BIRC7 promotes epithelial-mesenchymal transition and metastasis in papillary thyroid carcinoma through restraining autophagy. Am J Cancer Res 2020;10(1):78–94.

65. Pozuelo-Rubio M. Regulation of autophagic activity by 14-3-3ζ proteins associated with class III phosphatidylinositol-3-kinase. Cell Death Differ 2011;18(3):479–492.

66. Xu Y, Ren J, He X, Chen H, Wei T, Feng W. YWHA/14-3-3 proteins recognize phosphorylated TFEB by a noncanonical mode for controlling TFEB cytoplasmic localization. Autophagy 2019;15(6):1017–1030.

67. Awad O, Sarkar C, Panicker LM, et al. Altered TFEB-mediated lysosomal biogenesis in Gaucher disease iPSC-derived neuronal cells. Hum Mol Genet 2015;24(20):5775–5788.

68. Zhang YD, Zhao JJ. TFEB participates in the Aβ-induced pathogenesis of Alzheimer's disease by regulating the autophagy-lysosome pathway. DNA Cell Biol 2015;34(11):661–668.

69. Willett R, Martina JA, Zewe JP, Wills R, Hammond GRV, Puertollano R. TFEB regulates lysosomal positioning by modulating TMEM55B expression and JIP4 recruitment to lysosomes. Nat Commun 2017;8(1):1580.

70. Aqul A, Liu B, Ramirez CM, et al. Unesterified cholesterol accumulation in late endosomes/lysosomes causes neurodegeneration and is prevented by driving cholesterol export from this compartment. J Neurosci 2011;31(25):9404–9413.

71. Peake KB, Vance JE. Normalization of cholesterol homeostasis by 2-hydroxypropyl-β-cyclodextrin in neurons and glia from Niemann-pick C1 (NPC1)-deficient mice. J Biol Chem 2012;287(12):9290–9298.

72. Ramirez CM, Liu B, Aqul A, et al. Quantitative role of LAL, NPC2, and NPC1 in lysosomal cholesterol processing defined by genetic and pharmacological manipulations. J Lipid Res 2011;52(4):688–698.

73. Zhao C, Ling Z, Newman MB, Bhatia A, Carvey PM. TNF-alpha knockout and minocycline treatment attenuates blood-brain barrier leakage in MPTP-treated mice. Neurobiol Dis 2007;26(1):36–46.

74. Chen X, Lan X, Roche I, Liu R, Geiger JD. Caffeine protects against MPTP-induced blood-brain barrier dysfunction in mouse striatum. J Neurochem 2008;107(4):1147–1157.

Supporting Data

Additional Supporting Information may be found in the online version of this article at the publisher's web-site.

SGML and CITI Use Only
DO NOT PRINT

Author Roles

(1) Research Project: A. Conception, B. Organization, C. Execution; (2) Statistical Analysis: A. Design, B. Execution, C. Review and Critique; (3) Manuscript: A. Writing of the First Draft, B. Review and Critique.

J.J.: 1A, 1B, 1C, 2A, 2B, 3A
K.B.: 1C
J.M.: 1B, 1C, 2A, 2B
C. Saraiva: 1B, 1C, 2A, 2B
S.S.-S.: 1C, 2A, 2B
I.R.: 1B, 1C
A.G.: 1B, 1C, 2A, 2B
F.S.: 1B, 1C, 2A, 2B
G.Z.: 1B, 1C, 2A, 2B
L.M.S.: 1B, 1C, 3B
J.S.: 1C, 2A, 2B
J.A.-F.: 1B, 1C
J.W.: 1B, 1C, 3B
G.G.-G.: 1B, 1C
A.S.M.: 1B, 1C
X.Q.: 1B, 1C
A.V.: 1C, 2A, 2B
G.C.: 1B, 1C, 2A, 2B
I.B.: 1B
F.B.: 1C, 2A, 2B
C.J.: 1B, 1C
A.R.: 1B, 1C, 3B
W.L.: 1C, 2C
L.Y.: 1C, 2C
E.B.: 1B, 3B
G.A.: 1C, 2C, 3B
S.B.: 1B, 1C, 3B
R.S.: 1B, 1C, 2C
C. Schröder: 1B, 1C, 2C
P.M.A.A.: 1B, 1C, 3B
C.K.: 3B
R.K.: 3B
P.S.: 1B, 1C, 3B
J.C.S.: 1A, 2C, 3B

4.2. MANUSCRIPT II

Single-cell transcriptomics reveals multiple neuronal cell types in human midbrain-specific organoids

---

This article has been published in *Cell and Tissue Research.*

4.2.1. Preface

The establishment of midbrain organoids represented a big advance for the study of midbrain-specific processes, with respect to monolayer 2D cultures of dopaminergic neurons. 3D organoids better recapitulate the midbrain cytoarchitecture and cellular contacts and interactions. Midbrain organoids are composed by different cell types, including neurons – with an enrichment of dopaminergic neurons – macroglia and progenitor cells. Furthermore, 3D contacts such as synapses and neuron myelination by oligodendrocytes have been observed in these systems (Monzel et al., 2017; Smits et al., 2019) . However, until now, characterization of the cellular composition in midbrain was restricted to marker immunodetection. In this article, we study in detail the cellular heterogeneity in midbrain organoids based on gene expression. We studied the diversity of neuronal subtypes and their electrophysiological activity, and elucidated that dopaminergic, GABAergic, glutamatergic, and serotonergic neurons are present in midbrain organoids. Apart from neuronal clusters, other cell types such as progenitor and mesenchymal cells were detected amongst the 8 identified cell clusters. This paper represents a detailed characterisation of midbrain organoids, which allows us to better understand the cellular composition and functionality of cells in the system. These findings are crucial to discern mechanisms linked to development and disease, and to study cellular clusters that may have to be integrated in the system to increase its complexity.

In this article, I contributed by studying the presence of fibroblasts in midbrain organoids. I fixed and sectioned organoids, and I performed immunofluorescence stainings of organoid sections for the COL1A1 marker. We show the presence of mesenchymal cells in midbrain organoids, which were identified as fibroblast-like cells. Figure 5e shows the results of my participation in the manuscript.

Cell and Tissue Research (2020) 382:463–476
https://doi.org/10.1007/s00441-020-03249-y

REGULAR ARTICLE

Single-cell transcriptomics reveals multiple neuronal cell types in human midbrain-specific organoids

Lisa M. Smits[1] · Stefano Magni[1] · Kaoru Kinugawa[2] · Kamil Grzyb[1] · Joachim Luginbühl[3] · Sonia Sabate-Soler[1] · Silvia Bolognin[1] · Jay W. Shin[3] · Eiichiro Mori[2] · Alexander Skupin[1,4] · Jens C. Schwamborn[1]

Received: 23 January 2020 / Accepted: 22 June 2020 / Published online: 31 July 2020

Abstract

Human stem cell-derived organoids have great potential for modelling physiological and pathological processes. They recapitulate in vitro the organization and function of a respective organ or part of an organ. Human midbrain organoids (hMOs) have been described to contain midbrain-specific dopaminergic neurons that release the neurotransmitter dopamine. However, the human midbrain contains also additional neuronal cell types, which are functionally interacting with each other. Here, we analysed hMOs at high-resolution by means of single-cell RNA sequencing (scRNA-seq), imaging and electrophysiology to unravel cell heterogeneity. Our findings demonstrate that hMOs show essential neuronal functional properties as spontaneous electrophysiological activity of different neuronal subtypes, including dopaminergic, GABAergic, glutamatergic and serotonergic neurons. Recapitulating these in vivo features makes hMOs an excellent tool for in vitro disease phenotyping and drug discovery.

Keywords Neural stem cells · Midbrain organoids · Neuronal subtypes · Single-cell RNA sequencing · Electrophysiological activity

Introduction

Current in vitro approaches to model physiology and pathology of human neurons are mainly based on pure cultures of neurons grown under 2D conditions. It has been shown that the differentiation potential of human induced pluripotent stem cells (iPSCs) provides a unique source of different neural cell types (Takahashi and Yamanaka 2006). Until now, many protocols for generating iPSC-derived neural cultures have been described. The resulting cell culture monolayers have been proven as useful tools to study disease mechanisms and to identify potential neuroprotective compounds (Nguyen et al. 2011; Cooper et al. 2012; Sánchez-Danés et al. 2012; Reinhardt et al. 2013b; Ryan et al. 2013). However, these culture conditions do not recapitulate several characteristics, which are relevant to the human brain, like cyto-architecture or complex cell-cell interactions. This may result in inaccurate modelling of the human brain (patho-)physiology with the consequence that candidate compounds might prove efficacy in 2D in vitro studies but are ineffective in clinical trials or vice versa (Abe-Fukasawa et al. 2018). The recent establishment of new 3D neuronal cell culture models has contributed to mimic key aspects of human brain development (Lancaster et al. 2013; Tieng et al. 2014; Muguruma et al. 2015; Jo et al. 2016; Qian et al. 2016; Monzel et al. 2017). Studies using human cerebral brain organoids have shown the acquisition of neuronal maturity and network activity (Quadrato et al. 2017; Matsui et al. 2018). Their complex, multicellular architecture enables the study of neuronal diseases and has already led to novel insights on, e.g. Zika virus–induced microcephaly

Stefano Magni, Kaoru Kinugawa and Kamil Grzyb contributed equally to this work.

Electronic supplementary material The online version of this article (https://doi.org/10.1007/s00441-020-03249-y) contains supplementary material, which is available to authorized users.

✉ Jens C. Schwamborn
jens.schwamborn@uni.lu

Kaoru Kinugawa
kinugawa_kaoru@naramed-u.ac.jp

[1] Luxembourg Centre for Systems Biomedicine (LCSB), Developmental and Cellular Biology, University of Luxembourg, Belvaux, Luxembourg

[2] Department of Future Basic Medicine, Nara Medical University, Kashihara, Nara, Japan

[3] Division of Genomic Technologies, RIKEN Center for Life Science Technologies, Yokohama, Kanagawa, Japan

[4] University California San Diego, La Jolla, CA, USA

(Ming et al. 2016; Qian et al. 2017). Besides this unique in vitro disease modelling potential, human brain organoids provide a platform for advanced drug screening (Kelava and Lancaster 2016; Di Lullo and Kriegstein 2017). In this study, we focused on a detailed characterization of the different neuronal subtypes in human midbrain-specific organoids (hMOs). With single-cell transcriptome analysis, we examined the presence of different neuronal subtypes, and subsequently studied the effect of chemical compounds on the electrophysiological activity of the neuronal network. Our findings demonstrate that hMOs contain, beside dopaminergic neurons, other neuronal subtypes including GABAergic, glutamatergic and serotonergic neurons. hMOs showed essential neuronal functional properties during the course of differentiation, like synapse formation and spontaneous electrophysiological activity. These features indicate that hMOs recapitulate specific characteristics of functional human midbrain tissue, thus making them a valuable resource for in vitro disease modelling and drug discovery.

Material and methods

Data availability

The data that support the findings of this study, including the original single-cell RNA Sequencing data, are publicly available at this doi: www.doi.org/10.17881/lcsb.20190326.01.

Furthermore, a previous version of this manuscript is available as pre-print under: https://doi.org/10.1101/589598.

Pluripotent stem cell culture

hiPSC lines were provided by Bill Skarnes, Wellcome Trust Sanger Institute (iPSC Bill), Alstem (iPS15, derived from human peripheral blood mononuclear cells, episomal reprogrammed) or previously described in Reinhard et alia (Reinhardt et al. 2013b). The cells were cultured on Matrigel-coated (Corning, hESC-qualified matrix) plates, maintained in Essential 8 medium (Thermo Fisher Scientific) and cultured with and split 1:6 to 1:8 every 4 to 5 days using Accutase (Sigma). Ten μM ROCK inhibitor (Y-27632, Abcam) was added to the media for 24 h following splitting.

Derivation of midbrain floorplate neural progenitor cells

The derivation and maintenance of midbrain floorplate neural progenitor cells (mfNPCs) has been described previously (Smits et al. 2019).

In brief, embryoid bodies (EBs) were formed with 2000 iPSCs each, using AggreWell 400 (Stemcell Technologies). The cells were cultured in Knockout DMEM (Invitrogen) with 20% Knockout Serum Replacement (Invitrogen), 100-μM beta-mercaptoethanol (Gibco), 1% nonessential amino acids (NEAA, Invitrogen), 1% penicillin/streptomycin/glutamine (Invitrogen), freshly supplemented with 10-μM SB-431542 (SB, Ascent Scientific), 250-nM LDN-193189 (LDN, Sigma), 3-μM CHIR99021 (CHIR, Axon Medchem), 0.5-μM SAG (Merck) and 5-μM ROCK inhibitor (Sigma). After 24 h, EBs were transferred to a non-treated tissue culture plate (Corning). On day two, medium was replaced with N2B27 medium consists of DMEM-F12 (Invitrogen)/Neurobasal (Invitrogen) 50:50 with 1:200 N2 supplement (Invitrogen), 1:100 B27 supplement lacking vitamin A (Invitrogen) with 1% penicillin/streptomycin/glutamine, supplemented with 10-μM SB, 250-nM LDN, 3-μM CHIR and 0.5-μM SAG. On day four and six, medium was exchanged with the same but including 200-μM ascorbic acid (AA, Sigma). On day eight, EBs with neuroepithelial outgrowth were triturated into smaller pieces and diluted in a 1:10 ratio. For following passages, 1× TrypLE Select Enzyme (Gibco)/0.5-mM EDTA (Invitrogen) in 1× PBS was used and 10,000 to 20,000 cells per 96-well ultra-low attachment plate (round bottom, Corning) were seeded. The cells were always kept under 3D culture conditions and from passage 1 on cultured in N2B27 medium freshly supplemented with 2.5-μM SB, 100-nM LDN, 3-μM CHIR, 200-μM AA and 0.5-μM SAG. After every cell split, the ultra-low attachment plate was centrifuged for 3 min at 200×*g* to assure the aggregation of single cells at the bottom of the well. Additionally, a 5-μM ROCK inhibitor was added. The cells were split every 7 to 14 days and the medium was changed every third day. After four to five passages, mfNPCs were used as a starting population for hMOs.

Generation of midbrain-specific organoids

To start the generation of hMOs, 3000 cells per well were seeded to an ultra-low attachment 96-well round bottom plate, centrifuged for 3 min at 200×*g* and kept under maintenance conditions for 7 days. LDN and SB were withdrawn of mfNPC expansion medium and after three additional days, the concentration of CHIR was reduced to 0.7 μM. On day nine of differentiation, medium was changed to neuronal maturation N2B27 medium including 10-ng/ml BDNF (Peprotech), 10-ng/ml GDNF (Peprotech), 200-μM AA (Sigma), 500-μM dbcAMP (Sigma), 1-ng/ml TGF-β3 (Peprotech), 2.5-ng/ml ActivinA (Life Technologies) and 10-μM DAPT (Cayman). The organoids were kept under static culture conditions with media changes every third day for 35 or 70 days. Detailed information about the generation of hMOs has been published recently (Smits et al. 2019).

Immunofluorescence

hMOs were fixed with 4% PFA overnight at 4 °C and washed 3× with PBS for 15 min. After treatment, they were embedded in 3–4% low melting point agarose in PBS. The solid agarose block was sectioned with a vibratome (Leica VT1000s) into 50 or 70-μm sections. The sections were blocked on a shaker with 0.5% Triton X-100, 0.1% sodium azide, 0.1% sodium citrate, 2% BSA and 5% normal goat or donkey serum in PBS for 90 min at RT. Primary antibodies were diluted in the same solution but with only 0.1% Triton X-100 and were applied for 48 h at 4 °C.

After incubation with the primary antibodies (Supplementary Table 2), sections were washed 3× with PBS and subsequently blocked for 30 min at RT on a shaker. Then sections were incubated with the secondary antibodies in 0.05% Tween-20 in PBS for 2 h at RT and washed with 0.05% Tween-20 in PBS and Milli-Q water before they were mounted in Fluoromount-G mounting medium (Southern Biotech).

STAINperfect Immunostaining Kit (ImmuSmol) was used according to manufacturer's protocol to detect dopamine, serotonin, GABA and L-glutamine. Nuclei were counterstained with Hoechst 33342 (Invitrogen).

For qualitative analysis, three randomly selected fields per organoid section were acquired with a confocal laser scanning microscope (Zeiss LSM 710) and images were further processed with OMERO Software. Three-dimensional surface reconstructions of confocal z-stacks were created using Imaris software (Bitplane).

Quantitative image analysis

Immunofluorescence 3D images of hMOs were analysed in Matlab (Version 2017b, Mathworks). The in-house developed image analysis algorithms automate the segmentation of nuclei, astrocytes and neurons with structure-specific feature extraction. The image preprocessing for the segmentation of nuclei was computed by convolving the raw Hoechst channel with a Gaussian filter. By selecting a pixel threshold to identify apoptotic cells, a pyknotic nuclei mask was identified and subtracted from the nuclei mask.

For the segmentation of neurons, a median filter was applied to the raw TUJ1 channels. The expression levels were expressed in two ways as follows: (i) positive pixel of the marker, normalized by the pixel count of Hoechst; (ii) cells positive for a marker expressed as a percentage of the total number of cells. In this latter case, the nuclei were segmented and a watershed function was applied. Considering the high cell density of the specimens, steps to ensure high quality in the segmentation process were implemented and structures with a size higher than 10,000 pixels were removed (this indicated incorrected segmentation, e.g. clumps). In the nuclei successfully segmented as a single element, a perinuclear zone was identified. In case the marker of interest was positive in at least 1% of the perinuclear area, the corresponding cell was considered as positive.

Single-cell RNA sequencing using droplet-sequencing (Drop-Seq)

Single-cell RNA sequencing (scRNA-seq) data were generated using the Droplet-Sequencing (Drop-Seq) technique (Macosko et al. 2015) as described previously (Walter 2019). In this work, we performed scRNA-seq of hMOs derived from hiPSC line H4 (see Supplementary Table 1). For each time point, 35 days and 70 days after dopaminergic differentiation, we pooled and analysed 30 hMOs each.

Pre-processing of the digital expression matrices from scRNA-seq

The result of the Drop-Seq scRNA-seq pipeline and subsequent bioinformatics processing is a digital expression matrix (DEM) representing the number of mRNA molecules captured per gene per droplet. Here, we obtained two DEMs, one corresponding to 35-day hMOs and the other to 70-day hMOs. After quality cut based on knee plots, we retained for each sample 500 cells with the highest number of total transcripts measured and performed normalization of the DEM separately. Finally, the two DEMs were merged for the comparison analysis of the two time points based on 24,976 expressed genes in 1000 cells. The data was analysed by our customized Python analysis pipeline (Python version 3.6.0, with anaconda version 4.3.1) including dimensionality reduction by t-distributed stochastic neighbourhood embedding (t-SNE) (van der Maarten and Hinton 2008) and differential gene expression analysis.

Analysis of differentially expressed genes from scRNA-seq data

To determine which and how many genes were differentially expressed between 35-day and 70-day hMOs, we applied a one-way ANOVA test, a one-way ANOVA test on ranks (Kruskal-Wallis test), and a Mutual Information based test. The minimum p value obtained for each gene across these three tests was retained and statistical significance was set to $p < 0.01$ after Bonferroni correction for multiple hypothesis testing of differentially expressed genes (DEGs).

Cumulative gene expressions from scRNA-seq data

From literature, we extracted cell type–specific gene lists (Supplementary Table 3) for stem cells, neurons and neuronal subtypes (dopaminergic, glutamatergic, GABAergic and

serotonergic neurons) (Reinhardt et al. 2013a; La Manno et al. 2016; Cho et al. 2017). Note that not all genes listed therein have been measured in our dataset; these were highlighted in Supplementary Table 3.

For each list, we defined a score, which we refer to as cumulative gene expression, computed as the sum of the expression of the corresponding genes from normalized DEM for each cell. Since the expression levels were measured at single cell level, we can consider the cells' distributions across the cumulative genes expression scores (Fig. 2a). These histograms exhibit the cumulative gene expression scores normalized to their maxima on the horizontal axis. Thus, on the horizontal axis, a value of 1 corresponds to the maximal cumulative gene expression for one list of genes, while 0 corresponds to no expression of any genes from that list. The vertical axis exhibits the number of cells falling into the corresponding bin of the histogram. In each subpanel, the distributions for day 35 and for day 70 are shown. Population differences were assessed by Z-test of the means with Bonferroni correction.

Gene-gene correlations from scRNA-seq data

From the scRNA-seq data, we also computed gene-gene Pearson correlation coefficients for stemness-specific and neuron-specific genes. Analysis was performed independently for the two samples (35-day DA dif and 70-day DA dif) resulting in two correlation matrices (Fig. 1c).

In the lower triangular matrix, all correlation values are shown, whereas the upper triangular matrix contains only statistically significant correlations (p value < 0.05 after Bonferroni correction). For visual clarity, diagonal elements and undetected genes were excluded.

Fold changes of gene expression from scRNA-seq data

For individual genes, we considered the normalized gene expression across cell populations. For each selected gene, we compared its expression within the 35-day cells with the one within the 70-day cells by computing the logarithmic fold change (log2FC). We performed this analysis for the genes

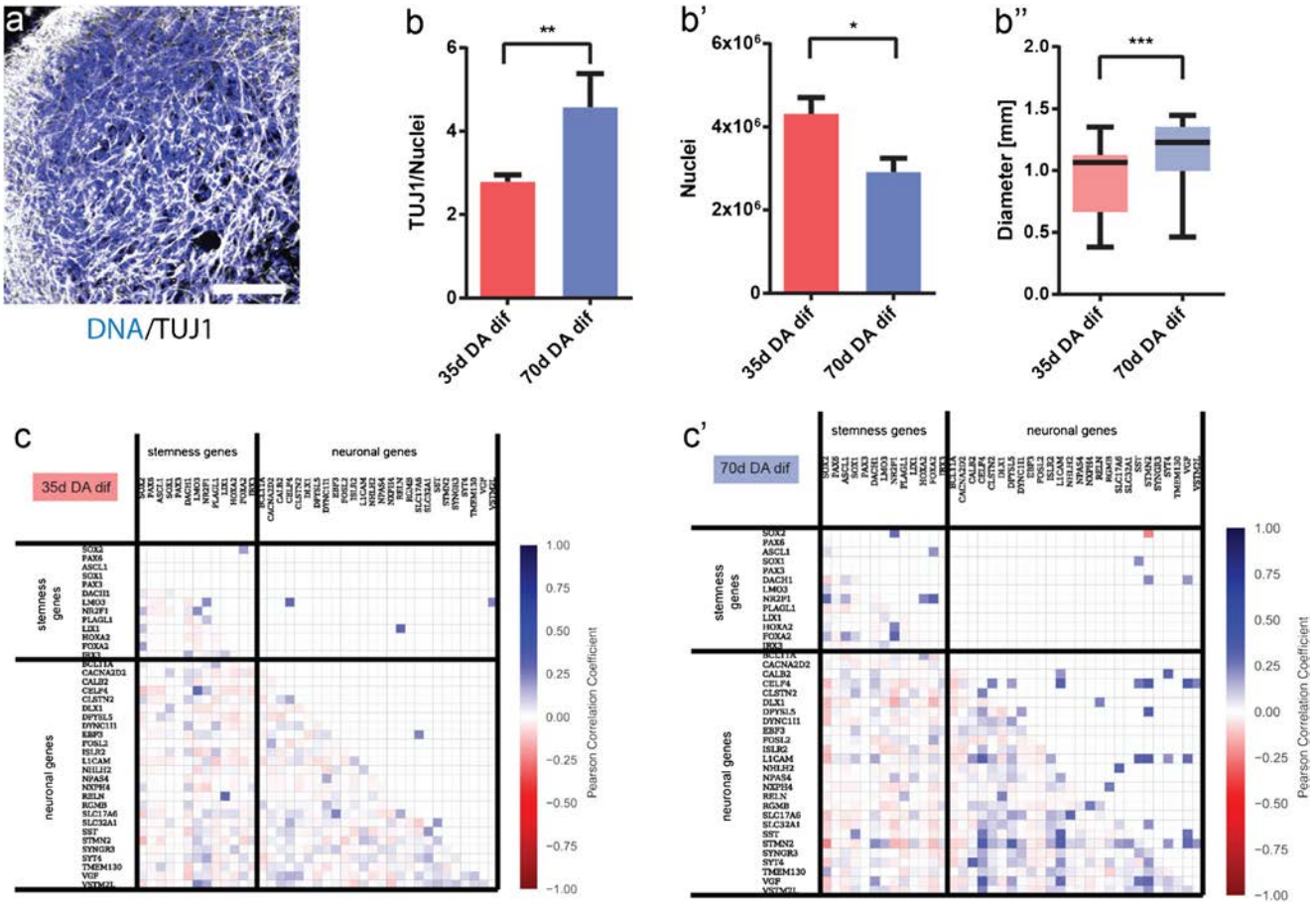

Fig. 1 Identification of neuronal population in midbrain-specific organoids. (**a**) Immunohistological staining of TUJ1 expressing neurons in 35-day organoid sections (50-µm thickness, scale bar 100 µm). (**b**) The ratio of TUJ1 positive pixels normalized against Hoechst (35 days $n = 59$, 70 days $n = 48$). (**b'**) Quantification of Hoechst positive pixel (35 days $n = 22$, 70 days $n = 29$). (**b"**) Average size of four different organoid lines. Whiskers present minimum and maximum (35 days $n = 21$, 70 days $n = 44$). Data presented as mean ± SEM. (**c**) Gene-gene correlation matrices, for genes at day 35 (**c**), and day 70 (**c'**)

specific of neuronal subtypes including glutamatergic neurons, GABAergic neurons and dopaminergic neurons (Fig. 2c–d), where negative values indicate that a gene is less expressed at day 35 than at day 70 and positive numbers the opposite. *p* values are based on Z-test with Bonferroni correction and significance levels correspond to * = *p* value <0.05, ** = *p* value <0.01, *** = *p* value < 0.001, and **** = *p* value < 0.0001. Error bars represent SEM based on the individual sample average and error propagation.

scRNA-seq data analysis for UMAP plot, dot plot and violin plot

ScRNA-seq data were generated using the Droplet-Sequencing (Drop-Seq) technique (1). After bioinformatics processing, we obtained two digital expression matrices (DEM), corresponding to day 35 and day 70 after differentiation into human midbrain organoids (hMOs).

In an alternative analysis approach, which is independent and complementary to the scRNA-Seq analysis described above, further data processing was performed using the Seurat v.3.0.0 R package (Satija et al. 2015). Cells with more than 4000 or less than 500 detected genes, as well as those with mitochondrial transcripts proportion higher than 7.5% were excluded. We collected a total of 1295 cells (505 cells at day 35 and 790 cells at day 70). The datasets were log normalized and scaled to 10,000 transcripts per cells. The top 2000 highly variable genes for day 35 and day 70 were determined using the variance-stabilizing transformation method. The datasets from day 35 and day 70 were integrated

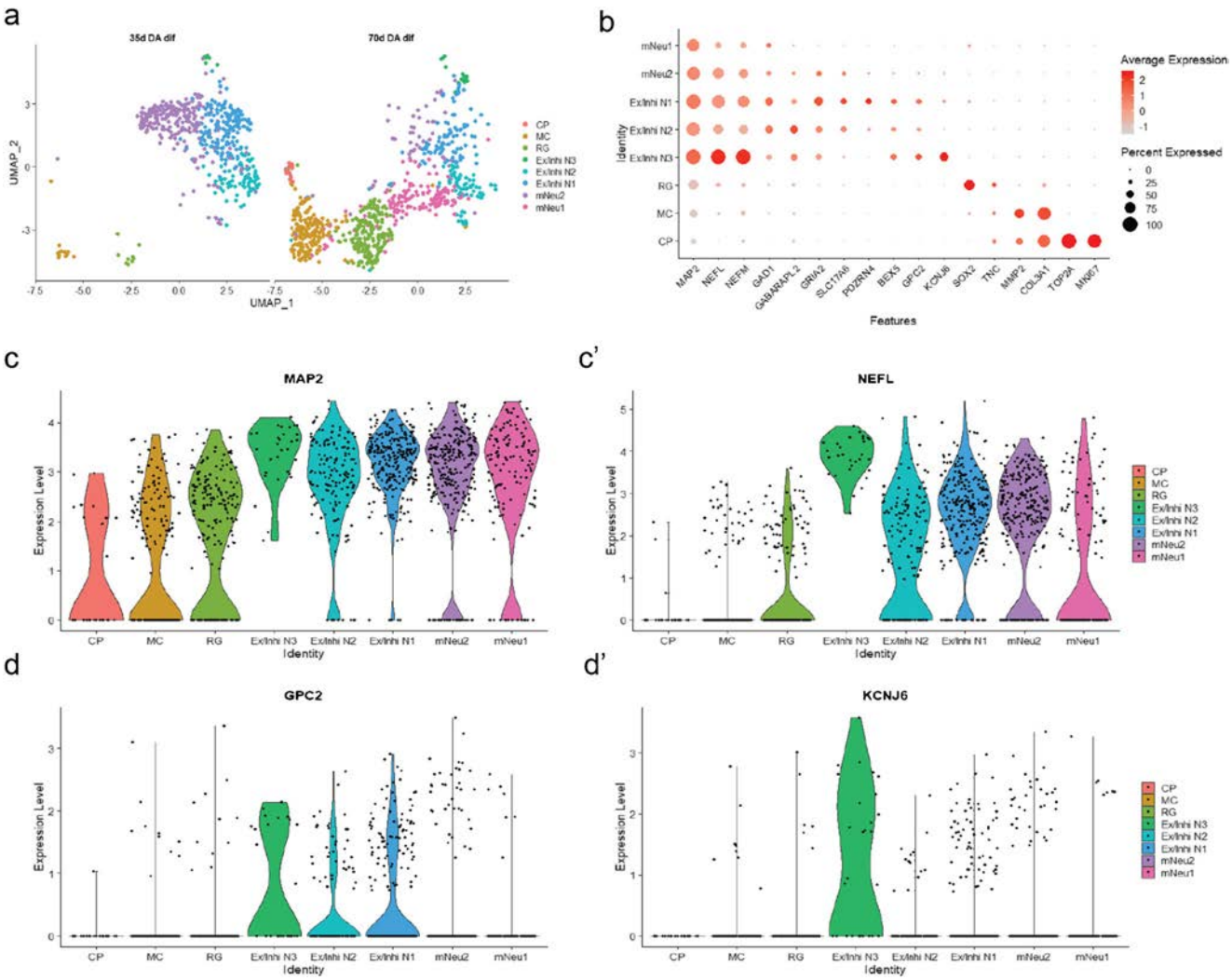

Fig. 2 Single-cell RNA sequencing analysis of midbrain-specific organoids. (**a**) Uniform manifold approximation and projection (UMAP) plot shows that the total 1295 cells identified 8 cell populations. Each dot corresponds to a single cell. Cell populations are coloured and annotated based on their expressing genes. CP, cycling progenitors; MC, mesenchymal cells; RG, radial glia cells; Ex/Inhi N, excitatory/inhibitory neurons; mNeu, mature neurons. UMAP plots shows difference in gene expressions between day 35 and day 70. (**b**) Dot plot shows the expression of each cell type–specific genes. (**c**–**d**) Violin plots show the distribution of expression of each marker gene. The mNeu clusters expressed MAP2 (**c**) and NEFL (**c'**), the Ex/Inhi N clusters expressed GPC2 (**d**) and KCNJ6 (**d'**)

using canonical correlation analysis (CCA) in the Seurat package (Stuart et al. 2019). The datasets were integrated based on the top 30 dimensions from CCA using the Seurat method by identifying anchors and integrating the datasets. The resulting integrated data were scaled and principal component analysis (PCA) was performed. Clustering was performed based on the top 30 principal components (PCs), using the shared nearest neighbour (SNN) modularity optimization with a resolution of 0.8. Cluster identities were assigned based on cluster gene markers as determined by the "FindAllMarkers" function in Seurat and gene expression of known marker genes.

TEM morphology

Sixty-three-day-old hMO specimens were immersion-fixed in a solution of 2% PFA and 2.5% glutaraldehyde in 0.1-M sodium cacodylate buffer (pH 7.4, Electron Microscopy Sciences, Hatfield, PA) for 3 h, rinsed several times in cacodylate buffer and further post-fixed in 2% glutaraldehyde in 0.1-M sodium cacodylate buffer for 2 h at room temperature on a gentle rotator; fixative was allowed to infiltrate an additional 48 h at 4 °C. Specimens were rinsed several times in cacodylate buffer, post-fixed in 1.0% osmium tetroxide for 1 h at room temperature and rinsed several times in cacodylate buffer. Samples were then dehydrated through a graded series of ethanols to 100% and dehydrated briefly in 100% propylene oxide. Tissue was then allowed to pre-infiltrate 2 h in a 2:1 mix of propylene oxide and Eponate resin (Ted Pella, Redding, CA), then transferred into a 1:1 mix of propylene oxide and Eponate resin and allowed to infiltrate overnight on a gentle rotator. The following day, specimens were transferred into a 2:1 mix of Eponate resin and propylene oxide for a minimum of 2 h, allowed to infiltrate in fresh 100% Eponate resin for several hours, and embedded in fresh 100% Eponate in flat moulds; polymerization occurred within 24–48 h at 60 °C. Thin (70 nm) sections were cut using a Leica EM UC7 ultramicrotome, collected onto formvar-coated grids, stained with uranyl acetate and Reynold's lead citrate and examined in a JEOL JEM 1011 transmission electron microscope at 80 kV. Images were collected using an AMT digital imaging system with proprietary image capture software (Advanced Microscopy Techniques, Danvers, MA).

Microelectrode array

The Maestro microelectrode array (MEA, Axion BioSystems) platform was used to record spontaneous activity of the hMOs. A 48-well MEA plate containing a 16-electrode array per well was precoated with 0.1-mg/ml poly-D-lysine hydrobromide (Sigma-Aldrich). Sixty to seventy days old organoids of two different passages were briefly treated for 5 min with 1× TrypLE Select Enzyme, resuspend in 10 µg/ml laminin (Sigma-Aldrich) and placed as a droplet onto the array. After 1 h incubation, neuronal maturation media was added and cells were cultured for 1–2 weeks. Spontaneous activity was recorded at a sampling rate of 12.5 kHz for 5 min at 37 °C over several days. Axion Integrated Studio (AxIS 2.1) was used to assay creation and analysis. A Butterworth band pass filter with 200–3000 Hz cutoff frequency and a threshold of 6× SD were set to minimize both false positives and missed detections. The spike raster plots were analysed using the Neural Metric Tool (Axion BioSystems). Electrodes with an average of ≥ 5 spikes/min were defined as active, for the pharmacological treatment 24 electrodes were analysed. The organoids were consecutively treated with Gabazine, D-AP-5, NBQX (Cayman Chemical, end concentration: 50 mM each), and Quinpirole (Sigma Aldrich, end concentration: 5 µM). To block all neuronal activity and thus verify spontaneous spiking activity of the cells, tetrodotoxin (TTX, Cayman Chemical, 1 µM) was applied at the end. The spike count files generated from the recordings were used to calculate the number of spikes/active electrode/min. Further details regarding the MEA system were previously described (Bardy et al. 2015).

Statistical analyses

If not stated otherwise, experiments were performed with three independently generated organoid cultures from three different cell lines ($n = 9$). Gaussian distribution was evaluated by performing D'Agostino and Pearson omnibus normality test. In case the data were normally distributed, Grubbs' test was performed to detect significant outliers. Unpaired *t* test with Welch's correction or nonparametric Kolmogorov-Smirnov test was performed to evaluate statistical significance. Data are presented as mean ± SEM. The statistical analyses of scRNA-seq data are described in the corresponding sections.

Results

Characterization of the neuronal differentiation dynamics in midbrain-specific organoids

Previously, we demonstrated that human iPSC-derived midbrain floor plate neural progenitor cells (mfNPCs) can give rise to 3D human organoids that contain high amounts of dopaminergic neurons (Smits et al. 2019). To have a better insight into the dynamics of the neuronal differentiation, we evaluated TUJ1 staining, as a marker for neuronal differentiation, at two time points during the differentiation of hMOs (Fig. 1 a and b). An in-house developed image analysis algorithm was used to segment Hoechst-positive nuclei and TUJ1-positive neurons to create specific nuclear and neuronal

masks. These masks contain all positive pixel counts for Hoechst and TUJ1, respectively.

The TUJ1 signal normalized to the Hoechst signal significantly increased after 70 days compared with 35 days, demonstrating a progressive differentiation into post-mitotic neurons. Whereas, the nuclear marker signal was significantly decreased at 70 days compared with 35 days, which might indicate selection in the cell population, as reported by Suzanne and Steller (2013) (Fig. 1 b and b'). Along with these findings, we observed that the size of the organoids significantly increased during the course of the differentiation. This suggests that the increased TUJ1 volume and organoid size are due to the increased tissue complexity (e.g. neuronal arborisation) within the hMO (Fig. 1b").

To further characterize the neuronal differentiation dynamics at the gene expression level, we performed scRNA-seq on samples from the two time points mentioned above. The experiments were conducted using the Drop-Seq technique (Macosko et al. 2015), and the standard bioinformatics processing of the data resulted in two sample-specific digital expression matrices (DEM), which were further normalized and merged (see Methods section).

To investigate how the differentiation of precursor cells into neurons evolves over time, we computed the gene-gene correlation for the genes of the neuron-specific list and of the stemness-specific list, altogether. Comparing these two lists, we found that at 35 days there are low values of correlation between genes exclusively specific for neurons or stem cells and also between neuron- and stemness-specific genes (Fig. 1c). Very few of the correlation values are significantly different from zero and were substituted by zeros in the upper triangular matrix (Fig. 1c). While correlations between stemness genes and neuron-stemness correlations at day 70 remain similar to day 35, correlations between neuron-specific genes increased considerably at day 70. This significant increase of neuron-specific gene correlations indicates a higher commitment of the cells towards the neuronal fate at day 70 compared with day 35 and supports the finding of a progressive maturation of post-mitotic neurons (Fig. 1 c and c').

To visualize the so-obtained high-dimensional single-cell data, we performed dimensionality reduction of the DEM by uniform manifold approximation and projection (UMAP) (van der Maarten and Hinton 2008), where each dot corresponds to a cell (Fig. 2a). After processing, quality control and filtering, we analysed a total of 1295 cells, 505 cells at day 35 and 790 cells at day 70 (Fig. S1 a and b). To identify distinct cell populations based on shared and unique patterns of gene expression, we performed dimensionality reduction and unsupervised cell clustering. All 1295 cells from the two time points were analysed together and plotted onto two uniform manifold approximation and projection (UMAP) plots (Fig. 2a). We identified eight distinct cell populations expressing known markers of major cell types (Fig. 2b). The cell populations comprised five neuronal clusters and three non-neuronal clusters. The five neuron clusters were divided into two mature neuron cluster (mNeu1 and mNeu2) and three excitatory/inhibitory neuron clusters (Ex/Inhi N1, Ex/Inhi N2, Ex/Inhi N3). The mNeu clusters expressed MAP2, NEFL and NEFM (Fig. 2 b, c and c'). The Ex/Inhi N clusters expressed BEX5, GPC2, KCNJ6, PDZRN4, GRIA2, SLC17A6, GAD1 and GABARAPL2 (Fig. 2 b, d and d'). Non-neuronal clusters were divided into radial glia cells (RG), mesenchymal cells (MC) and cycling progenitors (CP) subtypes (Fig. 2 b, S2 a and b). Cell populations distinctly changed between day 35 and day 70 (Fig. 2a). Interestingly the day 70 cell populations showed more non-neuronal clusters.

Midbrain-specific organoids consist of different neuronal subtypes

From previous studies, we know that hMOs are rich in dopaminergic neurons (Jo et al. 2016; Qian et al. 2016; Monzel et al. 2017; Smits et al. 2019; Kim et al. 2019). We wanted to further explore which other neuronal subtypes develop besides midbrain dopaminergic neurons within the hMOs.

Therefore, we investigated the expression of genes typical for dopaminergic, glutamatergic, GABAergic and serotonergic neurons by analysing the scRNA-seq data. We plotted the distributions of cells across the cumulative gene expression scores, which were obtained from the lists of genes specific of a neuronal subtype (Fig. 3a–a"'). While the cell distribution over cumulative expression score for GABAergic neurons was very similar between the samples at 35 days and 70 days (Fig. 3a"), we detected statistically significant differences between the distributions of cells over scores for the other three types of neurons. The expression of the selected genes for the glutamatergic and dopaminergic neurons was increased at day 35 compared with day 70, which is consistent with the observations for the neuron specific score (Fig. 2a).

In order to additionally highlight the presence of dopaminergic, glutamatergic, GABAergic and serotonergic neurons, we made use of the UMAP plots and highlighted the expression of marker genes for dopaminergic, glutamatergic, GABAergic and serotonergic neurons (Fig. 4 and S3). In agreement with the fact that the fraction of non-neuronal cells is higher in the day 70 organoids (Fig. 1), the counts for the various neuronal subtypes tend to be higher at day 35.

To further verify the presence of the addressed neuronal subtypes, we conducted an immunohistochemistry staining for the respective neurotransmitters. This allowed us to robustly detect dopaminergic, glutamatergic and GABAergic neurons as well as even a few serotonergic neurons within hMOs (Fig. 5a–d).

Finally, among the non-neuronal cells, we surprisingly found a cluster of mesenchymal cells (MC in Fig. 1d). A

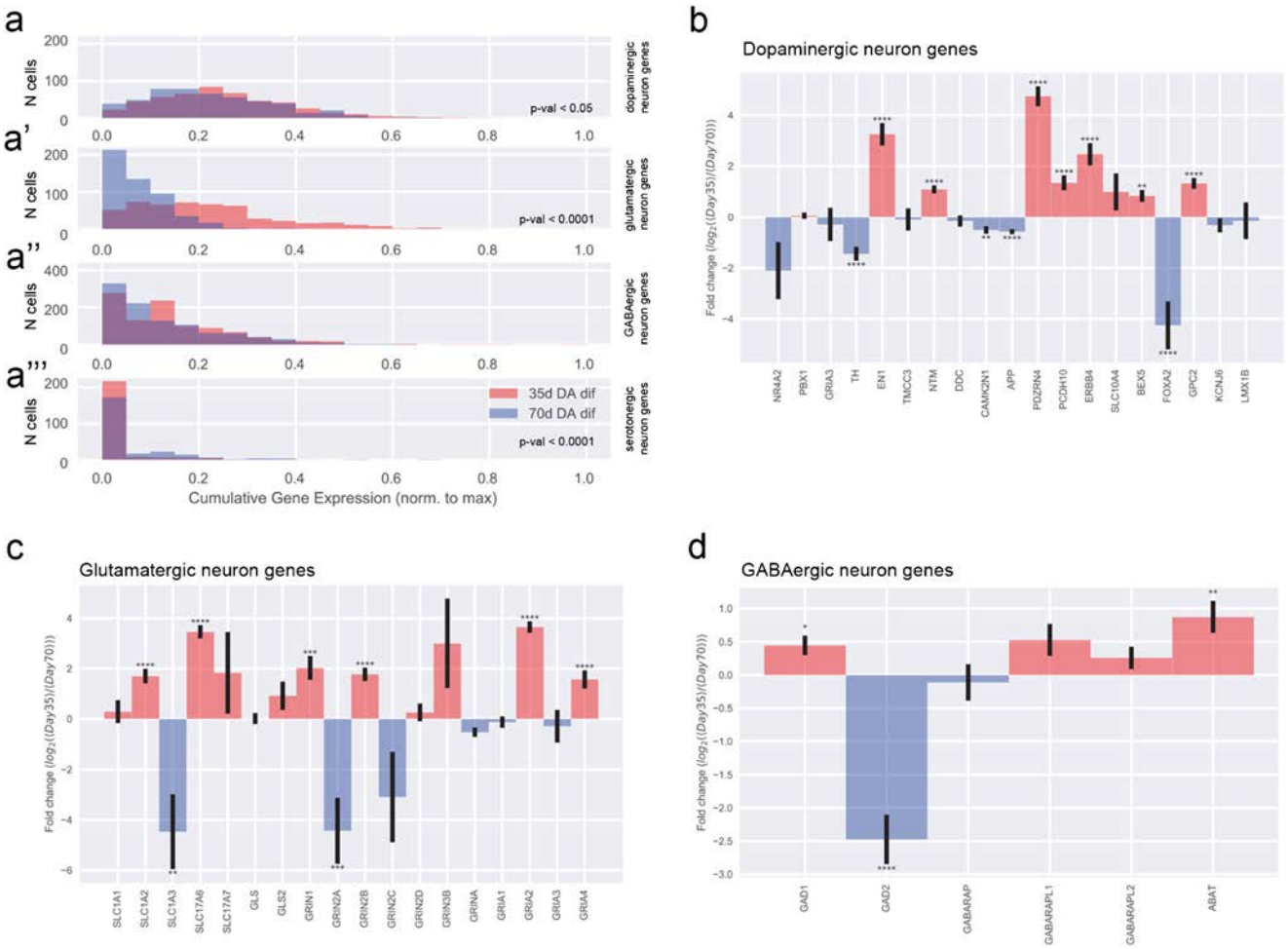

Fig. 3 Neuronal subtypes in midbrain-specific organoids. (**a**) Distributions (histograms) of cells across the cumulative gene expression scores, obtained from the lists of genes specific for the main neuronal subtypes present in the organoids, namely, dopaminergic (**a**), glutamatergic (**a'**), GABAergic (**a"**), and serotonergic neurons (**a"'**). (**b**–**d**) Log2 fold-changes between day 35 and day 70 in gene expression for individual genes corresponding to the lists of genes typical of the neuronal subtypes: (**b**) dopaminergic neurons, (**c**) glutamatergic neurons, and (**d**) GABAergic neurons

similarly surprising finding has been reported recently for a single-cell RNA sequencing analysis of dopaminergic neurons transplanted in the rodent brain, where fibroblast-like cells were detected (Tiklova et al. 2019). These cells are reported to be positive for the marker COL1A1. Hence, we also stained hMOs with an anti-COL1A1 antibody and indeed we were able to confirm the presence of this cell type (Fig. 5e).

Midbrain-specific organoids express synaptic proteins

After identifying the presence of neurons and even specific neuronal subtypes on transcriptome expression levels by means of neurotransmitter staining and scRNA-seq, we investigated the actual interaction among the neuronal cells within the hMOs. We previously showed that hMOs synthesize and release the neurotransmitter dopamine (Smits et al. 2019). This already suggests the establishment of a functional neuronal network. The basic requirement for neuronal network formation is the development of synapses. Hence, we evaluated the presence of synaptic connections using the presynaptic marker SYNAPTOPHYSIN and the postsynaptic marker PSD95 in organoid sections after 35 days and 70 days of culture (Fig. 6 a and b). Both proteins were detectable in a puncta-like organization, which is expected for synapses. With a subsequent 3D surface reconstruction, we observed that the signals for SYNAPTOPHYSIN and PSD95 were localized in close proximity, forming pre- and postsynaptic puncta (Fig. 3c). To further investigate whether actual functional synaptic connections were formed in the hMOs, we used a transmission electron microscopy (TEM) approach (Fig. 3d). EM micrographs show excitatory synapses characterized by electron dense post-synaptic density proteins (full arrow) and pre-synaptic synapse (asterisks) loaded with synaptic vesicles.

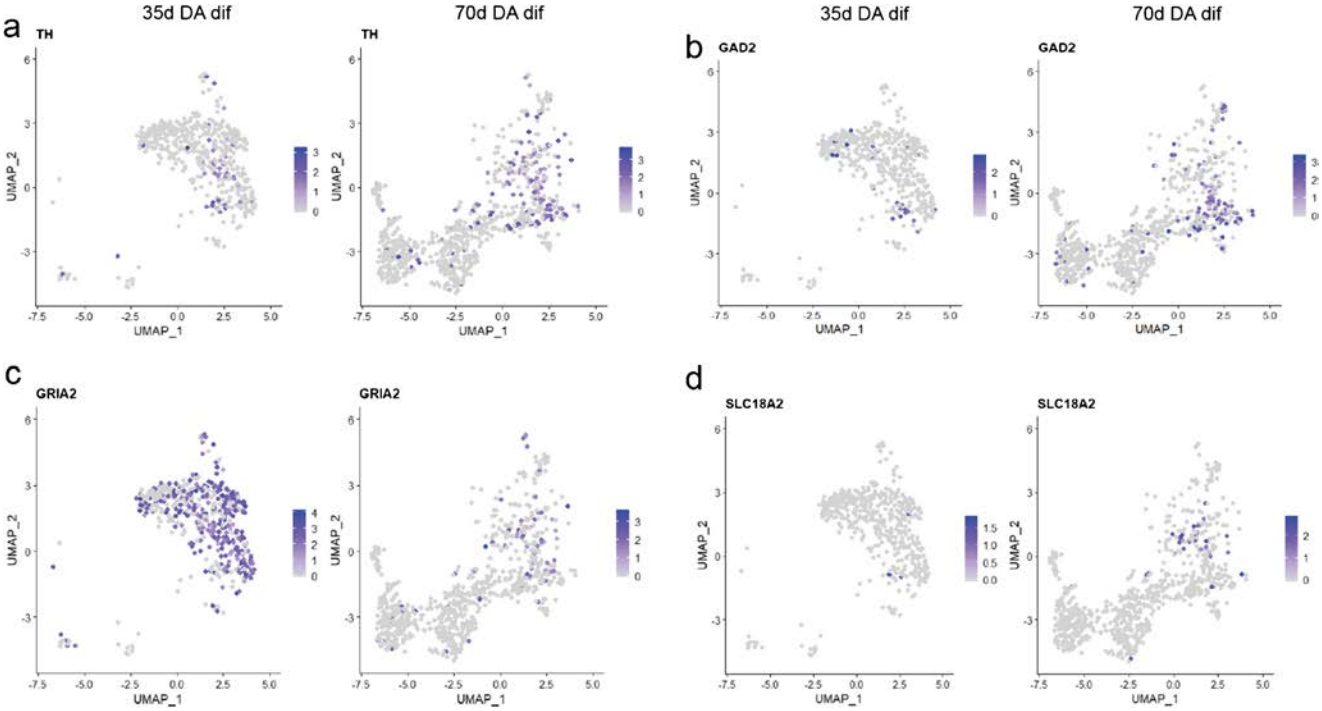

Fig. 4 UMAP plot analysis of neuronal subtypes. UMAP plots show the gene expressions at day 35 at day 70 for markers of dopaminergic (**a**), GABAergic (**b**), glutamatergic (**c**), and serotonergic (**d**) neurons. Each dot is coloured according to the expression level

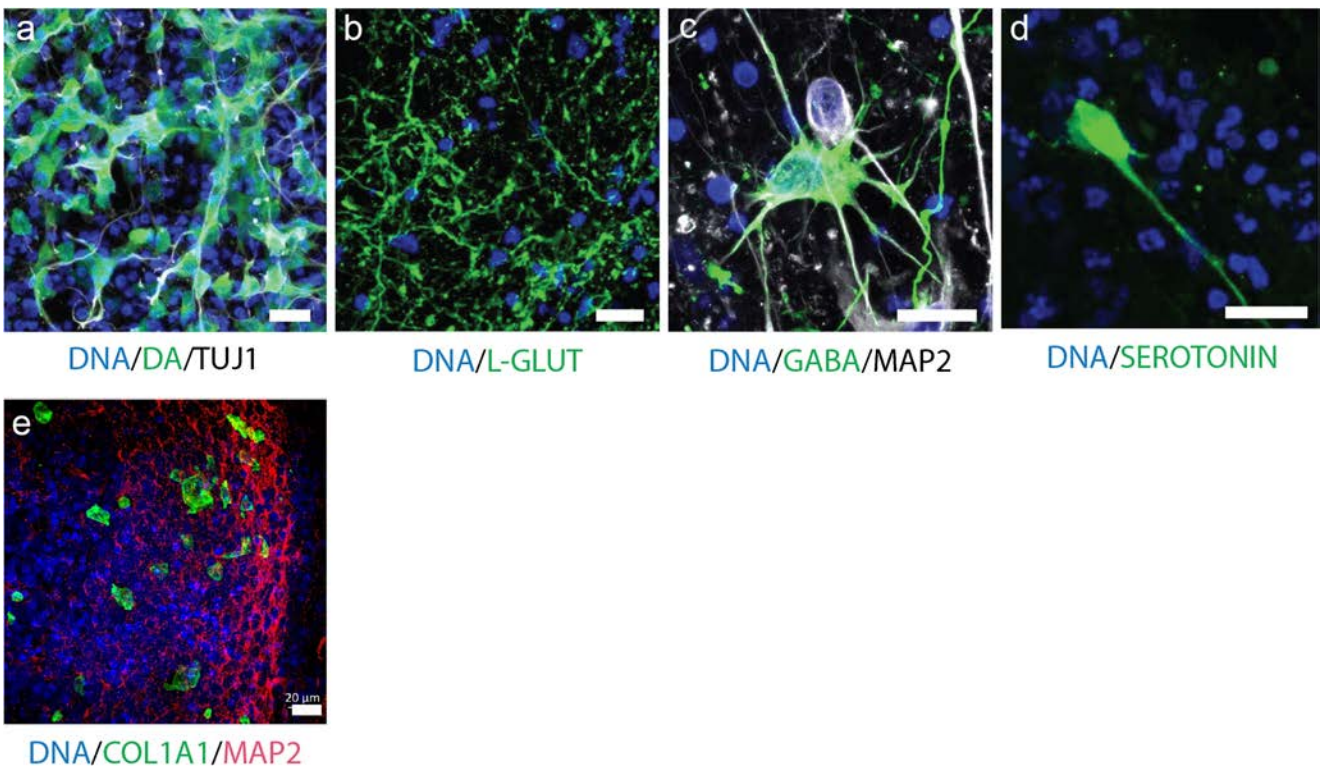

Fig. 5 Immunofluorescence staining analysis of neuronal subtypes. (**a**–**d**) Immunohistological staining of organoid sections (50-µm thickness). Detection of the neurotransmitters dopamine (**a**), L-glutamine (**b**), GABA (**c**), and serotonin (**d**). Scale bar is 20 µm. (**e**) Immunohistological staining of organoid sections (70-µm thickness) for the detection of the fibroblast marker COL1A1. Scale bar is 20 µm

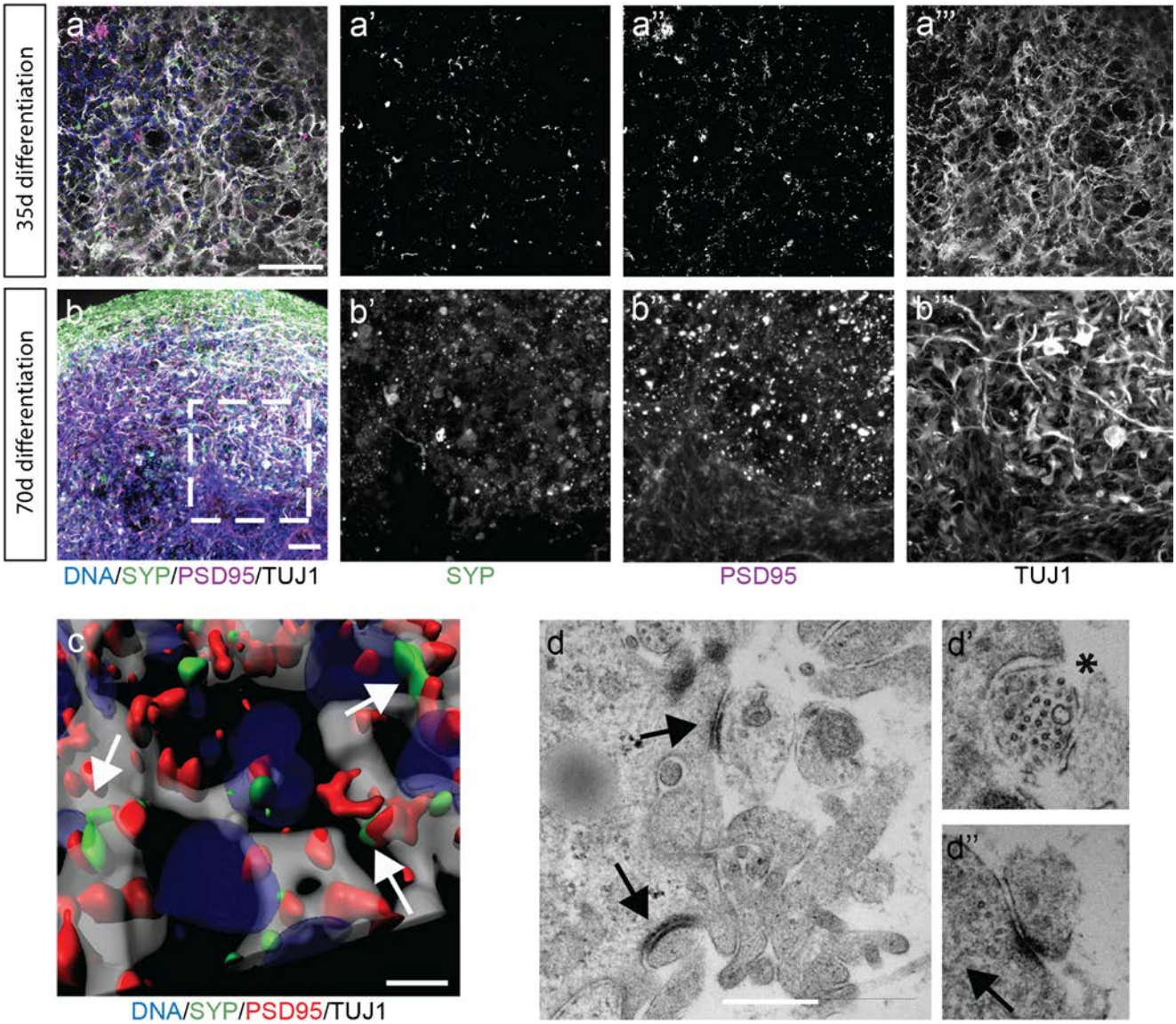

Fig. 6 Midbrain-specific organoids express synaptic proteins. (**a**–**b**) Immunostaining of pre- and the postsynaptic markers at day 35 (**a**) and day 70 (**b**). Dashed lines indicate the region of magnification. Scale bar is 50 μm. (**c**) 3D surface reconstructions of confocal z-stacks of an organoid at day 70 of differentiation. Scale bar is 10 μm. (**d**) Representative electron micrographs of synaptic terminals from 63-day organoids. Scale bar is 500 nm

Midbrain-specific organoids develop GABAergic, glutamatergic and dopaminergic electrophysiological activity

Non-invasive multielectrode array (MEA) measurements can give insights into physiological properties, like the generation of spontaneous neuronal activity of in vitro cultured, self-organized networks (Luhmann et al. 2016). As the assessment of neuronal activity is important to evaluate the functional maturation, we tested the spontaneous electrophysiological activity of hMOs by MEA measurements (Odawara et al. 2016). We measured extracellular field potentials, which are generated by action potentials. At days 50–60 of differentiation, hMOs were seeded in 48-well tissue culture MEA plates on a grid of 16 electrodes (Fig. 7 a and b). After 10–20 days of culturing, we recorded spontaneous activity, on several electrodes, over several days, in the form of mono- and biphasic spikes (Fig. 7 a' and a''). To investigate which neuronal subtypes were functionally active in the hMOs, we applied specific drugs following a previously reported experimental design (Illes et al. 2014). We recorded spiking patterns from 24 active electrodes: in Fig. 7 c and d representative recordings of one electrode are displayed. After treating the organoids with gabazine, a $GABA_A$ receptor antagonist, we detected an increase of spontaneous spiking (22.5% increase, Fig. 7d'). Following the gabazine-induced disinhibition, we applied the AMPA/Kainate-receptor antagonist NBQX and the NMDA-receptor antagonist D-AP-5. The inhibition of the

excitatory neurons resulted in a 28.1% decrease of spontaneous activity (Fig. 7d"). After the inhibition of GABAergic and glutamatergic neurons in the hMOs, we added the D2/D3 receptor agonist quinpirole (Fig. 7 c' and d"'), which resulted in a 47.8% decrease of neuronal activity. Confirming the findings displayed in Fig. 2, we conclude from these experiments that hMOs contain functional GABAergic, glutamatergic and dopaminergic neurons.

Discussion

The in vitro human brain organoid technology has become a valuable tool allowing advances in the field of basic research as well as in translational applications (Fatehullah et al. 2016). Organoids specifically modelling the human midbrain hold great promise for studying human development and for modelling Parkinson's disease (PD) (Jo et al. 2016; Monzel et al. 2017; Kim et al. 2019; Smits et al. 2019). In contrast to 2D monolayer cultures, hMOs can recapitulate complex interactions of midbrain dopaminergic neurons with other cell types of the central nervous system (CNS) in a 3D environment. However, human midbrain organoid research has so far focused mainly on dopaminergic neurons. In a detailed study of Borroto-Escuela et al. (2018), it has been described that released dopamine can diffuse into synaptic regions of glutamate and GABA synapses and directly affect other striatal cell types possessing dopamine receptors. Furthermore, *substantia nigra* dopaminergic neurons are directly controlled by GABAergic input (Tepper and Lee 2007). Evidences from these studies suggest that the presence of other neuronal subtypes is important to model multifactorial disease like PD. In our study, we have demonstrated that the derivation of hMOs leads to functional neuronal networks, containing different neuronal subtypes of the human midbrain. Single-cell transcriptomic data from hMOs demonstrated that there is an increased expression of neuronal-specific genes in 35 days compared with 70 days old hMOs. On the other hand, the gene-gene correlations between only neuron-specific genes increased considerably at day 70, suggesting an increased commitment of cells towards the neuronal cell fate during the course of the organoid development. This further supports the finding of a progressive maturation of post-mitotic neurons (Fig. 1c). The identification of these neuron-specific genes revealed that the genes upregulated at the earlier time point are relevant in the process of neurogenesis and neuronal migration and differentiation (EBF3 (Garcia-Dominguez et al. 2003), L1CAM (Patzke et al. 2016)). Whereas the upregulated genes at the later time point have been for instance implicated in subpopulations like GABAergic neurons (DLX1, CALB2 (Al-Jaberi et al. 2015)). This indicates a higher commitment of the cells towards their intended fate and a progressive maturation of the post-mitotic neurons within the hMOs. Furthermore, single-cell analysis of the hMOs also proved the presence of specific neuronal subtypes, like dopaminergic, glutamatergic, GABAergic and serotonergic neurons. Supporting the findings of currently published midbrain-specific organoid models (Jo et al. 2016; Qian et al. 2016; Monzel et al. 2017; Smits et al. 2019), we detected a significant upregulation of tyrosine hydroxylase (TH) within the cell population of 70 days old hMOs compared with 35 days old hMOs.

In the here presented data, we see a strong underrepresentation of neurons among recovered cells in the scRNA-seq data (see, e.g. data for 70 days of differentiation in Fig. 2a). However, this has been seen by others before and is explained by difficulties in the mechanic dissociated of complex 3D neuronal tissues into single cells. Particularly, neurons with their long and branched processes have the tendency to be lost in this process. Hence, while scRNA-seq is an excellent tool for the qualitative analysis of cell types, particularly for neural cultures, it might not be the ideal method for cell type quantification. In this context, the identification of mesenchymal cells was surprising. However, a previous study identified similar cells in human dopaminergic neuron grafts in the rodent brain (Tiklova et al. 2019). Therefore, these cells have been described as vascular leptomeningeal cells, a cell type that includes barrier forming fibroblasts. These data are consistent with our findings.

The activity of neurons and their different receptors can be analysed by the specific response to chemical compounds. It has been shown that quinpirole, a specific D2/D3 receptor agonist, suppresses the firing in hMOs (Jo et al. 2016; Monzel et al. 2017). In addition to the previously reported analyses in hMOs, we blocked inhibitory and excitatory communication, to further isolate and attribute the recorded signals to neuronal subtypes. Gabazine induces a disinhibition of GABAergic neurons, whereas NMDA-receptor and AMPA/Kainate-receptor antagonists inhibit glutamatergic excitatory communication (Illes et al. 2014). Together with the characteristic hallmarks of synapse formation (Fig. 6a–d) and the previous findings of dopamine release (Smits et al. 2019), these data confirm the presence of functional dopamine receptors in dopaminergic neurons as well as functional GABAergic and glutamatergic neurons within hMOs. As neurons do not exist in isolation in the CNS but form functional networks with other neurons and non-neuronal cells, it is important to expand our research of neurodegenerative diseases using 3D models that are able to recapitulate cell autonomous as well as non-cell autonomous aspects. Utilizing 3D cell culture models that comprise a variety of neuronal subtypes could lead to new insights into the selective vulnerabilities, which are observed in neurodegeneration. Indeed, evidence

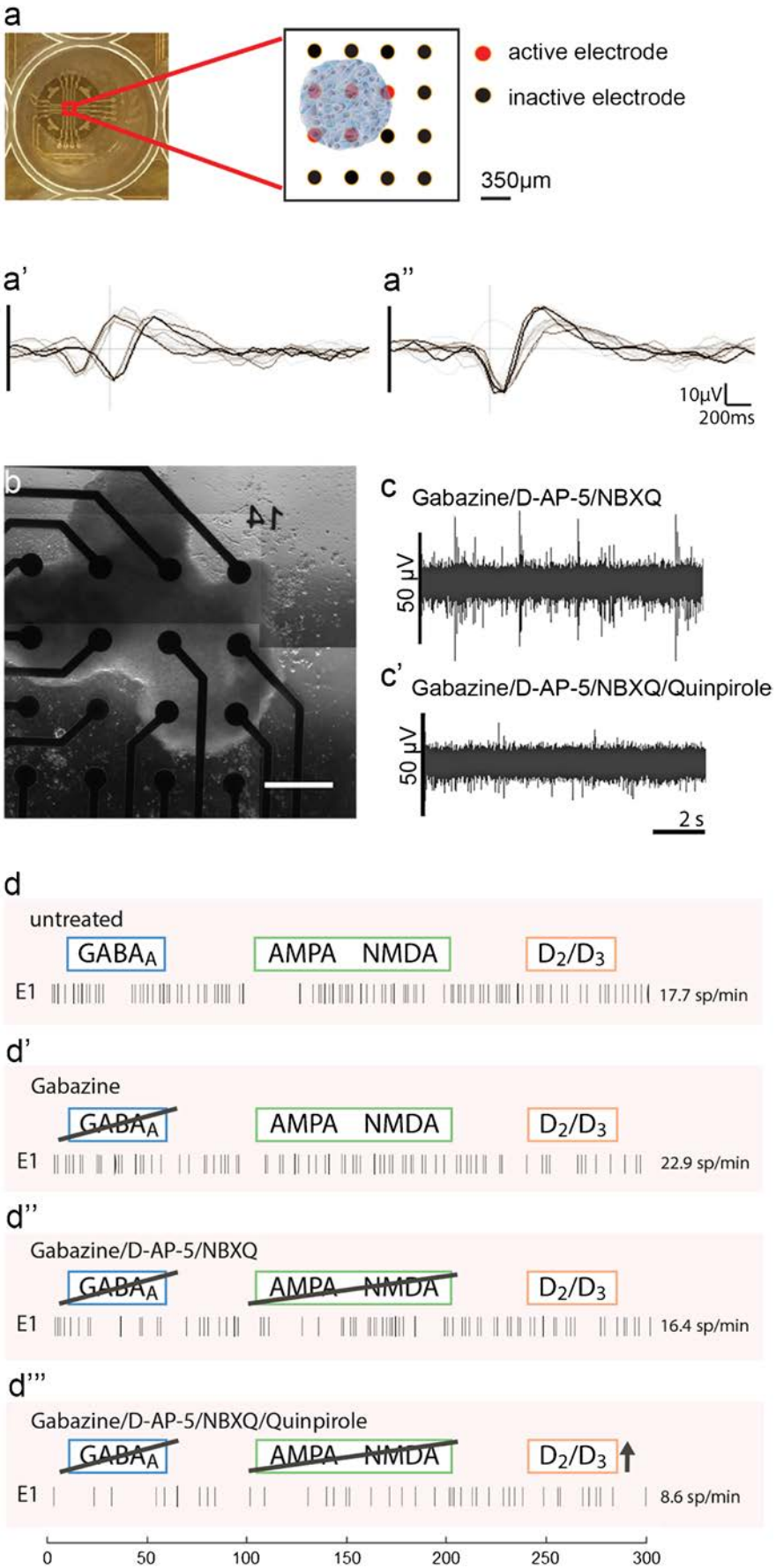
a
active electrode
inactive electrode
350µm
a'
a''
10µV
200ms
b
c
Gabazine/D-AP-5/NBXQ
50 µV
c'
Gabazine/D-AP-5/NBXQ/Quinpirole
50 µV
2 s
d
untreated
GABA$_A$
AMPA NMDA
D$_2$/D$_3$
E1
17.7 sp/min
d'
Gabazine
GABA$_A$
AMPA NMDA
D$_2$/D$_3$
E1
22.9 sp/min
d''
Gabazine/D-AP-5/NBXQ
GABA$_A$
AMPA NMDA
D$_2$/D$_3$
E1
16.4 sp/min
d'''
Gabazine/D-AP-5/NBXQ/Quinpirole
GABA$_A$
AMPA NMDA
D$_2$/D$_3$
E1
8.6 sp/min
0
50
100
150
200
250
300

◀ **Fig. 7** Electrophysiological activity in midbrain-specific organoids. (**a**) Representative scheme of positioned midbrain organoid on a 16-electrode array in a 48-well tissue culture plate. Examples of mono- and biphasic spikes detected by individual electrodes of a multielectrode array (MEA) system (**a'**, **a"**). (**b**) Representative image of midbrain organoid positioned on a 16-electrode array in a 48-well tissue culture plate. Scale bar is 350 μm. (**c**–**d**) Evaluation of the spontaneous activity by addressing inhibitory (blue) and excitatory (green) neurotransmitter receptors using multielectrode array (MEA) system. (**c**, **c'**) Representative raw data traces show the effect of Quinpirole in absence of inhibitory and excitatory synaptic communication. (**d**) Representative spike raster plots demonstrate effects of applied compounds

suggests that specific regulation of the excitability of dopaminergic neurons by other neuronal subtypes in the midbrain might explain their selective vulnerability in PD (Korotkova et al. 2004). This underlines the importance and the enormous potential for future disease modelling of the here described hMO model, as it contains functionally connected heterogeneous neuronal cell populations.

Acknowledgements We would like to thank Dr. Sebastian Illes (University of Gothenburg, Sweden) for his help with the experimental MEA design and Diane Capen (Massachusetts General Hospital, Boston, USA) for her EM work. We thank Dr. Jared Sterneckert (Technical University of Dresden, Germany) and Dr. Bill Skarnes (The Wellcome Trust Sanger Institute, Cambridge, UK) for human iPSC lines. Furthermore, we would like to thank Yohan Jarosz from the LCSB Bioinformatics Core Group for his support in data management. This project was supported by the LCSB pluripotent stem cell core facility.

Authors' contributions LMS designed and performed cell culture and imaging experiments, prepared the figures and wrote the original draft. KG performed the scRNA-seq experiments and related bioinformatics approaches. SSS did the fibroblast analysis. SM, KK, JL and JWS performed the computational analysis of the single-cell RNA-Seq data, edited the manuscript and contributed to the figs. AS, JWS and EM supervised the design and implementation of the single-cell experiments and associated computational data analysis. SB initiated the project, supervised it and edited the manuscript. JCS conceived and supervised the project, designed the experiments and edited the manuscript.

Funding information The JCS lab is supported by the Fonds National de la Recherché (FNR) (CORE, C13/BM/5791363 and Proof-of-Concept program PoC15/11180855 & PoC16/11559169). This is an EU Joint Programme-Neurodegenerative Disease Research (JPND) project (INTER/JPND/14/02; INTER/JPND/15/11092422). Further support comes from the SysMedPD project which has received funding from the European Union's Horizon 2020 research and innovation programme under grant agreement No 668738. LMS is supported by fellowships from the FNR (AFR, Aides à la Formation-Recherche). Electron microscopy was performed in the Microscopy Core of the Center for Systems Biology/Program in Membrane Biology, which is partially supported by an Inflammatory Bowel Disease Grant DK043351 and a Boston Area Diabetes and Endocrinology Research Center (BADERC) Award DK057521. SM is supported by the University of Luxembourg and the National Research Fund through the CriTiCS DTU FNR PRIDE/10907093/CRITICS. KG and AS were supported by the Luxembourg National Research Fund (FNR) through the C14/BM/7975668/CaSCAD project and AS additionally by the National Biomedical Computation Resource (NBCR) through the NIH P41 GM103426 grant from the National Institutes of Health.

Compliance with ethical standards

Conflict of interest JCS is co-founder of the biotech company OrganoTherapeutics SARL.

Ethical approval Written informed consent was obtained from all individuals who donated samples to this study and the here conduced work was approved by the responsible ethics commissions. The cell lines used in this study are summarized in Supplementary Table 1.

References

Abe-Fukasawa N, Otsuka K, Aihara A, Itasaki N, Nishino T (2018) Novel 3D liquid cell culture method for anchorage-independent cell growth, cell imaging and automated drug screening. Sci Rep 8(1): 3627. https://doi.org/10.1038/s41598-018-21950-5

Al-Jaberi N, Lindsay S, Sarma S, Bayatti N, Clowry GJ (2015) The early fetal development of human neocortical GABAergic interneurons. Cereb Cortex 25(3):631–645. https://doi.org/10.1093/cercor/bht254

Bardy C, van den Hurk M, Eames T, Marchand C, Hernandez RV, Kellogg M et al (2015) Neuronal medium that supports basic synaptic functions and activity of human neurons in vitro. Proc Natl Acad Sci:201504393. https://doi.org/10.1073/pnas.1504393112

Borroto-Escuela DO, Perez De La Mora M, Manger P, Narvaez M, Beggiato S, Crespo-Ramirez M et al (2018) Brain dopamine transmission in health and Parkinson's disease: modulation of synaptic transmission and plasticity through volume transmission and dopamine heteroreceptors. Front Synaptic Neurosci 10:20. https://doi.org/10.3389/fnsyn.2018.00020

Cho GS, Lee DI, Tampakakis E, Murphy S, Andersen P, Uosaki H et al (2017) Neonatal transplantation confers maturation of PSC-derived cardiomyocytes conducive to modeling cardiomyopathy. Cell Rep 18(2):571–582. https://doi.org/10.1016/j.celrep.2016.12.040

Cooper O, Seo H, Andrabi S, Guardia-Laguarta C, Graziotto J, Sundberg M et al (2012) Pharmacological rescue of mitochondrial deficits in iPSC-derived neural cells from patients with familial Parkinson's disease. Sci Transl Med 4(141):141ra190. https://doi.org/10.1126/scitranslmed.3003985

Di Lullo E, Kriegstein AR (2017) The use of brain organoids to investigate neural development and disease. Nat Rev Neurosci 18(10): 573–584. https://doi.org/10.1038/nrn.2017.107

Fatehullah A, Tan SH, Barker N (2016) Organoids as an in vitro model of human development and disease. Nat Publ Group 18:246–254. https://doi.org/10.1038/ncb3312

Garcia-Dominguez M, Poquet C, Garel S, Charnay P (2003) Ebf gene function is required for coupling neuronal differentiation and cell cycle exit. Development 130(24):6013–6025. https://doi.org/10.1242/dev.00840

Illes S, Jakab M, Beyer F, Gelfert R, Couillard-Despres S, Schnitzler A et al (2014) Intrinsically active and pacemaker neurons in pluripotent stem cell-derived neuronal populations. Stem Cell Reports 2(3): 323–336. https://doi.org/10.1016/j.stemcr.2014.01.006

Jo J, Xiao Y, Sun AX, Cukuroglu E, Tran HD, Goke J et al (2016) Midbrain-like organoids from human pluripotent stem cells contain functional dopaminergic and neuromelanin-producing neurons. Cell Stem Cell 19(2):248–257. https://doi.org/10.1016/j.stem.2016.07.005

Kelava I, Lancaster MA (2016) Dishing out mini-brains : current progress and future prospects in brain organoid research. Dev Biol 420:199–209. https://doi.org/10.1016/j.ydbio.2016.06.037

Kim H, Park HJ, Choi H, Chang Y, Park H, Shin J et al (2019) Modeling G2019S-LRRK2 sporadic Parkinson's disease in 3D midbrain organoids. Stem Cell Reports 12(3):518–531. https://doi.org/10.1016/j.stemcr.2019.01.020

Korotkova TM, Ponomarenko AA, Brown RE, Haas HL (2004) Functional diversity of ventral midbrain dopamine and GABAergic neurons. Mol Neurobiol 29(3):243–259. https://doi.org/10.1385/MN:29:3:243

La Manno G, Gyllborg D, Codeluppi S, Nishimura K, Salto C, Zeisel A et al (2016) Molecular diversity of midbrain development in mouse, human, and stem cells. Cell 167(2):566–580.e519. https://doi.org/10.1016/j.cell.2016.09.027

Lancaster MA, Renner M, Martin CA, Wenzel D, Bicknell LS, Hurles ME et al (2013) Cerebral organoids model human brain development and microcephaly. Nature 501(7467):373–379. https://doi.org/10.1038/nature12517

Luhmann HJ, Sinning A, Yang JW, Reyes-Puerta V, Stuttgen MC, Kirischuk S et al (2016) Spontaneous neuronal activity in developing neocortical networks: from single cells to large-scale interactions. Front Neural Circuits 10:40. https://doi.org/10.3389/fncir.2016.00040

Macosko EZ, Basu A, Satija R, Nemesh J, Shekhar K, Goldman M et al (2015) Highly parallel genome-wide expression profiling of individual cells using nanoliter droplets. Cell 161(5):1202–1214. https://doi.org/10.1016/j.cell.2015.05.002

Matsui TK, Matsubayashi M, Sakaguchi YM, Hayashi RK, Zheng C, Sugie K et al (2018) Six-month cultured cerebral organoids from human ES cells contain matured neural cells. Neurosci Lett 670:75–82. https://doi.org/10.1016/j.neulet.2018.01.040

Ming GL, Tang H, Song H (2016) Advances in Zika virus research: stem cell models, challenges, and opportunities. Cell Stem Cell 19(6): 690–702. https://doi.org/10.1016/j.stem.2016.11.014

Monzel AS, Smits LM, Hemmer K, Hachi S, Moreno EL, van Wuellen T et al (2017) Derivation of human midbrain-specific organoids from neuroepithelial stem cells. Stem Cell Reports 8(5):1144–1154. https://doi.org/10.1016/j.stemcr.2017.03.010

Muguruma K, Nishiyama A, Kawakami H, Hashimoto K, Sasai Y (2015) Self-organization of polarized cerebellar tissue in 3D culture of human pluripotent stem cells. Cell Rep 10:537–550. https://doi.org/10.1016/j.celrep.2014.12.051

Nguyen HN, Byers B, Cord B, Shcheglovitov A, Byrne J, Gujar P et al (2011) LRRK2 mutant iPSC-derived DA neurons demonstrate increased susceptibility to oxidative stress. Cell Stem Cell 8:267–280. https://doi.org/10.1016/j.stem.2011.01.013

Odawara A, Katoh H, Matsuda N, Suzuki I (2016) Physiological maturation and drug responses of human induced pluripotent stem cell-derived cortical neuronal networks in long-term culture. Sci Rep 6: 26181. https://doi.org/10.1038/srep26181

Patzke C, Acuna C, Giam LR, Wernig M, Sudhof TC (2016) Conditional deletion of L1CAM in human neurons impairs both axonal and dendritic arborization and action potential generation. J Exp Med 213(4):499–515. https://doi.org/10.1084/jem.20150951

Qian X, Nguyen HN, Song MM, Hadiono C, Ogden SC, Hammack C et al (2016) Brain-region-specific organoids using mini-bioreactors for modeling ZIKV exposure. Cell 165(5):1238–1254. https://doi.org/10.1016/j.cell.2016.04.032

Qian X, Nguyen HN, Jacob F, Song H, Ming GL (2017) Using brain organoids to understand Zika virus-induced microcephaly. Development 144(6):952–957. https://doi.org/10.1242/dev.140707

Quadrato G, Nguyen T, Macosko EZ, Sherwood JL, Min Yang S, Berger DR et al (2017) Cell diversity and network dynamics in photosensitive human brain organoids. Nature 545(7652):48–53. https://doi.org/10.1038/nature22047

Reinhardt P, Glatza M, Hemmer K, Tsytsyura Y, Thiel CS, Hoing S et al (2013a) Derivation and expansion using only small molecules of human neural progenitors for neurodegenerative disease modeling. PLoS One 8(3):e59252. https://doi.org/10.1371/journal.pone.0059252

Reinhardt P, Schmid B, Burbulla LF, Schondorf DC, Wagner L, Glatza M et al (2013b) Genetic correction of a LRRK2 mutation in human iPSCs links parkinsonian neurodegeneration to ERK-dependent changes in gene expression. Cell Stem Cell 12(3):354–367. https://doi.org/10.1016/j.stem.2013.01.008

Ryan SD, Dolatabadi N, Chan SF, Zhang X, Akhtar MW, Parker J et al (2013) Isogenic human iPSC Parkinson's model shows nitrosative stress-induced dysfunction in MEF2-PGC1α transcription. Cell 155:1351–1364. https://doi.org/10.1016/j.cell.2013.11.009

Sánchez-Danés A, Richaud-Patin Y, Carballo-Carbajal I, Jiménez-Delgado S, Caig C, Mora S et al (2012) Disease-specific phenotypes in dopamine neurons from human iPS-based models of genetic and sporadic Parkinson's disease. EMBO Mol Med 4:380–395. https://doi.org/10.1002/emmm.201200215

Satija R, Farrell JA, Gennert D, Schier AF, Regev A (2015) Spatial reconstruction of single-cell gene expression data. Nat Biotechnol 33(5):495–502. https://doi.org/10.1038/nbt.3192

Smits LM, Reinhardt L, Reinhardt P, Glatza M, Monzel AS, Stanslowsky N et al (2019) Modeling Parkinson's disease in midbrain-like organoids. npj Parkinson's Dis in press. https://doi.org/10.1038/s41531-019-0078-4

Stuart T, Butler A, Hoffman P, Hafemeister C, Papalexi E, Mauck WM, Hao Y, Stoeckius M, Smibert P, Satija R (2019) Comprehensive integration of single-cell data. Cell 177(7):1888–1902. https://doi.org/10.1016/j.cell.2019.05.031

Suzanne M, Steller H (2013) Shaping organisms with apoptosis. Cell Death Differ 20(5):669–675. https://doi.org/10.1038/cdd.2013.11

Takahashi K, Yamanaka S (2006) Induction of pluripotent stem cells from mouse embryonic and adult fibroblast cultures by defined factors. Cell 126(4):663–676. https://doi.org/10.1016/j.cell.2006.07.024

Tepper JM, Lee CR (2007) GABAergic control of substantia nigra dopaminergic neurons. Prog Brain Res 160:189–208. https://doi.org/10.1016/S0079-6123(06)60011-3

Tieng V, Stoppini L, Villy S, Fathi M, Dubois-Dauphin M, Krause KH (2014) Engineering of midbrain organoids containing long-lived dopaminergic neurons. Stem Cells Dev 23(13):1535–1547. https://doi.org/10.1089/scd.2013.0442

Tiklová K, Nolbrant S, Fiorenzano A, Björklund ÅK, Sharma V, Heuer A, Gillberg L, Hoban DB, Cardoso T, Adler AF, Birtele M, Lundén-Miguel H, Volakakis N, Kirkeby A, Perlmann T, Parmar M (2019) Single cell gene expression analysis reveals human stem cell-derived graft composition in a cell therapy model of Parkinson's disease. bioRxiv:720870. https://doi.org/10.1101/720870

van der Maarten L, Hinton G (2008) Visualizaing data unsin t-SNE. In: Journal of Machine Learning Research.)

Walter J (2019) Neural stem cells of Parkinson's disease patients exhibit aberrant mitochondrial morphology and functionality. Stem Cell Reports in press

4.3. MANUSCRIPT III

Microglia integration into human midbrain organoids leads to increased neuronal maturation and functionality

This article has been submitted in *Glia.*

4.3.1. Preface

The human brain consists on groups of neurons that communicate with each other through synaptic contacts (Lovinger, 2008; Pereda, 2014). The functionality and viability of these neurons is supported by macroglia – astrocytes and oligodendrocytes -, microglia and vasculature (Araque et al., 2014; Bautch and James, 2009b; Duncan et al., 2021; Hughes and Appel, 2019; Ueno et al., 2013). Microglia participate in the remodelling of neuronal networks. They provide neurons with neurotrophic factors, and maintain brain homeostasis by phagocytosing cell debris and metabolic waste products (Nimmerjahn et al., 2005; Witting et al., 2000). Midbrain organoids consist on a high amount of dopaminergic neurons, together with other neuronal types, astrocytes, oligodendrocytes and different progenitor populations (Monzel et al., 2017; Nickels et al., 2020; Smits et al., 2019) However, the absence of microglia makes midbrain organoids incomplete in terms of accurate representation of cellular diversity in the midbrain.

In this article, we successfully integrate iPSC-derived human microglia into midbrain organoids. We characterize the system via snRNA-Seq, and studied not only microglial identity within organoids, but also the effects microglia have on other cell types and pathways. We observed differences in cell death, oxidative stress and synaptic remodelling-related gene expression. We also show that neuronal excitability is increased in the presence of microglia. Overall, the integration of microglia into midbrain organoids leads to beneficial effects for the organoid functionality, and makes the system a potential candidate to study neuroinflammation in PD.

This publication is the main result of my PhD studies. I derived macrophage precursors for co-culture, and neural precursor cells for the generation of organoids. I performed the co-cultures that were analysed in this manuscript. Y.Lan, T. Kouno, J. Sharif and H. Koseki carried out the pre-processing of samples for snRNA-Seq, and S. L. Nickels analysed the data. U. Dubonyte helped maintaining the cell cultures, K. Barmpa performed the synapse analysis with western blot, and J. Jarazo participated in the live imaging and made the supplementary videos. C. Thome performed and analysed the patch clamp experiments. C. Saraiva revised and edited the manuscript. I conducted and analysed the rest of the experiments, prepared the figures and wrote the original manuscript.

Microglia integration into human midbrain organoids leads to increased neuronal maturation and functionality

Sonia Sabate-Soler[1], Sarah Louise Nickels[1], Cláudia Saraiva[1], Emanuel Berger[1], Ugne Dubonyte[1], Kyriaki Barmpa[1], Yan Jun Lan[3,4], Tsukasa Kouno[3], Javier Jarazo[1,2], Graham Robertson[1], Jafar Sharif[3], Haruhiko Koseki[3], Christian Thome[5], Jay W. Shin[3], Sally A. Cowley[6], Jens C. Schwamborn*[1]

[1] Luxembourg Centre for Systems Biomedicine (LCSB), Developmental and Cellular Biology, University of Luxembourg, Belvaux, Luxembourg.
[2] OrganoTherapeutics SARL-S, Esch-sur-Alzette, Luxembourg
[3] RIKEN Center for Integrative Medical Sciences, Yokohama, Kanagawa 230-0045, Japan.
[4] ETH Zurich, Institute of Pharmaceutical Sciences, Zurich 8057 Switzerland
[5] Institute of Physiology and Pathophysiology, Heidelberg University, Heidelberg, Germany.
[6] Oxford Parkinson's Disease Centre, James Martin Stem Cell Facility, Sir William Dunn School of Pathology, University of Oxford, Oxford, UK.
Contact information: jens.schwamborn@uni.lu

Summary

The human brain is a complex, three-dimensional structure. To better recapitulate brain complexity, recent efforts have focused on the development of human specific midbrain organoids. Human iPSC-derived midbrain organoids consist of differentiated and functional neurons, which contain active synapses, as well as astrocytes and oligodendrocytes. However, the absence of microglia, with their ability to remodel neuronal networks and phagocytose apoptotic cells and debris, represents a major disadvantage for the current midbrain organoid systems. Additionally, neuro-inflammation related disease modelling is not possible in the absence of microglia. So far, no studies about the effects of human iPSC-derived microglia on midbrain organoid neural cells have been published. Here we describe an approach to derive microglia from human iPSCs and integrate them into iPSC-derived midbrain organoids. Using single nuclear RNA Sequencing, we provide a detailed characterization of microglia in midbrain organoids as well as the influence of their presence on the other cells of the organoids. Furthermore, we describe the effects that microglia have on cell death and oxidative stress-related gene expression. Finally, we show that microglia in midbrain organoids affect synaptic remodelling and increase neuronal excitability. Altogether, we show a more suitable system to further investigate brain development, as well as neurodegenerative diseases and neuro-inflammation.

Introduction

The human brain is a highly complex organ in terms of structure, molecular and cellular composition, making it a challenging target for research. Three-dimensional (3D) brain models have been recently developed to better mimic the spatial and functional complexity of the human brain. Over the last decade, different protocols were developed to generate either whole brain organoids (Lancaster *et al.*, 2013; Lindborg *et al.*, 2016) or discrete regions of the brain(Shi *et al.*, 2012; Jo *et al.*, 2016; Qian *et al.*, 2016; Birey *et al.*, 2017; Monzel *et al.*, 2017). These models have proven to be suitable to model neurological disorders, including microcephaly (Lancaster *et al.*, 2013), Batten disease (Gomez-Giro *et al.*, 2019), Parkinson's disease (PD) (Smits *et al.*, 2019) and others (Choi *et al.*, 2014; Qian *et al.*, 2016). In fact, to better model PD recent efforts have focused on the development of PD patient specific midbrain organoids (Kim *et al.*, 2019; Smits *et al.*, 2019). Midbrain organoids contain spatially patterned groups of dopaminergic neurons, making them a suitable model to study PD. They consist of differentiated and functional neurons, which contain active synapses, as well as astrocytes and oligodendrocytes (Monzel *et al.*, 2017; Smits *et al.*, 2019). Moreover, they are able to recapitulate cardinal features of PD, including loss of dopaminergic neurons (Smits *et al.*, 2019), and protein aggregation (Kim *et al.*, 2019).

A major feature of neurological disorders is chronic inflammation (Bradburn, Murgatroyd and Ray, 2019; Tu *et al.*, 2019). Previous studies have shown integration of iPSC-derived microglia in cerebral organoids (Muffat *et al.*, 2016; Abud *et al.*, 2017). Furthermore, innate differentiation of microglia within whole brain organoids has also been achieved(PR *et al.*, 2018; Ramani *et al.*, 2020). Those systems used iPSCs to generate their cerebral organoids, instead of a neuro-epithelial stem cell population, used normally to generate midbrain region-specific brain organoids. The current midbrain organoid system derived from neuro-epithelial stem cells– with ectodermal origin –lacks microglia, due to their mesodermal origin. The absence of microglia, with their ability to prune neuronal synapses as well as phagocytose apoptotic cells and debris represents a major disadvantage for the understanding of the physiological brain. Additionally, neuro-inflammation related disease modelling is not possible in a system that lacks microglia.

Microglia, the largest population of immune cells in the brain, are tissue-resident macrophages. In the adult brain they represent 5 to 15% of the adult brain cells, depending on the brain region (Thion, Ginhoux and Garel, 2018). Microglia have a unique ontogeny; they are derived from Yolk sac progenitors in a very early embryonic age (Ginhoux *et al.*, 2010; Schulz *et al.*, 2012; Li and Barres, 2017). Microglia have particular functions during brain development. Among others, they establish contacts with neural progenitors to support neurogenesis and proliferation (Choi *et al.*,

2008; Ueno *et al.*, 2013). In the adult brain, they interact with neurons, astrocytes and oligodendrocytes, and their major functions are maintenance of brain homeostasis and immune defence. They also interact with synapses, modulating neuronal activity, and perform synaptic pruning (Wake *et al.*, 2009; Tremblay *et al.*, 2011). They phagocytose apoptotic neurons, induce programmed cell death (Witting *et al.*, 2000), guide sprouting blood vessels, and participate in neuronal maturation (Rymo *et al.*, 2011). Chronic neuro-inflammation is one of the neuropathological characteristics of neurodegenerative disorders, including PD (Shabab *et al.*, 2017).

Here, we describe the stable integration of functional human iPSC-derived microglia into midbrain organoids. This represents a significant advancement of the midbrain model, increasing its complexity and making a step forward from organoids to multi-lineage assembloids (Pasca, 2019; Marton and Pașca, 2020). Moreover, microglia within assembloids express phagocytosis-related genes and release cytokines and chemokines, demonstrating relevant cellular communication abilities. Moreover, we demonstrate that assembloids display a reduction of cell death and oxidative stress-related genes in the system, compared to midbrain organoids without microglia. Furthermore, microglia seem to affect synapse remodelling, and lead to increased electrophysiology properties in neurons. Overall, we have established a stable and reproducible way to integrate functional microglia into midbrain organoids, leading to a next generation of midbrain organoid modelling. Our technology represents a step forward for the understanding and modulation of the complexity of the healthy and diseased human brain, with especial relevance for neuro-inflammatory conditions.

Results

hiPSC-derived microglia express specific markers and are functional

The work presented here is based on the use of quality controlled hiPSC lines (lines: K7, 163, EPI, table S1) from three different healthy individuals that express the pluripotency markers SSEA-4, OCT-4, TRA-1-60, NANOG, TRA-1-81 and SOX2 (Figure S1A). We started by deriving macrophage precursors from hiPSCs that were then differentiated into microglia for 10 days, as previously described (Haenseler, Zambon, *et al.*, 2017). hiPSC-derived microglia in monoculture expressed macrophage-specific markers, including IBA1, PU1 and CD45, and microglia markers, notably TMEM119 and P2RY12, as detected by immunostaining (Fig. 1A). Moreover, PCR confirmed that microglia also expressed the macrophage specific genes *IBA1* and *CD68*, and the microglia-specific genes *TMEM119* and *P2RY12* (Fig. 1B). After confirming the microglia cell

identity, we next assessed their phagocytic capacity. Incubation of microglia with Zymosan particles showed the cells' ability in phagocytosing these particles, detectable within their cell bodies (Figure 1C, Figure S1B, Video S1, S2 and S3).

A major challenge in assembloid generation is the compatibility of cell culture conditions for different cell types. In order to assess the microglia compatibility with the organoid culture medium, we first examined the toxicity of each midbrain organoid medium supplement on microglia survival. Macrophage precursors were cultured for 10 days with organoid maturation medium (containing BDNF, GDNF, TGFβ3, db cAMP, DAPT and Activin A), microglia differentiation medium (containing IL-34 and GM-CSF), or microglia medium individually supplemented with each of the neurotrophic factors contained in the organoid medium. After 10 days of exposure to the different media, an MTT viability assay showed a significant decrease in cell viability in the presence of TGFβ3 (69.18% ± 8.371, $p=0.0024$), db cAMP (47.10% ± 8.371, $p<0.0001$) and Activin A (76.01% ± 8.371, $p=0.0292$) compared to microglia medium (Figure 1D and E). After only 7 days of exposure, an impairment of differentiation and a lower viability were already observed visually in the cells cultured with organoid medium as well as the microglia medium supplemented with TGFβ3 or db cAMP (Figure 1E). These results indicate that the midbrain organoid medium, containing TGFβ3, db cAMP and Activin A might not be suitable for the cultivation of microglia containing midbrain organoids.

The co-culture medium allows microglial survival and neuronal differentiation in midbrain organoids

After testing the organoid medium on microglia, we next assessed the effects of the different media compositions on the neuronal population of the midbrain organoids. Taking into consideration the cytotoxic effect on 2D monoculture microglia, we combined the microglia differentiation medium with the least microglia-toxic neurotrophic factors from the organoid maturation medium. Hence, we supplemented the microglia differentiation medium with BDNF, GDNF, DAPT and Activin A – since they play an important role in neuronal maturation - and refer to this medium combination as the "co-culture medium" (Table S2). In order to study the effects of the co-culture medium on the organoids, we used midbrain organoids from the line K7 as a control, and 3 groups of assembloids: K7 organoids co-cultured with K7 macrophage precursors, K7 organoids co-cultured with 163 macrophage precursors and K7 organoids co-cultured with EPI macrophage precursors (Figure 1F. The "assembloids" group in graphs represents the pooled results from the three co-cultured groups). We cultured those groups with midbrain organoid medium, microglia differentiation medium or co-culture medium for 20 more days (Figure 1F). As

expected, the IBA1 positive microglial population was significantly reduced when organoid medium was used, whereas no difference was observed when cultured with microglia or co-culture medium (Figure 1G, Figure S1C). The major neuronal cell type in midbrain organoids are TH positive dopaminergic neurons. Interestingly, we observed a significant decrease in TH positive neurons in both midbrain organoids and assembloids in the presence of microglia differentiation medium (Figure 1H, Figure S1C). This decrease was not observed in the MAP2 positive pan neuronal population (Figure S1D, Figure 2C, Figure S1I). The reduction of TH positive cells indicates an impairment of dopaminergic neuron differentiation under microglia medium culture conditions. Notably, in the presence of co-culture medium, the levels of TH in both midbrain organoids and assembloids remained at similar levels as for the organoids cultured with midbrain organoid maturation medium (Figure 1H, Figure S1C). In summary, we here developed a unique co-culture medium that is optimal for both microglial survival and dopaminergic neuron differentiation in human midbrain organoids.

Assembloids contain IBA1 positive functional microglia and express midbrain specific neuronal markers

After successfully optimizing the co-culture conditions, midbrain organoids were generated using a pure ventral midbrain-patterned NESC population (Figure S1E) from the hiPSC line K7 (Smits *et al.*, 2019; Nickels *et al.*, 2020). After 2 days of maintenance, and 15 days of dopaminergic neuron differentiation induction, we proceeded to the co-cultures (Figure 2A). They were performed as described in the previous section, using K7 midbrain organoids as controls, and co culturing K7 organoids with K7 macrophage precursors, with 163 macrophage precursors or with EPI macrophage precursors (following Figure 1F excluding the media testing). During the whole study, we did not observe any major line specific differences. During the co-culture, the macrophage precursors first aggregated, forming smaller round colonies that attached to the surface of the organoid and then incorporated within that same structure (Figure S1F).

After 20 days of co-culture (35 days of dopaminergic differentiation), we validated the incorporation of microglia into the organoids by IBA1 immunostaining. We then assessed the percentage of IBA1 positive cells in assembloids using a previously published computer-assisted image analysis pipeline for marker identification and quantification with small modifications (Smits *et al.*, 2019). On average, 6.4% of the assembloid cells were IBA1 positive (Figure 2B). The morphology of the incorporated microglial cells varied between round and partially ramified (Figure S1G). We confirmed the presence of a neuronal population by a Beta-tubulin III (TUJ1) staining, and assessed further neuronal differentiation by MAP2 staining. In addition, FOXA2

positive midbrain specific dopaminergic neuron precursors and TH positive differentiated dopaminergic neurons were observed in assembloids (Figure 2C, Figure S1I). After culturing the assembloids for 70 days, we further confirm the presence of a GFAP positive astrocytic population in the assembloids (Figure S1H).

Single nuclear RNA-sequencing reveals eight different cell populations within midbrain-microglia assembloids.

In order to further characterize the microglia within assembloids we performed single nuclear RNA-sequencing (snRNA-Seq). Separation of clusters in cells coming from midbrain organoids and assembloids clearly showed that the microglia cluster is specific for assembloids and not present in midbrain organoids (Figure 2D). Cell types were identified based on marker gene expression from La Mano et al. 2016 (G *et al.*, 2016). Moreover, the identified cell clusters were validated and neuronal subtypes were specified (Figure S2 and Table S5). Quality controlled clustering of single cells (Figure S3) showed eight different cell types: radial glia (RGL), midbrain specific neural epithelial stem cells (midNESC), neuronal progenitors (PROG), neuroblasts (NB), young dopaminergic and cholinergic neurons yDN&CN, mature A10 specific dopaminergic neurons, GABAergic and glutamatergic neurons (mDN(A10)&GABA&GLUT), mature A9 specific dopaminergic neurons and serotonergic neurons (mDN(A9)&SN) as well as microglia (MGL, Figure S2).

Proportions of the different clusters in midbrain organoids and assembloids are represented in pie charts (Figure 2E). midNESC were the most prominent cell type by representing 35% of total cells. More than 60% of the organoid and assembloid cells showed neuronal identity (corresponding to the groups NB, yDN&CN, mDN(A10)&GIN&Gan, mDN(A9)&SN). Less than 5% were represented by glial cells (astrocytes, oligodendrocytes and microglia) at this stage of differentiation. Because of a considerable sample and cell loss, we believe the proportion of microglia cells represented in the Figure 2E is not accurate. However, we proceeded with the analysis of microglial identity and functionality-related genes, as well as for the other cell clusters. Progenitors were closest to neuroblasts and young neurons, whereas radial glial cells were very similar to midNESCs. The different mature neuronal groups clustered together. Clustering of the marker genes showed the relation between different cell clusters (Figure 2F). As expected, MGL cells clustered apart from all other cell types. A distinct genetic signature of the microglia cells was further validated by a Spearman correlation analysis (Figure 2G).

Microglia in assembloids show a typical immune cell signature

Next, we aimed at identifying gene signatures unique to microglia in comparison to the other cell types in assembloids. Firstly, we used the expression of the 100 most variable genes obtained from the snRNA-Seq analysis to cluster the different cell populations observed in assembloids (Figure 3A). Indeed most variability between cells clusters came from the microglia, which had a completely different genetic signature (Figure 3A). Then, we identified the top 100 markers defining microglia identity (Figure 3B). From those, several canonical marker genes were chosen in order to characterize the main functions of microglia. General microglia marker genes such as *IBA1* and *PU1* were significantly and specifically expressed in microglia. In addition, the microglia core signature revealed genes involved in antigen presentation (*HLA-DMB*), cytokine and complement signalling (*CSF1R, IL18, C1QC*) as well as pathogen and self-recognition such as toll-like receptor signalling (*TLR2*), C-type lectins (*CLEC7A*) and mannose and nod-like receptors (*MRC1, NAIP*). Moreover, genes involved in microglial adhesion (*ITGAM*) and motility through chemokine signalling (*CCL2*), as well as purinergic signalling (*P2RX4*) were significantly expressed in microglia (Figure 3C). Furthermore, several chemokines and cytokines were expressed predominantly in microglia (Figure 3D).

In order to address microglia functionality, we then measured chemokine and cytokine release in midbrain organoids and assembloids. For that, culture medium from midbrain organoids and assembloids at day 20 of co-culture was used. The medium collected was in contact with the organoids or assembloids for 3 days. As expected, in a hierarchical clustering analysis, midbrain organoids clustered in a different group than the microglia containing assembloids (Figure 4A). For a total of 18 analysed cytokines (IL-7, IL-12p17, IL-3, TNFα, IL-1α, IL-1ß, IL-6, IFNα, IL-10 and IFNγ) and chemokines (CXCL8, CCL2, CXCL2, CCL3, CXCL1, CCL4, CX3CL1 and MIP-3ß) we observed a significant increase in the medium from assembloids compared to midbrain organoids, suggesting that immune functionality was acquired through the microglia incorporation (Figure 4B). Interestingly, although the RNA expression levels for IL-6, IL-7 and CX3CL1 were higher in non-microglia cells (Figure 4C), the levels of released cytokines were higher in the assembloids medium (Figure 4B). Hence, potentially the released cytokines are not necessarily produced in the microglia, but their secretion is stimulated by the presence of microglia.

Microglia in assembloids are functional and affect the expression of cell survival-related genes

As we previously demonstrated, microglia have the ability to phagocytose Zymosan particles in 2D monoculture (Figure 1C). Therefore, we assessed if microglia in assembloids express genes involved in phagocytosis. Indeed, in assembloids we observed a higher expression of phagocytic genes suggesting the presence of a functional phagolysosomal pathway (Figure 3D). Genes included antigen recognition (*HLA-A,B,C*), receptor (*TLR2,4*) and internal signalling (*ATG7*), as well as autophagic vesicle formation (*LAMP2*, *SQSTM1* (*p62*)) and lysosomal degradation/oxidation (*CYBB*). These results indicate these microglia should have phagocytic capacity and hence the ability to remove dead cells. Interestingly and in agreement with this hypothesis, when we measured the organoid size throughout the culture period we observed a decrease of the assembloid size over time (Figure 4D). Midbrain organoids and assembloids were stained using the DNA dye Hoechst, and using our computer-assisted image analysis pipeline for cell type segmentation(Smits *et al.*, 2019), we quantified Hoechst signal. Levels of total cells, live cells and necrotic/late apoptotic cells were evaluated. We observed that the total amount of cells was lower in assembloids compared to midbrain organoids, correlating with the size measurements. Particularly, the amount of dead cells was significantly lower in the assembloids (Figure 4E), suggesting that microglia may eliminate dead cells in assembloids.

Microglia have an effect on oxidative stress and immune response in assembloids

After establishing the successful integration of microglia into midbrain organoids and showing important aspects of microglia functionality, we investigated the potential influence of microglia on the neural cells in midbrain organoids. We performed differential gene expression analysis over the neural cells in assembloids and midbrain organoids, which revealed 423 significantly different genes ($p<0.05$). The top 100 differentially expressed genes (DEGs) across all cells are represented in a heat-map and clustered by cell type (Figure S4A). We assigned DEGs to each cell type and represented their overlap in Venn diagrams ($p<0.05$, Figure S4B). The left Venn diagram shows an overlap of all three neuronal clusters and the right Venn diagram overlaps NB, RGL, PROG and midNESCs. Most DEG were cell type specific, although some cell types shared DEGs, which was especially the case between both mature neuronal clusters.

Next, a pathway enrichment analysis was performed MetaCore using the DEG across all cell types in midbrain organoids and assembloids (Figure 5A). The analysis revealed 12 significantly enriched biological pathways. Besides ribosomal and cytoskeletal genes, genes for oxidative

stress (10/160 genes), the immune response (12/242 genes) as well as neurogenesis and axonal guidance were significantly different (13/229). Interestingly, we found 10 enriched genes involved in hypoxia and oxidative stress. Among those, six genes showed a clear downregulation of this pathway in the presence of microglial cells; the expression of mitochondrial cytochrome oxidase 1 (complex IV) (*COX1*), peroxiredoxin1 (*PRDX1*), superoxide dismutase 1 (*SOD1*), glutathione peroxidase 4 (*GPX4*), ATPase (complex V) (*MT-ATP6*), as well as glutathione S-transferase 1 (*GSTP1*) was significantly lower in assembloids (Figure 5B).

Next, we assessed the 12 genes involved in the immune response and in the antigen presentation processes (Figure 5C). Indeed, non-microglial cells expressed genes from the MHCII such as *HLA-C* and *B*. Moreover, the *STAT2* and *STAT3* genes were upregulated in the presence of microglia. The MRC2 (ENDO180) receptor involved in collagen internalization and remodelling was upregulated, while genes involved in cytokine mediated phagocytosis (*ELMO1*) and autophagy (MAP1LC3A (LC3), SQSTM1 (p62)) were downregulated (Figure 5C). An enrichment analysis of the DEGs for each cell cluster showed differences in genes involved in immune response, inflammation, phagocytosis and response to hypoxia and oxidative stress, among others (Figure S4C).

Microglia are important to main brain homeostasis. However, neuro-inflammation might occur when this homeostasis is compromised. Therefore, we assessed the expression of genes involved in pyroptosis – inflammation related cell death through inflammasome activation – including CASP1, NLRP3, PYCARD (data not shown) PPIA (Figure S5A). Neuro-inflammation related genes were unchanged or decreased in assembloids, suggesting that presence of microglia in organoids does not lead to neuro-inflammation in physiological conditions.

Microglia affect the expression of synaptic remodelling-related genes in assembloids

Enrichment analysis of the DEGs for each cell cluster showed differences in genes involved in synaptic vesicle exocytosis, synaptic contact, synaptogenesis and axonal guidance in assembloids (Figure 5D and Figure S4C). To further investigate the microglia effects on synaptic pathways, we performed an extensive analysis of genes involved in synaptic processes. In assembloids, general synaptic markers such as *Synaptotagmin* (*SYT1*) and *Synaptophysin* (*SYP*), as well as the dopaminergic neuron circuit formation genes *ROBO1* and *DCC* were significantly downregulated across cell types (Figure 6A). Other important genes involved in synaptic vesicle exocytosis – such as *VMAT2* and *SNAP25* - were differentially expressed (Figure S5B). Moreover, we assessed axonal guidance and growth molecules, such as semaphorins

(*SEMA3C*, *DPYSL2*), plexins, ephrins (*EPHA5*), neuropilins, neurofilaments and actin cytoskeleton (*NEFM, ACTB*) (Figure S5C). These genes were all differentially expressed, depending on the cell type, indicating that axonal remodelling is influenced by the presence of microglia. Furthermore, we examined some cell specific genes in mature neurons involved in action potential (*CASK, CACNA1A, CACNA1E, CACNA1B*) and active zones (*HCN1, KCNC3, KCND3*) within synapses and observed that those genes are upregulated in assembloids (Figure 6B). Apart from assessing the synapse-related gene expression, we observed reduced protein levels of the synaptic vesicle protein VAMP2 in assembloids compared to midbrain organoids (Figure 6C). Together these results suggest a role of microglia in synaptic remodelling and maturation within midbrain organoids.

In order to investigate the functional impact of microglia in midbrain organoids we performed electrophysiological measurements of passive and active membrane properties as well as firing behaviour. We performed patch-clamp experiments of visually identified neurons in the intact organoids from 20 to 35 days after microglia addition (Figure 6D). Neurons in midbrain organoids and assembloids exhibited similar resting membrane potentials and input resistances and reliably fired repetitive action potentials in response to somatic current injections (n midbrain organoids =14; n assembloids = 13 cells; Figure S5D). Depolarizing steps in voltage-clamp configuration triggered strong inward currents in all tested neurons, indicative of fast voltage-activated sodium currents (Figure S5E). The amplitude of these currents was not different between both groups. Firing characteristics and action potential waveforms (Figure 6D) varied considerably, which was expected from neurons at different degrees of maturation. Importantly, the voltage threshold for the action potential generation was more negative in the group of assembloid neurons (-39.86 (midbrain organoids) against -36.35 (assembloids) ± 3.281, p=0.0480, Fig 6d), which is a common and strong indicator of increased neuronal excitability in mature neurons. In sum, neurons in assembloids develop fully mature electrophysiological properties with a lower threshold for action potential generation than in midbrain organoids. Furthermore, we performed multi-electrode array (MEA) analysis with midbrain organoids and assembloids containing microglia from line K7, 163 or EPI (Figure 6E). The results showed that, after 40 days of co-culture, which corresponds with the time point when the Patch clamp measurements were performed, assembloids had a lower interspike interval than midbrain organoids (Figure 6E). These results back up the observed lower action potential threshold observed in the patch-clamp experiment.

In order to support these findings and investigate further the differences between midbrain organoids and assembloids, we performed a non-polar exo-metabolomic analysis from culture

supernatants 20 days after microglia addition. The assay showed a different metabolic profile in midbrain organoids compared to assembloids (Figure S5F). A total number of 14 metabolites were significantly different. Among them, we observed a higher uptake of glucose and pyruvic acid from assembloids (Figure S6A). Regarding amino-acid metabolism, we observed a lower secretion of phenylalanine, tyrosine, methionine, lysine, putrescine, threonine, leucine, isoleucine and valine by the assembloids compared to midbrain organoids. Furthermore, the levels of uptaken asparagine and serine from the medium were higher in assembloids. The secretion of glutamine was higher assembloids (Figure S6B).

Discussion

Microglia can be efficiently integrated into Midbrain organoids

Here we described the generation of human midbrain assembloids containing microglia as well as the effect that microglia have on midbrain organoid structure and function. Although some studies have shown a microglia-like population in brain organoids (Mansour *et al.*, 2018; Ormel *et al.*, 2018), integration of human iPSC-microglia cells into midbrain organoids has not previously been reported. Moreover, particularly the assessment of how microglia are affecting brain organoid physiology is heavily under-investigated.

In this study, we have shown for the first time the successful incorporation of a significant amount of microglia into midbrain organoids, obtaining an average of 6.4% of IBA1 positive cells in assembloids. Studies based on immunocytochemistry show around 10% of IBA1 positive cells in human substantia nigra (Mittelbronn *et al.*, 2001). One of the main challenges we faced during the integration were the cytotoxic effects of the midbrain organoid medium on microglia, and the unsuitability of the microglia differentiation medium on the organoids. Interestingly, while TGF-beta 1 and 2 have been associated with microglia function and inflammatory response (Hu *et al.*, 1995; Lieb, Engels and Fiebich, 2003; WK *et al.*, 2004; Taylor *et al.*, 2017) , very little is known about the relationship between TGF-beta 3 and microglia. TGF-beta 3 has been associated with dopaminergic neuron differentiation (Roussa *et al.*, 2006), which is the reason why the dopaminergic neuron differentiation medium contains this recombinant molecule. However, no studies associating a beneficial relationship between TGF-beta3 and microglia have been found. We hypothesize that this subtype of the TFG-beta family may be acting differently than TGF-beta 1 and 2, since the 3D structure of TGF-beta 1 and 2 are considerably different than TGF-beta3, which could lead to functional differences with respect to their effect towards microglia (Andrew P. Hinck *et al.*, 1996; EV *et al.*, 2000; Grütter *et al.*, 2008). The absence of neurotrophic factors

– which promote dopaminergic differentiation – in the microglia differentiation medium, led to a significantly lower amount of dopaminergic neurons in midbrain organoids and assembloids. This incompatibility might be one of the reasons why, so far, no studies have shown an efficient co-culture of dopaminergic neurons with microglia. Here, we developed an optimized co-culture medium, which allowed the survival of microglia within the organoids as well as an efficient dopaminergic neuron differentiation. The incorporated microglia clustered separately from the cells of ectodermal origin in the midbrain organoids, showing that both cell lines keep their cellular identity under co-culture conditions. This is in line with in vivo development, as microglia are derived from primitive hematopoietic stem cells and as such have a completely different genetic signature (Alliot, Godin and Pessac, 1999; Ginhoux *et al.*, 2010; Schulz *et al.*, 2012). Unfortunately, and as stated before, the sample loss during the pre-processing for snRNA-Seq makes the cell proportions from the sequencing inaccurate. Thus, additional runs of sequencing would allow us to obtain more reliable results concerning the cell proportions. However, the obtained data is still of good quality to proceed with gene expression analysis for cell clustering and for assessing functionality-related genes. Apart from clustering separately from the rest of the assembloid cells, microglial cells express genetic markers for all the major functions of the human microglial core signature (Galatro *et al.*, 2017). This confirms that the population we integrated into the organoid is, indeed, microglial.

Until now, no studies analysed which effect the integration of microglia cells have on the functionality of midbrain organoids. Our data demonstrate that the integration of microglia influence neural stress, cell death, neuronal cyto-architecture and synapse remodelling- related gene expression in the neuronal network.

Microglia communicate with neurons and play a role in midbrain organoid stress response

Microglia have cell-cell communication ability through cytokine and chemokine signalling (Carbonell *et al.*, 2005; Arnò *et al.*, 2014; Siddiqui, Lively and Schlichter, 2016; Haenseler, Sansom, *et al.*, 2017). They can move towards apoptotic cells in order to phagocyte and eliminate cell debris (Chan *et al.*, 2003). Apoptotic neurons generate chemotactic signals recognized by microglial receptors, which attract them to the apoptotic area in order to phagocytose dying cells (Witting *et al.*, 2000). Our data suggest that microglia are functional in assembloids. Phagocytic genes were significantly expressed. These gene expression data were experimentally confirmed through a 2D Zymosan phagocytosis assay. Furthermore, our gene expression analysis via snRNA-Seq showed the expression of multiple cytokines and chemokines, as well as cyto- and

chemokine receptors, in microglia from assembloids. We also measured many cytokines and chemokines in culture media, and observed that their levels were significantly higher in assembloid medium compared to midbrain organoids medium. We observed a reduced size of assembloids compared to midbrain organoids, and a lower amount of dead cells in assembloids. These results lead us to hypothesize that microglia in assembloids may be attracted to apoptotic areas and phagocytose apoptotic cells and cell debris. High levels of cell death and absence of removal mechanisms for dead cells, particularly in the centre of organoids, was previously a key limitation of organoid technology (Berger *et al.*, 2018; Nickels *et al.*, 2020).

Previous work on organoids suggested that neurons in organoids have unusual high stress levels (Bhaduri *et al.*, 2020). Interestingly, the DEG analysis shows differences in oxidative cell stress-related genes (often linked to cell death). Moreover, the downregulation of autophagy within non-microglial cells might be linked to reduced overall stress due to starvation, which is in line with the increased metabolite uptake from the media. Additionally, the metabolomics analysis revealed a significantly lower amount of Leucine, Isoleucine, Valine, Phenylalanine and Tyrosine in the assembloid culture medium. Increased plasma levels of those metabolites have been associated with acute hypoxic exposure in rats (Muratsubaki and Yamaki, 2011).
We also observed upregulated genes involved in the immune response in assembloids. Non-microglial cells may have reacted towards microglia by upregulating antigen presenting factors, and STAT2 and STAT3 pathways involved in the inflammatory response. Although neuronal cells respond to microglia, no inflammasome activation was observed in the current study. This, together with reduced oxidative stress and cell death in assembloids, suggests that the communication could be neuroprotective. In addition, ER stress and UFPR remained unaffected or reduced in assembloids. Overall, these results indicates alterations in cell signalling, oxidative stress and inflammation. Further studies on cell death and oxidative stress would be of value to confirm the observed results and support our hypothesis.

Microglia induce alterations in synaptic gene expression in assembloids

In the current study, the expression of synaptic marker genes is reduced in assembloids. Furthermore, protein levels of the pre-synaptic protein VAMP2 were lower in assembloids compared to midbrain organoids. Physiologically, microglia are responsible, among other functions, for remodelling the cyto-architecture and connectivity of the brain by stripping unnecessary or misguided synapses (Wake *et al.*, 2009; Tremblay *et al.*, 2011). Here we could show that genes in axonal guidance and cytoskeletal organization are deregulated upon microglia presence. Moreover, whereas the expression of most synaptic genes are reduced, the expression

of genes involved in triggering action potential are increased. These results lead us to hypothesize that inactive synapses may be eliminated while active synapses are strengthened. This phenomenon would be in line with the previously described synaptic pruning function of microglia (Paolicelli *et al.*, 2011; Sellgren *et al.*, 2019). The metabolomics results may be supporting this theory; there was an increase in glucose metabolism in assembloids via a higher uptake of glucose and pyruvic acid from the medium. The higher metabolic activity in the glucose metabolism may indicate a higher need for substrates for the TCA cycle, which leads to amino-acid production and, eventually, to neuro-transmitter production (Tiwari, Ambadipudi and Patel, 2013). Further, we observed a lower release of methionine to the medium. Methionine is related to processes of neurotransmission and neuromodulation (Kurbat and Lelevich, 2009). The secretion of glutamine to the medium was higher in assembloids. Since this amino acid is directly linked to the neurotransmitter glutamate production, this might indicate a higher production of glutamate. The uptake of the amino acids phenylalanine and tyrosine was higher in assembloids. Interestingly, tyrosine can be metabolized from phenylalanine, which can be metabolized to L-DOPA and, after that, to dopamine (Weinberg *et al.*, 2019). Further experiments assessing synapse pruning would be of great value to confirm these observations.

Finally, the electrophysiology analysis showed that neurons in assembloids form a functional network. Interestingly, the voltage threshold for action potential generation, a common marker of neuronal excitability, was lower in assembloids compared to midbrain. Furthermore, the MEA results show a lower inter-spike interval in assembloids compared to midbrain organoids. Together with a tendency to higher membrane potentials, this indicates elevated levels of excitability in these neurons. Since the intrinsic excitability of neurons is often fine-tuned to the amount and frequency of external inputs and network activity, this change might in fact compensate for the possible degree of synaptic pruning previously discussed. Furthermore, these results are in line with previous reports, which describe that microglia increase neuronal excitability (Klapal, Igelhorst and Dietzel-Meyer, 2016).

Thus, our results suggest that microglia in assembloids may perform synaptic pruning, leaving the system with fewer inactive synapses. Microglia could strengthen and support active synapses, and lead to a more active TCA cycle in the assembloids. Furthermore, the electrophysiological properties of assembloids suggest a higher excitability of neurons.

Midbrain-microglia assembloids as a new model for neuro-inflammation in Parkinson's disease

Microglia play an important role in neurodegenerative diseases. Reactive microgliosis and neuro-inflammation are known to promote neuronal cell death and the pathophysiology of those disorders (Block, Zecca and Hong, 2007; Duffy *et al.*, 2018). Midbrain organoids have been used to model neurodegeneration in PD *in vitro* (Kim *et al.*, 2019; Smits *et al.*, 2019). However, until now, no 3D in vitro model for studying neuro-inflammation in PD was described. The new assembloid model presented here will enable to study reactive microgliosis and neuro-inflammation in PD. Furthermore, a personalized approach, in which patient-specific assembloids are used, can be assessed for genetic and idiopathic cases of PD. This opens doors to studies of neuro-inflammation related pathways and, to new therapeutic targets for compounds that focus on the immune system in the brain.

Resource availability

All original and processed data as well as scripts that support the findings of this study are public available at this https://doi.org/10.17881/cx25-ht49.

Author contributions

SSS designed and conducted the experiments, interpreted the data and drafted the manuscript. SLN analysed data. EB, UD, KB, YJL, TK, JJ, GR, Js, HK and CT conducted specific experiments. CS contributed to the manuscript. JWS, SC and JCS coordinated and conceptualized the study. All authors reviewed and approved the final manuscript and agreed to be accountable for their contributions.

Acknowledgments

The authors would like to thank Dr. Jared Sterneckert for providing us with the cells from K7 line, and Dr. Christine Klein from the Institute of Neurogenetics, University of Lübeck for providing the 163 line. J.J. is supported by a Pelican award from the Fondation du Pelican de Mie et Pierre Hippert-Faber. SLN is supported by the National Centre of Excellence in Research on Parkinson's Disease (NCER-PD) is funded by the Luxembourg National Research Fund (FNR/NCER13/BM/11264123). We thank the LCSB Metabolomics Platform, and specially Christian Jäger and Xiangyi Dong for their contribution to this manuscript. We also thank Dr. Paul

Antony and Dr. Silvia Bolognin for the development of the codes used in this study. The JCS lab is supported by the Fonds National de la Recherche (FNR) Luxembourg (PRIDE17/12244779/PARK-QC; FNR/PoC16/11559169, FNR/ NCER13/BM/11264123). This is an EU Joint Program - Neurodegenerative Disease Research (JPND) project (INTER/JPND/15/11092422). We also would like to thank the private donors who support our work at the Luxembourg Centre for Systems Biomedicine. JWS and JYL are supported by research grant to RIKEN Integrative Medical Sciences (IMS) from the Japanese Ministry of Education, Culture, Sports, Science and Technology (MEXT) and JYL is part of the International Program Associate (IPA) program in RIKEN.

Declaration of interests

JCS and JJ are co-founders and shareholder of the biotech company Organo Therapeutics SARL. This company used midbrain organoids and assembloids for in vitro disease modelling and drug discovery.

Ethics Statement

Written informed consent was obtained from all individuals who donated samples to this study and all work with human stem cells was done after approval of the national ethics board, Comité National d'Ethique de Recherche (CNER), under the approval numbers 201305/04 and 201901/01.

Rights retention statement

Methods

2D cell culture

iPSCs

Generation of iPSCs was performed as described in (Reinhardt *et al.*, 2013). iPSCs (Table S1) where cultured in Matrigel® (Corning, 354277) coated 6-well plates (Thermo Scientific, 140675), using Essential 8 Basal medium (Thermo Scientific, A1517001) supplemented with ROCK Inhibitor (Y-27632, Millipore, SCM075) for the first 24 hours after plating. The medium was exchanged on a daily basis. Confluence iPSCs (~70-90%) slipt using Accutase® (Sigma, A6964) and plated at around 300,000 cells per well. Neural progenitor cells needed to generated organoids were derived from iPSCs and maintained in culture as described previously (Smits *et al.*, 2019; Nickels *et al.*, 2020). iPSCs were also used to generate Macrophage precursors (van Wilgenburg *et al.*, 2013) and further differentiate them into microglia as described previously (Haenseler, Sansom, *et al.*, 2017).

Microglia

50K macrophage precursors were plated per well in a glass bottom 96-glass bottom well plate (IBL Baustoff, 220.230.042). Cells were cultured with microglia differentiation medium (Advanced DMEM/F12 (Thermo Fisher, 12634010), 1x N2 (Thermo Fisher, 17502001), 1x Pen/Strep (Invitrogen, 15140122), 1x GlutaMax (Thermo Fisher, 35050061), 50 µM 2-mercaptoethanol (Thermo Fisher, 31350-010), 100 ng/mL IL-34 (Peprotech, 200-34), 10 ng/mL GM-CSF (Peprotech, 300-03). Cells were kept in culture for 10 days, with a medium change every 3-4 days, and then fixed with 4 % formaldehyde (Millipore, 1.00496.5000) for immunostaining or used for a phagocytosis or MTT assay.

3D cell culture

Midbrain organoid generation and culture

Midbrain organoids generation is described in (Smits *et al.*, 2019; Nickels *et al.*, 2020). Shortly, 6,000 cells per well were seeded in an Ultra-Low Attachment 96-well Well plate (Merck, CLS3474) and kept under maintenance conditions (N2B27 medium supplemented with 0.2 mM Ascorbic acid (Sigma, A4544-100G), 3 µM CHIR 99021 (Axon,

CT 99021), 0.5 µM Smoothened Agonist (SAG, Stem cell technologies, 73412), , 2.5 µM SB-431542 (Abcam, ab120163), 0.1 µM LDN-193189 (Sigma, SML0559)) for 2 days. After that, we started the pre-patterning (day 0 of dopaminergic differentiation) by removing SB and LDN from the medium. Two days after, CHIR concentration was reduced to 0.7 µM. On day 6 of dopaminergic differentiation, the medium was changed into maturation medium (N2B27 plus 0.2 mM Ascorbic acid, 10ng/mL Brain Derived Neurotrophic Factor, BDNF (Peprotech, 450-02), 10 ng/mL Glial-Derived Neurotrophic Factor, GDNF (Peprotech, 450-10), 1pg/mL TGF-β3 (Peprotech, 100-36E), 0.5 mM db cAMP (Sigma, D0627-5X1G), 10 µM DAPT (R&D Systems, 2634/10) and 2.5ng/mL Activin A (Thermo Scientific, PHC9564)). Organoids were kept under static culture conditions with media changes every third day until day 15 of dopaminergic differentiation.

Medium optimization for co-culture with macrophage precursors

Two batches of organoids and assembloids were used for the media optimization. Midbrain organoids from line K7 were used as controls. Midbrain organoids from line K7 were co-cultured with macrophage precursors, either from line K7, 163 or EPI. Therefore, graphs indicating “Midbrain organoids” refer to K7 midbrain organoids, and “Assembloids” refer to pooled results from K7 organoids co-cultured with K7, 163 and EPI microglia separately. For the media test, midbrain organoids and assembloids were cultured in the previously described maturation medium until day 15 of dopaminergic differentiation. Then, independently of the addition or not of macrophage precursors, the medium was kept the same, exchanged by microglia differentiation medium or co-culture medium (Table S2; Advanced DMEM/F12, 1x N2 supplement, 1x GlutaMAX™, 50 µM 2-mercaptoethanol, 100 U/mL Penicillin-Streptomycin, 100ng/mL IL-34, 10 ng/mL GM-CSF, 10 ng/mL BDNF, 10 ng/mL GDNF, 10 µM DAPT and 2.5 ng/mL Activin A). We kept the culture until day 35 of differentiation, fixed with 4 % formaldehyde (Millipore, 1.00496.5000) and proceeded to immunofluorescence staining.

Co-culture of midbrain organoids with macrophage precursors

From day 15 of dopaminergic differentiation,– when the co-culture started - the culture medium of midbrain organoids and assembloids was replaced by co-culture medium containing 186,000 freshly harvested macrophage precursor cells per organoid. As described in the previous Methods and Results sections, K7 midbrain organoids were

used as controls, and K7 organoids were separately co-cultured with macrophage precursors from lines K7, 163 or EPI. The “Assembloids” group on graphs represent the pooled results from organoids co-cultured with the K7, 163 and EPI microglia lines. After, the plate was centrifuged at 100 xg for 3 minutes to promote the attachment of the cells to the surface of the organoids. Medium was changed every 2-3 days and the system was kept for 20 or 70 days (until day 35 or 85 of dopaminergic differentiation, respectively). Then, organoids and assembloids were snap-frozen for sequencing and protein extraction or fixed with 4 % formaldehyde (Millipore, 1.00496.5000) for immunofluorescence staining.

Phagocytosis assay

For immunofluorescence staining macrophage precursors were harvested and 30,000 cells per well were plated in 96-glass bottom well plates (IBL Baustoff, 220.230.042) and differentiated into microglia. At day 10, two Zymosan A (S. cerevisiae) BioParticles™ (Thermo Fisher, Z23373) per cell were added (60,000 particles / well). Then, cells were incubated for 30 minutes at 37C, washed with 1x PBS and fixed with 4 % formaldehyde (Millipore, 1.00496.5000). Then fixed samples were used for immunofluorescence staining. For live imaging (Video S1, S2 and S3), 100,000 cells per well were seeded in 8-well Nunc™ Lab-Tek™ Chamber Slides (Thermo Fisher, 177402PK) and immediately imaged.

Viability assay (MTT)

50K macrophage precursors were plated per well in a 96-glass bottom well plate (IBL Baustoff, 220.230.042). After 10 days of microglia differentiation induction, 10ul of 5 mg/ml MTT (3-[4,5-dimethylthiazol-2-yl]-2,5-diphenyltetrazolium bromide (Sigma, M2128)) were added to each well. Cells were incubated for 4h at 37C. Then, the medium was aspirated and 100ul of DMSO were added to each well, pipetting vigorously in order to detach and disrupt the cells. Absorbance was measure at 570 nm. Results were compared to midbrain organoid medium (MOm).

Immunofluorescence staining in 2D

Cells cultured in glass coverslips (150K cells/well) or 96-well imaging plates were fixed for 15 min with 4 % formaldehyde (Sigma, 100496) and washed 3x with PBS. Permeabilization was done by using 0.3% Triton X-100 in 1x PBS for 15 minutes. The cells were washed 3 times with PBS and blocked the cells with 3% BSA (Carl Roth, 80764) in PBS at room temperature. Cells were then incubated in a wet chamber, overnight (16h) at 4°C with the primary antibodies (diluted in 3%

BSA + 0.3% Triton X-100 in 1xPBS). Cells were rinsed 3 times with PBS and further incubated with secondary antibodies diluted in 3% BSA + 0.3% Triton X-100 in 1x PBS for 1 hour at room temperature. After 3 more PBS washes, the plates were directly imaged and the coverslips were mounted in a glass slide with Fluoromount-G® (Southern Biotech, Cat. No. 0100-01). The antibodies used are listed in Table S3.

Immunofluorescence staining in 3D

Midbrain organoids and assembloids were fixed with 4 % Formaldehyde overnight at 4 °C and washed 3 times with PBS for 15 min. Organoids were embedded in 4 % low-melting point agarose (Biozym, Cat. No. 840100) in PBS. 70 µm sections were obtained using a vibratome (Leica VT1000 S). We selected sections coming from the centre of the organoids and assembloids, rather than border sections. The sections were blocked with 0.5 % Triton X-100, 0.1 % sodium azide, 0.1 % sodium citrate, 2 % BSA and 5 % donkey serum in PBS for 90 min at room temperature. Primary antibodies were diluted in 0.1 % Triton X-100, 0.1 % sodium azide, 0.1 % sodium citrate, 2 % BSA and 5 % donkey serum and were incubated for 48 h at 4 °C in a shaker. After incubation with the primary antibodies (Table S3), sections were washed 3x with PBS and subsequently incubated with secondary antibodies (Table S3) in 0.05 % Tween-20 in PBS for 2 h at RT and washed with 0.05 % Tween-20 in PBS. Sections were mounted in Fluoromount-G mounting medium on a glass slide.

Imaging

Qualitative images were acquired with a confocal laser-scanning microscope (Zeiss LSM 710). For quantitative image analysis, the Operetta CLS High-Content Analysis System (Perkin Elmer) was used to automatically acquire 25 planes per organoid section, with an spacing between planes of 1 µm. Images were modified with the ZEN blue Software. For live imaging (supplemental videos), the Cell Observer SD and the CSU-X1 Spinning Disc Unit (ZEISS) were used. 100 frames were acquired in each video using the ZEN blue software, during 3054.06s (163 line), 3053.27s (EPI line) and 3053.66s (K7 line). The videos were processed and modified with Adobe Premiere and Screenpresso software in order to obtain a representative time-line of the phagocytosis process. The shown videos represent 29.97 frames per second, resulting on a total number of 659.34 frames (163 line), 689.31 frames (EPI line) and 449.55 frames (K7 line).

Image analysis

To measure the area of organoids and assembloids, we used ImageJ. We delimited the perimeter of the organoids and assembloids and used the “Measure” tool to obtain a pixel surface. Surfaces were then compared using Graphpad Prism and displayed as ‘fold change’ in graphs.

For immunofluorescence staining analysis, 3D images of midbrain organoids and assembloids were analysed in Matlab (Version 2017b, Mathworks) following (Bolognin *et al.*, 2019; Smits *et al.*, 2019). The in-house developed image analysis algorithms facilitate the segmentation of Nuclei, neurons and microglia, obtaining as a result the positive pixel surface for a selected marker. To estimate the Iba1 positive cell number, we used the *regionprops* Matlab function in 8 sections coming from 4 assembloids from 2 different batches. This function detected different a total number of 310 IBA1$^+$ events. We separated the Hoechst$^+$ detection by ‘live nuclei” (bigger and less intense) and “pyknotic nuclei” (smaller and more intense due to the chromatin condensation). A total number of 776 live nuclei and 4178 pyknotic nuclei were detected. After that, we averaged the volume results for IBA1, live nuclei and pyknotic nuclei, and we added a new line in the main image analysis function to automatically divide the IBA1 Mask (pixel volume) by the averaged IBA1 volume number previously calculated. We did the same for the live nuclei, obtaining then an approximate IBA1$^+$ cell number, and live nuclei number. We obtained the percentage of IBA1$^+$ cells following this formula: (IBA1$^+$ cell number /live nuclei number) x 100. The reason why we used the live nuclei number is that dead cells may lose the IBA1 expression.

Western blot

Protein was extracted from midbrain organoids from 3 batches, and from assembloids with microglia from line K7, 163 and EPI from 3 batches. Protein extraction was done from 5 or 4 pooled organoids using the 1x RIPA buffer (Abcam, ab156034) containing 1x Phosphatase inhibitor cocktail (Merck Millipore, 524629-1ML) and 1x cOmplete™ Protease Inhibitor Cocktail (Sigma, 11697498001). The lysates were sonicated in the Bioruptor (Diagenode) for 10 cycles of 30 sec on and 30 sec off. The amount of protein was measured using the Pierce BCA Protein Assay Kit (Thermofisher, 23227) and the BIOTEK Cytation 5 Imaging reader. 30 µg of protein was used from each sample in the western blot. 6x loading buffer containing 0.375M Tris (MW 121.14 g/mol), 9% SDS, 50% Glycerol, 0.2% Bromphenolblue, 0.3M DTT was added in each sample and boiled at 95oC for 5 min. The protein samples were loaded into precast polyacrylamide gels (Thermofisher, NW04120BOX). The iBlot2 device from Invitrogen was used

for transferring the proteins from the gel to PVDF membranes (Thermofisher, IB24001). The membranes were blocked in 1xPBS containing 0.2% Tween-20 and 5% Milk in for 60 min at RT. Primary antibodies were incubated in 1XPBS containing 0.02% Tween-20, 5% BSA at 4°C overnight. Secondary antibodies were incubated for 60 min at RT in the same buffer as the one for primary antibodies. Enhanced fluorescent signal was detected in the LI-COR OdysseyFc imaging system. Band quantifications were performed with ImageJ and statistics were run using GraphPad Prism. A Mann-Whitney test was run to compare the midbrain organoid against the assembloid group.

RT-PCR

Between one and three million microglia cells were used per RNA extraction. We used the RNeasy Mini Kit (Qiagen) as well as DNase I Amplification Grade (Sigma-Aldrich) to isolate RNA. After conducting reverse395 transcription by following the protocol of the High Capacity RNA to DNA Kit (Thermo Fisher Scientific), RT–PCRs were performed using GreenTaq polymerase and 50ng of cDNA per reaction. An initial denaturing step, 5 min at 95 °C, 40 cycles of denaturation for 30 s at 95 °C, annealing for 45 s at 55 °C (for Iba-1, CD68, and TMEM119) or 61 °C (for RPL37A and P2RY12), extension for 30 s at 72 °C and a final extension for 5 min at 72 °C. The used primers are listed in Table S4.

Cytokine and chemokine release assay

Cytokine and chemokine measurements were performed using the Human XL Cytokine Discovery Luminex® Performance Assay (RD Systems, #FCTSM18). We collected supernatants from three midbrain organoid and assembloid batches and three biological replicates (microglia lines K7, 163 and EPI). When values were too low to be detected, they appeared as ‘out of range’. In order to consider them statistically, they were assigned the lowest measured value of the standard curve for that metabolite. The statistics were run with three batches and three cell lines for the assembloid group (midbrain organoids vs assembloids K7, 163 and EPI).

Metabolomics

For the extracellular metabolomics analysis, we used snap frozen media from 20 days of co-culture old midbrain organoids or assembloids after 48h of culture. We also incubated co-culture media, not in contact with organoids, as a control. 3 organoids or assembloids were used per batch, 3 batches were analysed, and the 3 different cell lines were used for the assembloid group.

From the measured results, the control (basal medium) was subtracted in order to discriminate secreted (positive numbers) against uptaken (negative numbers) metabolites.

Polar metabolite extraction, derivatization, and GC-MS measurement

Extracellular metabolites from media samples were extracted using a methanolic extraction fluid (5:1, methanol/water mixture, v/v). The water fraction contained two internal standards Pentanedioic acid-D6 (c = 10 µg/mL; C/D/N Isotopes Inc.) and [UL-13C5]-Ribitol (c = 20 µg/mL; Omicron Biochemicals). 40 µL of medium was added to 240 µL ice-cold extraction fluid. After adding 100 µl ice-cold chloroform, the mixture was shaken for 5 min at 4 °C. For phase separation, 100 µl chloroform and 100 µl water were added and vortexed for 1 min. Then, the mixture was centrifuged at 21,000 xg for 5 min at 4 °C. 250 µL of the polar (upper) phase was transferred to GC glass vial with micro insert (5-250 µL) and evaporated to dry under vacuum at -4 °C.

Metabolite derivatization was performed by using a multi-purpose sample preparation robot (Gerstel). Dried medium extracts were dissolved in 30 µl pyridine, containing 20 mg/mL methoxyamine hydrochloride (Sigma-Aldrich), for 120 min at 45 °C under shaking. After adding 30 µl N-methyl-N-trimethylsilyl-trifluoroacetamide (Macherey-Nagel), samples were incubated for 30 min at 45 °C under continuous shaking.

GC-MS analysis was performed by using an Agilent 7890A GC coupled to an Agilent 5975C inert XL Mass Selective Detector (Agilent Technologies). A sample volume of 1 µl was injected into a Split/Splitless inlet, operating in split mode (10:1) at 270 °C. The gas chromatograph was equipped with a 30 m (I.D. 0.25 mm, film 0.25 µm) DB-5ms capillary column (Agilent J&W GC Column) with 5 m guard column in front of the analytical column. Helium was used as carrier gas with a constant flow rate of 1.2 ml/min. The GC oven temperature was held at 90 °C for 1 min and increased to 220 °C at 10 °C/min. Then, the temperature was increased to 280 °C at 20 °C/min followed by 5 min post run time at 325 °C. The total run time was 22 min. The transfer line temperature was set to 280 °C. The MSD was operating under electron ionization at 70 eV. The MS source was held at 230 °C and the quadrupole at 150 °C. Mass spectra were acquired in full scan mode (m/z 70 to 700).

Data normalization and data processing

All GC-MS chromatograms were processed using MetaboliteDetector, v3.220190704 (REF). Compounds were annotated by retention time and mass spectrum using an in-house mass spectral library. The internal standards were added at the same concentration to every medium sample to correct for uncontrolled sample losses and analyte degradation during metabolite extraction. The data set was normalized by using the response ratio of the integrated peak area_analyte and the integrated peak area_internal standard. The results correspond to triplicates from three co-cultured batches and three biological replicates (midbrain organoids against assembloids with microglia from lines K7, 163 and EPI).

Patch clamp

Passive and active electrophysiological properties of cells in assembloids (with microglia from line 163) and midbrain organoids were characterized by whole-cell patch-clamp recordings in voltage and current clamp.

Each organoid was transferred from the incubator to a submerged type recording chamber with constant perfusion of carbogen-buffered artificial cerebrospinal fluid (ACSF) at 32°C. The ACSF contained (in mM): 124 NaCl, 3 KCl, 1.8 MgSO4, 1.6 CaCl2, 10 glucose, 1.25 NaH2PO4, 26 NaH2CO3 with an osmolarity of 295 mOsm/l. The organoid was fixated between a large diameter pipette and a custom made platinum harp. Cells were visualized using phase-contrast on an upright BX51 microscope (Olympus, Hamburg, Germany) with a 60x water-immersion objective. Recording electrodes were pulled using borosilicate glass on a Flaming/Brown P-97 Puller (Sutter Instrument, Novato, CA, USA) to yield a resistance of 3–6 MΩ. The electrode solution contained (in mM): 126 potassium gluconate, 4 KCl, 10 HEPES, 0.3 EGTA, 4 MgATP, 0.3 Na2GTP, and 10 phosphocreatine adjusted to pH 7.2 using KOH and to 288 mOsm/l by adding sucrose. Recordings were obtained in voltage and current-clamp mode with an ELC-03XS amplifier (NPI electronic, Tamm, Germany). Signals were low-pass filtered at 3 kHz and digitized with 20 kHz using a Micros 1401MKII AC-converter (CED, Cambridge, UK). Data were collected using the Signal 4.10 software (CED). Voltages were not corrected for the calculated liquid-junction potential of +14.5 mV. Test pulses of -50 pA and 100 ms were applied regularly to control for changes in series resistance.

Putative neurons were visually identified by their size and shape. After obtaining the whole-cell configuration, the resting membrane potential was determined in current clamp and the cell subsequently stabilized at -70 mV by continuous current injection. To assess active and passive membrane properties, hyper- and depolarizing current steps were injected at increments of 10 pA and of 500 ms length starting from -50 pA. Passive parameters were assessed by the smallest negative current step that yielded a constant plateau potential, which varied due to the heterogeneity of input resistances. To measure maximum firing rates, cells were depolarized by voltage steps of increasing amplitudes until APs started to fail due to sodium channel inactivation (up to +500 pA depending on input resistance). Action potential waveforms characteristics were analyzed for the first action potential that fired 50 ms after the onset of current injections. The voltage threshold was defined as the potential at which the rising slope exceeded 5 mV/ms and amplitudes were measured from threshold to peak. In voltage-clamp mode, cells were held at -70 mV and positive voltage steps of 300 ms duration and 10 mV increments were applied every 5 s. Maximal voltage was +30 mV. The power of voltage-gated cation channels (predominantly sodium) was quantified at -30mV and used for statistical comparison. Data analysis was performed using Stimfit (Guzman, 2014) and custom-written Phyton routines. Values were tested for Gaussian distribution by D'Agostino-Pearson omnibus normality test. Unpaired t-tests were used to assess statistical significance in normally distributed data and Mann-Whitney tests for non-normally distributed data (indicated as p in Figures). Outliers deviating 2.5 standard deviations were excluded from statistical analysis but indicated in the Figures.

The presence of microglia in the recorded assembloids was confirmed using immunohistochemical staining and confocal imaging. Organoids were fixed in 4% formaldehyde and stained for nuclei (Fluoroshield with DAPI, Sigma-Aldrich), neuronal markers (MAP2, Sigma-Aldrich Chemie GmbH), and microglia (anti-Iba1, WAKO Chemicals). Imaging was carried out on an A1 Nikon confocal microscope at the Nikon Imaging Center Heidelberg, Germany.

Statistical analyses

First, Gaussian distribution was evaluated by performing D'Agostino & Pearson omnibus normality test. According to this distribution, either a 1way ANOVA or a Kruskal-Wallis test with a Dunnett's test for multiple comparisons were used to evaluate statistical significance. For the pooled results (organoids against assembloids), Gaussian distribution was also tested. Depending on the outcome, an unpaired t-test or Mann-Whitney test was used to assess the difference between groups. Outliers deviating 2.5 standard deviations were excluded from statistical analysis but indicated in the Figures.

Cells that showed a resting membrane potential above -40 mV and action potentials shorter than 50 mV and wider than 3 ms in half-width were excluded from analysis, assuming that these cells were either not fully matured neurons or recording conditions were poor. The presence of microglia in the recorded organoids was confirmed using immunohistochemical staining and confocal imaging. For the image analysis, a 2way ANOVA, Tukey's multiple comparisons test was performed to evaluate statistical significance. Data is presented as mean ± SEM. All analyses were performed with three different biological replicates (assembloids microglia from three different cell lines).

Multi-electrode array (MEA)

48-well MEA plates (Axion, M768-tMEA-48B-5) were coated as follows: 24 h incubation with 0.1 mg/ml poly-D-lysine (Sigma, P7886) followed by a 24 h incubation with 1 mg/ml laminin (Sigma, L2020). At day 20 of co-culture (or 35 days of dopaminergic differentiation), midbrain organoids and assembloids were transferred to 48-well pre-coated MEA plates. Midbrain organoids and assembloids were placed in the centre of the wells, and left in the incubator for 25 minutes to ensure the maximum media evaporation and adherence of the organoids and assembloids to the well bottom. Then, we added 25 ul of Geltrex (Invitrogen, A1413302) to the top, to avoid the detachment from the wells. Data was acquired with an Axion Maestro Multiwell 768-channel MEA System (Axion Biosystems) and using the Axis software (Axon Biosystems). Data was exported and analysed using the available R script (see ‘Resource availability’).

Single-nuclei RNA sequencing (snRNAseq)

Five snap-frozen organoids or assembloids from one batch per condition were used to perform snRNAseq.

Data generation

Whole frozen organoids and assembloids (with microglia from lines K7, 163 and EPI) were dissociated for generating single-nuclei gene-expression libraries. The following steps were performed on ice using chilled and freshly prepared buffers. In brief, organoids and assembloids were gently dissociated using 500 mL of 0.1X Lysis Buffer (10 mM Tris-HCl pH 7.4, 10 mM NaCl, 3 mM MgCl2, 0.1% Tween-20, 0.1% Nonidet P40 Substitute, 0.01% digitonin, 1% BSA, nuclease-free water) by pipetting 10X with a wide-pore 1000 µL pipette, followed by a 10 min incubation period on ice. This was repeated for 2 cycles. To reduce batch effects and increase the number of nuclei per experiment, material from 4 different

organoids or assembloids were pooled for each group. Cells were filtered through a 40-µM strainer using 300 µL at a time, using a new 40-µM strainer. The same procedure was done with 20-µM (Sysmex, AN777717) and 10-µM (Sysmex, AP275603) strainers, followed by centrifugation for 5 min at 500 xg, at 4°C. Nuclei were then stained using Hoechst 33342 (1:2000) for 5 min at room temperature and counted on the Countess II. Using Diluted Nuclei Buffer (10x Genomics, 2000153) each sample was adjusted to a concentration of 4000 nuclei/µL. We generated one library for each sample, aiming for 6000 nuclei. Single-nuclei experiments were performed using the 10x Genomics Next GEM Single Cell 5′ Library Kit v1.1 (1000168) to encapsulate nuclei and amplify cDNA, to generate sequencing libraries. Each library was barcoded using i7 barcodes provided by 10x Genomics. cDNA and sequencing library quality and quantity were determined using Agilent's High Sensitivity DNA Assay (5067-4626) and KAPA (KK4824). Final libraries were pooled, loaded on two lanes of the Illumina's HiSeq X and sequenced in 150PE mode.

Count matrix generation

Following steps are performed on default settings if not otherwise specified. Single-nucleus libraries were demultiplexed based on their i7 index sequences and for each library mapping to the human genome was performed using the Cell Ranger 4.0.0 software and human reference GRCh38 3.0.0, both provided by 10x Genomics. Next, count matrix files for each sample were generated using cellranger count.

Data pre-processing

Since the material coming from assembloids with the EPI microglia line was lost, count matrixes for the assembloids with K7 and 163 microglia, as well as the midbrain organoid control were uploaded and Seurat Objects were created. Data was pre-processed as described by https://satijalab.org/seurat/v3.2/pbmc3k_tutorial.html. An independent data quality control was performed of all three objects, by checking levels of ribosomal genes, and by removing cells with a high mitochondrial gene fraction (Lake *et al.*, 2019; D and JJ, 2021). Moreover, cells containing less than 100 or more than 5000 (100 < RNA n Feature < 5000) genes were removed from the analysis, being considered empty droplets or doublets, respectively. After quality assessment all three objects were combined, log normalized, scaled, and a linear dimensional reduction was performed (PCA).

Dimensionality was assessed (20) and cells were clustered with a resolution of 0.5. A non-linear dimensional reduction using “umap” was performed, and cluster markers were assessed. Cluster names were defined by their characteristic marker gene expression.

Cell type identification

Cell clustering was performed based on the top 20 principal components using Louvain algorithm modularity optimization with a resolution of 0.5. UMAP was used for cell cluster visualization (Becht *et al.*, 2018). The distinct cell clusters were identified in the UMAP plot. For cell type identification, binarized gene list across cell types from La Manno et al., 2016 was used. This list of genes comprises information about the marker genes in a binarized manner, where 1 means that gene is marking a specific cell population and 0 means that it cannot be considered as a marker gene. For more details on how this list is generated please refer to La Manno et al., 2016. Expression of each cluster defining gene was overlapped with the marker gene (1) in the La Manno marker matrix. Cell types were assigned based on the highest number of major cluster marker genes being expressed in the respective clusters. Cellular subtypes were verified and grouped in neuronal identity clusters based on neuronal marker gene lists (Table S5). (Chen *et al.*, 2016; Smits *et al.*, 2020). Moreover manual marker verifications were done using known marker genes for each cluster. For instance, RGLs expressed *SLC1A3 (Glast*). MidNESCs expressed midbrain markers *SHH*, *LMX1A* and *FOXA2* and stem cell markers *SOX2* and *MSI1* (*Musashi*). PROG highly expressed *VIM (Vimentin*) and lower levels of stem cell markers. NB were positive for young neuronal markers *DCX* (*doublecortin*) and *STMN1* (*sthaminin*) without expressing mature neuronal markers. YDN&CN still expressed *DCX* and *STMN1* but also some mature neuronal markers for synapses such as *SYP (synaptophysin*) and subtype specification markers such as *TH* (dopaminergic neurons) and *SLC18A3* (cholinergic neurons). Mature neurons expressed low levels of *STMN1* and *DCX* but high levels of *SYP*. Subtype specification revealed that mDN(A10)&GaN&GlN expressed high levels of genes that define neurons from the ventral tegmental area (VTA). Besides, cells expressing dopaminergic marker *TH* also expressed the marker for A10 DN *CALB1*, as well as *ADCYAP1*. Moreover, the glutamatergic *SLC18A1* and GABAergic *GAD1* transporters were highly expressed in these neurons. Last mDN(A9)&SN were qualified by high amounts of *TH* and KCNJ6 (*Girk2)* as well as DN defining synaptic markers *ROBO1*. Moreover, also serotonergic transporters *SLC*18A2 were expressed in that cluster. Microglial cells expressed *IBA1.* Cell type proportions were calculated by counting

the cells of each cluster. A spearman correlation and a heatmap clustering (pheatmap) were performed on the average expression of clusters defining genes. Because of a substantial sample loss during sample processing, that affected the microglia cell count,. 26 microglial cells were detected (Table S6). The microglial cluster, 26 cells, was subsetted and an independent analysis was performed. The top 100 genes defining the microglial cluster are shown in a heatmap. Moreover, the average gene expression across all microglial cells was exported, and representative genes (Galatro et al. 2017). are presented in a violin plot. Significances were calculated based on a one sample Wilcoxon test *p<0.05. The same was done for genes involved in the phagocytic pathway. Cytokines and chemokines were represented in a heatmap.

Differential expressed gene and enrichment analysis

The most variable features were identified and a heatmap clustering (pheatmap) was performed on the average expression of the top 100 most variable genes. DEG were identified between assembloids and midbrain organoids. This was done for all the cell types together and each cell type independently. Data of the DEG lists is represented in heatmaps (top 100), or underwent metacore enrichment analysis. Metacore analysis was based on the following arbitrary threshold p<0.05, adj p<0.5. Moreover, Venn diagrams were formed using nVenn http://degradome.uniovi.es/cgi-bin/nVenn/nvenn.cgi. Genes involved in the enriched pathways are shown separately in box plots. Statistics were performed using a Wilcoxon test p<0.05*.

References

Abud, E. M. *et al.* (2017) 'iPSC-Derived Human Microglia-like Cells to Study Neurological Diseases', *Neuron*. Cell Press, 94(2), pp. 278-293.e9. doi: 10.1016/j.neuron.2017.03.042.

Alliot, F., Godin, I. and Pessac, B. (1999) 'Microglia derive from progenitors, originating from the yolk sac, and which proliferate in the brain', *Developmental Brain Research*. Elsevier, 117(2), pp. 145–152. doi: 10.1016/S0165-3806(99)00113-3.

Andrew P. Hinck, § *et al.* (1996) 'Transforming Growth Factor β1: Three-Dimensional Structure in Solution and Comparison with the X-ray Structure of Transforming Growth Factor β2†,‡', *Biochemistry*. American Chemical Society , 35(26), pp. 8517–8534. doi: 10.1021/BI9604946.

Arnò, B. *et al.* (2014) 'Neural progenitor cells orchestrate microglia migration and positioning into the developing cortex', *Nature Communications*. Nature Publishing Group, 5. doi: 10.1038/ncomms6611.

Becht, E. *et al.* (2018) 'Dimensionality reduction for visualizing single-cell data using UMAP', *Nature Biotechnology*, 37(1), pp. 38–47. doi: 10.1038/nbt.4314.

Berger, E. *et al.* (2018) 'Millifluidic culture improves human midbrain organoid vitality and differentiation', *Lab on a Chip*. Royal Society of Chemistry, 18(20), pp. 3172–3183. doi: 10.1039/c8lc00206a.

Bhaduri, A. *et al.* (2020) 'Cell stress in cortical organoids impairs molecular subtype specification', *Nature*. Nature Research, 578(7793), pp. 142–148. doi: 10.1038/s41586-020-1962-0.

Birey, F. *et al.* (2017) 'Assembly of functionally integrated human forebrain spheroids', *Nature*. Nature Publishing Group, 545(7652), pp. 54–59. doi: 10.1038/nature22330.

Block, M. L., Zecca, L. and Hong, J.-S. (2007) 'Microglia-mediated neurotoxicity: uncovering the molecular mechanisms.', *Nature reviews. Neuroscience*, 8(1), pp. 57–69. doi: 10.1038/nrn2038.

Bolognin, S. *et al.* (2019) '3D Cultures of Parkinson's Disease-Specific Dopaminergic Neurons for High Content Phenotyping and Drug Testing', *Advanced Science*. Wiley-Blackwell, 6(1). doi: 10.1002/ADVS.201800927.

Bradburn, S., Murgatroyd, C. and Ray, N. (2019) 'Neuroinflammation in mild cognitive impairment and Alzheimer's disease: A meta-analysis', *Ageing Research Reviews*. Elsevier Ireland Ltd, pp. 1–8. doi: 10.1016/j.arr.2019.01.002.

Carbonell, W. S. *et al.* (2005) 'Migration of perilesional microglia after focal brain injury and modulation by CC chemokine receptor 5: An in situ time-lapse confocal imaging study', *Journal of Neuroscience*. J Neurosci, 25(30), pp. 7040–7047. doi: 10.1523/JNEUROSCI.5171-04.2005.

Chan, A. *et al.* (2003) 'Phagocytosis of apoptotic inflammatory cells by microglia and its therapeutic implications: Termination of CNS autoimmune inflammation and modulation by interferon-beta', *GLIA*. Glia, 43(3), pp. 231–242. doi: 10.1002/glia.10258.

Chen, X. *et al.* (2016) 'Coupled electrophysiological recording and single cell transcriptome analyses revealed molecular mechanisms underlying neuronal maturation', *Protein and Cell*. Higher Education Press, 7(3), pp. 175–186. doi: 10.1007/s13238-016-0247-8.

Choi, S. H. *et al.* (2008) 'FAD-linked human Presenilin 1 variants impair environmental enrichment-induced hippocampal neural progenitor cell proliferation and differentiation in a non-cell-autonomous manner', *Neuron*. NIH Public Access, 59(4), p. 568. doi: 10.1016/J.NEURON.2008.07.033.

Choi, S. H. *et al.* (2014) 'A three-dimensional human neural cell culture model of Alzheimer's disease', *Nature*. Nature Publishing Group, 515(7526), pp. 274–278. doi: 10.1038/nature13800.

Osorio, D. and Cai, JJ. (2021) 'Systematic determination of the mitochondrial proportion in human and mice tissues for single-cell RNA-sequencing data quality control', *Bioinformatics (Oxford, England)*. Bioinformatics, 37(7), pp. 963–967. doi: 10.1093/BIOINFORMATICS/BTAA751.

Duffy, M. F. *et al.* (2018) 'Lewy body-like alpha-synuclein inclusions trigger reactive microgliosis prior to nigral degeneration', *Journal of Neuroinflammation*. BioMed Central Ltd., 15(1). doi: 10.1186/s12974-018-1171-z.

Bocharov, E. V. et al. (2000) 'Sequence-specific 1H and 15N assignment and secondary structure of transforming growth factor beta3', *Journal of biomolecular NMR*. J Biomol NMR, 16(2), pp. 179–180. doi: 10.1023/A:1008315600134.

La Manno, G. et al. (2016) 'Molecular Diversity of Midbrain Development in Mouse, Human, and Stem Cells', *Cell*. Cell, 167(2), pp. 566-580.e19. doi: 10.1016/J.CELL.2016.09.027.

Galatro, T. F. *et al.* (2017) 'Transcriptomic analysis of purified human cortical microglia reveals age-associated changes', *Nature Neuroscience*. Nature Publishing Group, 20(8), pp. 1162–1171. doi: 10.1038/nn.4597.

Ginhoux, F. *et al.* (2010) 'Fate mapping analysis reveals that adult microglia derive from primitive macrophages', *Science*, 330(6005), pp. 841–845. doi: 10.1126/science.1194637.

Gomez-Giro, G. *et al.* (2019) 'Synapse alterations precede neuronal damage and storage pathology in a human cerebral organoid model of CLN3-juvenile neuronal ceroid lipofuscinosis', *Acta Neuropathologica Communications*. BioMed Central Ltd., 7(1). doi: 10.1186/s40478-019-0871-7.

Grütter, C. *et al.* (2008) 'A cytokine-neutralizing antibody as a structural mimetic of 2 receptor interactions', *Proceedings of the National Academy of Sciences of the United States of America*, 105(51), pp. 20251–20256. doi: 10.1073/pnas.0807200106.

Haenseler, W., Sansom, S. N., *et al.* (2017) 'A Highly Efficient Human Pluripotent Stem Cell Microglia Model Displays a Neuronal-Co-culture-Specific Expression Profile and Inflammatory Response', *Stem Cell Reports*. ElsevierCompany., 8(6), pp. 1727–1742. doi: 10.1016/j.stemcr.2017.05.017.

Haenseler, W., Zambon, F., *et al.* (2017) 'Excess α-synuclein compromises phagocytosis in iPSC-derived

macrophages', *Scientific Reports*. Springer US, 7(1), pp. 1–11. doi: 10.1038/s41598-017-09362-3.

Hu, S. *et al.* (1995) 'Cytokine modulation of murine microglial cell superoxide production', *Glia*. John Wiley & Sons, Ltd, 13(1), pp. 45–50. doi: 10.1002/GLIA.440130106.

Jo, J. *et al.* (2016) 'Midbrain-like organoids from human pluripotent stem cells contain functional dopaminergic and neuromelanin producing neurons', *Cell stem cell*. NIH Public Access, 19(2), p. 248. doi: 10.1016/J.STEM.2016.07.005.

Kim, H. *et al.* (2019) 'Modeling G2019S-LRRK2 Sporadic Parkinson's Disease in 3D Midbrain Organoids', *Stem Cell Reports*. ElsevierCompany., 12(3), pp. 518–531. doi: 10.1016/j.stemcr.2019.01.020.

Klapal, L., Igelhorst, B. A. and Dietzel-Meyer, I. D. (2016) 'Changes in neuronal excitability by activated microglia: Differential Na+ current upregulation in pyramid-shaped and bipolar neurons by TNF-α and IL-18', *Frontiers in Neurology*. Frontiers Media S.A., 7(MAR). doi: 10.3389/fneur.2016.00044.

Kurbat, M. N. and Lelevich, V. V. (2009) 'Metabolism of amino acids in the brain', *Neurochemical Journal*. Springer, pp. 23–28. doi: 10.1134/S1819712409010036.

Lake, B. B. *et al.* (2019) 'A single-nucleus RNA-sequencing pipeline to decipher the molecular anatomy and pathophysiology of human kidneys', *Nature Communications*. Springer US, 10(1), pp. 1–15. doi: 10.1038/s41467-019-10861-2.

Lancaster, M. A. *et al.* (2013) 'Cerebral organoids model human brain development and microcephaly', *Nature*, 501(7467), pp. 373–379. doi: 10.1038/nature12517.

Li, Q. and Barres, B. A. (2017) 'Microglia and macrophages in brain homeostasis and disease', *Nature Publishing Group*. Nature Publishing Group, 18(4), pp. 225–242. doi: 10.1038/nri.2017.125.

Lieb, K., Engels, S. and Fiebich, B. L. (2003) 'Inhibition of LPS-induced iNOS and NO synthesis in primary rat microglial cells', *Neurochemistry International*, 42(2), pp. 131–137. doi: 10.1016/S0197-0186(02)00076-1.

Lindborg, B. A. *et al.* (2016) 'Rapid Induction of Cerebral Organoids From Human Induced Pluripotent Stem Cells Using a Chemically Defined Hydrogel and Defined Cell Culture Medium', *STEM CELLS Translational Medicine*. Wiley, 5(7), pp. 970–979. doi: 10.5966/sctm.2015-0305.

Mansour, A. A. *et al.* (2018) 'An in vivo model of functional and vascularized human brain organoids', *Nature Biotechnology*. Nature Publishing Group, 36(5), pp. 432–441. doi: 10.1038/nbt.4127.

Marton, R. M. and Pașca, S. P. (2020) 'Organoid and Assembloid Technologies for Investigating Cellular Crosstalk in Human Brain Development and Disease', *Trends in Cell Biology*, 30(2), pp. 133–143. doi: 10.1016/j.tcb.2019.11.004.

Mittelbronn, M. *et al.* (2001) 'Local distribution of microglia in the normal adult human central nervous system differs by up to one order of magnitude', *Acta Neuropathologica*. Acta Neuropathol, 101(3), pp. 249–255. doi: 10.1007/s004010000284.

Monzel, A. S. *et al.* (2017) 'Derivation of Human Midbrain-Specific Organoids from Neuroepithelial Stem Cells', *Stem Cell Reports*, 8(5), pp. 1144–1154. doi: 10.1016/j.stemcr.2017.03.010.

Muffat, J. *et al.* (2016) 'Efficient derivation of microglia-like cells from human pluripotent stem cells', *Nature Medicine*. Nature Publishing Group, 22(11), pp. 1358–1367. doi: 10.1038/nm.4189.

Muratsubaki, H. and Yamaki, A. (2011) 'Profile of plasma amino acid levels in rats exposed to acute hypoxic hypoxia', *Indian Journal of Clinical Biochemistry*. Indian J Clin Biochem, 26(4), pp. 416–419. doi: 10.1007/s12291-011-0125-3.

Nickels, S. L. *et al.* (2020) 'Reproducible generation of human midbrain organoids for in vitro modeling of Parkinson's disease', *Stem Cell Research*. Elsevier B.V., 46. doi: 10.1016/j.scr.2020.101870.

Ormel, P. R. *et al.* (2018) 'Microglia innately develop within cerebral organoids', *Nature Communications*. Springer US, 9(1). doi: 10.1038/s41467-018-06684-2.

Paolicelli, R. C. *et al.* (2011) 'Synaptic pruning by microglia is necessary for normal brain development', *Science*. Science, 333(6048), pp. 1456–1458. doi: 10.1126/science.1202529.

Pasca, S. P. (2019) 'Assembling human brain organoids', *Science*, 363(6423), pp. 126–127. doi: 10.1126/science.aau5729.

PR, O. *et al.* (2018) 'Microglia innately develop within cerebral organoids', *Nature communications*. Nat Commun, 9(1). doi: 10.1038/S41467-018-06684-2.

Qian, X. *et al.* (2016) 'Brain-Region-Specific Organoids Using Mini-bioreactors for Modeling ZIKV Exposure', *Cell*. Cell Press, 165(5), pp. 1238–1254. doi: 10.1016/j.cell.2016.04.032.

Ramani, A. *et al.* (2020) 'SARS-CoV-2 targets neurons of 3D human brain organoids', *The EMBO Journal*. John Wiley & Sons, Ltd, 39(20), p. e106230. doi: 10.15252/EMBJ.2020106230.

Reinhardt, P. *et al.* (2013) 'Correction: Derivation and Expansion Using Only Small Molecules of Human Neural Progenitors for Neurodegenerative Disease Modeling', *PLoS ONE*. Public Library of Science (PLoS), 8(11), p. 59252. doi: 10.1371/annotation/6a917a2e-df4a-4ad9-99bb-6aa7218b833e.

Roussa, E. *et al.* (2006) 'Transforming Growth Factor β Is Required for Differentiation of Mouse Mesencephalic Progenitors into Dopaminergic Neurons In Vitro and In Vivo: Ectopic Induction in Dorsal Mesencephalon', *STEM CELLS*. John Wiley & Sons, Ltd, 24(9), pp. 2120–2129. doi: 10.1634/STEMCELLS.2005-0514.

Rymo, S. F. *et al.* (2011) 'A two-way communication between microglial cells and angiogenic sprouts regulates angiogenesis in aortic ring cultures', *PLoS ONE*, 6(1), p. e15846. doi: 10.1371/journal.pone.0015846.

Schulz, C. *et al.* (2012) 'A lineage of myeloid cells independent of Myb and hematopoietic stem cells.', *Science (New York, N.Y.)*, 336(6077), pp. 86–90. doi: 10.1126/science.1219179.

Sellgren, C. M. *et al.* (2019) 'Increased synapse elimination by microglia in schizophrenia patient-derived models of synaptic pruning', *Nature Neuroscience*. Nature Publishing Group, 22(3), pp. 374–385. doi: 10.1038/s41593-018-0334-7.

Shabab, T. *et al.* (2017) 'Neuroinflammation pathways: a general review', *International Journal of Neuroscience*, 127(7), pp. 624–633. doi: 10.1080/00207454.2016.1212854.

Shi, Y. *et al.* (2012) 'Human cerebral cortex development from pluripotent stem cells to functional excitatory synapses', *Nature Neuroscience*, 15(3), pp. 477–486. doi: 10.1038/nn.3041.

Siddiqui, T. A., Lively, S. and Schlichter, L. C. (2016) 'Complex molecular and functional outcomes of single versus sequential cytokine stimulation of rat microglia', *Journal of Neuroinflammation*. BioMed Central Ltd., 13(1). doi: 10.1186/s12974-016-0531-9.

Smits, L. M. *et al.* (2019) 'Modeling Parkinson's disease in midbrain-like organoids', *npj Parkinson's Disease*. Springer US, 5(1). doi: 10.1038/s41531-019-0078-4.

Smits, L. M. *et al.* (2020) 'Single-cell transcriptomics reveals multiple neuronal cell types in human midbrain-specific organoids', *Cell and Tissue Research*. Springer, 382(3), p. 463. doi: 10.1007/S00441-020-03249-Y.

Taylor, R. A. *et al.* (2017) 'TGF-β1 modulates microglial phenotype and promotes recovery after intracerebral hemorrhage', *Journal of Clinical Investigation*, 127(1), pp. 280–292. doi: 10.1172/JCI88647.

Thion, M. S., Ginhoux, F. and Garel, S. (2018) 'Microglia and early brain development: An intimate journey', *Science*, 362(6411), pp. 185–189. doi: 10.1126/science.aat0474.

Tiwari, V., Ambadipudi, S. and Patel, A. B. (2013) 'Glutamatergic and GABAergic TCA cycle and neurotransmitter cycling fluxes in different regions of mouse brain', *Journal of Cerebral Blood Flow and Metabolism*. J Cereb Blood Flow Metab, 33(10), pp. 1523–1531. doi: 10.1038/jcbfm.2013.114.

Tremblay, M. È. *et al.* (2011) 'The role of microglia in the healthy brain', *Journal of Neuroscience*, 31(45), pp. 16064–16069. doi: 10.1523/JNEUROSCI.4158-11.2011.

Tu, D. *et al.* (2019) 'The pentose phosphate pathway regulates chronic neuroinflammation and dopaminergic neurodegeneration', *Journal of Neuroinflammation*. BioMed Central Ltd., 16(1). doi: 10.1186/s12974-019-1659-1.

Ueno, M. *et al.* (2013) 'Layer v cortical neurons require microglial support for survival during postnatal development', *Nature Neuroscience*, 16(5), pp. 543–551. doi: 10.1038/nn.3358.

Wake, H. *et al.* (2009) 'Resting microglia directly monitor the functional state of synapses in vivo and determine the fate of ischemic terminals', *Journal of Neuroscience*. J Neurosci, 29(13), pp. 3974–3980. doi: 10.1523/JNEUROSCI.4363-08.2009.

Weinberg, R. P. *et al.* (2019) 'Palm Fruit Bioactives augment expression of Tyrosine Hydroxylase in the Nile Grass Rat basal ganglia and alter the colonic microbiome', *Scientific Reports*. Nature Research, 9(1),

p. 18625. doi: 10.1038/s41598-019-54461-y.

van Wilgenburg, B. *et al.* (2013) ‘Efficient, Long Term Production of Monocyte-Derived Macrophages from Human Pluripotent Stem Cells under Partly-Defined and Fully-Defined Conditions’, *PLoS ONE*, 8(8). doi: 10.1371/journal.pone.0071098.

Witting, A. *et al.* (2000) ‘Phagocytic clearance of apoptotic neurons by microglia/brain macrophages in vitro: Involvement of lectin-, integrin-, and phosphatidylserine-mediated recognition’, *Journal of Neurochemistry*, 75(3), pp. 1060–1070. doi: 10.1046/j.1471-4159.2000.0751060.x.

WK, K. *et al.* (2004) ‘TGF-beta1 represses activation and resultant death of microglia via inhibition of phosphatidylinositol 3-kinase activity’, *Journal of immunology (Baltimore, Md. : 1950)*. J Immunol, 172(11), pp. 7015–7023. doi: 10.4049/JIMMUNOL.172.11.7015.

Figure titles and legends

Figure 1. iPSC-derived microglia express specific markers, have phagocytosis ability and are compatible with the engineered co-culture medium. **A.** Immunofluorescence staining of microglia from line 163 for IBA1, PU.1 (upper panels), TMEM119 and CD45 (middle panels) and P2RY12 (bottom panels). **B.** IBA1, CD68, TMEM119 and P2RY12 gene expression in microglia from the three used lines. The Ribosomal Protein RPL37A coding gene was used as a housekeeping gene due to its stable expression. **C.** Immunofluorescence staining of microglia from the EPI line for IBA1 and Zymosan. For lines K7 and 163 see Figure S1B. **D.** Cell viability of 2D microglia from lines 163 and EPI (MTT assay) after 10 days of treatment with midbrain organoid media (MOm) or microglia medium (MGLm) without further supplementation or supplemented with neurotrophic factors. (n=3, 3 batches). **E**. Representative bright field images of the microglia morphology (line 163) at day 0 and 7 of culture with MOm, MGLm, MGLm supplemented with TGFβ3 (MGL + TGFβ3), with cAMP (MGL + cAMP) or with Activin A (MGL + ActA). **F.** Schematic diagram of the steps for the media optimization in assembloids and midbrain organoids. **G.** IBA1 positive ($IBA1^+$) population in assembloids upon culture with MOm, MGLm or co-culture medium (cc med). Y axis represents the fold change with respect to the control (MOm). **H.** TH positive (TH^+) neuron population in midbrain organoids (left) and assembloids (right). Y axis represents the fold change with respect to the control (MOm) (n (midbrain organoids) = 2, 2 batches, n (assembloids) = 5, 2 batches and 3 cell lines). Data are represented as mean ± SEM. *p<0.05, **p<0.01, ***p<0.001, ****p<0.0001 using a 2way ANOVA with Dunnett's multiple comparisons test. Abbreviations: BDNF, brain-derived neurotrophic factor; GDNF, glial cell-derived neurotrophic factor; TGFβ3, Transforming growth factor beta-3, cAMP, cyclic adenosine monophosphate; ActA, activin A.

Figure 2. **The co-culture medium allows a successful microglia integration and seven other neural cell populations in assembloids**. **A.** Timeline of the co-culture of midbrain organoids with macrophage precursors. DOD = Day of Differentiation, DOC = Day of co-culture. **B.** IBA1 positive ($IBA1^+$) cell percentage in midbrain organoids and assembloids. Assembloids present around 6.4% of $IBA1^+$ cells (n (midbrain organoids) = 5, 5 batches, n (assembloids) = 15, 5 batches, 3 cell lines). Data are represented as mean ± SEM. **C.** Immunofluorescence staining of midbrain organoids and assembloids with microglia from the line K7 for IBA1, FOXA2 and MAP2 (left panels), and for TH and TUJ1 (right panels). For lines 163 and EPI see Figure S1H. **D.** UMAP visualization of scRNA-seq data - split by microglial presence - shows 8 different defined cell clusters in assembloids. RGL, radial glia; midNESC, midbrain specific neural epithelial stem cells;

PROG, neuronal progenitors; NB, neuroblasts; yDN&CN, young dopaminergic and cholinergic neurons; mDN(A10)&gaN&GlN, mature A10 specific dopaminergic neurons, gabaergic and glutamatergic neurons; mDN(A9)&SN, mature A9 specific dopaminergic neurons and serotonergic neurons, MGL, microglia. **E.** Proportions of different cell types in midbrain organoids and assembloids**. F.** Average expression of cluster defining genes in assembloids. **G.** Spearman's correlation between different cell types in assembloids. *p < 0.05, **p<0.01, ***p<0.001, ****p<0.0001 using a Kruskal-Wallis 1way ANOVA with Dunn's multiple comparisons test (for MGLm and cc med vs MOm), and a Mann-Whitney test (for MGLm vs cc med) in A and B, and a Mann-Whitney test in E.

Figure 3. Microglia in assembloids have a typical immune cell signature. A. Heatmap showing the average expression of 100 most variable genes between midbrain organoids and assembloids. **B.** Expression of top 100 microglial marker genes across microglia cells in assembloids. **C.** Microglia core signature, expression of microglia marker genes as well as genes involved in adhesion, immune response, pathogen recognition and purinergic signalling. **D.** Gene expression levels of genes related to phagocytic activity. Violin plot shows average expression level. *p <0.05, **p<0.01, ***p<0.001, ****p<0.0001 using a Wilcox one-sample tests, median in red, quantiles in black. Dots represent single cells.

Figure 4. Microglia in assembloids have phagocytic capacities and release cytokines and chemokines. A. Heatmap representing the measured levels of cytokines and chemokines in cell culture media (pg/ml) shows two different clusters corresponding to midbrain organoids and assembloids (n=9, 3 batches, 3 lines). **B.** Cytokine (upper graph) and chemokine (bottom graph) levels in midbrain organoids and assembloids (n=9, 3 batches, 3 lines). **C.** Average expression of cytokine and chemokine genes across cell types. **D.** Organoid surface area in midbrain organoids and assembloids over time (left graph, n=3, 3 batches). Comparison of the organoid size, measuring the same organoids and assembloids, in four time points during culture (right graph, n=3, 3 batches). **E.** Cell number (total nuclei count, left panel) and dead cells (pyknotic nuclei, right panel) in midbrain organoids and assembloids after 20 days of culture (n (midbrain organoids) = 5, 5 batches, n (assembloids) =15, 5 batches, 3 lines). Data are represented as mean ± SEM. *p < 0.05, **p<0.01, ***p<0.001, ****p<0.0001 using a Mann-Whitney test in A and B, a multiple t test with the Holm-Sidak method for D (left panel), a 2way ANOVA with Tukey's multiple comparisons test for D (right panel) and a Mann-Whitney test in E.

Figure 5. Microglia affect the expression of oxidative stress and immune response-related genes in assembloids. A. Differentially expressed gene enrichment analysis in assembloids

against midbrain organoids reveals 12 significant network process pathways (FDR<0.05). **B.** Expression of genes related to response to oxidative stress in assembloids compared to midbrain organoids. **C.** Gene expression of genes related to immune response of assembloids. The presence of microglia increases the expression of genes related to antigen presentation and immune response, and decreases the expression of those related to autophagy in non-microglia cells. Box plots show mean expression and standard deviation. **D.** Enrichment analysis of cluster specific DEG p<0.05 between assembloids and midbrain organoids reveals significant FDR<0.05 network processes involved in oxidative stress, immune response as well as synaptic regulation. Dots represent single cells. Data are represented as mean ± SD. *p < 0.05, **p<0.01, ***p<0.001, ****p<0.0001 using a Wilcox test.

Figure 6. Microglia affect the expression of genes related to synaptic remodeling in assembloids and develop mature electrophysiological characteristics. A. Gene expression of general synaptic markers such as *Synaptotagmin* (*SYT1*) and *Synaptophysin* (*SYP*), and the dopaminergic neuron circuit formation genes *ROBO1* and DCC across cell clusters in midbrain organoids and assembloids. Data are represented as mean ± SD. * p< 0.05 using a Wilcox test. Dots represent single cells **B.** Expression of genes involved in action potential (*CASK, CACNA1A, CACNA1E, CACNA1B*) and active zones (*HCN1, KCNC3, KCND3*) within synapses in the dopaminergic neuron cluster (mDN(A9)&SN) in midbrain organoids and assembloids. Data are represented as mean ± SD. * p< 0.05 using a Wilcox test. Dots represent single cells. **C.** Western blot showing protein levels of the synaptic vesicle marker VAMP2 and the housekeeping protein β-actin (upper panels). Bar graph showing the Western blot quantification from the upper panels (n (midbrain organoids) = 3, 3 batches, n (assembloids) = 9, 3 batches, 3 cell lines). **p<0.01 using a Mann-Whitney test. Data are represented as mean ± SEM. **D.** Fixation of organoid during recording and post hoc verification of microglia presence. The left half shows an infra-red phase-contrast life image with the fixation pipette (upper left panel). The right half shows the same organoid after immunofluorescence staining for MAP2 and IBA1. Example traces show voltage response to hyperpolarizing and depolarizing current injections of a neuron inside an assembloid measured by whole-cell patch-clamp. Voltage responses that exhibited action potential (AP) following 50ms after stimulus onset were used for AP analysis (upper right panel). Analysis of AP waveform characteristics (bottom left panel). Voltage thresholds were significantly more depolarized in assembloid neurons (bottom middle-left panel, n =14 neurons in midbrain organoids and n =13 cells in assembloids), although analysis of AP amplitude (bottom middle-right panel) and half width (bottom right panel) shows no systematic differences between both groups. Box plots indicate median, 25th, and 75th percentiles and raw data points. Outliers

deviating 2.5 standard deviations are marked translucent and were excluded from statistical analysis for normally distributed data. P-values were determined using unpaired t-tests or Mann-Whitney rank test (indicated as p, see Supplemental Experimental Procedures). **E.** Multi-electrode array results showed a lower inter-spike interval in assembloids compared to midbrain organoids (n (midbrain organoids) = 3, 3 batches, n (assembloids) = 9, 3 batches, 3 cell lines). ***p=0.001, **p=0.01, *p=0.05 using a Wilcox test. Boxes cover data from the first to the third quartile. The whiskers go from each quartile to the minimum or maximum.

Figures

Figure 1

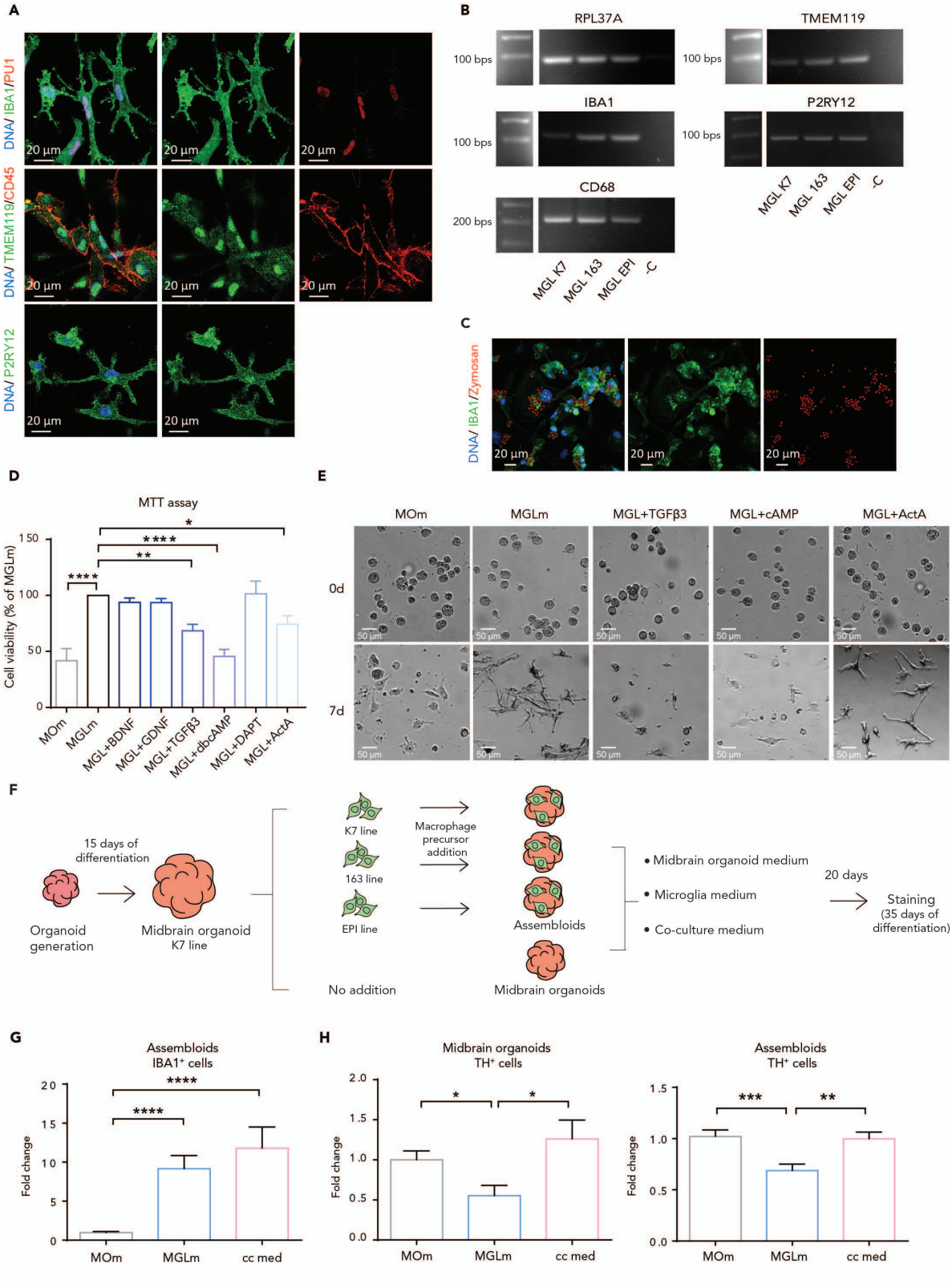

Figure 2

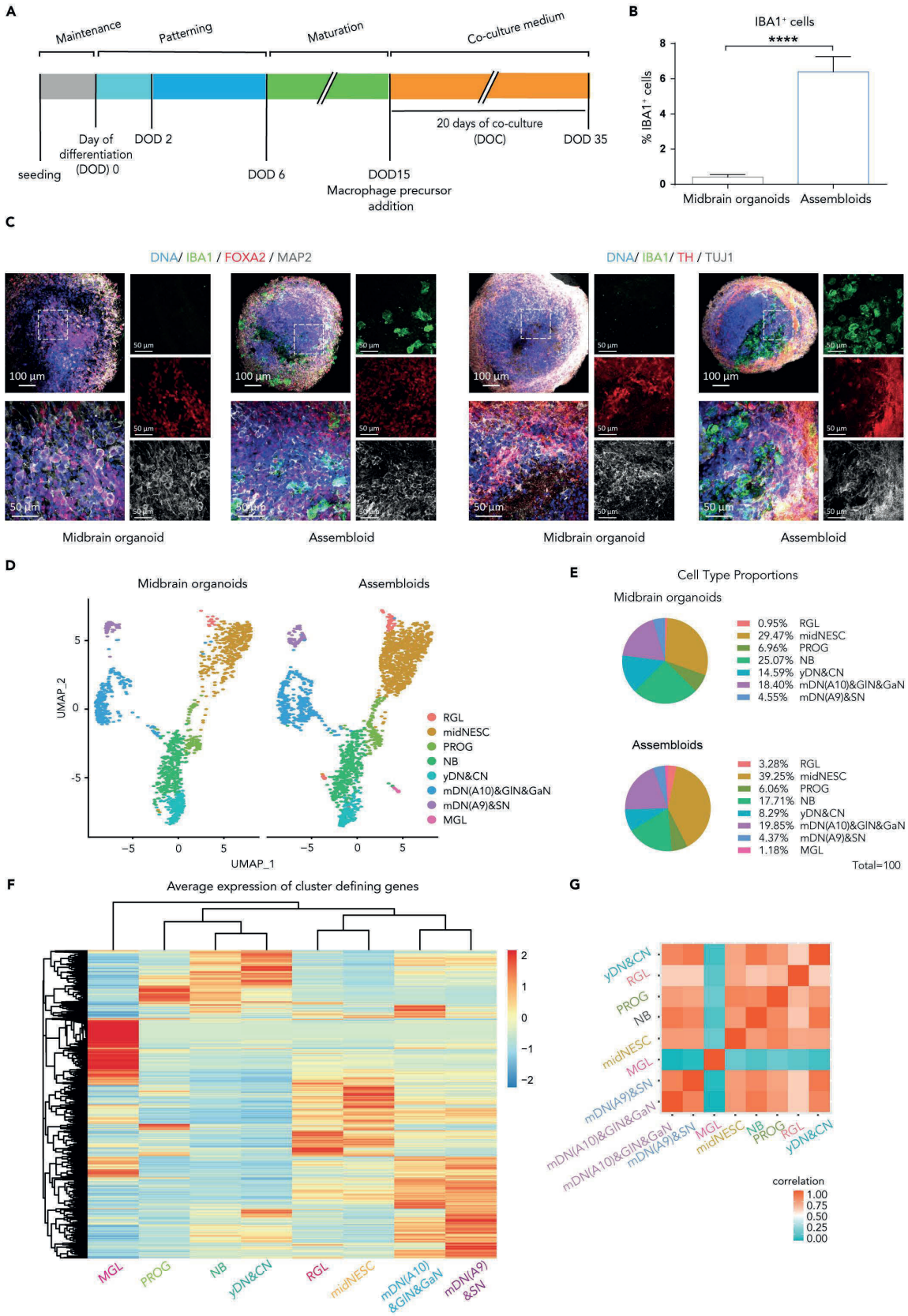
A
Maintenance
Patterning
Maturation
Co-culture medium
seeding
Day of differentiation (DOD) 0
DOD 2
DOD 6
DOD15 Macrophage precursor addition
20 days of co-culture (DOC)
DOD 35
B
IBA1+ cells
****
% IBA1+ cells
Midbrain organoids
Assembloids
C
DNA/ IBA1 / FOXA2 / MAP2
DNA/ IBA1/ TH / TUJ1
Midbrain organoid
Assembloid
Midbrain organoid
Assembloid
D
Midbrain organoids
Assembloids
UMAP_2
UMAP_1
RGL
midNESC
PROG
NB
yDN&CN
mDN(A10)&GlN&GaN
mDN(A9)&SN
MGL
E
Cell Type Proportions
Midbrain organoids
0.95% RGL
29.47% midNESC
6.96% PROG
25.07% NB
14.59% yDN&CN
18.40% mDN(A10)&GlN&GaN
4.55% mDN(A9)&SN
Assembloids
3.28% RGL
39.25% midNESC
6.06% PROG
17.71% NB
8.29% yDN&CN
19.85% mDN(A10)&GlN&GaN
4.37% mDN(A9)&SN
1.18% MGL
Total=100
F
Average expression of cluster defining genes
MGL
PROG
NB
yDN&CN
RGL
midNESC
mDN(A10) &GlN&GaN
mDN(A9) &SN
G
correlation
1.00
0.75
0.50
0.25
0.00

Figure 3

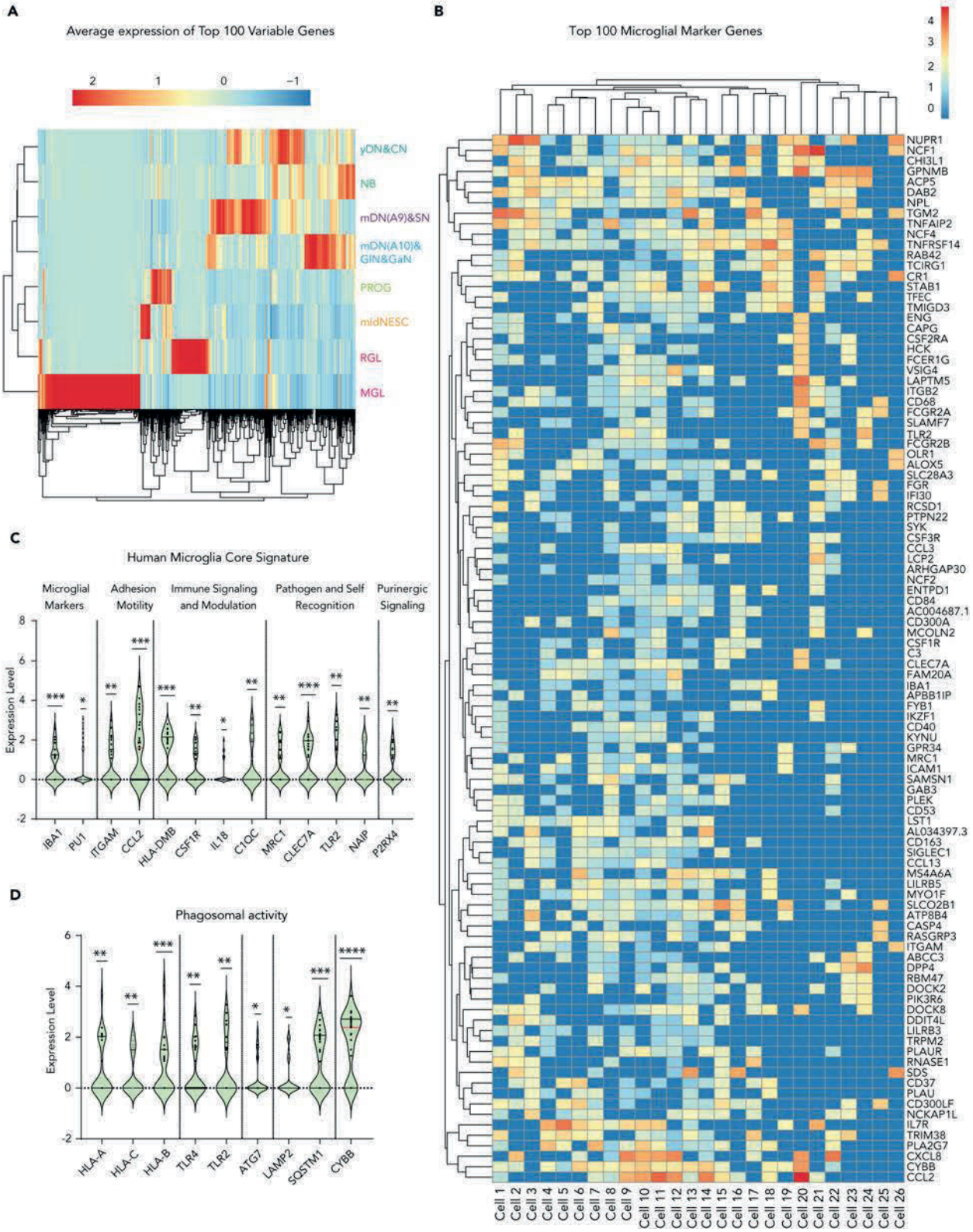
A
Average expression of Top 100 Variable Genes
2
1
0
−1
yDN&CN
NB
mDN(A9)&SN
mDN(A10)&
GIN&GaN
PROG
midNESC
RGL
MGL
B
Top 100 Microglial Marker Genes
4
3
2
1
0
NUPR1
NCF1
CHI3L1
GPNMB
ACP5
DAB2
NPL
TGM2
TNFAIP2
NCF4
TNFRSF14
RAB42
TCIRG1
CR1
STAB1
TFEC
TMIGD3
ENG
CAPG
CSF2RA
HCK
FCER1G
VSIG4
LAPTM5
ITGB2
CD68
FCGR2A
SLAMF7
TLR2
FCGR2B
OLR1
ALOX5
SLC28A3
FGR
IFI30
RCSD1
PTPN22
SYK
CSF3R
CCL3
LCP2
ARHGAP30
NCF2
ENTPD1
CD84
AC004687.1
CD300A
MCOLN2
CSF1R
C3
CLEC7A
FAM20A
IBA1
APBB1IP
FYB1
IKZF1
CD40
KYNU
GPR34
MRC1
ICAM1
SAMSN1
GAB3
PLEK
CD53
LST1
AL034397.3
CD163
SIGLEC1
CCL13
MS4A6A
LILRB5
MYO1F
SLCO2B1
ATP8B4
CASP4
RASGRP3
ITGAM
ABCC3
DPP4
RBM47
DOCK2
PIK3R6
DOCK8
DDIT4L
LILRB3
TRPM2
PLAUR
RNASE1
SDS
CD37
PLAU
CD300LF
NCKAP1L
IL7R
TRIM38
PLA2G7
CXCL8
CYBB
CCL2
Cell 1
Cell 2
Cell 3
Cell 4
Cell 5
Cell 6
Cell 7
Cell 8
Cell 9
Cell 10
Cell 11
Cell 12
Cell 13
Cell 14
Cell 15
Cell 16
Cell 17
Cell 18
Cell 19
Cell 20
Cell 21
Cell 22
Cell 23
Cell 24
Cell 25
Cell 26
C
Human Microglia Core Signature
Microglial Markers
Adhesion Motility
Immune Signaling and Modulation
Pathogen and Self Recognition
Purinergic Signaling
Expression Level
IBA1
PU1
ITGAM
CCL2
HLA-DMB
CSF1R
IL18
C1QC
MRC1
CLEC7A
TLR2
NAIP
P2RX4
D
Phagosomal activity
Expression Level
HLA-A
HLA-C
HLA-B
TLR4
TLR2
ATG7
LAMP2
SQSTM1
CYBB

Figure 4

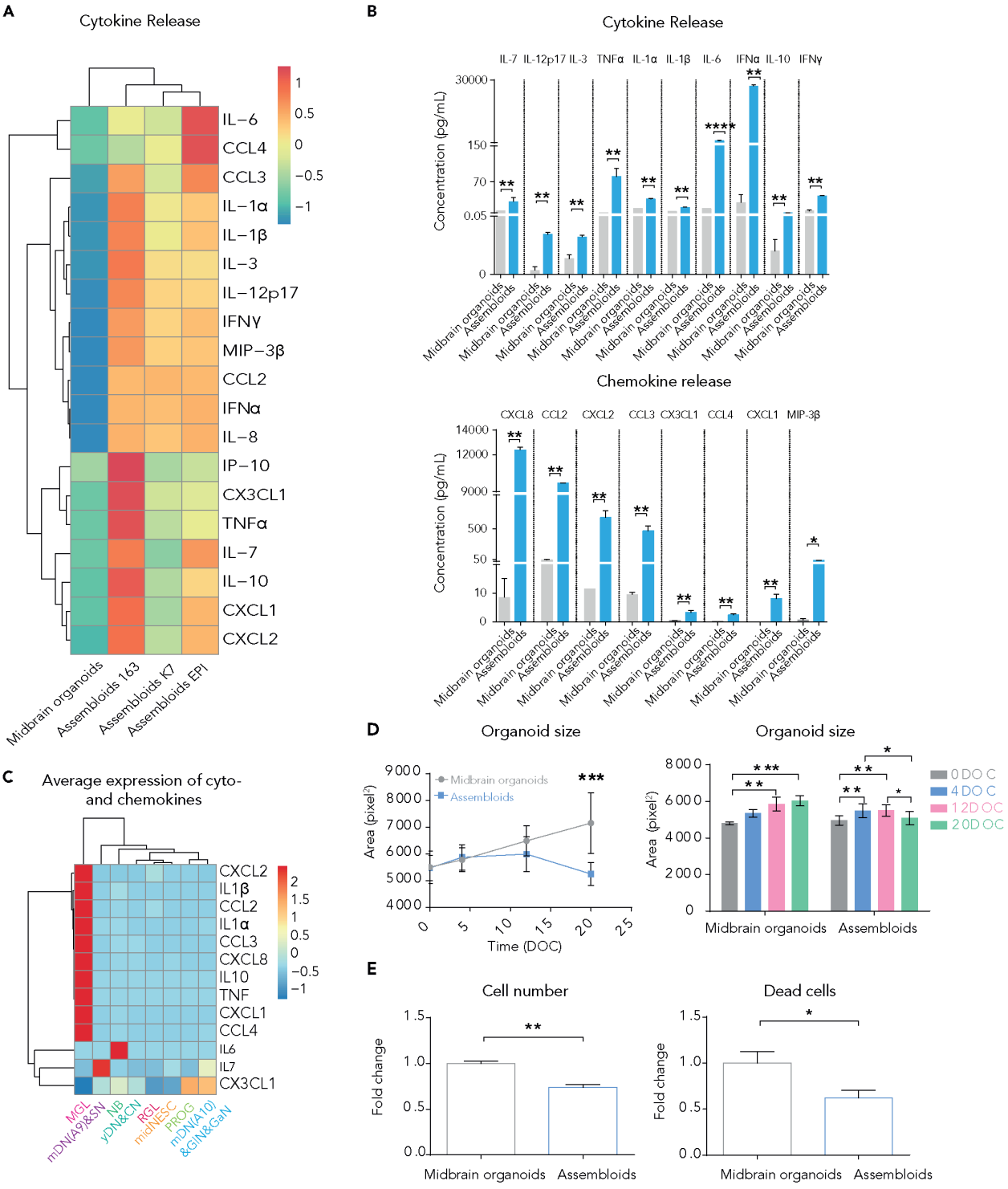
A
Cytokine Release
IL−6
CCL4
CCL3
IL−1α
IL−1β
IL−3
IL−12p17
IFNγ
MIP−3β
CCL2
IFNα
IL−8
IP−10
CX3CL1
TNFα
IL−7
IL−10
CXCL1
CXCL2
Midbrain organoids
Assembloids 163
Assembloids K7
Assembloids EPI
B
Cytokine Release
IL-7 IL-12p17 IL-3 TNFα IL-1α IL-1β IL-6 IFNα IL-10 IFNγ
Concentration (pg/mL)
Chemokine release
CXCL8 CCL2 CXCL2 CCL3 CX3CL1 CCL4 CXCL1 MIP-3β
Midbrain organoids
Assembloids
C
Average expression of cyto- and chemokines
CXCL2
IL1β
CCL2
IL1α
CCL3
CXCL8
IL10
TNF
CXCL1
CCL4
IL6
IL7
CX3CL1
MGL
mDN(A9)&SN
NB
yDN&CN
RGL
midNESC
PROG
mDN(A10)
&GlN&GaN
D
Organoid size
Midbrain organoids
Assembloids
Area (pixel²)
Time (DOC)
Organoid size
0 DOC
4 DOC
12 DOC
20 DOC
Midbrain organoids
Assembloids
E
Cell number
Dead cells
Fold change
Midbrain organoids
Assembloids

Figure 5

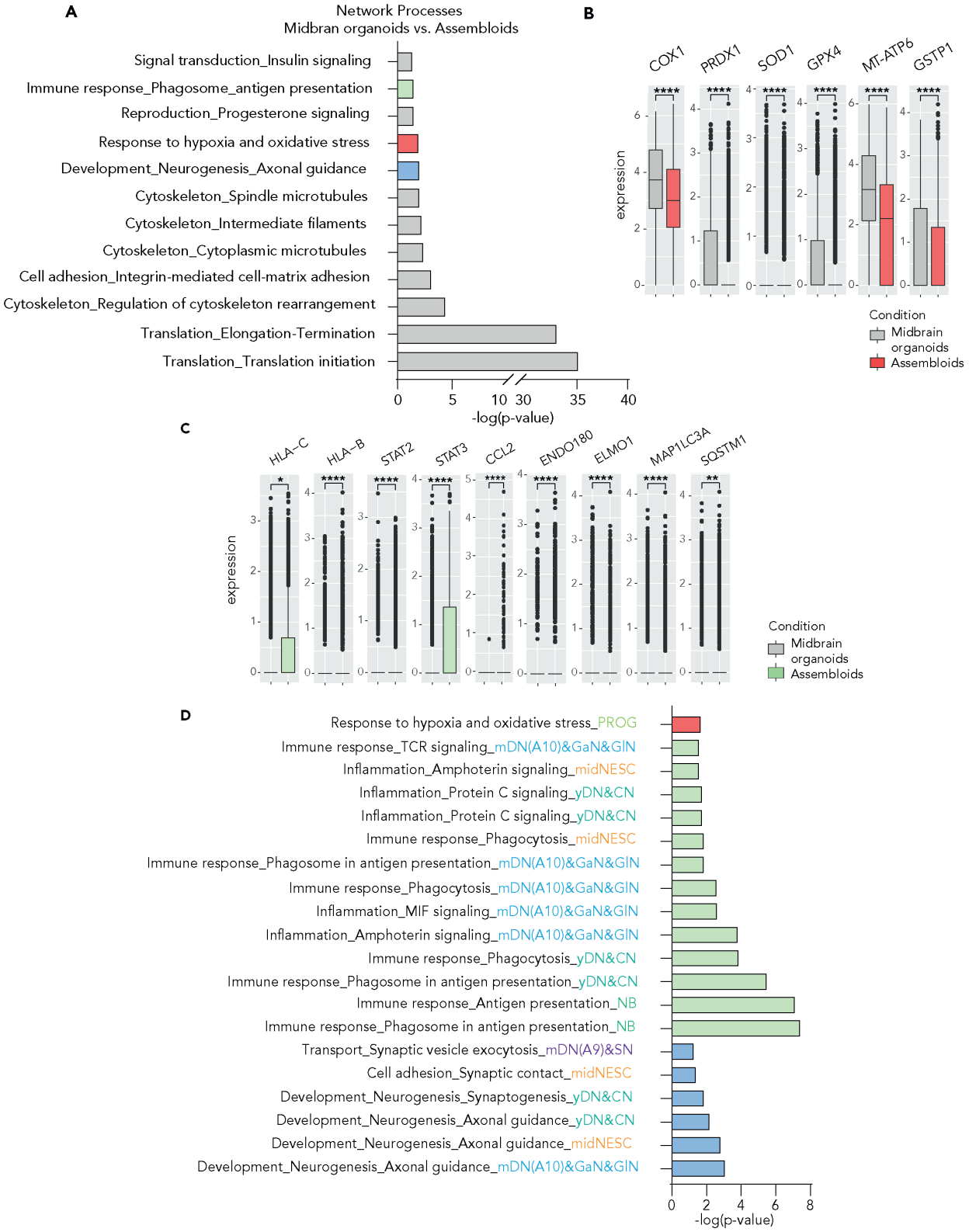
A
Network Processes
Midbran organoids vs. Assembloids
Signal transduction_Insulin signaling
Immune response_Phagosome_antigen presentation
Reproduction_Progesterone signaling
Response to hypoxia and oxidative stress
Development_Neurogenesis_Axonal guidance
Cytoskeleton_Spindle microtubules
Cytoskeleton_Intermediate filaments
Cytoskeleton_Cytoplasmic microtubules
Cell adhesion_Integrin-mediated cell-matrix adhesion
Cytoskeleton_Regulation of cytoskeleton rearrangement
Translation_Elongation-Termination
Translation_Translation initiation
0 5 10 30 35 40
-log(p-value)
B
COX1
PRDX1
SOD1
GPX4
MT-ATP6
GSTP1
expression
Condition
Midbrain organoids
Assembloids
C
HLA–C
HLA–B
STAT2
STAT3
CCL2
ENDO180
ELMO1
MAP1LC3A
SQSTM1
expression
Condition
Midbrain organoids
Assembloids
D
Response to hypoxia and oxidative stress_PROG
Immune response_TCR signaling_mDN(A10)&GaN&GlN
Inflammation_Amphoterin signaling_midNESC
Inflammation_Protein C signaling_yDN&CN
Inflammation_Protein C signaling_yDN&CN
Immune response_Phagocytosis_midNESC
Immune response_Phagosome in antigen presentation_mDN(A10)&GaN&GlN
Immune response_Phagocytosis_mDN(A10)&GaN&GlN
Inflammation_MIF signaling_mDN(A10)&GaN&GlN
Inflammation_Amphoterin signaling_mDN(A10)&GaN&GlN
Immune response_Phagocytosis_yDN&CN
Immune response_Phagosome in antigen presentation_yDN&CN
Immune response_Antigen presentation_NB
Immune response_Phagosome in antigen presentation_NB
Transport_Synaptic vesicle exocytosis_mDN(A9)&SN
Cell adhesion_Synaptic contact_midNESC
Development_Neurogenesis_Synaptogenesis_yDN&CN
Development_Neurogenesis_Axonal guidance_yDN&CN
Development_Neurogenesis_Axonal guidance_midNESC
Development_Neurogenesis_Axonal guidance_mDN(A10)&GaN&GlN
0 2 4 6 8
-log(p-value)

Figure 6

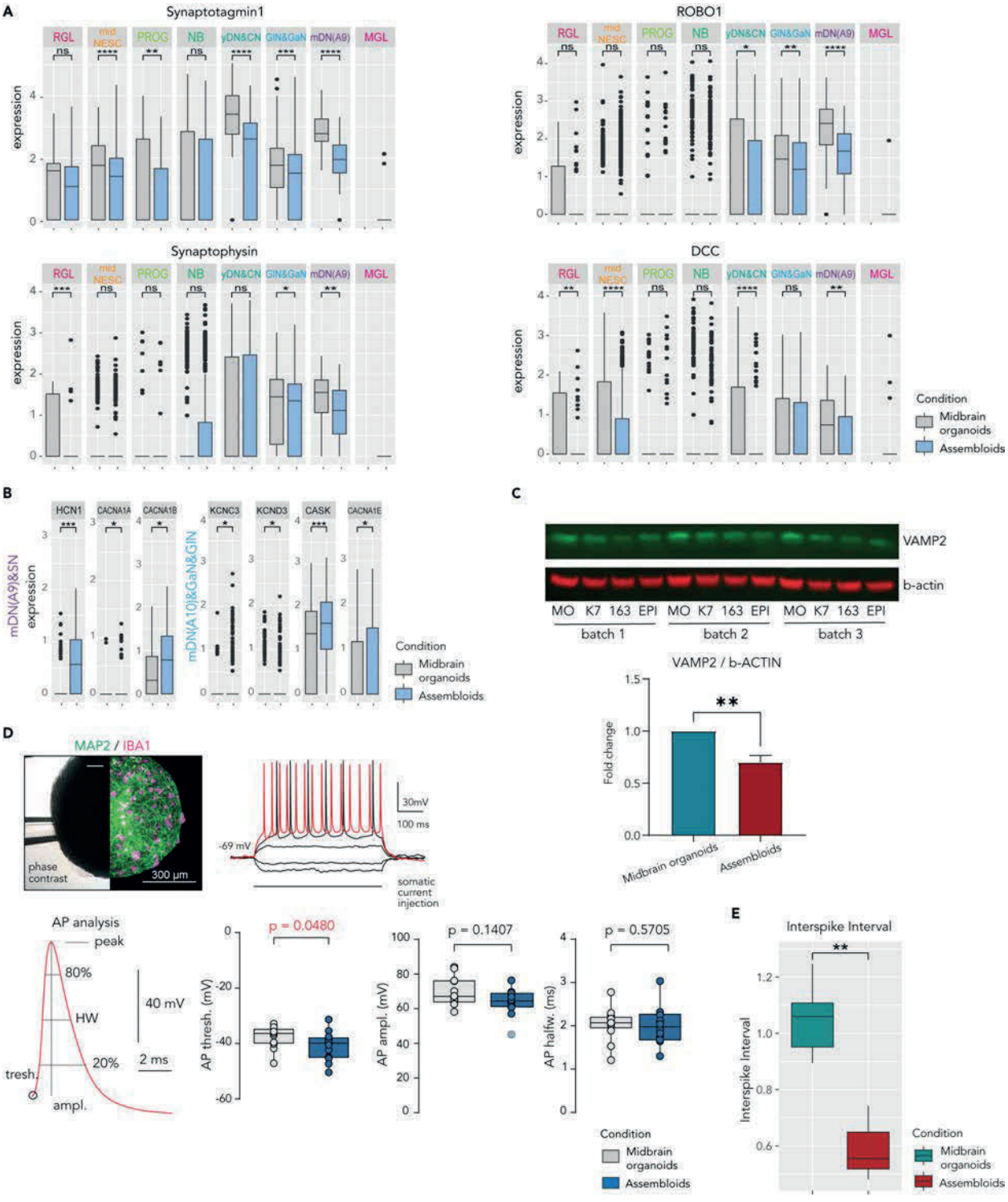
A
Synaptotagmin1
ROBO1
Synaptophysin
DCC
RGL
mid NESC
PROG
NB
yDN&CN
GIN&GaN
mDN(A9)
MGL
expression
Condition
Midbrain organoids
Assembloids
B
HCN1
CACNA1A
CACNA1B
KCNC3
KCND3
CASK
CACNA1E
mDN(A9)&SN
mDN(A10)&GaN&GIN
C
VAMP2
b-actin
MO K7 163 EPI
batch 1
batch 2
batch 3
VAMP2 / b-ACTIN
Fold change
Midbrain organoids
Assembloids
D
MAP2 / IBA1
phase contrast
300 µm
30mV
100 ms
-69 mV
somatic current injection
AP analysis
peak
80%
HW
20%
tresh.
ampl.
40 mV
2 ms
AP thresh. (mV)
p = 0.0480
AP ampl. (mV)
p = 0.1407
AP halfw. (ms)
p = 0.5705
E
Interspike Interval
Interspike Interval

Supplemental information

Supplemental figure legends

Figure S1. Microglia in assembloids show different morphologies and allow astrocyte differentiation A. iPSCs from the line K7 (upper row), 163 (middle row) and EPI (bottom row) stained for the pluripotency markers TRA-1-60, Nanog (left), TRA-1-81, SOX2 (middle), SSEA-4 and Oct-4 (right). **B.** Zymosan and IBA1 staining on microglia from line K7 (top) and 163 (bottom) differentiated for 10 days. **C.** Immunostaining for IBA1, TH and TUJ1 of midbrain organoids and assembloids with microglia from line K7, 163 and EPI upon culture with midbrain organoid (MOm), microglia (MGLm) or co-culture (cc med) media). **D.** MAP2 positive ($MAP2^+$) cells in midbrain organoids and assembloids (n (midbrain organoids) =5, 5 batches, n (assembloids) =15, 5 batches, 3 cell lines). For immunofluorescence images see Figure 2C and S1H. Data are represented as mean ± SEM. Y axis is fold change compared to midbrain organoids. **E.** Immunostaining of neural precursor cells from line K7 for the pluripotency marker SOX2, the neural precursor marker Nestin and the forebrain and hindbrain marker PAX6, whose absence confirms the midbrain patterning of the cells. **F.** Bright field images of midbrain organoids (upper panels) and assembloids (bottom panels) at the co-culture day (0DOC, days of co-culture, left) and at 20DOC (right). **G.** Immunostaining of assembloids for IBA1 showing ramified (left), elongated (middle) and round (right) microglia. **H.** Immunostaining of an assembloid from the line 163 after 70 days of co-culture, for GFAP, IBA1 and MAP2. **I.** Immunofluorescence staining of midbrain organoids (left panels) and assembloids with microglia from line 163 (middle panels) and EPI (right panels) for IBA1, FOXA2 and MAP2 (upper panels), and for TH and TUJ1 (bottom panels). The images correspond to a maximum intensity projection from a z-stack of 70µm organoid sections.

Figure S2. Cell type specific gene expression in assembloids. Heatmap showing the cell type-specific gene expression throughout the different cell clusters in assembloids.

Figure S3. Quality control of sn-RNAseq data using the Seurat R Package. Quality controls of **A.** Midbrain organoids. **B**. Assembloids with microglia from line K7. **C**. Assembloids with microglia from line 163. i) Before quality controls; ii) After quality controls (100 < nFeature_RNA < 5000 or percent_mt < 25); iii) Correlation between features and counts; iv) Correlation between microglial genes and counts. **D.** Volcano plot showing the most variable genes between midbrain organoids and assembloids. **E.** UMAP visualization of scRNA-seq data grouped by samples: Assembloids with microglia from 163 Assembloids_163), Assembloids with microglia from K7

(Assembloids_K7) and midbrain organoids. **F.** Principle components analysis. 20 dimensions were chosen.

Figure S4. Microglia in assembloids lead to differential expression of multiple genes. A. Heatmap of the average expression of 100 most significant differentially expressed genes across cell clusters in midbrain organoids and assembloids ($p<0.05$). **B.** Venn diagrams showing the number of DEG across cell types. Overlap within three neuronal clusters (left pannel) and midNESC, PROG, RGL and NB (right panel). **C.** Complete enrichment analysis of cluster specific DEG between midbrain organoids and assembloids reveals significant network processes (FDR<0.05).

Figure S5. Microglia lead to a decrease in the inflammasome-related gene PPIA, and differences in synapse-related genes. A. Expression of PPIA gene, involved in pyroptosis, across cell clusters in midbrain organoids and assembloids. **B.** Expression of *VMAT2* and *SNAP25*, involved in synaptic vesicle exocytosis, across cell clusters in midbrain organoids and assembloids. **C.** Expression levels of axonal guidance and growth-related genes: semaphorins (*SEMA3C*, *DPYSL2*), plexins, ephrins (*EPHA5*), neuropilins, neurofilaments and actin cytoskeleton (*NEFM, ACTB*) across cell clusters in midbrain organoids and assembloids. Data are represented as mean ± SD. * $p< 0.05$ using a Wilcox test. Dots represent single cells. **D.** Boxplot from patch clamp data showing that neurons in midbrain organoids and assembloids show similar resting membrane potentials (left) and input resistances (middle), and fired repetitive action potentials in response to somatic current injections (right, n midbrain organoids =14; n assembloids = 13 cells). **E.** Inward currents of an assembloid neuron triggered by voltage steps to different potentials starting from -70 mV in voltage-clamp mode. Voltage-gated currents appeared at -40mV and persisted until +30mV under whole-cell voltage-clamp conditions (left). Inward currents generated at -30 mV (red trace in left panel) between midbrain organoids and assembloids showed no significant difference between both groups (right). **F.** Heatmap showing extracellular metabolite levels in culture supernatants (n (midbrain organoids) = 5, 5 batches, n (assembloids) = 15, 5 batches, 3 cell lines). Midbrain organoids cluster separately from assembloids from lines K7, 163 and EPI.

Figure S6. Assembloids show a different extracellular metabolite profile compared to midbrain organoids. A. Metabolite levels in the culture media from organoids and assembloids after 48h of culture. The levels of glucose and pyruvic acid were lower in media from assembloids compared to midbrain organoids. **B.** The levels of the amino acids phenylalanine, tyrosine, methionine, lysine, putrescine, threonine, leucine, isoleucine, valine, asparagine and serine in the

media were lower in assembloids, whereas the glutamate levels were higher (n (midbrain organoids)= 3, 3 batches, n(assembloids)= 9, 3 batches, 3 cell lines). Each dot represents a replicate (medium 3 organoids or assembloids pooled). Data are represented as mean ± SEM. *p < 0.05, **p<0.01, ***p<0.001, ****p<0.0001 using a Mann-Whitney or an unpaired t test.

Supplemental Figures

Figure S1

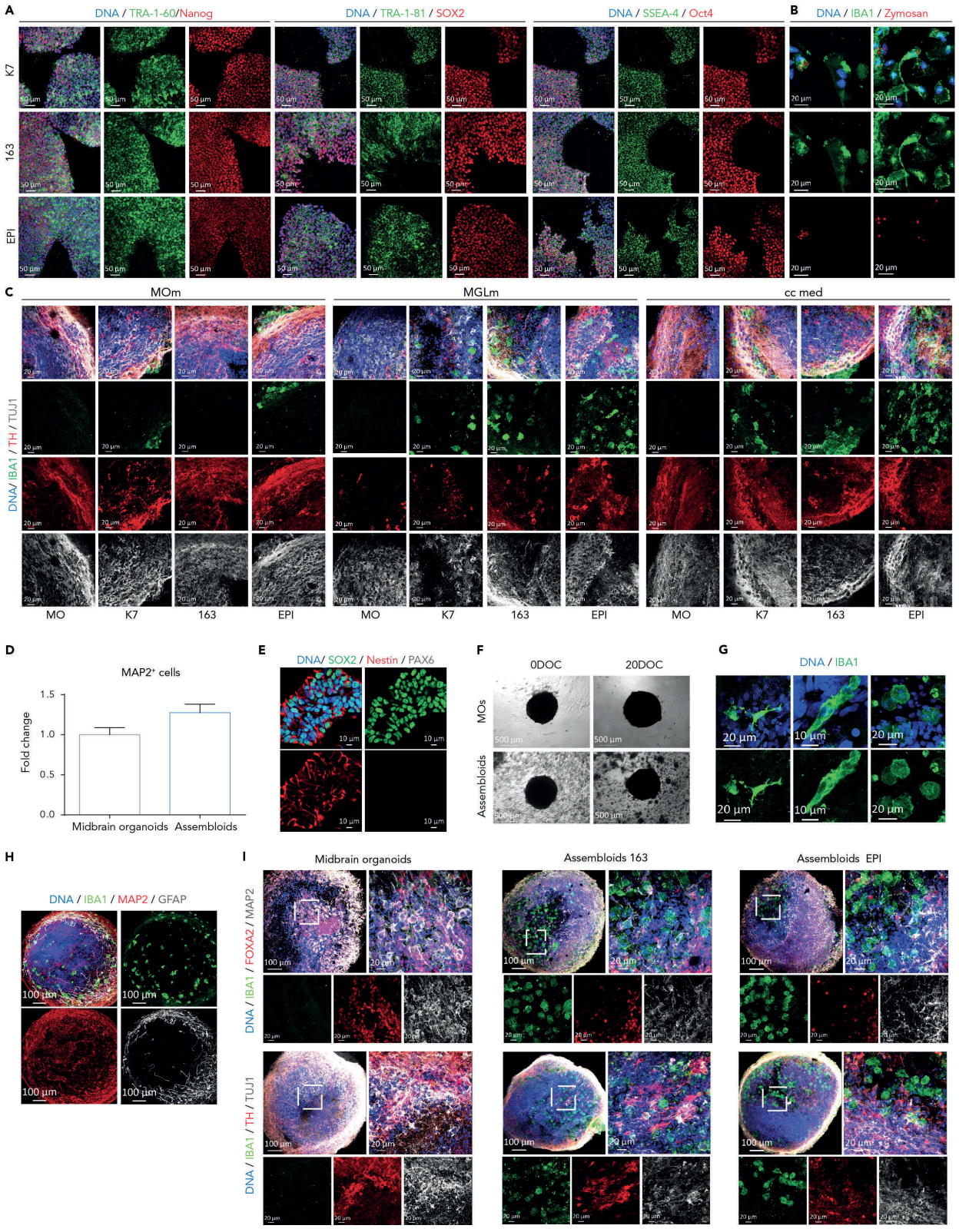

Figure S2

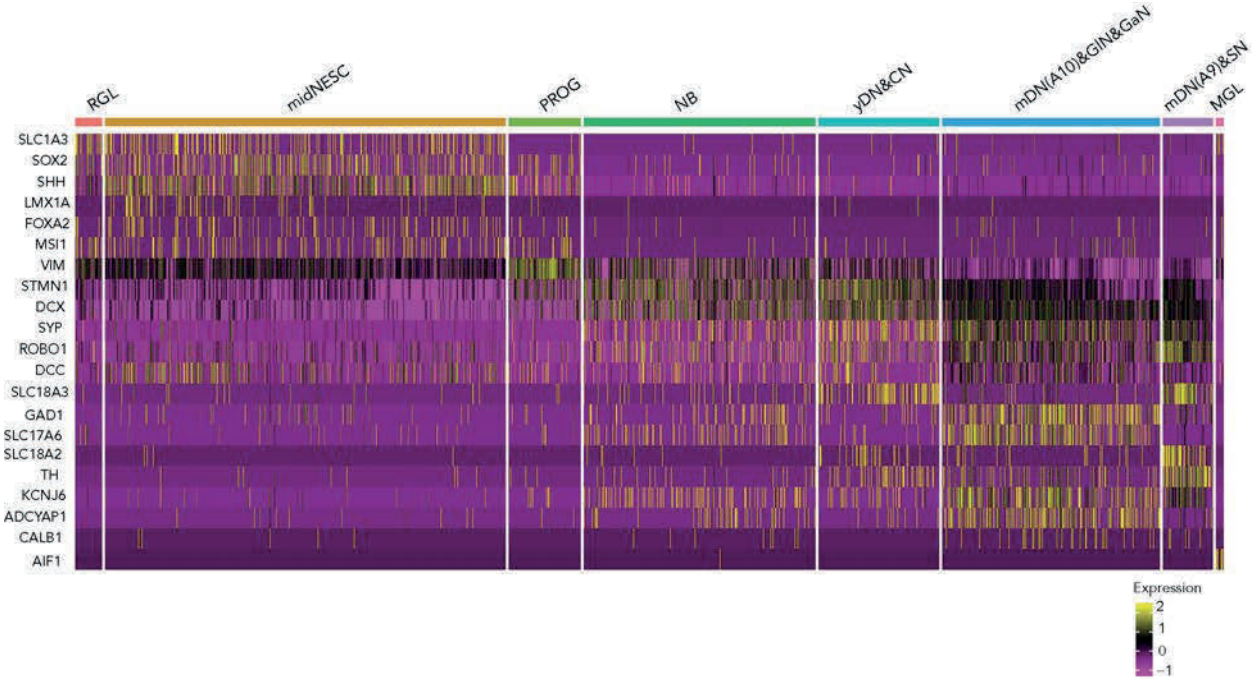
RGL
midNESC
PROG
NB
yDN&CN
mDN(A10)&GlN&GaN
mDN(A9)&SN
MGL
SLC1A3
SOX2
SHH
LMX1A
FOXA2
MSI1
VIM
STMN1
DCX
SYP
ROBO1
DCC
SLC18A3
GAD1
SLC17A6
SLC18A2
TH
KCNJ6
ADCYAP1
CALB1
AIF1
Expression
2
1
0
−1

Figure S3

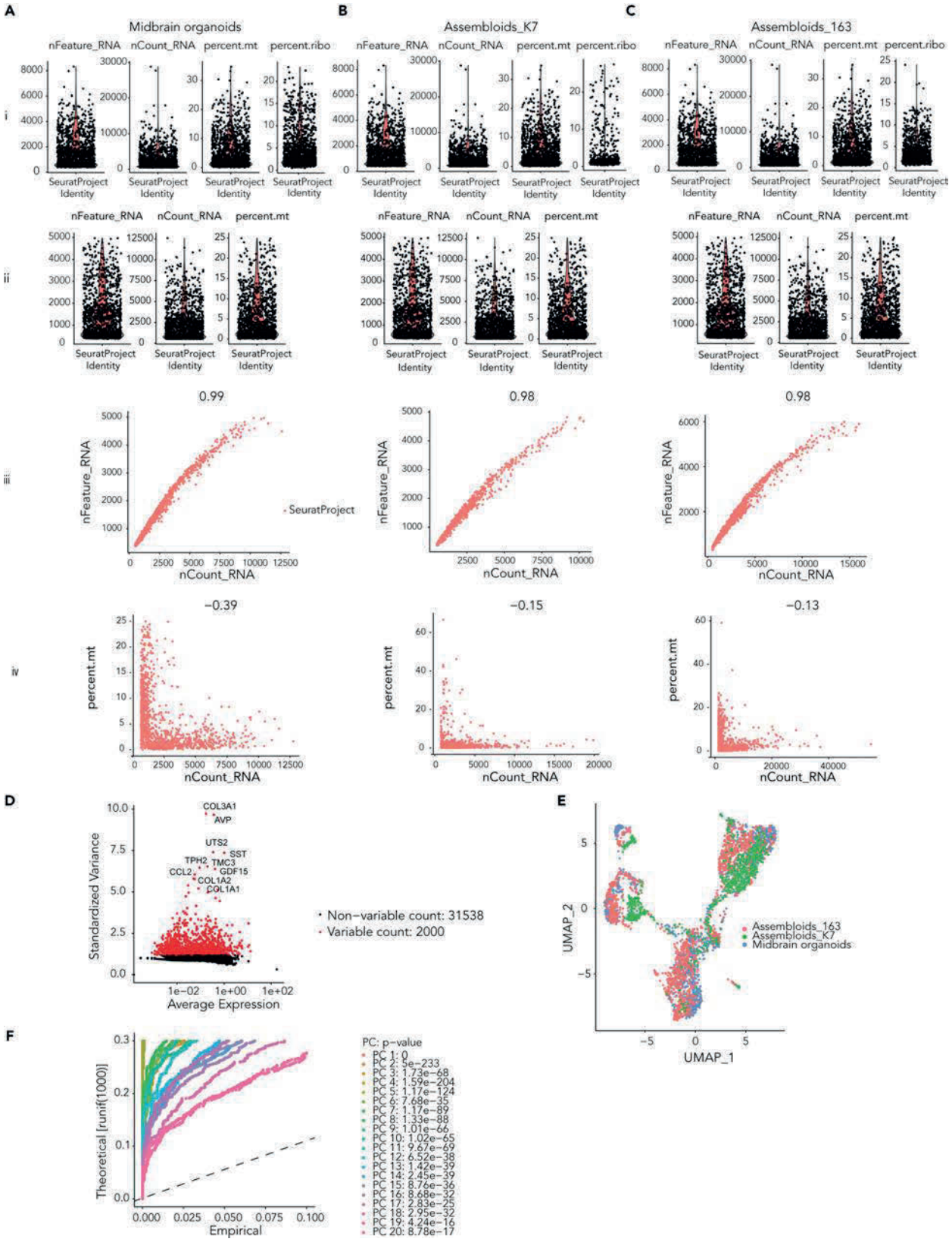
A
Midbrain organoids
B
Assembloids_K7
C
Assembloids_163
nFeature_RNA
nCount_RNA
percent.mt
percent.ribo
SeuratProject
Identity
i
ii
iii
iv
0.99
0.98
0.98
−0.39
−0.15
−0.13
nFeature_RNA
nCount_RNA
percent.mt
SeuratProject
D
Standardized Variance
Average Expression
COL3A1
AVP
UTS2
SST
TPH2
TMC3
CCL2
GDF15
COL1A2
COL1A1
Non−variable count: 31538
Variable count: 2000
E
UMAP_1
UMAP_2
Assembloids_163
Assembloids_K7
Midbrain organoids
F
Theoretical [runif(1000)]
Empirical
PC: p−value
PC 1: 0
PC 2: 5e−233
PC 3: 1.73e−68
PC 4: 1.59e−204
PC 5: 1.17e−124
PC 6: 7.68e−35
PC 7: 1.17e−89
PC 8: 1.33e−88
PC 9: 1.01e−66
PC 10: 1.02e−65
PC 11: 9.67e−69
PC 12: 6.52e−38
PC 13: 1.42e−39
PC 14: 2.45e−39
PC 15: 8.76e−36
PC 16: 8.68e−32
PC 17: 2.83e−25
PC 18: 2.95e−32
PC 19: 4.24e−16
PC 20: 8.78e−17

Figure S4

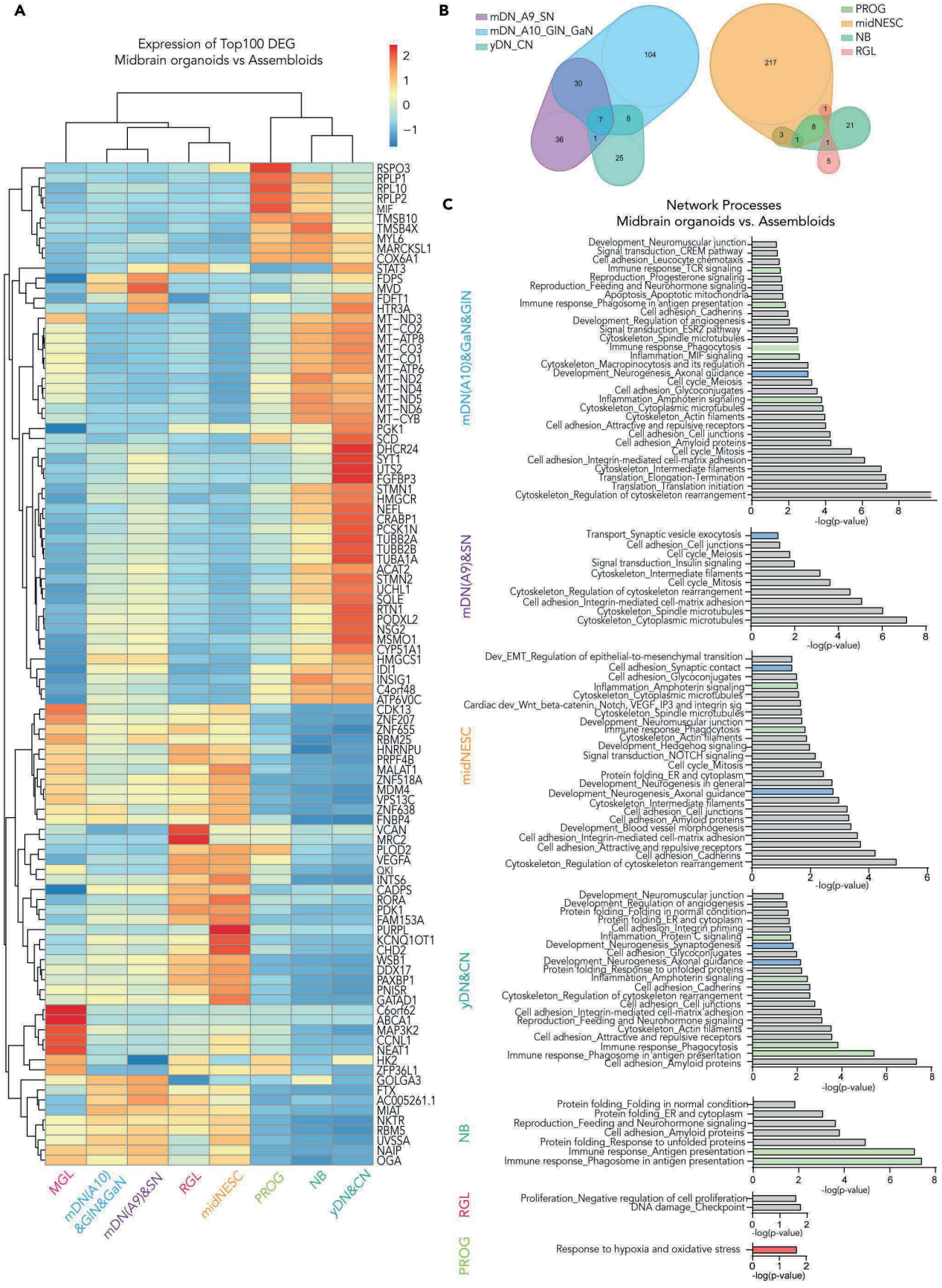
A
Expression of Top100 DEG
Midbrain organoids vs Assembloids
2
1
0
−1
RSPO3
RPLP1
RPL10
RPLP2
MIF
TMSB10
TMSB4X
MYL6
MARCKSL1
COX6A1
STAT3
FDPS
MVD
FDFT1
HTR3A
MT−ND3
MT−CO2
MT−ATP8
MT−CO3
MT−CO1
MT−ATP6
MT−ND2
MT−ND4
MT−ND5
MT−ND6
MT−CYB
PGK1
SCD
DHCR24
SYT1
UTS2
FGFBP3
STMN1
HMGCR
NEFL
CRABP1
PCSK1N
TUBB2A
TUBB2B
TUBA1A
ACAT2
STMN2
UCHL1
SQLE
RTN1
PODXL2
NSG2
MSMO1
CYP51A1
HMGCS1
IDI1
INSIG1
C4orf48
ATP6V0C
CDK13
ZNF207
ZNF655
RBM25
HNRNPU
PRPF4B
MALAT1
ZNF518A
MDM4
VPS13C
ZNF638
FNBP4
VCAN
MRC2
PLOD2
VEGFA
OKI
INTS6
CADPS
RORA
PDK1
FAM153A
PURPL
KCNQ1OT1
CHD2
WSB1
DDX17
PAXBP1
PNISR
GATAD1
C6orf62
ABCA1
MAP3K2
CCNL1
NEAT1
HK2
ZFP36L1
GOLGA3
FTX
AC005261.1
MIAT
NKTR
RBM5
UVSSA
NAIP
OGA
MGL
mDN(A10) &GlN&GaN
mDN(A9)&SN
RGL
midNESC
PROG
NB
yDN&CN
B
mDN_A9_SN
mDN_A10_GlN_GaN
yDN_CN
PROG
midNESC
NB
RGL
104
30
7
8
36
1
25
217
1
8
21
3
1
1
5
C
Network Processes
Midbrain organoids vs. Assembloids
mDN(A10)&GaN&GlN
Development_Neuromuscular junction
Signal transduction_CREM pathway
Cell adhesion_Leucocyte chemotaxis
Immune response_TCR signaling
Reproduction_Progesterone signaling
Reproduction_Feeding and Neurohormone signaling
Apoptosis_Apoptotic mitochondria
Immune response_Phagosome in antigen presentation
Cell adhesion_Cadherins
Development_Regulation of angiogenesis
Signal transduction_ESR2 pathway
Cytoskeleton_Spindle microtubules
Immune response_Phagocytosis
Inflammation_MIF signaling
Cytoskeleton_Macropinocytosis and its regulation
Development_Neurogenesis_Axonal guidance
Cell cycle_Meiosis
Cell adhesion_Glycoconjugates
Inflammation_Amphoterin signaling
Cytoskeleton_Cytoplasmic microtubules
Cytoskeleton_Actin filaments
Cell adhesion_Attractive and repulsive receptors
Cell adhesion_Cell junctions
Cell adhesion_Amyloid proteins
Cell cycle_Mitosis
Cell adhesion_Integrin-mediated cell-matrix adhesion
Cytoskeleton_Intermediate filaments
Translation_Elongation-Termination
Translation_Translation initiation
Cytoskeleton_Regulation of cytoskeleton rearrangement
0 2 4 6 8
-log(p-value)
mDN(A9)&SN
Transport_Synaptic vesicle exocytosis
Cell adhesion_Cell junctions
Cell cycle_Meiosis
Signal transduction_Insulin signaling
Cytoskeleton_Intermediate filaments
Cell cycle_Mitosis
Cytoskeleton_Regulation of cytoskeleton rearrangement
Cell adhesion_Integrin-mediated cell-matrix adhesion
Cytoskeleton_Spindle microtubules
Cytoskeleton_Cytoplasmic microtubules
0 2 4 6 8
-log(p-value)
midNESC
Dev_EMT_Regulation of epithelial-to-mesenchymal transition
Cell adhesion_Synaptic contact
Cell adhesion_Glycoconjugates
Inflammation_Amphoterin signaling
Cytoskeleton_Cytoplasmic microtubules
Cardiac dev_Wnt_beta-catenin_Notch_VEGF_IP3 and integrin sig
Cytoskeleton_Spindle microtubules
Development_Neuromuscular junction
Immune response_Phagocytosis
Cytoskeleton_Actin filaments
Development_Hedgehog signaling
Signal transduction_NOTCH signaling
Cell cycle_Mitosis
Protein folding_ER and cytoplasm
Development_Neurogenesis in general
Development_Neurogenesis_Axonal guidance
Cytoskeleton_Intermediate filaments
Cell adhesion_Cell junctions
Cell adhesion_Amyloid proteins
Development_Blood vessel morphogenesis
Cell adhesion_Integrin-mediated cell-matrix adhesion
Cell adhesion_Attractive and repulsive receptors
Cell adhesion_Cadherins
Cytoskeleton_Regulation of cytoskeleton rearrangement
0 2 4 6
-log(p-value)
yDN&CN
Development_Neuromuscular junction
Development_Regulation of angiogenesis
Protein folding_Folding in normal condition
Protein folding_ER and cytoplasm
Cell adhesion_Integrin priming
Inflammation_Protein C signaling
Development_Neurogenesis_Synaptogenesis
Cell adhesion_Glycoconjugates
Development_Neurogenesis_Axonal guidance
Protein folding_Response to unfolded proteins
Inflammation_Amphoterin signaling
Cell adhesion_Cadherins
Cytoskeleton_Regulation of cytoskeleton rearrangement
Cell adhesion_Cell junctions
Cell adhesion_Integrin-mediated cell-matrix adhesion
Reproduction_Feeding and Neurohormone signaling
Cytoskeleton_Actin filaments
Cell adhesion_Attractive and repulsive receptors
Immune response_Phagocytosis
Immune response_Phagosome in antigen presentation
Cell adhesion_Amyloid proteins
0 2 4 6 8
-log(p-value)
NB
Protein folding_Folding in normal condition
Protein folding_ER and cytoplasm
Reproduction_Feeding and Neurohormone signaling
Cell adhesion_Amyloid proteins
Protein folding_Response to unfolded proteins
Immune response_Antigen presentation
Immune response_Phagosome in antigen presentation
0 2 4 6 8
-log(p-value)
RGL
Proliferation_Negative regulation of cell proliferation
DNA damage_Checkpoint
0 1 2
-log(p-value)
PROG
Response to hypoxia and oxidative stress
0 1 2
-log(p-value)

Figure S5

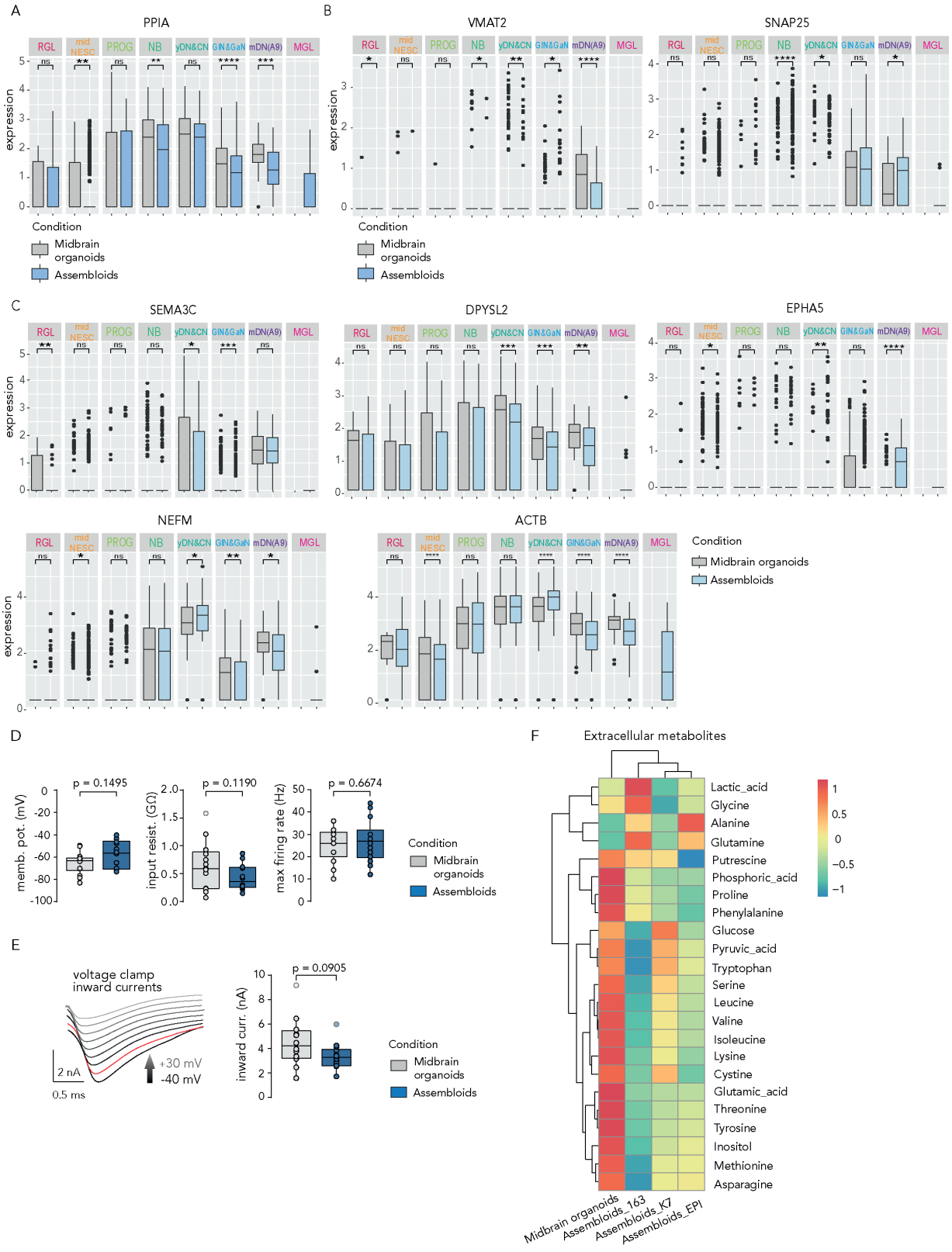
A
PPIA
B
VMAT2
SNAP25
RGL
mid NESC
PROG
NB
yDN&CN
GIN&GaN
mDN(A9)
MGL
expression
Condition
Midbrain organoids
Assembloids
C
SEMA3C
DPYSL2
EPHA5
NEFM
ACTB
D
memb. pot. (mV)
p = 0.1495
input resist. (GΩ)
p = 0.1190
max firing rate (Hz)
p = 0.6674
E
voltage clamp
inward currents
2 nA
0.5 ms
+30 mV
-40 mV
inward curr. (nA)
p = 0.0905
F
Extracellular metabolites
Lactic_acid
Glycine
Alanine
Glutamine
Putrescine
Phosphoric_acid
Proline
Phenylalanine
Glucose
Pyruvic_acid
Tryptophan
Serine
Leucine
Valine
Isoleucine
Lysine
Cystine
Glutamic_acid
Threonine
Tyrosine
Inositol
Methionine
Asparagine
Midbrain organoids
Assembloids_163
Assembloids_K7
Assembloids_EPI

Figure S6

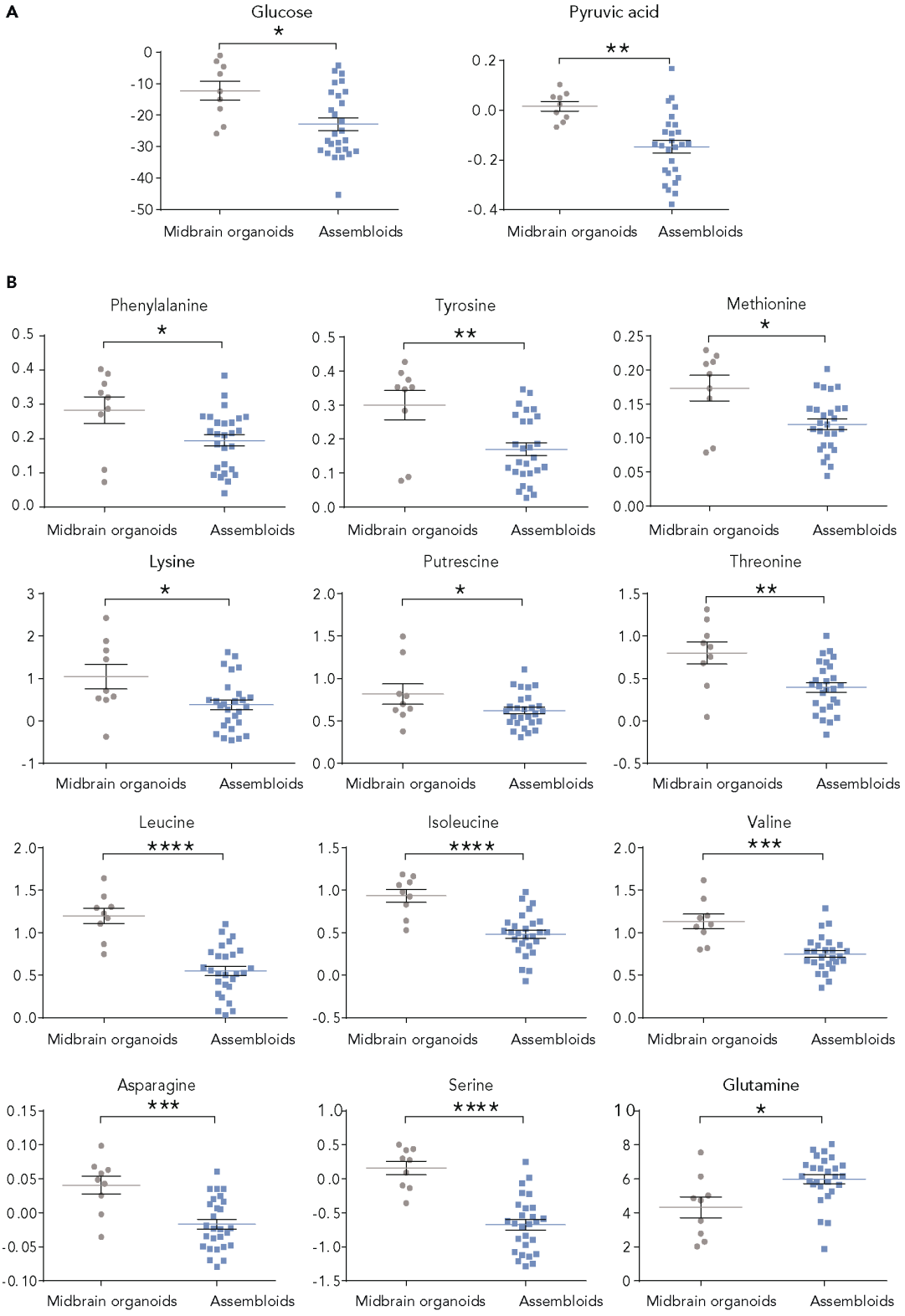
A
Glucose
*
0
-10
-20
-30
-40
-50
Midbrain organoids
Assembloids
Pyruvic acid
**
0.2
0.0
-0.2
-0.4
Midbrain organoids
Assembloids
B
Phenylalanine
*
0.5
0.4
0.3
0.2
0.1
0.0
Midbrain organoids
Assembloids
Tyrosine
**
0.5
0.4
0.3
0.2
0.1
0.0
Midbrain organoids
Assembloids
Methionine
*
0.25
0.20
0.15
0.10
0.05
0.00
Midbrain organoids
Assembloids
Lysine
*
3
2
1
0
-1
Midbrain organoids
Assembloids
Putrescine
*
2.0
1.5
1.0
0.5
0.0
Midbrain organoids
Assembloids
Threonine
**
1.5
1.0
0.5
0.0
-0.5
Midbrain organoids
Assembloids
Leucine
****
2.0
1.5
1.0
0.5
0.0
Midbrain organoids
Assembloids
Isoleucine
****
1.5
1.0
0.5
0.0
-0.5
Midbrain organoids
Assembloids
Valine
***
2.0
1.5
1.0
0.5
0.0
Midbrain organoids
Assembloids
Asparagine
***
0.15
0.10
0.05
0.00
-0.05
-0.10
Midbrain organoids
Assembloids
Serine
****
1.0
0.5
0.0
-0.5
-1.0
-1.5
Midbrain organoids
Assembloids
Glutamine
*
10
8
6
4
2
0
Midbrain organoids
Assembloids

Supplemental video legends

Video S1. Time-lapse of K7 microglia phagocytosing Zymosan particles. 449.55 frames, 29.97 frames per second.
Video S2. Time-lapse of 163 microglia phagocytosing Zymosan particles. 659.34 frames, 29.97 frames per second.
Video S3. Time-lapse of EPI microglia phagocytosing Zymosan particles. 689.31, 29.97 frames per second.

Supplemental Tables

Name	Simplified identifier	Identifier	Patient	Gender	Age of sampling	Source
K7	200	2.0.0.10.1.0	K7.1 WT/C4 WT	Female	81	Reinhardt et al., 2013
EPI	201	2.0.0.15.0.0	A13777	Female	Cord Blood	GIBCO/A13777
163	304	2.0.0.79.0.0	163	Male	66	SYSMED

Table S1 related to experimental procedures. iPS cell lines used in this study. Macrophage precursors were derived from iPSCs as described in the Experimental procedures section. Human neural precursors were derived from human iPSCs from the simplified identifier 200. Human midbrain-specific organoids were generated with neural precursors as described in the Experimental procedures section.

Reagent name	Company	Catalog number	Concentration
Advanced DMEM/F12	Thermo Fisher	12634010	-
N2	Thermo Fisher	17502001	1x
Pen/Strep	Invitrogen	15140122	1x
GlutaMax	Thermo Fisher	35050061	1x
2-mercaptoethanol	Thermo Fisher	31350-010	50 µM
IL-34	Peprotech	200-34	100 ng/mL
GM-CSF	Peprotech	300-03	10 ng/mL
BDNF	Peprotech	450-02	10 ng/mL
GDNF	Peprotech	450-10	10 ng/mL
DAPT	R&D Systems	2634/10	10 µM
Activin A	Thermo Fisher	PHC9564	2.5 ng/mL

Table S2 related to experimental procedures. Co-culture medium composition.

Antibody	Host species	Source	Ref.-No.	Dilution
IBA1	Goat	Abcam	ab5076	1:250
PU1	Rabbit	Cell signalling	2258S	1:250
CD45	Mouse	Biolegend	304002	1:1000
TMEM119	Rabbit	Sigma	HPA051870	1:250
P2RY12	Rabbit	Sigma	HPA014518	1:250
FOXA2	Mouse	Santa Cruz	sc-101060	1:250
LMX1A	Rabbit	Abcam	ab139726	1:100
PAX6	Rabbit	Biolegend	901301	1:300
SOX2	Goat	R&D systems	AF2018	1:100
SOX2	Rabbit	Abcam	ab97959	1:100
Nestin	Mouse	Millipore	MAB5326	1:100
TH	Rabbit	Abcam	ab112	1:1000
TUJ1	Chicken	Millipore	AB9354	1:1000
MAP2	Chicken	Abcam	ab5392	1:1000
MAP2	Mouse	Millipore	MAB3418	1:200
GFAP	Chicken	Millipore	AB5541	1:1000
SSEA-4	Mouse	Millipore	MAB4304	1:50
Oct-4	Rabbit	Abcam	ab19857	1:400
TRA-1-60	Mouse	Millipore	MAB4360	1:50
Nanog	Rabbit	Millipore	AB5731	1:200
TRA-1-81	Mouse	Millipore	MAB4381	1:50
VAMP2	Rabbit	Abcam	ab215721	1:1000
Actin-β	Mouse	Cell signalling	3700	1:100000
Alexa Fluor® 647 Anti-chicken	Donkey	Jackson Immuno	703-605-155	1:1000
Alexa Fluor® 488 anti-goat	Donkey	Invitrogen	A-11055	1:1000
Alexa Fluor® 568 anti-goat	Donkey	Thermo Fisher	a11057	1:1000
Alexa Fluor® 647 anti-goat	Donkey	Invitrogen	a21447	1:1000
Alexa Fluor® 488 anti-rabbit	Donkey	Thermo Fisher	a21206	1:1000
Alexa Fluor® 568 anti-rabbit	Donkey	Invitrogen	a10042	1:1000
Alexa Fluor® 647 anti-rabbit	Donkey	Invitrogen	a31573	1:1000
Alexa Fluor® 488 anti-mouse	Donkey	Invitrogen	a21202	1:1000
Alexa Fluor® 568 anti-mouse	Donkey	Invitrogen	a10037	1:1000

Hoechst 33342 Solution (20 mM)	-	Invitrogen	62249	1:10000
IgG H+L 800	Rabbit	Cell signalling	5151	1:10000
IgG H+L 680	Mouse	Cell signalling	5470	1:10000

Table S3 related to experimental procedures. Antibodies used in this study.

Primer	Sequence (5' to 3')	Region (Purpose)
h-RPL37A-F	GTGGTTCCTGCATGAAGACAGTG	RT-PCR
h-RPL37A-R	TTCTGATGGCGGACTTTACCG	RT-PCR
2241_AIF1_F	AGACGTTCAGCTACCCTGACTT	RT-PCR
2242_AIF1_R	GGCCTGTTGGCTTTTCCTTTTCTC	RT-PCR
2243_CD68_F	CTTCTCTCATTCCCCTATGGACA	RT-PCR
2244_CD68_R	GAAGGACACATTGTACTCCACC	RT-PCR
2289_P2RY12 FW	AAGAGCACTCAAGACTTTAC	RT-PCR
2290_P2RY12 RV	GGGTTTGAATGTATCCAGTAAG	RT-PCR
2291_TMEM119 FW	AGTCCTGTACGCCAAGGAAC	RT-PCR
2292_TMEM119 RV	GCAGCAACAGAAGGATGAGG	RT-PCR

Table S4 related to experimental procedures. Primers used in this study.

Stem cells	DA	VTA	Maturity	CN	GAN	GLN	SN
SOX2	NR4A2	ALDH1A1	SPRYD7	CHAT	GAD1	SLC1A1	SLC6A4
PAX6	PBX1	TUBB2A	SLC18A3	GAD2	SLC1A2	SLC18A2
HES5	GRIA3	TRHR	SKP1	GABARAP	SLC1A3	TPH1
ASCL1	TH	CD24	GNAI1	ACHE	GABARAP	SLC17A6	TPH2
SOX1	EN1	SLC18A2	MRAS	L1	FEV
PAX3	TMCC3	ATP1A3	GABARAP	SLC17A7	HTR1D
DACH1	NTM	FGF1	MAGED1	L2	HTR1E
LMO3	DDC	NRIP3	ARL2	ABAT	GLS	HTR1F
NR2F1	CAMK2N1	MPP6	MCFD2	GLS2	HTR2A
PLAGL1	ALDH1A1	NTS	MORF4L2	GRIN1	HTR2A−AS1
LIX1	APP	CCK	NRSN2	GRIN2A	HTR2B
HOXA2	PDZRN4	SOX6	NAP1L3	GRIN2B	HTR2C
FOXA2	PCDH10	GRIN2C	NGRN	GRIN2C	HTR3A
SLC1A3	ERBB4	SNCG	OLFM1	GRIN2D	HTR3B
MSI1	SLC10A4	IGF1	DKK3	GRIN3A	HTR3D
VIM	BEX5	ADCYAP1	CCDC136	GRIN3B	HTR4
NES	NPY1R	GRP	COX6C	GRINA	HTR5A
SHH	GPC2	LPL	HSP90AB1	GRIA1	HTR5A−AS1
CALB1	GRIA2
GRIA3
GRIA4

	HTRA2 HTRA3 HTRA4 PTX3 OTX2 EN2 SOX6 FOXA2 LMX1A LMX1B KCNJ6 CALB1 SLC6A3 SHH NKX6−1	SLC32A 1 VIP TACR3 DCC OTX2 SATB1	CALM2 ATP1B1 UQCRB COX4I1 PSMB5 FXYD7 RTN1 SEC62 COX7C CNTN1 FAIM2 SLC48A1 RAB3B NPTXR PDGFA NDUFC2 BEX2 UCHL1			HTRA1	

Table S5 related to results. Genes used for defining neuronal cell clusters and maturity. DA = Dopaminergic; VTA = ventral tegmental area; CN = Cholinergic; GAN = Gabaergic; GLN = Glutamatergic; SN = Serotonergic.

Name	Identifier
Cell 1	MglK7_CATCAGAAGGCCATAG.1
Cell 2	MglK7_AGGGATGGTGTCCTCT.1
Cell 3	MglK7_CTAAGACGTCTAGCGC.1
Cell 4	MglK7_CCGTGGACATCCTTGC.1
Cell 5	MglK7_AGTTGGTCAGCCTTTC.1
Cell 6	Mgl163_ACGCCAGTCATTGCCC.1
Cell 7	Mgl163_CATATTCTCCAATGGT.1
Cell 8	MglK7_CGCTGGAGTCCAGTTA.1
Cell 9	MglK7_AAGCCGCAGCTTCGCG.1
Cell 10	MglK7_CTCCTAGTCCTGCTTG.1
Cell 11	MglK7_CAAGGCCGTAGGCATG.1
Cell 12	MglK7_ACAGCCGCAGCTGCAC.1
Cell 13	MglK7_CAACCAACAGGAATGC.1
Cell 14	MglK7_ACGGGCTGTACAAGTA.1
Cell 15	MglK7_GTCTTCGCAATCCGAT.1
Cell 16	Mgl163_GCACATACATCGGACC.1
Cell 17	Mgl163_AGATCTGCAAACGTGG.1
Cell 18	Mgl163_ACGTCAAAGTTTAGGA.1
Cell 19	MglK7_GGATGTTGTCGCCATG.1
Cell 20	MglK7_TGTTCCGCAAGAGGCT.1
Cell 21	MglK7_GACTACAAGTAGGCCA.1
Cell 22	MglK7_TTAGGACAGGTTACCT.1
Cell 23	MglK7_GCTGGGTAGCGATATA.1
Cell 24	MglK7_GCTTGAAAGATACACA.1
Cell 25	MglK7_AAAGTAGGTGACTACT.1
Cell 26	MglK7_TATCTCACAGGTTTCA.1

Table S6 related to results. Identifiers of the 26 microglia cells.

4.4. MANUSCRIPT IV

Vascularization of human midbrain organoids leads to reduced hypoxia and a complex microglia morphology

This article is currently in preparation.

4.4.1. Preface

iPSC-derived midbrain organoids represent the human midbrain and its cellular heterogeneity. They contain functional neurons, which connect amongst each other through synaptic contacts and show electrophysiological activity and neurotransmitter release. Neurons in the system differentiate from neural progenitors, together with other cell types including astrocytes and oligodendrocytes (Monzel et al., 2017; Smits et al., 2019, 2020). Midbrain organoids have been used to investigate genetic Parkinson's disease associated with *LRRK2* and *PINK1* mutations (Jarazo et al., 2021; Smits et al., 2019). Furthermore, they have been applied for compound testing (Jarazo et al., 2021). However, midbrain organoids do not fully recapitulate the human midbrain, since cell types with other developmental origin than neuroectodermal do not occur innately in the system. Vasculature in the brain supports cells with oxygen and nutrients, and compose the BBB, a system with major importance for brain homeostasis regulation. The vasculature interacts with other cell types in the brain forming complexes such as the neurovascular unit, which are affected in neurodegenerative diseases like PD.

In this work, we developed and characterized midbrain-vascular assembloids by fusion of midbrain and blood vessel organoids. Assembloids contained endothelial cells that made contacts through adherens junctions. Pericyte and basal lamina markers were detected in assembloids. After establishing the model, we studied the effects that endothelial networks had on assembloids. We hypothesized that a vasculature-like system would ameliorate hypoxia and viability in the assembloid cells. These speculations were validated by lower levels of hypoxia and cell death in assembloids. To study cellular interactions in a complex midbrain-specific model containing all cell types in the brain, we successfully integrated microglia into vascularized assembloids. We observed contacts between microglia, endothelial cells and neurons. Furthermore, both microglia and endothelial cells showed increased process elongation when they were co-cultured together. This advanced midbrain organoid system better recapitulates the cellular diversity and complex contacts in the human midbrain.

This article is the second main result of my PhD studies. I derived neural progenitor cells and generated vascular and midbrain organoids for co-culture. I generated assembloids and co-cultured them with macrophage precursors for further analysis. K. Haendler did the pre-processing of samples for snRNA-Seq. A. Zagare and K. Barmpa analysed the sequencing data. C. Saraiva participated in the experiment design and performance. She supervised the work and revised the manuscript. I performed and analysed the rest of the experiments, made the figures and wrote the manuscript.

Vascularization of human midbrain organoids leads to reduced hypoxia and increases the morphological complexity of microglia

Sonia Sabate-Soler[1], Alise Zagare[1], Kyriaki Barmpa[1], Kristian Haendler[2], Malte Spielman[2], Cláudia Saraiva[1*], Jens Schwamborn[1*,]

1 Luxembourg Centre for Systems Biomedicine (LCSB), Developmental and Cellular Biology, University of Luxembourg, Belvaux, Luxembourg.

2 Institut für Humangenetik, Universitätsklinikum Schleswig-Holstein, Lübeck, Germany

* Joint corresponding authors

Abstract

The use of complex human-based cell culture systems has rapidly increased in the last years, due to their translatability and heterogeneous cellular composition, which allows the study of molecular and cellular interactions. Study of brain specific regions such as the midbrain are of importance not only to better understand human development but also neurodegeneration. In fact, we have developed midbrain organoids containing neuroectoderm-derived cell types, such as neurons, astrocytes and oligodendrocytes. Functionality of neurons in the system has been proven, and the model has been used to investigate genetic Parkinson's disease. However, this midbrain organoid model does not contain all cell types in the midbrain. The lack of a vasculature system represents a limitation in terms of oxygen and nutrient supply. Furthermore, interactions between neurons and glia with blood vessels cannot be studied in the absence of a vasculature network. In this work, we successfully incorporated a vasculature network into midbrain organoids by fusion with vascular organoids. We developed midbrain-vascular assembloids that contain endothelial cells, adherens junction markers, pericytes and basal lamina markers. The integration of a vasculature system leads to a decrease of hypoxia and cell death in assembloids. Finally, incorporation of microglia into vascularized assembloids showed an increase of microglia elongation and ramification in the presence of vasculature. Altogether, we present an optimized midbrain model, containing neuronal cells (including dopaminergic neurons), glia cells, as well as microglia and vasculature, which makes it more similar to the actual human midbrain in terms of cellular composition.

Introduction

Three dimensional (3D) organoid models have been increasingly developed and used over the last years, since they accurately represent the cellular organization and functionality of human organs (Broutier et al., 2016; Lancaster et al., 2013; Morizane et al., 2015). The brain is a highly complex system, with many different cell types organized in different regions. Whole brain (Lancaster et al., 2013; Lindborg et al., 2016) and region-specific (Birey et al., 2017; Jo et al., 2016; Monzel et al., 2017) organoid models have been developed in the last years. Our efforts have focused on the development of midbrain-specific organoids, which have been proven a suitable model for Parkinson's Disease (PD, Jarazo et al., 2021; Monzel et al., 2017). Midbrain organoids have a heterogeneous cellular composition, containing neuroectoderm-derived cell types and progenitor cells. Neurons in midbrain organoids are functional, and able to communicate with one another through synaptic contacts (Smits et al 2019).

In order to increase the complexity of brain organoid models, researchers have focused on the incorporation of a vasculature system and microglia over the last years. Because of their mesodermal origin, microglia and endothelial cells do not occur innately in neuroectoderm-patterned brain organoid systems. However, in Ormel et al., 2018, a protocol to innately induce microglia differentiation in iPSC-derived cerebral organoids is described. In the case of microglia, scientists have achieved successful co-cultures of cerebral organoids with microglia (Mansour et al., 2018). Integration of a vasculature system in whole brain and region-specific organoids has been attempted over the last decade (Bergmann et al., 2018; Miller et al., 2012; Pham et al., 2018). Several approaches have been applied, including an external incorporation of mesoderm-derived cells, (Bergmann et al., 2018; Wörsdörfer et al., 2020) and integration of artificial scaffolds (Miller et al., 2012; Nashimoto et al., 2017). Furthermore, transplantation of organoids into mice has been achieved in order to benefit from external angiogenesis into the organoid structure (Mansour et al., 2018; Pham et al., 2018). Recently, a study where cerebral organoids were co-cultured with vascular organoids showed promising results in terms of blood vessel integration into cerebral tissue (Ahn et al., 2021). Until now, there are no studies showing an integration of human iPSC-derived vasculature into midbrain organoids. We believe that an approach based on the co-culture of two types of human organoids, where vascular cells invade the midbrain tissue to form a complex assembloid would avoid high stress conditions due to tissue disaggregation, single-cell handling or incorporation of artificial scaffolds. Furthermore, not relying on animal models represents an advantage in terms of reproducibility, cost-efficiency and ethical concerns.

Vascularization in the brain starts its development externally in the perineural vascular plexus, and invades the developing brain at early embryonic age (Jones, 1970; Kurz et al., 1996;

Raybaud, 2010; Ruhrberg and Bautch, 2013). Vascularization in the brain is organized in arterioles and capillaries, which structurally compose the blood-brain-barrier (BBB) and the blood-cerebrospinal fluid-barrier (Abbott et al., 2010; Di Giovanna et al., 2018; Ohtsuki and Terasaki, 2007). Blood vessels are composed by endothelial cells connected by specific junctions, pericytes and the basal lamina containing smooth muscle cells (Imagawa et al., 1994; Mcdonald and Larue, 1983; Stehbens et al., 2009). In the brain, they interact with neuronal projections, astrocyte feet and microglia in the neurovascular unit (Bell et al., 2010; McConnell et al., 2017; Ruhrberg and Bautch, 2013). In this article, we show the successful integration of a vasculature system in midbrain organoids by co-culture of midbrain and vascular organoids. Midbrain-vascular assembloids express endothelium markers, and preserve the proportion of dopaminergic neurons in the system.

We hypothesized that the presence of a vasculature system in midbrain organoids would not only bring the model closer to the actual situation in the human brain, but also help the oxygen flow in the organoid centre. The lack of oxygen and nutrients in the inner core of the organoid is a common issue in 3D models, often leading to high levels of cell death and the so called “dead core” (Monzel et al., 2017). This phenomenon is not restricted to midbrain organoids, since it has been observed in other types of organoids (Beauchamp et al., 2015; Lancaster et al., 2013; Ramachandran et al., 2015). Midbrain organoids miss a functional vasculature system that would provide the inner centre with oxygen and nutrient supplies, decreasing the hypoxia levels in the system by allowing for a better oxygen flow. We show that hypoxia levels in assembloids are significantly lower than in midbrain organoids, proving the successful oxygen supply by the endothelial network.

Furthermore, by co-culture of assembloids with macrophage precursors and differentiation into microglia in 3D, we obtained a complex assembloid system where microglia spatially interact with endothelial cells and neuron processes, mimicking the neurovascular unit *in vitro*. Finally, microglia in assembloids display a more complex morphology compared to non-vascularized midbrain organoids, further demonstrating the importance of a vasculature network in the organoid system. We advanced the midbrain organoid model into midbrain-vascular assembloid containing microglia, a system that could be further explored to study blood vessel and BBB instability as well as neuroinflammation in physiology and pathology.

Results

Midbrain-vascular assembloids show different cell clusters and preserve the dopaminergic neuron identity

In order to integrate a vascular system into midbrain organoids, we derived neuro-epithelial stem cells (NESCs) from quality-controlled iPSCs (Figure S1) and generated vascular organoids following Wimmer et al., 2019. We used two *wild-type* cell lines (#200 and #201) and cultured the organoids until day 13. At that time point we embedded them in an extracellular matrix gel together with midbrain organoids (generated following Nickels et al., 2020), which were at day 8 of culture (day 6 of differentiation). We cultured the system together for 24 more days, until day 30 of dopaminergic differentiation. Midbrain organoids cultured in the absence of vascular organoids were used as control (Figure 1A). After performing single nuclear RNA sequencing (snRNA-Seq) and quality-control the data (Figure S2), we studied cell type clustering based on published information about the gene identity of human embryonic midbrain populations (La Manno et al., 2016). We observed different cell clusters in midbrain organoids and assembloids (Figure 1B and C). While there were clusters identified as pericytes or endothelial cells in midbrain organoids, there were only containing one or few cells. However, in assembloids and in lower measure in midbrain organoids, two pericyte-like cell clusters were identified (Figure 1B and C). Interestingly, a shift on the progenitor cell clusters was observed between groups; while in midbrain organoids we observed few cells in the three radial glia clusters, two big neural progenitor clusters were shown (Figure 1C and D).. On the other hand, in assembloids the neural progenitor cell cluster was composed by few cells, while the radial glia clusters were represented by a considerably higher amount of cells (Figure 1C and D, Figure S3). In line with that observation, cell type clustering by gene expression showed two different main clusters; one formed by two dopaminergic neuron and two neural progenitor sub-clusters, and another one composed by three radial glia and two pericyte-like sub-clusters (Figure 1E). To verify that the dopaminergic neuron clusters were not affected by the co-culture, we checked the gene expression of the dopaminergic genes *TH* and *FOXA2,* and observed a similar expression in both groups (Figure 1F). Western blot for TH and analysis of TH over the neuronal population (TUJ1-positive) confirmed the snRNA-Seq observation (Figure 1G), confirming that the dopaminergic neuron population is not compromised by the assembloid generation procedure.

Assembloids express specific vascular markers and show blood vessel-like organization

By day 30 of differentiation, assembloids from lines #200 and #201 showed the presence of the endothelial cell marker CD31, as well as the dopaminergic neuron marker TH and the pan-neuronal marker MAP2 (Figure 2A). Since non-vascularized midbrain organoids did not show any positive CD31 structure, we focused on studying the components of endothelial networks in vascularized assembloids. Immunofluorescence staining for the basement membrane and extracellular matrix protein Collagen IV showed positive structures in assembloids, which organized spatially in a similar way as CD31-positive endothelial cells (Figure 2B). Staining for alpha smooth muscle actin, a capillary pericyte and vascular smooth muscle cell and marker, showed positive cells (Figure 2C). The presence of vascular-specific adherens junctions between endothelial cells was confirmed by VE-Cadherin staining in assembloids (Figure 2D). Flow cytometry analysis with organoid and assembloid cells stained for VE-Cadherin, showed a tendency of an increase in assembloids. In addition, the amount of cells expressing the pericyte marker PDGFRβ increased around 20 times in assembloids compared to midbrain organoids (Figure 2E). High magnification immunofluorescence images showed a cell organization of CD31-positive endothelial cells in a tubular-like manner (Figure 2F). Overall, we show the presence of endothelial cells connected by tight junctions, pericytes and basal lamina in assembloids, which seem to be organized in vessel-like structures.

In line with these results, snRNA-Seq data showed differences in several pathways, and extracellular matrix (ECM) remodelling and cell adhesion pathways were often represented amongst them (Figure 3A). Several cell adhesion and ECM-related genes were differentially expressed between midbrain organoids and assembloids (Figure 3B). Interestingly, an up-regulation of gene markers related to astrocyte differentiation was observed in assembloids compared to midbrain organoids (Figure 3C).

Assembloids show lower LDH release and hypoxia levels

After confirming the presence of an endothelium network in assembloids, we assessed the effects that it has on hypoxia and cell viability. After measuring the midbrain organoid and assembloid area at day 30 of differentiation, we confirmed that assembloids are significantly larger than midbrain organoids (Figure 4A and B). We performed a viability LDH assay, and observed a significantly lower LDH release in assembloids compared to midbrain organoids (Figure 4C), suggesting that considering the total cell population assembloids have lower levels of cell death. To understand if this lower cell death level was related with a better oxygenation of the organoids we assess hypoxia levels using the hypoxyprobe assay and staining, which allows the detection of hypoxic cells in the system. We used midbrain

organoids and assembloids at day 15 of differentiation. Assembloids showed a significantly lower amount of hypoxic cells, suggesting that the endothelial system participates in decreasing hypoxia in assembloids (Figure 4D).

Microglia in assembloids show a more complex morphology compared to midbrain organoids

After confirming the endothelial identity in assembloids and assessing differences in terms of cell death, hypoxia and gene expression, we investigated the assembly of a neurovascular unit in assembloids. For that, we co-cultured midbrain organoids or assembloids from the cell line #201 with macrophage precursors, and cultured the system until day 30 of differentiation (Figure 5A). First, to confirm that macrophage precursor cells differentiate into microglia, we plated a subset in 2D, cultured them for 14 days with microglia differentiation medium and fixed them. Then, we performed an immunofluorescence staining for the microglia markers IBA1 and PU1, and confirmed that 2D-differentiated microglia expressed those markers (Figure 5B). Then, we proceeded to the co-cultures, and observed that throughout the co-culture time macrophage precursors are attracted to the organoid and assembloid surroundings and eventually integrate into the system (Figure 5C). After sectioning and immunostaining organoids and assembloids, we observed IBA1-positive cells in organoids and assembloids that had been co-cultured with macrophage precursors and CD31-positive cells in assembloids (Figure 5D). 3D reconstructions of immunostaining images showed a close interaction between microglia and endothelial cells (Figure 5E, upper panels). Furthermore, this microglia-endothelial complex made contacts with TH-positive projections, showing neurovascular unit-like interactions (Figure 5E, bottom panels). We observed that microglia and endothelial cells in assembloids seemed to have a more ramified morphology in compared to midbrain organoids. These observations were confirmed with image analysis, where we measured the length sum of processes per cell using the Imaris software. Microglia processes were significantly longer in assembloids compared to midbrain organoids (Figure 5F). Furthermore, the length of endothelial cell processes was higher in assembloids with microglia compared to the ones without microglia (Figure 5G). Thus, in terms of morphology and process length, both microglia and endothelial cells seemed to benefit from each other's presence in the system.

Discussion

Midbrain-vascular assembloids contain endothelial cell and pericyte clusters while maintaining the dopaminergic neuron population

Recent efforts have focused on integrating a vascular-like system in human brain organoids. Amongst the approaches that have been assessed are the co-culture of endothelial progenitor cells with organoids or neural cells (Bergmann et al., 2018; Wörsdörfer et al., 2019). However, these organoids missed some neural cell types, or needed transplantation into mice to fully develop their endothelium network. Transplantation of human brain organoids into mice has been one of the most successful approaches to promote angiogenesis. This has been done either without previous endothelial participation (Mansour et al., 2018) or with prior organoid coating with endothelial cells (Pham et al., 2018) Genetically modifying embryonic stem cells to ectopically overexpress the gene *ETV2*, involved in endothelial cell development, have also been explored prior to transplantation into mice (Cakir et al., 2019). However, the need of transplantation into animal models makes the experimental aspects of the studies more difficult in terms of reproducibility, cost, ethical concerns and amount of replicates.

In this study, we successfully integrated a vascular network into midbrain organoids by co-culture with vascular organoids. snRNA-Seq results show the presence of 9 different cell clusters in assembloids, including two pericyte-like clusters. Pericyte-like clusters were characterized by the expression of genes related to mesenchyme and vasoconstriction (cluster 1), and to junction proteins and ECM processes (cluster 2). These clusters were also represented in midbrain organoids, although the number of cells of both clusters were much lower than in assembloids. This observation is not too surprising, considering that in previous analysis of midbrain organoids, cells identified as ‘pericyte-like’, also named ‘mesenchymal cells’ or ‘fibroblasts have been identified (Smits et al., 2020; Zagare et al., 2022).

Interestingly, we observed a shift in the cell type distribution in assembloids compared to midbrain organoids. Midbrain organoids presented two big neural progenitor clusters, and three radial glia clusters represented by few cells. Assembloids’ cell distribution was shifted in favour of the radial glia clusters, while the neural progenitor groups contained few cells. This could be due to the different origins of the starting cell population in midbrain organoids (neuro-epithelial stem cells) and vascular organoids (iPSCs), and the different media composition of both systems prior to co-culture (Wimmer et al., 2019). Moreover, recent studies confirmed that endothelial cells and vasculature have close interactions with radial glia in the developing brain. At embryonic and post-natal stages, endothelial cells participate in the docking of radial glia processes into the pial surface – the barrier between grey matter and cerebrospinal fluid (Segarra et al., 2018). Neural precursor cells use vasculature processes to migrate through

the nervous system (Snapyan et al., 2009). Furthermore, vasculature cells contribute to radial glia maturation and differentiation into astrocytes (Segarra et al., 2018; da Silva et al., 2019). On the other hand, radial glia participates in the angiogenesis process in the developing brain (Matsuoka et al., 2016; Siqueira et al., 2018; Zhang et al., 2020). Thus, endothelial cells and vasculature networks in assembloids may participate in the development and differentiation of radial glia cells, while neuronal progenitors are, in proportion, less represented in assembloids compared to midbrain organoids. Nevertheless, the fact that TH and FOXA2 positive neurons are preserved in assembloids indicates that the dopaminergic neuron population is not affected by the assembloid generation, and that they hold a vascularized midbrain identity.

Radial glia-like cells in the midbrain can differentiate into dopaminergic neurons (Bonilla et al., 2008). Therefore, studying the amount of dopaminergic neurons in later time points of culture would be interesting to explore whether the dopaminergic neuron population increases with respect to non-vascularized organoids, which have a lower radial glia population. Furthermore, radial glia cells act as a scaffold that developing neurons use to migrate in the brain (Rakic, 1972; Sidman and Rakic, 1973). This could mean that the regionalization of neuronal populations in midbrain organoids could be accentuated in vascularized organoids thanks to the radial glia populations. Finally, radial glia fibres have been proven to enhance neuronal regeneration and functionality upon injury via neuroblast migration (Jinnou et al., 2018). Studying the recovery of neurons upon injury in vascularised organoids would be of interest to compare the neuron regeneration capacity in organoids and assembloids.

Endothelial networks in midbrain-vascular assembloids express specific markers and displays vessel-like structures

After assessing the presence of different cell clusters, including two pericyte-like clusters, we focused on blood vessel-like structures in assembloids. Immunostaining images showed visibly different structures between organoids and assembloids, which seemed to have an overall less compact tissue with more cavities. We showed the presence of endothelial cells, the main cell type in vasculature networks. Positive immunofluorescence and FACS staining for VE-Cadherin indicate that endothelial cells make contacts with each other through adherens junctions. Studies have demonstrated the high importance of VE-Cadherin in vascular networks, since it controls the development of tight junctions by up-regulation of the gene encoding for tight junction adhesive protein Claudin-5 (Duong and Vestweber, 2020; Taddei et al., 2008). Staining for type IV Collagen showed positive structures, proving the presence of an extracellular matrix and basal lamina. Furthermore, FACS analysis showed positive cells for the pericyte marker PDGFRβ, with a tendency to an increase in assembloids. Positive structures for alpha-smooth muscle actin, marker of brain capillary pericytes and

vascular smooth muscle cells were also observed in immunofluorescence staining in assembloids. The endothelial cell marker CD31 seemed to spatially organize with VE-cadherin, collagen IV and alpha-smooth muscle actin, indicating that there is an endothelial network organized in a blood vessel-like manner. Immunofluorescence assays showed a tubular-like organization of CD31-positive endothelial cells, suggesting that blood vessel structures have tubular-like shape in assembloids.

SnRNA-Seq analysis showed that multiple pathways were differentially regulated in assembloids compared to midbrain organoids. Amongst these pathways, the ones related to ECM remodelling and cell adhesion were the most significant ones. Since cell adhesion molecules – such as integrins and fibronectin – and ECM processes are highly related (Deem and Cook-Mills, 2004; Francis et al., 2002; McCarty et al., 2002), the observed up-regulation of cell adhesion and ECM-related genes could be due to the blood vessel development and angiogenesis in the system.

Initial studies about astrocyte development and differentiation showed that they originate from radial glia cells during brain development (Levitt and Cooper, 1981; Levitt et al., 1983; Misson et al., 1988). Later studies proved that astrocytes, but also a neuronal subset derive from radial glia (Barry and McDermott, 2005; Malatesta et al., 2000; Noctor et al., 2001). In our dataset, snRNA-Seq results showed a higher expression of genes related to astrocyte differentiation. This could be because there is a much higher representation of radial glia clusters in assembloids. Furthermore, previous studies have shown that vasculature and angiogenesis participate in astrocyte differentiation in the developing brain and retina (Duan et al., 2017; Mi et al., 2001; Segarra et al., 2018; da Silva et al., 2019). Thus, the vasculature network in assembloid could be participating in astrocyte differentiation. To verify this observation, a comparison of the astrocyte amount in assembloids against midbrain organoids should be assessed with later time point cultures. Next steps could focus on later time points, where astrocyte differentiation is more abundant, and explore whether astrocyte feet interact with the neurovascular-like complex.

Hypoxia levels in assembloids against midbrain organoids suggest an improvement in oxygen supply

In 3D cell culture models, we can often observe high cell death levels in the inner core of the tissue. This is mainly caused by the lack of oxygen and nutrients, leading to high hypoxia levels in the core. Multiple studies with organoids – including midbrain – have showed this phenomenon (Beauchamp et al., 2015; Lancaster et al., 2013; Monzel et al., 2017; Ramachandran et al., 2015). Some attempts to overcome this issue include protocol optimisation in order to decrease organoid size and therefore allow nutrient and oxygen

diffusion to the organoid tissue (Nickels et al., 2020). Other approaches focused on slicing of live organoids and culture of organoid sections to avoid big structures where the core receives limited oxygen and nutrients (Qian et al., 2020).

We assessed cell viability and hypoxia in our iPSC-derived vascularized assembloids and compare the levels to midbrain organoids. We performed an LDH assay using culture supernatants. We normalized the LDH release results to organoid and assembloid size, since assembloids are significantly bigger. The results show a significantly lower LDH release in assembloids, indicating lower cell death. Furthermore, we studied hypoxia levels in both groups thanks to the Hypoxyprobe kit. We observed that the percentage of hypoxic cells decrease significantly in assembloids compared to midbrain organoids at day 15 of dopaminergic differentiation. These results suggest that the integration of an endothelial network by co-culture with vascular organoids may result in an overall less compact tissue, allowing for oxygen to better flow through the structure. The presence of blood vessel-like structures may result in a more efficient organoid oxygenation and nutrient supply in assembloids. Previous studies have shown that reduction of hypoxia by angiogenesis leads to neural stem cell differentiation (Lange et al., 2016). This could indicate that in later time points there may be differences in stem cell differentiation in assembloids compared to midbrain organoids.

Microglia interact with endothelial cells and display a more complex morphology in assembloids

In order to study microglia morphology and their interaction with endothelial cells in 3D, we co-cultured midbrain organoids with macrophage precursors at an early culture stage to promote microglia differentiation within organoids and assembloids. Immunofluorescence images show that microglia seem to make contacts with endothelial cells and TH-positive neuron projections. Those contacts can be also observed in 3D reconstructions, suggesting neurovascular-like interactions in assembloids. We visibly observed that microglia in assembloids displayed a different morphology than in non-vascularized midbrain organoids. After image analysis of IBA1-positive cells, we confirmed, in the presence of vasculature, microglia processes are longer. Furthermore, we showed that CD31-positive endothelial cell processes are also longer in the presence of microglia. Thus, it seems that the co-habitation of vasculature with microglia leads to an increase of process elongation in both cell types. Upon injury or disease, microglia morphology tends to become amoeboid and migrate to the injury site, however in healthy conditions, microglia display motile processes that survey the environment (Morrison et al., 2017; Yang et al., 2019). Furthermore, there is a positive correlation between microglia elongation and ramification and developmental age (Cengiz et

al., 2019; Harry and Kraft, 2012). These previous evidences indicate that microglia in assembloids could fit a more mature morphological profile. Assessing cytokine and chemokine secretion, as well as microglial maturation, would be of high value to decipher the molecular implications of these morphological changes.

Endothelial cells showed longer processes in the presence of microglia. Endothelial cells undergo an elongation and sprouting prior to vessel formation and closure (Tsuji-Tamura and Ogawa, 2018). Thus, the higher elongation of endothelial cells in assembloids with microglia compared to the ones without microglia could indicate that the process of tube formation could be enhanced. Analysis of later time points, where vessel formation may be advanced and tubular structures may close completely would be of high value to confirm this hypothesis. Furthermore, studies have showed that elongated endothelial cells suppress the activation of monocytes *in vitro*, and culture of monocytes with supernatant of elongated endothelial cells had the same effect (Liang et al., 2020). This suggests that factors in the endothelial secretome may contribute to the suppression of immune cell activation. Oppositely, dysfunction of endothelial cells in pathological conditions such as stroke and ischemic injury leads to microglial activation, where microglia secrete pro-inflammatory cytokines and change their morphology into an amoeboid shape (Iadecola and Anrather, 2011; Perego et al., 2011).

Methods

2D cell culture

Generation of iPSCs (Table 1) was done as described in Reinhardt et al., 2013. In short, 6-well plates (Thermo Scientific, 140675) were coated with Matrigel® (Corning, 354277) and 300K cells were plated per well. We used Essential 8 Basal medium (Thermo Scientific, A1517001) for cell maintenance, with a daily medium change. The first 24 h after cell splitting or thawing, the medium was supplemented with 10 µM ROCK Inhibitor (Y-27632, Millipore, SCM075). When confluence reached 70-90%, cells were split by incubating for 5 minutes with Accutase® (Sigma, A6964). The generation of neural progenitor cells from iPSCs and their maintenance were performed as described in Nickels et al., 2020; (Smits et al., 2019). The derivation of macrophage precursors from iPSCs and their maintenance were performed as described in Haenseler et al., 2017.

3D cell culture

Midbrain organoid generation and culture

We generated and cultured midbrain organoids as described in Nickels et al., 2020 and Smits et al., 2019. In short, 6,000 cells were seeded per well in an Ultra-Low Attachment 96-well plate (Merck, CLS3474) and cultured in maintenance medium (N2B27 medium supplemented with 0.2 mM Ascorbic acid (Sigma, A4544), 3 µM CHIR 99021 (Axon Medchem, CT 99021), 0.5 µM Smoothened Agonist, SAG (Merk Millipore, 566660), 2.5 µM SB-431542 (Abcam, ab120163), 0.1 µM LDN-193189 (Sigma, SML0559)) for 2 days. Then, the medium was replaced to induce a ventral midbrain patterning (day 0 of dopaminergic differentiation) by removing SB and LDN. Two days after, CHIR concentration was reduced to 0.7 µM. On day 6 of dopaminergic differentiation, the medium was replaced by maturation medium (N2B27 plus 0.2 mM Ascorbic acid, 10ng/mL Brain Derived Neurotrophic Factor, BDNF (Peprotech, 450-02), 10 ng/mL Glial-Derived Neurotrophic Factor, GDNF (Peprotech, 450-10), 1 pg/mL TGF-β3 (Peprotech, 100-36E), 10 µM DAPT (R&D Systems, 2634/10) and 2.5 ng/mL Activin A (Thermo Scientific, PHC9564)). We kept the spheroids in static conditions (without shaking) until day 4 of dopaminergic differentiation - when they were co-cultured with macrophage precursors - or day 6, when they were embedded in Matrigel® (Corning, 354277) as described in Monzel et al., 2017 or co-cultured with vascular organoids.

Vascular organoid generation and culture

We generated and cultured vascular organoids as described in Wimmer et al., 2019 with slight modifications. In short, 3000 iPSCs were seeded per well in a 96-well plate resuspended in vascular differentiation medium (DMEM/F12 medium (Thermo Fisher, 21331020), 20% KOSR (Thermo Fisher, 10828028), 1x Glutamax (Thermo Fisher, 35050061), 1x NEAA (Thermo Fisher, 11140050)), supplemented with 50 µM ROCK Inhibitor (Y-27632, Millipore, SCM075) and placed in an incubator with hypoxic conditions (5% O_2). On day 3 after seeding, the medium was exchanged and supplemented with 12 µM CHIR99021. On days 5, 7 and 9, the medium was exchanged again, and supplemented with 30 ng/mL BMP4 (Peprotech, 120-05), 30 ng/mL VEGF-A (Peprotech, 100-20) and 30 ng/mL FGF-2 (Peprotech, 100-18B). On day 11, the exchanged medium contained 30 ng/mL VEGF-A, 30 ng/mL FGF-2 and 10 µM SB-43152. On day 13, vascular organoids were used for co-culture with midbrain organoids and embedded in Matrigel® as described in Monzel et al., 2017 (Figure 1A).

Co-culture of midbrain organoids with vascular organoids

Co-culture of midbrain and vascular organoids was done by co-embedding at day 6 of midbrain dopaminergic differentiation and day 13 of vascular organoid culture (Figure 1A). Midbrain and vascular organoids were placed together in a Matrigel® droplet of around 30 µl, and let polymerize for 25 minutes at 37°C. After that, they were transferred into 24-well plates and cultured with midbrain maturation medium on an orbital shaker rotating at 80 rpm.

Co-culture of midbrain organoids and midbrain-vascular assembloids with macrophage precursors

Two days before the embedding, at day 4 of dopaminergic differentiation, midbrain spheroids were organized into four sub-groups; midbrain organoids, midbrain organoids with microglia, midbrain-vascular assembloids and midbrain-vascular assembloids with microglia. The culture medium of the four groups was exchanged into co-culture medium (Advanced DMEM/F12 (Thermo Fisher, 12634010), 1x N2 (Thermo Fisher, 17502001), 1x Pen/Strep (Invitrogen, 15140122), 1x Glutamax (Thermo Fisher, 35050061), 50 µM 2-mercaptoethanol (Thermo Fisher, 31350-010), 100 ng/mL IL-34 (Peprotech, 200-34), 10 ng/mL GM-CSF (Peprotech, 300-03), 10 ng/mL BDNF, 10 ng/mL GDNF, 10 µM DAPT and 2.5 ng/mL Activin A. For the groups that would contain microglia, macrophage precursors were resuspended in the culture medium and added on the well (186K macrophage precursors per midbrain organoid, and 450K macrophage precursors per midbrain-vascular assembloid, Sabate-Soler et al., 2022). Two days after, we proceeded with the embedding as described previously.

Immunofluorescence staining in 2D

For immunofluorescence staining of iPSCs and neural cell precursors, cells were cultured in glass coverslips. When they reached a confluence of about 60%, they were fixed for 15 min with 4% formaldehyde (Sigma, 100496) and washed 3x with PBS. Then, permeabilization was done by using 0.3% Triton X-100 in 1x PBS for 15 minutes, followed by 3 washes with PBS and blocking with 3% BSA (Carl Roth, 80764) in PBS at room temperature for 1h. After that, we incubated the cells in a wet chamber, overnight (16h) at 4°C with the primary antibodies (diluted in 3% BSA + 0.3% Triton X-100 in 1xPBS, Table 2). Cells were rinsed 3x with PBS and further incubated with secondary antibodies diluted in 3% BSA + 0.3% Triton X-100 in 1x PBS for 1 hour at room temperature. They were washed 3 more times with PBS and one time

with water, and the coverslips were then mounted in a glass slide using Fluoromount-G® (Southern Biotech, Cat. No. 0100-01).

Immunofluorescence staining in 3D

At day 30 of dopaminergic differentiation, midbrain organoids and assembloids were fixed with 4 % Formaldehyde overnight (16h) at 4°C and washed 3 times with PBS for 15 min.

For immunostainings of organoid and assembloid sections, they were embedded in 4 % low-melting point agarose (Biozym, Cat. No. 840100) in PBS. A vibratome (Leica VT1000 S) was used to slice the organoids and assembloids into 70 or 120 µm sections. Blocking and permeabilization of sections was done with 0.5% Triton X-100, 0.1% sodium azide, 0.1% sodium citrate, 2% BSA and 5% donkey serum in PBS for 90 min at room temperature. Primary antibodies (Table 2) were diluted in 0.1% Triton X-100, 0.1% sodium azide, 0.1% sodium citrate, 2% BSA and 5% donkey serum, and sections were incubated with the primary antibody solution for 48 h at 4°C in a shaker. Then, sections were washed 3 times with PBS and incubated with secondary antibodies in 0.05% Tween-20 in PBS for 2 h at RT. After that, they were 3 times washed with 0.05% Tween-20 in PBS and one time with water. Sections were mounted in Fluoromount-G mounting medium on a glass slide.

For whole mount staining of organoids and assembloids, blocking and permeabilization of the entire organoid or assembloid tissue was done with 1% Triton X-100, 10% donkey serum in PBS for one day (18-24h) at room temperature on a shaker. Primary antibody solutions were prepared in 0.5% Triton X-100, 3% donkey serum in PBS. Organoids and assembloids were incubated with the primary antibody solution 4 days at 4°C on a shaker. Then, they were washed 3 times with PBS, for 1h, at room temperature. Secondary antibody solutions were prepared in 0.5% Triton X-100, 3% donkey serum in PBS, and organoids and assembloids were incubated for 2 days at 4°C on a shaker. After that, they were washed 3 times with 0.05% Tween-20 in PBS, 5 minutes at room temperature and they were mounted in Fluoromount-G mounting medium on a glass slide. To reduce possible squeezing of organoids and assembloids, several layers were drew on the glass slide with a hydrophobic pen.

Imaging

We used a Zeiss LSM 710 confocal laser-scanning microscope for representative images, and the ZEN blue Software for adjustments and modifications. For High-Content acquisitions followed by image analysis and quantification the Operetta CLS High-Content Analysis System (Perkin Elmer) was used. 25 planes were acquired per organoid section, with 1 µm of spacing between planes.

Image analysis

Image acquisitions of midbrain organoids and assembloids were analysed in Matlab (Version 2017b, Mathworks) as described in Monzel et al., 2017 and Smits et al., 2019. For image analysis of IBA1 and CD31 morphology, we used the Imaris software (Oxford instruments). We used the 'Filaments' tracer in order to segment positive cells, detect and modify seeding points and trace filaments and processes. Statistics were run with data per cell in GraphPad Prism.

Hypoxyprobe assay

The Hypoxyprobe™ Omni Kit (Hypoxyprobe, HP3-XXX) was used to measure hypoxia levels in organoids and assembloids. 250 µM pimonidazole was diluted in media, and organoids and assembloids were incubated in pimonidazole solution for 2h at 37°C. Then, fixation was performed with 4% Formaldehyde, overnight at room temperature, followed by agarose embedding and sectioning into 70 µm sections. The staining was done as described in "Immunofluorescence staining in 3D", using the PAb2627AP antibody against pimonidazole and a secondary HRP-conjugated antibody. Diaminobenzidine (DAB) tablets were used to proceed with the staining (SIGMAFAST™ 3,3′-Diaminobenzidine tablets, Sigma, D4293). A DAB tablet and a Urea hydrogen peroxide tablet were mixed in 5 ml of water. The solution was applied to the organoid and assembloid sections for < 1 min, when the colour developed visibly. Then, sections were washed with water and mounted with Fluoromount-G mounting medium on a glass slide. Images were acquired in a stereomicroscope (Nikon, SMZ25-SMZ18) and positive area quantification was done with ImageJ.

LDH assay

For the LDH viability assay, we used supernatant pooled from 3 organoids or assembloids per batch, and 3 batches were considered. We used the line #201 for this assay. We snap-froze supernatants the day of collection, and kept them at -80°C until the day the assay was performed. The LDH-Glo™ Cytotoxicity Assay (Promega, J2380 and J2381) kit was used, and samples were loaded into 96-well plates with opaque walls. Reagents were thawed at RT, and samples were thawed on ice. We used 25 µl of supernatant and 25 µl of LDH detection reagent per well, and incubated for 60 min at RT. Luminescence was recorded in a TECAN reader. We normalized the OD values to organoid and assembloid size (area measured in ImageJ), since there was a significant difference between them. After assessing the normality of the data, statistics were run using a t-test in Graphpad prism.

Western Blot

We used midbrain organoids and assembloids from the lines #200 and #201, and 3 batches per line. To extract protein, 3 to 5 organoids or assembloids were pooled. Samples were washed once with 1x PBS and snap-frozen. Until the day of the extraction, they were stored at -80°C. Organoid and assembloid dissociation was done with 1x RIPA buffer (Abcam, ab156034) containing 1x Phosphatase inhibitor cocktail (Merck Millipore, 524629-1ML) and 1x Complete™ Protease Inhibitor Cocktail (Sigma, 11697498001). Then, we sonicated the samples with a Bioruptor (Diagenode) for 10 cycles of 30 sec on and 30 sec off. We quantified the protein with a Pierce BCA Protein Assay Kit (Thermofisher, 23227) and a TECAN reader. For the western blot, we used 30 µg of protein per sample, and prepared it for loading with 6x loading buffer containing 0.375M Tris (MW 121.14 g/mol), 9% SDS, 50% Glycerol, 0.2% Bromphenolblue, 0.3M DTT. Prior to loading, samples were boiled at 95°C for 5 min. The protein samples were loaded into precast polyacrylamide gels (Thermofisher, NW04120BOX). To transfer the proteins to PVDF membranes (Thermofisher, IB24001) we used an iBlot2 device (Invitrogen). Membranes were blocked in 0.2% Tween-20 and 5% BSA in 1x PBS containing 60 min at RT. Primary antibodies (Table 2) were incubated in antibody buffer (0.02% Tween-20, 5% BSA in 1x PBS) at 4°C overnight. Secondary antibodies (Table 2) were diluted in antibody buffer, and membranes were incubated for 60 min at RT in the secondary antibody solution. Enhanced fluorescent signal was detected in the LI-COR OdysseyFc imaging system. Band quantifications were performed with ImageJ and, after assessing the normality of the data statistics were run using a Mann-Whitney test in GraphPad Prism.

Single-nuclei RNA sequencing (snRNAseq)

Sample pre-processing

Organoids and assembloids from the line #201 were used for this protocol. We collected 3 organoids or assembloids per batch, and 3 batches. At day 30 of dopaminergic differentiation, organoids and assembloids were snap-frozen and stored at -80°C. For the nuclei extraction, the samples from the 3 batches were pooled, resulting in two sample groups: organoids and assembloids.

Nuclei extraction and library preparation

To extract nuclei, frozen organoids and assembloids were transferred into a 1.5 ml vial with 0.5ml ice cold cell lysis buffer containing 10 mM Tris-HCl, pH 7.4, 10 mM NaCl, 3 mM MgCl2, 0.1% IGEPAL CA-630, 1% SUPERase In RNase Inhibitor (20 U/µL, Ambion) and 2% BSA and physically disrupted using a disposable pistille. The mixture

was filtered through a 10um filter and the nuclei were centrifuged down at 500g for 5min at 4°C. The supernatant was discarded and the nuclei were resuspended in 0.5 ml nuclei suspension buffer containing 10 mM Tris-HCl, pH 7.4, 10 mM NaCl, 3 mM MgCl2, 1% SUPERase In RNase Inhibitor (20 U/µL, Ambion) and 2% BSA. Nuclei were counted via Neubauer chamber and Trypan Blue staining, centrifuged down at 500g for 5min at 4°C, the supernatant was discarded and the nuclei were resuspended in the appropriate amount of nuclei suspension buffer to yield a single nuclei solution of ~1000 nuclei/ul. The single nuclei suspensions were processed into labelled cDNA and subsequently NGS libraries following manufacturer's instructions using Chromium Single Cell 3' chemistry (10X Genomics) cDNA and libraries were quantified using HS dsDNA assays on a Qubit 2 instrument (Thermo fisher) and fragment size distribution was determined via High Sensitivity DNA assay on a Bioanalyzer2100 instrument (Agilent). Final library molarity was determined via NEBNext Library Quant Kit for Illumina (NEB) on a QuantStudio 5 Real-Time PCR System (Applied Biosystems). Libraries were equimolarly pooled, clustered at 1000pM on a P3 flowcell and sequenced PE R1 28 cycles 2*10 index cycles and R2 90 cycles using 100 cylce SBS chemistry on a NextSeq2000 instrument (Illumina). Data was demultiplexed, converted to fastq format and aligned to reference genome hg19 using the cellranger software (10X Genomics).

Data analysis

Data was analyzed using Seurat package (version 4.0.2.) on R (version 4.0.2). Cells having at least 200 but not more than 5000 unique feature counts were removed as low-quality cells or probable doublets respectively. In addition, mitochondrial and ribosomal genes were filtered out. After QC, midbrain organoid data set included 9332 cells, but midbrain-vascular organoid – 14217 cells. Datasets were merged and log-normalized and scaled based on all features. Using vst method 2000 highly variable genes were identified, following the principal component analysis (PCA). Nine distinct cells clusters were identified, applying Louvain algorithm with a resolution of 0.5, based on the top 10 principal components. Cell types were identified using binarized marker gene list of embryonic midbrain cell types given by G et al., 2016. Cell identity detection was based on the amount of marker genes from embryonic midbrain cell populations, expressed in every cell cluster of our dataset. In addition, cell cluster identity was verified with GeneAnalystics online tool. Here, marker genes of each cell cluster found using FindAllMarkers function of Seurat, were given in the tool for cell type identification choosing *in vitro* parameter for brain cells. Differentially expressed genes (DEGs) were

detected using the FindMarkers function of the Seurat comparing midbrain-vascular dataset (ident.1) against midbrain dataset (ident.2). Significantly differentially expressed genes (p.adjust<0.05 and logfc.threshold = 0.25) were selected for further enrichment analysis using MetaCore (version 21.4). The fold change of the genes from the most enriched pathways was visualized using GraphPad Prism 9.

Author contributions

SSS and CS designed and conducted the experiments, interpreted the data and drafted the manuscript. AZ and KB analysed data. KH conducted specific experiments. MS and JCS coordinated and conceptualized the study. All authors reviewed and approved the final manuscript and agreed to be accountable for their contributions.

Acknowledgments

The authors would like to thank Dr. Jared Sterneckert for providing us with the cells from K7 line. CS is supported by Fonds National de la Recherche Luxembourg (C19/BM/13535609). t. We thank Dr. Paul Antony and Dr. Silvia Bolognin for the development of the codes used in this study. The JCS lab is supported by the Fonds National de la Recherche (FNR) Luxembourg (PRIDE17/12244779/PARK-QC; FNR/PoC16/11559169, FNR/ NCER13/BM/11264123). This is an EU Joint Program - Neurodegenerative Disease Research (JPND) project (INTER/JPND/15/11092422). We also would like to thank the private donors who support our work at the Luxembourg Centre for Systems Biomedicine.

Declaration of interests

JCS is co-founder and shareholder of the biotech company Organo Therapeutics SARL. This company used midbrain organoids and assembloids for *in vitro* disease modelling and drug discovery.

Ethics Statement

Written informed consent was obtained from all individuals who donated samples to this study and all work with human stem cells was done after approval of the national ethics board, Comité National d'Ethique de Recherche (CNER), under the approval numbers 201305/04 and 201901/01.

Rights retention statement

This research was funded in part by the Fonds National de la Recherche (FNR) Luxembourg. For the purpose of Open Access, the author has applied a CC BY public copyright license to any Author Accepted Manuscript (AAM) version arising from this submission.

References

Abbott, N.J., Patabendige, A.A.K., Dolman, D.E.M., Yusof, S.R., and Begley, D.J. (2010). Structure and function of the blood-brain barrier. Neurobiol. Dis. *37*, 13–25.

Ahn, Y., An, J.H., Yang, H.J., Lee, D.G., Kim, J., Koh, H., Park, Y.H., Song, B.S., Sim, B.W., Lee, H.J., et al. (2021). Human blood vessel organoids penetrate human cerebral organoids and form a vessel-like system. Cells *10*.

Barry, D., and McDermott, H. (2005). Differentiation of radial glia from radial precursor cells and transformation into astrocytes in the developing rat spinal cord. Glia *50*, 187–197.

Beauchamp, P., Moritz, W., Kelm, J.M., Ullrich, N.D., Agarkova, I., Anson, B.D., Suter, T.M., and Zuppinger, C. (2015). Development and Characterization of a Scaffold-Free 3D Spheroid Model of Induced Pluripotent Stem Cell-Derived Human Cardiomyocytes. Tissue Eng. Part C. Methods *21*, 852–861.

Bell, R.D., Winkler, E.A., Sagare, A.P., Singh, I., LaRue, B., Deane, R., and Zlokovic, B. V. (2010). Pericytes control key neurovascular functions and neuronal phenotype in the adult brain and during brain aging. Neuron *68*, 409–427.

Bergmann, S., Lawler, S.E., Qu, Y., Fadzen, C.M., Wolfe, J.M., Regan, M.S., Pentelute, B.L., Agar, N.Y.R., and Cho, C.F. (2018). Blood-brain-barrier organoids for investigating the permeability of CNS therapeutics. Nat. Protoc. *13*, 2827–2843.

Birey, F., Andersen, J., Makinson, C.D., Islam, S., Wei, W., Huber, N., Fan, H.C., Metzler, K.R.C., Panagiotakos, G., Thom, N., et al. (2017). Assembly of functionally integrated human forebrain spheroids. Nature *545*, 54–59.

Bonilla, S., Hall, A.C., Pinto, L., Attardo, A., Götz, M., Huttner, W.B., and Arenas, E. (2008). Identification of midbrain floor plate radial glia-like cells as dopaminergic progenitors. Glia *56*, 809–820.

Broutier, L., Andersson-Rolf, A., Hindley, C.J., Boj, S.F., Clevers, H., Koo, B.K., and Huch, M. (2016). Culture and establishment of self-renewing human and mouse adult liver and pancreas 3D organoids and their genetic manipulation. Nat. Protoc. 2016 119 *11*, 1724–1743.

Cakir, B., Xiang, Y., Tanaka, Y., Kural, M.H., Parent, M., Kang, Y.J., Chapeton, K.,

Patterson, B., Yuan, Y., He, C.S., et al. (2019). Engineering of human brain organoids with a functional vascular-like system. Nat. Methods *16*, 1169–1175.

Cengiz, P., Zafer, D., Chandrashekhar, J.H., Chanana, V., Bogost, J., Waldman, A., Novak, B., Kintner, D.B., and Ferrazzano, P.A. (2019). Developmental differences in microglia morphology and gene expression during normal brain development and in response to hypoxia-ischemia HHS Public Access. Neurochem Int *127*, 137–147.

Deem, T.L., and Cook-Mills, J.M. (2004). Vascular cell adhesion molecule 1 (VCAM-1) activation of endothelial cell matrix metalloproteinases: role of reactive oxygen species. Blood *104*, 2385–2393.

Duan, L.J., Pan, S.J., Sato, T.N., and Fong, G.H. (2017). Retinal Angiogenesis Regulates Astrocytic Differentiation in Neonatal Mouse Retinas by Oxygen Dependent Mechanisms. Sci. Reports 2017 71 *7*, 1–16.

Duong, C.N., and Vestweber, D. (2020). Mechanisms Ensuring Endothelial Junction Integrity Beyond VE-Cadherin. Front. Physiol. *11*, 519.

Francis, S.E., Goh, K.L., Hodivala-Dilke, K., Bader, B.L., Stark, M., Davidson, D., and Hynes, R.O. (2002). Central roles of alpha5beta1 integrin and fibronectin in vascular development in mouse embryos and embryoid bodies. Arterioscler. Thromb. Vasc. Biol. *22*, 927–933.

Di Giovanna, A.P., Tibo, A., Silvestri, L., Müllenbroich, M.C., Costantini, I., Allegra Mascaro, A.L., Sacconi, L., Frasconi, P., and Pavone, F.S. (2018). Whole-Brain Vasculature Reconstruction at the Single Capillary Level. Sci. Rep. *8*.

Haenseler, W., Sansom, S.N., Buchrieser, J., Newey, S.E., Moore, C.S., Nicholls, F.J., Chintawar, S., Schnell, C., Antel, J.P., Allen, N.D., et al. (2017). A Highly Efficient Human Pluripotent Stem Cell Microglia Model Displays a Neuronal-Co-culture-Specific Expression Profile and Inflammatory Response. Stem Cell Reports *8*, 1727–1742.

Harry, G.J., and Kraft, A.D. (2012). Microglia in the developing brain: a potential target with lifetime effects. Neurotoxicology *33*, 191.

Iadecola, C., and Anrather, J. (2011). The immunology of stroke: from mechanisms to translation. Nat. Med. *17*, 796.

Imagawa, T., Kitagawa, H., and Uehara, M. (1994). Ultrastructure of blood vessels in the head kidney of the carp, Cyprinus carpio. J. Anat. *185*, 521.

Jarazo, J., Barmpa, K., Modamio, J., Saraiva, C., Sabaté-Soler, S., Rosety, I., Griesbeck, A., Skwirblies, F., Zaffaroni, G., Smits, L.M., et al. (2021). Parkinson's Disease Phenotypes in Patient Neuronal Cultures and Brain Organoids Improved by 2-Hydroxypropyl-β-Cyclodextrin Treatment. Mov. Disord. 1–16.

Jinnou, H., Sawada, M., Kawase, K., Kaneko, N., Herranz-Pérez, V., Miyamoto, T., Kawaue, T., Miyata, T., Tabata, Y., Akaike, T., et al. (2018). Radial Glial Fibers Promote Neuronal Migration and Functional Recovery after Neonatal Brain Injury. Cell Stem Cell *22*, 128-137.e9.

Jo, J., Xiao, Y., Sun, A.X., Cukuroglu, E., Tran, H.-D., Göke, J., Tan, Z.Y., Saw, T.Y., Tan, C.-P., Lokman, H., et al. (2016). Midbrain-like organoids from human pluripotent stem cells contain functional dopaminergic and neuromelanin producing neurons. Cell Stem Cell *19*, 248.

Jones, E.G. (1970). On the mode of entry of blood vessels into the cerebral cortex. J. Anat. *106*, 507.

Kurz, H., Gärtner, T., Eggli, P.S., and Christ, B. (1996). First Blood Vessels in the Avian Neural Tube Are Formed by a Combination of Dorsal Angioblast Immigration and Ventral Sprouting of Endothelial Cells. Dev. Biol. *173*, 133–147.

Lancaster, M.A., Renner, M., Martin, C.A., Wenzel, D., Bicknell, L.S., Hurles, M.E., Homfray, T., Penninger, J.M., Jackson, A.P., and Knoblich, J.A. (2013). Cerebral organoids model human brain development and microcephaly. Nature *501*, 373–379.

Lange, C., Garcia, M.T., Decimo, I., Bifari, F., Eelen, G., Quaegebeur, A., Boon, R., Zhao, H., Boeckx, B., Chang, J., et al. (2016). Relief of hypoxia by angiogenesis promotes neural stem cell differentiation by targeting glycolysis. EMBO J. *35*, 924.

Levitt, P., and Cooper, M.L. (1981). COEXISTENCE OF NEURONAL AND GLIAL PRECURSOR CELLS IN THE CEREBRAL VENTRICULAR ZONE OF THE FETAL MONKEY: AN ULTRASTRUCTURAL IMMUNOPEROXIDASE ANALYSIS'. J. Neurosci Ence *1*, 27–39.

Levitt, P., Cooper, M.L., and Rakic, P. (1983). Early divergence and changing proportions of neuronal and glial precursor cells in the primate cerebral ventricular zone. Dev. Biol. *96*, 472–484.

Liang, J., Gu, S., Mao, X., Tan, Y., Wang, H., Li, S., and Zhou, Y. (2020). Endothelial Cell Morphology Regulates Inflammatory Cells Through MicroRNA Transferred by Extracellular Vesicles. Front. Bioeng. Biotechnol. *8*, 369.

Lindborg, B.A., Brekke, J.H., Vegoe, A.L., Ulrich, C.B., Haider, K.T., Subramaniam, S., Venhuizen, S.L., Eide, C.R., Orchard, P.J., Chen, W., et al. (2016). Rapid Induction of Cerebral Organoids From Human Induced Pluripotent Stem Cells Using a Chemically Defined Hydrogel and Defined Cell Culture Medium. Stem Cells Transl. Med. *5*, 970–979.

Malatesta, P., Hartfuss, E., and Götz, M. (2000). Isolation of radial glial cells by fluorescent-

activated cell sorting reveals a neuronal lineage. Development *127*, 5253–5263.

La Manno, G., Gyllborg, D., Codeluppi, S., Nishimura, K., Salto, C., Zeisel, A., Borm, L.E., Stott, S.R.W., Toledo, E.M., Villaescusa, J.C., et al. (2016). Molecular Diversity of Midbrain Development in Mouse, Human, and Stem Cells. Cell *167*, 566.

Mansour, A.A., Gonçalves, J.T., Bloyd, C.W., Li, H., Fernandes, S., Quang, D., Johnston, S., Parylak, S.L., Jin, X., and Gage, F.H. (2018). An in vivo model of functional and vascularized human brain organoids. Nat. Biotechnol. *36*, 432–441.

Matsuoka, R.L., Marass, M., Avdesh, A., Helker, C.S.M., Maischein, H.M., Grosse, A.S., Kaur, H., Lawson, N.D., Herzog, W., and Stainier, D.Y.R. (2016). Radial glia regulate vascular patterning around the developing spinal cord. Elife *5*.

McCarty, J.H., Monahan-Earley, R.A., Brown, L.F., Keller, M., Gerhardt, H., Rubin, K., Shani, M., Dvorak, H.F., Wolburg, H., Bader, B.L., et al. (2002). Defective associations between blood vessels and brain parenchyma lead to cerebral hemorrhage in mice lacking alphav integrins. Mol. Cell. Biol. *22*, 7667–7677.

McConnell, H.L., Kersch, C.N., Woltjer, R.L., and Neuwelt, E.A. (2017). The translational significance of the neurovascular unit. J. Biol. Chem. *292*, 762–770.

Mcdonald, D.M., and Larue, D.T. (1983). The ultrastructure vessels supplying carotid sinus and connections of blood the rat carotid body and. J. Neurocytol. *12*, 117–153.

Mi, H., Haeberle, H., and Barres, B.A. (2001). Induction of Astrocyte Differentiation by Endothelial Cells. J. Neurosci. *21*, 1538.

Miller, J.S., Stevens, K.R., Yang, M.T., Baker, B.M., Nguyen, D.H.T., Cohen, D.M., Toro, E., Chen, A.A., Galie, P.A., Yu, X., et al. (2012). Rapid casting of patterned vascular networks for perfusable engineered three-dimensional tissues. Nat. Mater. *11*, 768–774.

Misson, J.P., Edwards, M.A., Yamamoto, M., and Caviness, V.S. (1988). Mitotic cycling of radial glial cells of the fetal murine cerebral wall: a combined autoradiographic and immunohistochemical study. Dev. Brain Res. *38*, 183–190.

Monzel, A.S., Smits, L.M., Hemmer, K., Hachi, S., Moreno, E.L., van Wuellen, T., Jarazo, J., Walter, J., Brüggemann, I., Boussaad, I., et al. (2017). Derivation of Human Midbrain-Specific Organoids from Neuroepithelial Stem Cells. Stem Cell Reports *8*, 1144–1154.

Morizane, R., Lam, A.Q., Freedman, B.S., Kishi, S., Valerius, M.T., and Bonventre, J. V. (2015). Nephron organoids derived from human pluripotent stem cells model kidney development and injury. Nat. Biotechnol. *33*, 1193–1200.

Morrison, H., Young, K., Qureshi, M., Rowe, R.K., and Lifshitz, J. (2017). Quantitative

microglia analyses reveal diverse morphologic responses in the rat cortex after diffuse brain injury. Sci. Reports 2017 71 *7*, 1–12.

Nashimoto, Y., Hayashi, T., Kunita, I., Nakamasu, A., Torisawa, Y.S., Nakayama, M., Takigawa-Imamura, H., Kotera, H., Nishiyama, K., Miura, T., et al. (2017). Integrating perfusable vascular networks with a three-dimensional tissue in a microfluidic device. Integr. Biol. (United Kingdom) *9*, 506–518.

Nickels, S.L., Modamio, J., Mendes-Pinheiro, B., Monzel, A.S., Betsou, F., and Schwamborn, J.C. (2020). Reproducible generation of human midbrain organoids for in vitro modeling of Parkinson's disease. Stem Cell Res. *46*.

Noctor, S.C., Flint, A.C., Weissman, T.A., Dammerman, R.S., and Kriegstein, A.R. (2001). Neurons derived from radial glial cells establish radial units in neocortex. Nature *409*, 714–720.

Ohtsuki, S., and Terasaki, T. (2007). Contribution of carrier-mediated transport systems to the blood-brain barrier as a supporting and protecting interface for the brain; importance for CNS drug discovery and development. Pharm. Res. *24*, 1745–1758.

Ormel, P.R., Vieira de Sá, R., van Bodegraven, E.J., Karst, H., Harschnitz, O., Sneeboer, M.A.M., Johansen, L.E., van Dijk, R.E., Scheefhals, N., Berdenis van Berlekom, A., et al. (2018). Microglia innately develop within cerebral organoids. Nat. Commun. *9*.

Perego, C., Fumagalli, S., and De Simoni, M.-G. (2011). Temporal pattern of expression and colocalization of microglia/macrophage phenotype markers following brain ischemic injury in mice. J. Neuroinflammation *8*, 174.

Pham, M.T., Pollock, K.M., Rose, M.D., Cary, W.A., Stewart, H.R., Zhou, P., Nolta, J.A., and Waldau, B. (2018). Generation of human vascularized brain organoids. Neuroreport *29*, 588–593.

Qian, X., Su, Y., Adam, C.D., Deutschmann, A.U., Pather, S.R., Goldberg, E.M., Su, K., Li, S., Lu, L., Jacob, F., et al. (2020). Sliced Human Cortical Organoids for Modeling Distinct Cortical Layer Formation. Cell Stem Cell *26*, 766.

Rakic, P. (1972). Mode of cell migration to the superficial layers of fetal monkey neocortex. J. Comp. Neurol. *145*, 61–83.

Ramachandran, S.D., Schirmer, K., Münst, B., Heinz, S., Ghafoory, S., Wölfl, S., Simon-Keller, K., Marx, A., Oie, C.I., Ebert, M.P., et al. (2015). In Vitro Generation of Functional Liver Organoid-Like Structures Using Adult Human Cells. PLoS One *10*.

Raybaud, C. (2010). Normal and Abnormal Embryology and Development of the Intracranial Vascular System. Neurosurg. Clin. NA *21*, 399–426.

Reinhardt, P., Glatza, M., Hemmer, K., Tsytsyura, Y., Thiel, C.S., HÃ¶ing, S., Moritz, S., Parga, J.A., Wagner, L., Bruder, J.M., et al. (2013). Correction: Derivation and Expansion Using Only Small Molecules of Human Neural Progenitors for Neurodegenerative Disease Modeling. PLoS One *8*, 59252.

Ruhrberg, C., and Bautch, V.L. (2013). Neurovascular development and links to disease. Cell. Mol. Life Sci. *70*, 1675–1684.

Sabate-Soler, S., Nickels, S.L., Saraiva, C., Berger, E., Dubonyte, U., Barmpa, K., Lan, Y.J., Kouno, T., Jarazo, J., Robertson, G., et al. (2022). Microglia integration into human midbrain organoids leads to increased neuronal maturation and functionality. BioRxiv 2022.01.21.477192.

Segarra, M., Aburto, M.R., Cop, F., Llaó-Cid, C., Härtl, R., Damm, M., Bethani, I., Parrilla, M., Husainie, D., Schänzer, A., et al. (2018). Endothelial Dab1 signaling orchestrates neuro-glia-vessel communication in the central nervous system. Science (80-.). *361*.

Sidman, R.L., and Rakic, P. (1973). Neuronal migration, with special reference to developing human brain: a review. Brain Res. *62*, 1–35.

da Silva, S.M., Campos, G.D., Gomes, F.C.A., and Stipursky, J. (2019). Radial Glia-endothelial Cells' Bidirectional Interactions Control Vascular Maturation and Astrocyte Differentiation: Impact for Blood-brain Barrier Formation. Curr. Neurovasc. Res. *16*, 291–300.

Siqueira, M., Francis, D., Gisbert, D., Gomes, F.C.A., and Stipursky, J. (2018). Radial Glia Cells Control Angiogenesis in the Developing Cerebral Cortex Through TGF-β1 Signaling. Mol. Neurobiol. *55*, 3660–3675.

Smits, L.M., Reinhardt, L., Reinhardt, P., Glatza, M., Monzel, A.S., Stanslowsky, N., Rosato-Siri, M.D., Zanon, A., Antony, P.M., Bellmann, J., et al. (2019b). Modeling Parkinson's disease in midbrain-like organoids. NPJ Park. Dis. *5*.

Smits, L.M., Magni, S., Kinugawa, K., Grzyb, K., Luginbühl, J., Sabate-Soler, S., Bolognin, S., Shin, J.W., Mori, E., Skupin, A., et al. (2020). Single-cell transcriptomics reveals multiple neuronal cell types in human midbrain-specific organoids. Cell Tissue Res. *382*, 463–476.

Snapyan, M., Lemasson, M., Brill, M.S., Blais, M., Massouh, M., Ninkovic, J., Gravel, C., Berthod, F., Götz, M., Barker, P.A., et al. (2009). Cellular/Molecular Vasculature Guides Migrating Neuronal Precursors in the Adult Mammalian Forebrain via Brain-Derived Neurotrophic Factor Signaling.

Stehbens, W., Wakefield, J.S., Gilbert-Barness, E., and Zuccollo, J. (2009). HISTOPATHOLOGY AND ULTRASTRUCTURE OF HUMAN UMBILICAL BLOOD

VESSELS. Http://Dx.Doi.Org/10.1080/15227950500503660 *24*, 297–315.

Taddei, A., Giampietro, C., Conti, A., Orsenigo, F., Breviario, F., Pirazzoli, V., Potente, M., Daly, C., Dimmeler, S., and Dejana, E. (2008). Endothelial adherens junctions control tight junctions by VE-cadherin-mediated upregulation of claudin-5. Nat. Cell Biol. *10*, 923–934.

Tsuji-Tamura, K., and Ogawa, M. (2018). Morphology regulation in vascular endothelial cells. Inflamm. Regen. 2018 381 *38*, 1–13.

Wimmer, R.A., Leopoldi, A., Aichinger, M., Kerjaschki, D., and Penninger, J.M. (2019). Generation of blood vessel organoids from human pluripotent stem cells. Nat. Protoc. 2019 1411 *14*, 3082–3100.

Wörsdörfer, P., Dalda, N., Kern, A., Krüger, S., Wagner, N., Kwok, C.K., Henke, E., and Ergün, S. (2019). Generation of complex human organoid models including vascular networks by incorporation of mesodermal progenitor cells. Sci. Rep. *9*, 1–13.

Wörsdörfer, P., Rockel, A., Alt, Y., Kern, A., and Ergün, S. (2020). Generation of Vascularized Neural Organoids by Co-culturing with Mesodermal Progenitor Cells. STAR Protoc. *1*, 100041.

Yang, R., Wang, H., Wen, J., Ma, K., Chen, D., Chen, Z., and Huang, C. (2019). Regulation of microglial process elongation, a featured characteristic of microglial plasticity. Pharmacol. Res. *139*, 286–297.

Zagare, A., Barmpa, K., Smajic, S., Smits, L.M., Grzyb, K., Gruenewald, A., Skupin, A., Nickels, S.L., and Schwamborn, J. (2022). Midbrain organoids represent a physiologically relevant model that recapitulates a LRRK2-G2019S-associated gene expression signature during early neurodevelopment. Am. J. Hum. Genet.

Zhang, S., Wang, H.J., Li, J., Hu, X.L., and Shen, Q. (2020). Radial Glial Cell-Derived VCAM1 Regulates Cortical Angiogenesis Through Distinct Enrichments in the Proximal and Distal Radial Processes. Cereb. Cortex *30*, 3717–3730.

Figure titles and legends

Figure 1. Co-culture of midbrain and vascular organoids to obtain vascularized assembloids. A. Diagram of the organoid co-culture and generation of assembloids. **B.** snRNA-Seq UMAP of cell clusters in vascularized assembloids. Each dot represents a single cell and they are colour-identified **C**. snRNA-Seq UMAP showing the cell cluster distribution in organoids and assembloids. **D.** Bar graph representing the amount of cells composing each cluster in midbrain organoids and assembloids. **E.** Heatmap showing different expression on cluster-defining genes throughout cell clusters. Two main sub-clusters show cell populations corresponding to midbrain organoids or assembloids. **F.** Gene expression analysis showed similar *TH* and *FOXA2* expression in midbrain organoids and assembloids, indicating that the dopaminergic neuron population does not seem to be altered. **G.** Western blot results show no differences in TH levels in midbrain organoids and assembloids (each dot represents a pool of 3-5 organoids or assembloids from one batch (n = 6, 2 cell lines, 3 batches). Error bars = SEM). MO = Midbrain organoid, MOVO = assembloid.

Figure 2. Assembloids include blood vessel markers and tube-like structures. A. Immunofluorescence images in midbrain organoids and assembloids from lines #200 and #201, showing the presence of endothelial marker CD31, the dopaminergic neuron marker TH and the neuronal marker MAP2 at day 30 of dopaminergic differentiation (scale bar = 200 µm, 70 µm sections for line #200 and 120 µm for line #201). **B.** Immunofluorescence staining showing the endothelial cell marker CD31 and the basement membrane marker Collagen IV in assembloids (scale bar = 50 µm in upper panels, 20 µm in bottom panels, line #200, 70 µm sections). **C.** Staining for CD31 and the brain capillary and vascular smooth muscle cell alpha smooth muscle actin (aSMA) in an assembloid (scale bar = 50 µm, line #200, 70 µm sections). **D.** Staining for CD31 and the adherens junction marker VE-Cadherin in an assembloid (scale bar = 20 µm, line #200, 70 µm sections). **E.** Bar graphs representing the FACS results for VE-Cadherin (left) and the pericyte marker PDGFRβ (PDGFRb) in midbrain organoids and assembloids (each dot represents a pool of 3 organoids or assembloids from one batch, n = 2 (2 batches), line #201. Error bars = SEM). **F.** High magnification immunofluorescence image showing a CD31-positive structure with tubular morphology in an assembloid (scale bar = 5 µm, line #200, 70 µm sections).

Figure 3. Changes in cell adhesion, ECM remodelling and astrocyte differentiation in assembloids. A. Bar graph represented the significant enriched pathway maps based on the differential gene expression analysis between assembloids and midbrain organoids. The most significantly enriched pathway in assembloids compared to midbrain organoids related to cell adhesion and ECM remodelling (p adj. value <0.05, logfc threshold >0.25). **B.** Bar graph

showing the average log fold change of the differentially expressed genes related to cell adhesion and ECM remodelling (p adj. value <0.05, logfc threshold >0.25). **C.** Bar graph showing the average log fold change of the differentially expressed genes related to astrocyte differentiation (p adj. value <0.05, logfc threshold >0.25).

Figure 4. Assembloids show reduced levels of LDH release and hypoxia. A. Representative bright field images showing organoids (left) and assembloids (right) from lines #200 (upper panels) and #201 (bottom panels) at day 30 of dopaminergic differentiation. **B.** Bar graph representing organoid and assembloid area at day 30 of dopaminergic differentiation measured with ImageJ (each dot represents an organoid or assembloid, n = 6 (3 batches, 2 cell lines (#200 and #201)). Error bars = SEM). **B.** LDH release normalized to size in midbrain organoids and assembloids from line #201 at day 30 of dopaminergic differentiation (each dot represents a pooled supernatant sample from 3 organoids or assembloids from one batch, n = 3, 3 batches. Error bars are SEM). **C.** Representative images showing the Hypoxyprobe staining in a midbrain organoid (up) and an assembloid (bottom, left panels). Bar graph representing the percentage of hypoxic area in midbrain organoids and assembloids at day 15 of dopaminergic differentiation (each dot represents an organoid (1-3 organoids used per condition, n= 4, 2 cell lines, 2 batches per line). Error bars = SEM, right panel). *p < 0.05, **p<0.01, ***p<0.001, ****p<0.0001 using an unpaired t test in A, B and C.

Figure 5. Microglia connect with endothelial cells and neurons in co-culture and display an increased morphological complexity. A. Diagram showing the co-culture procedure for the integration of microglia into midbrain organoids and assembloids. **B.** Immunofluorescence image showing the expression of the microglia markers IBA1 and PU1 in 2D differentiated microglia after 14 days of culture .Scale bar = 50 µm. **C.** Bright field images showing midbrain organoids and assembloids co-cultured with microglia and their respective controls. Scale bar = 200 µm. **D.** Immunostaining images of midbrain organoids and assembloids with and without microglia, for IBA1, CD31 and TH (Scale bar = 50 µm. Images correspond to an orthogonal projection of 45 planes and 0.78 µm between planes). **E.** 3D reconstruction of the interaction between endothelial cells (CD31) and microglia (IBA1) from different angles (upper panels, scale bar = 15 µm in upper left panel and 20 µm in upper right panel). Interactions between endothelial cells, microglia and dopaminergic neurons (TH, filaments on image, bottom panels, scale bar = 8 µm in bottom left panel and 10 µm in bottom right panel). MO = Midbrain organoid, MOVO = assembloid. **F.** Graph showing a significant increase in microglia length measured in IMARIS. **G.** Graph showing a significant increase in endothelial cell length measured in IMARIS. In F and G; each dot represents one cell. The length is calculated as a sum of all processes in a cell (2 organoids used per condition, n= 2, 1 cell line, 2 batches. Error bars = SEM). *p < 0.05, **p<0.01, ***p<0.001, ****p<0.0001 using a Mann-Whitney test.

Figures

Figure 1

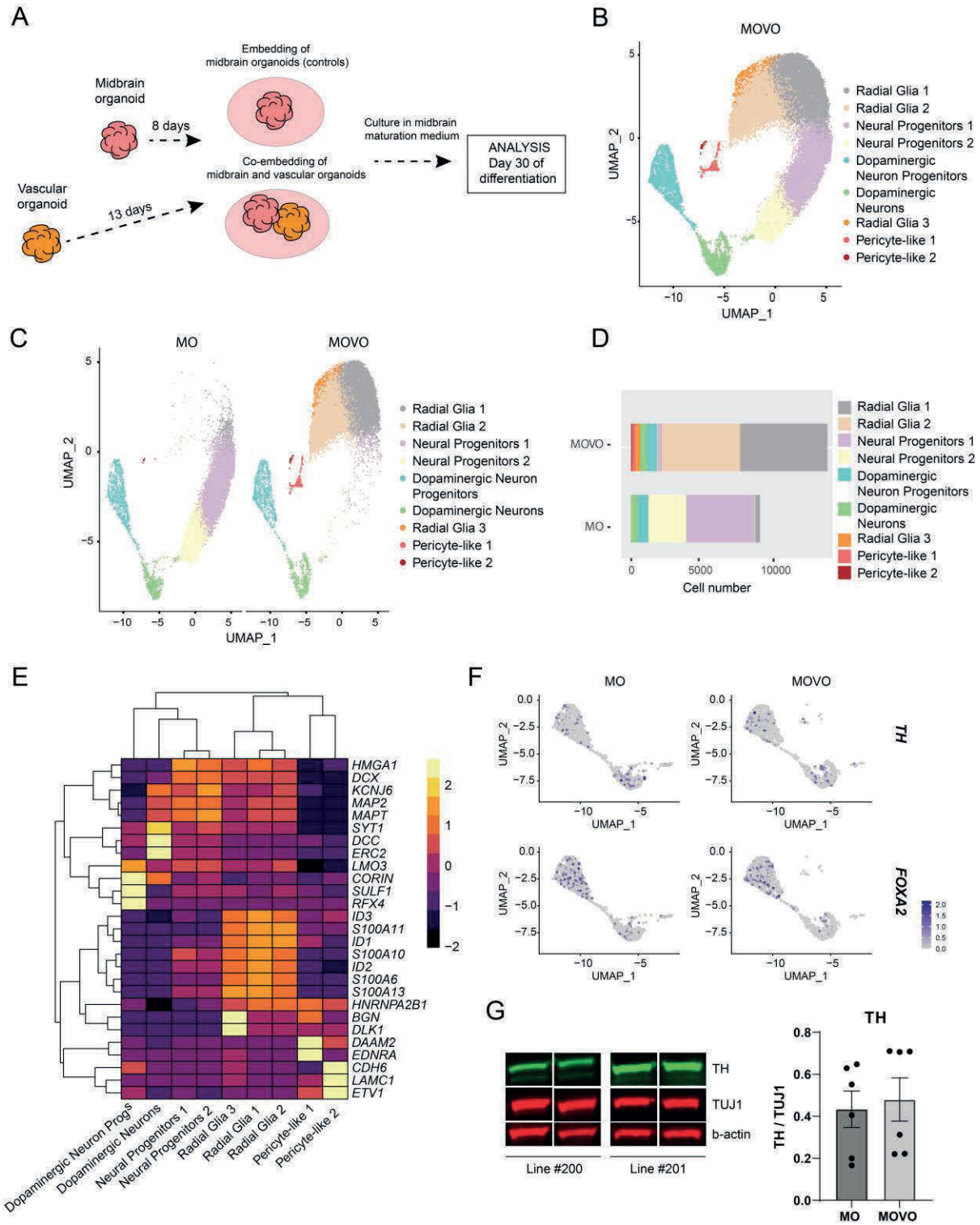

Figure 2

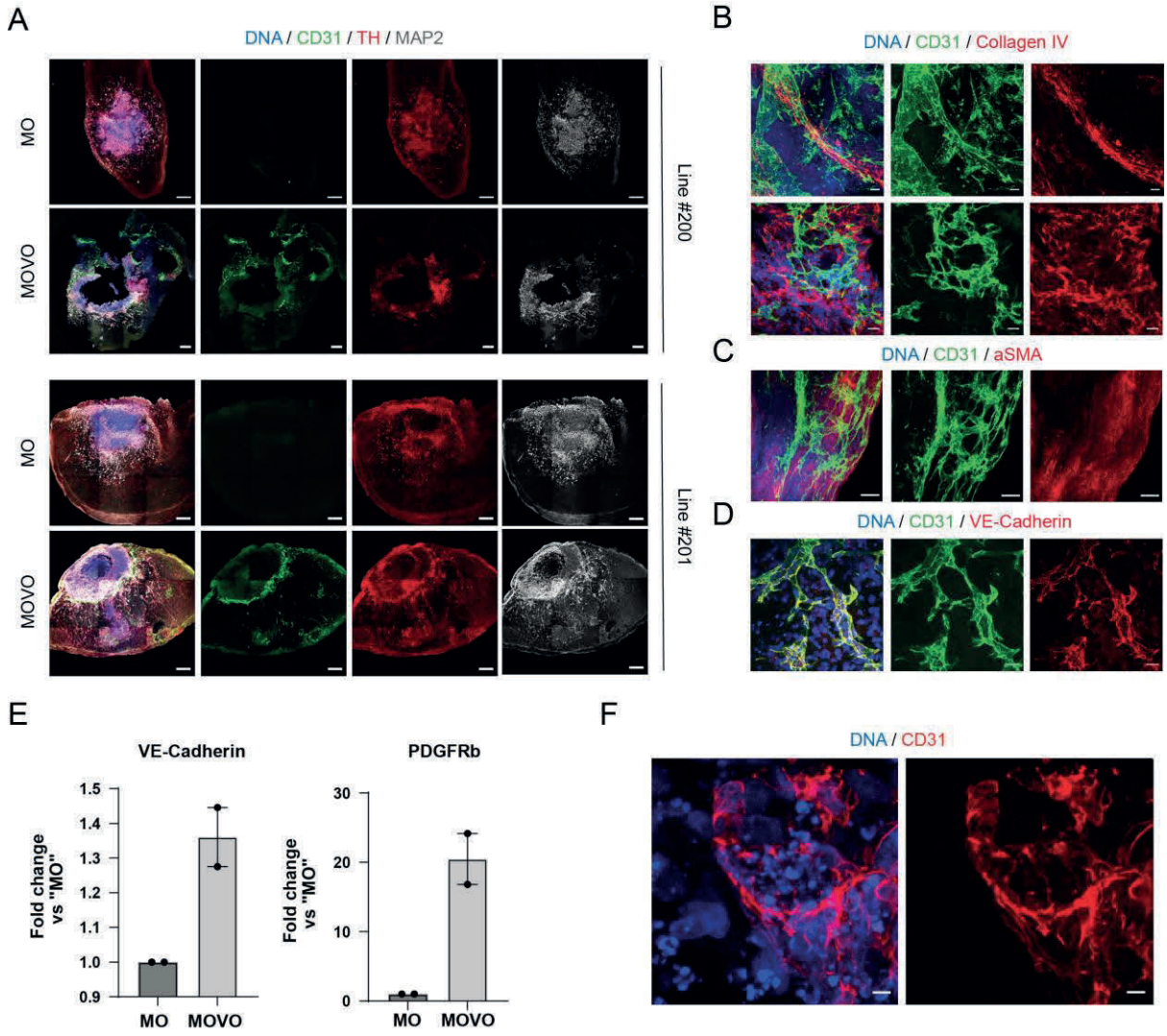
A
DNA / CD31 / TH / MAP2
MO
MOVO
Line #200
MO
MOVO
Line #201
B
DNA / CD31 / Collagen IV
C
DNA / CD31 / aSMA
D
DNA / CD31 / VE-Cadherin
E
VE-Cadherin
Fold change vs "MO"
1.5
1.4
1.3
1.2
1.1
1.0
0.9
MO
MOVO
PDGFRb
Fold change vs "MO"
30
20
10
0
MO
MOVO
F
DNA / CD31

Figure 3

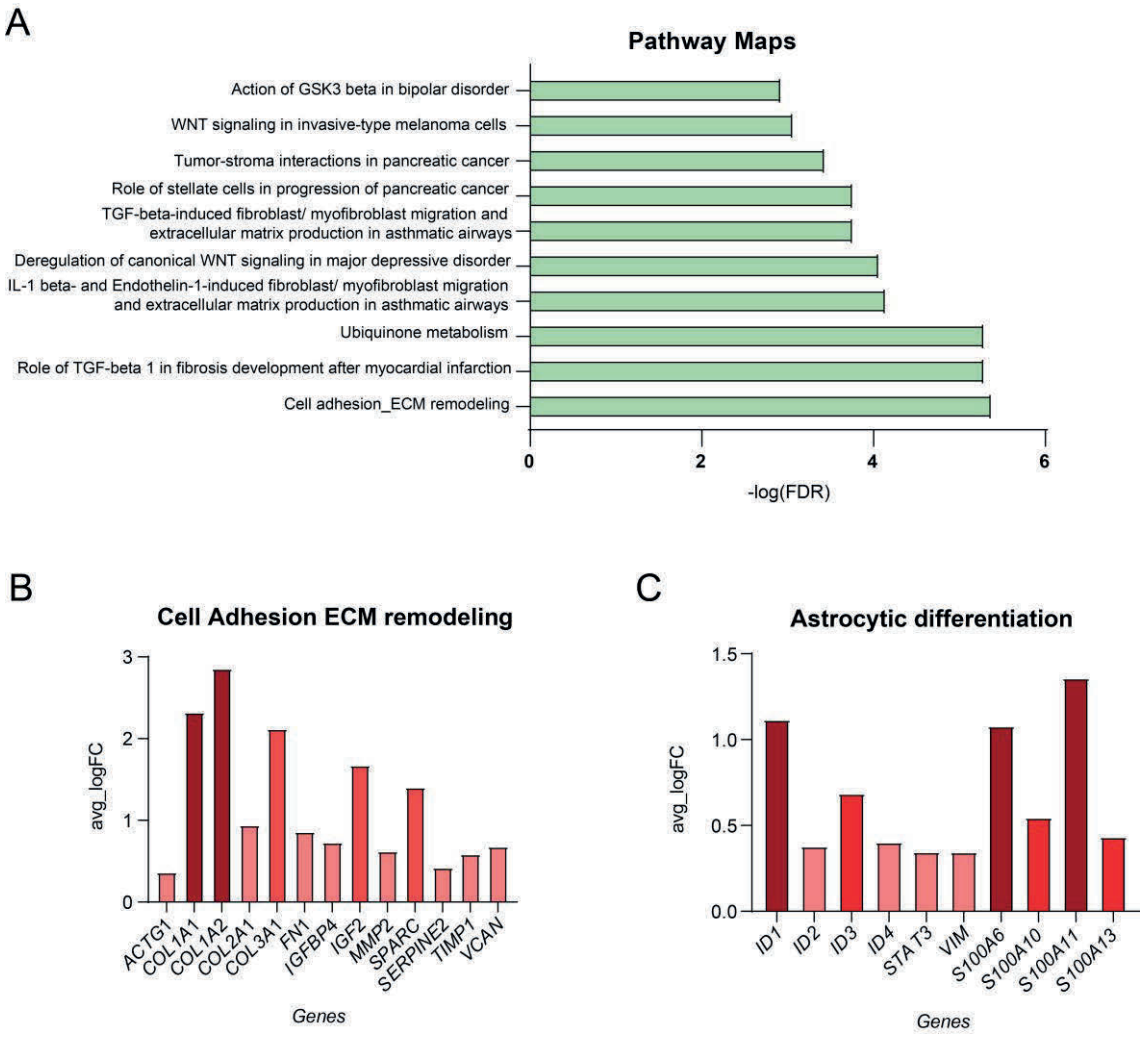
A
Pathway Maps
Action of GSK3 beta in bipolar disorder
WNT signaling in invasive-type melanoma cells
Tumor-stroma interactions in pancreatic cancer
Role of stellate cells in progression of pancreatic cancer
TGF-beta-induced fibroblast/ myofibroblast migration and extracellular matrix production in asthmatic airways
Deregulation of canonical WNT signaling in major depressive disorder
IL-1 beta- and Endothelin-1-induced fibroblast/ myofibroblast migration and extracellular matrix production in asthmatic airways
Ubiquinone metabolism
Role of TGF-beta 1 in fibrosis development after myocardial infarction
Cell adhesion_ECM remodeling
0
2
4
6
-log(FDR)
B
Cell Adhesion ECM remodeling
avg_logFC
0
1
2
3
ACTG1
COL1A1
COL1A2
COL2A1
COL3A1
FN1
IGFBP4
IGF2
MMP2
SPARC
SERPINE2
TIMP1
VCAN
Genes
C
Astrocytic differentiation
avg_logFC
0.0
0.5
1.0
1.5
ID1
ID2
ID3
ID4
STAT3
VIM
S100A6
S100A10
S100A11
S100A13
Genes

Figure 4

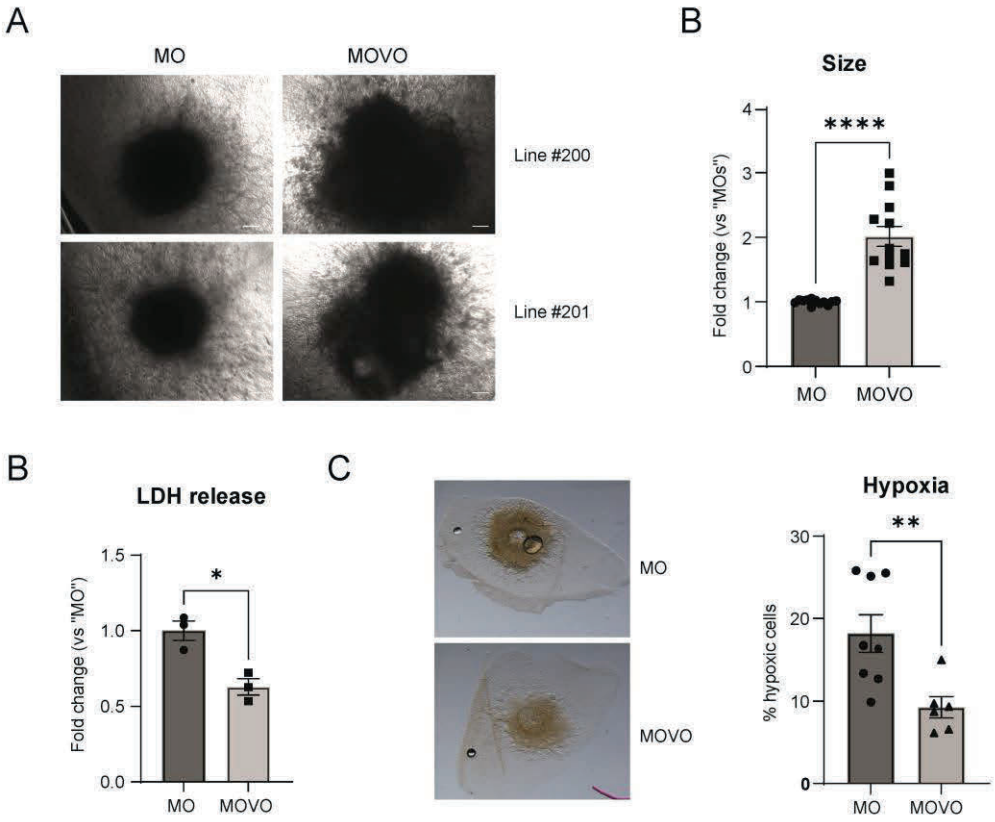
A
MO
MOVO
Line #200
Line #201
B
Size
****
Fold change (vs "MOs")
MO
MOVO
B
LDH release
*
Fold change (vs "MO")
MO
MOVO
C
MO
MOVO
Hypoxia
**
% hypoxic cells
MO
MOVO

Figure 5

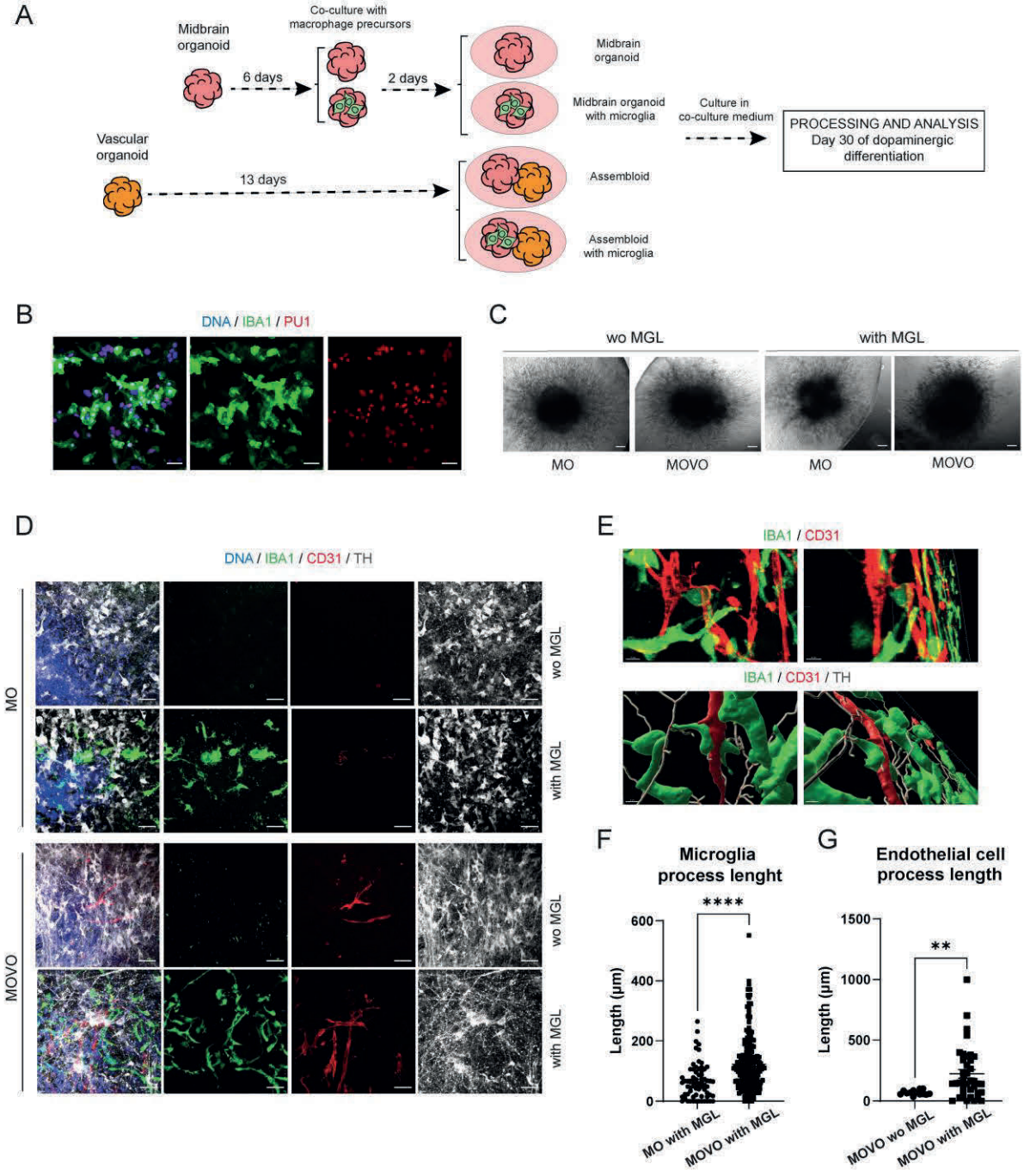
A
Midbrain organoid
Co-culture with macrophage precursors
6 days
2 days
Midbrain organoid
Midbrain organoid with microglia
Culture in co-culture medium
PROCESSING AND ANALYSIS Day 30 of dopaminergic differentiation
Vascular organoid
13 days
Assembloid
Assembloid with microglia
B
DNA / IBA1 / PU1
C
wo MGL
with MGL
MO
MOVO
MO
MOVO
D
DNA / IBA1 / CD31 / TH
MO
MOVO
wo MGL
with MGL
wo MGL
with MGL
E
IBA1 / CD31
IBA1 / CD31 / TH
F
Microglia process lenght
****
Length (µm)
600
400
200
0
MO with MGL
MOVO with MGL
G
Endothelial cell process length
**
Length (µm)
1500
1000
500
0
MOVO wo MGL
MOVO with MGL

Supplemental Information

Supplemental figure legends

Figure S1. iPSC and NESC characterization. A. Immunofluorescence staining of iPSCs from line #200 and #201 for the pluripotency markers TRA-1-81, SOX2 (upper panels), TRA-1-60, NANOG (middle panels), SSEA-4 and OCT4 (bottom panels, scale bar = 50 μm). B. Immunofluorescence staining of NESCs from line #200 and #201 for the midbrain and pluripotency markers NESTIN and SOX2. The absence of the forebrain and hindbrain marker PAX6 confirms the ventral midbrain identity (scale bar = 50 μm).

Figure S2. snRNA-Seq quality control. A. Violin plots of the gene number (nFeatures), molecules number (nCount), percentage of mitochondrial and ribosomal genes that were present in the MO and MOVO dataset before the quality control. **B.** Correlation plots between the number of genes and molecules in MO and MOVO datasets. **C.** Number of genes and molecules after the quality control of the MO and MOVO datasets. Mitochondria and ribosomal genes were removed. **D**. Correlation plots between the number of genes and the molecules in MO and MOVO datasets after the quality control. MO = Midbrain organoid, MOVO = assembloid.

Figure S3. snRNA-Seq clustering shows 9 different cell types. A. Dot plot representing gene markers defining different cell clusters. **B.** Dot plot showing high expression of radial glia-specific genes in the 3 radial glia cell clusters.

Supplemental Figures

Figure S1

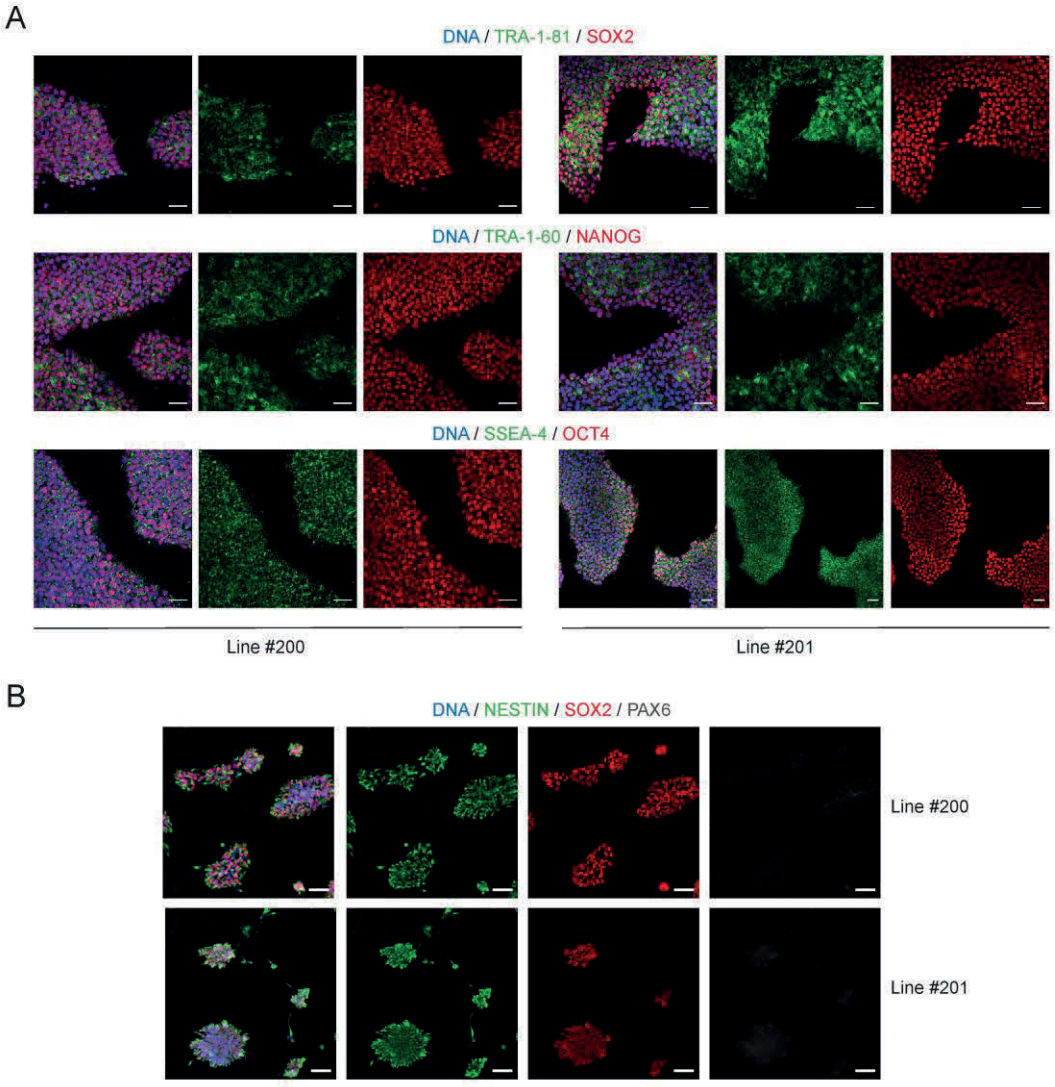

Figure S2

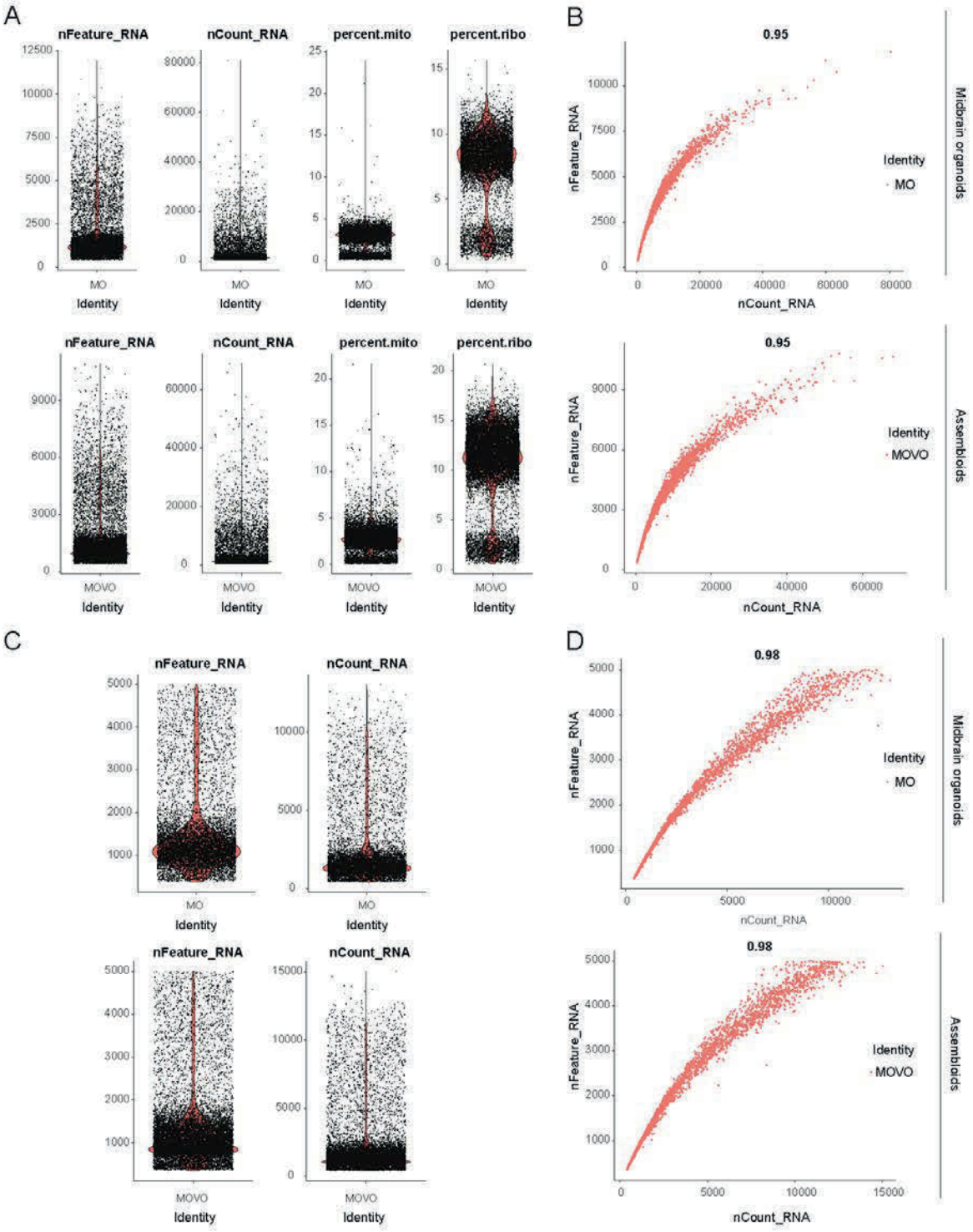
A
nFeature_RNA
nCount_RNA
percent.mito
percent.ribo
MO
MOVO
Identity
B
0.95
nFeature_RNA
nCount_RNA
Identity
MO
MOVO
Midbrain organoids
Assembloids
C
D
0.98

Figure S3

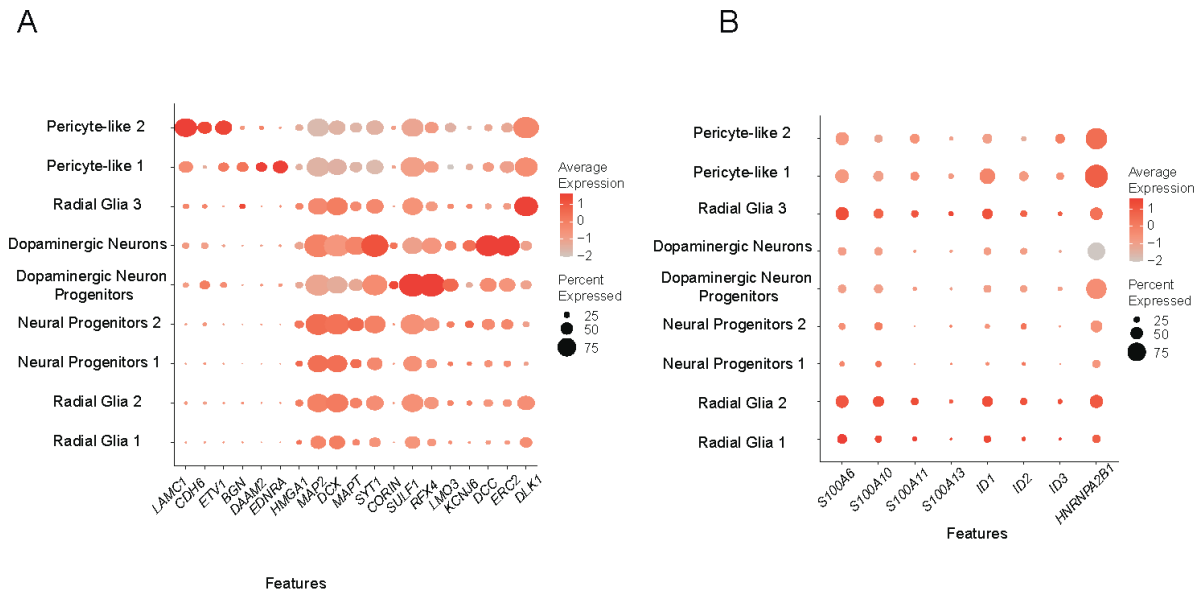
A
Pericyte-like 2
Pericyte-like 1
Radial Glia 3
Dopaminergic Neurons
Dopaminergic Neuron Progenitors
Neural Progenitors 2
Neural Progenitors 1
Radial Glia 2
Radial Glia 1
LAMC1
CDH6
ETV1
BGN
DAAM2
EDNRA
HMGA1
MAP2
DCX
MAPT
SYT1
CORIN
SULF1
RFX4
LMO3
KCNJ6
DCC
ERC2
DLK1
Features
Average Expression
1
0
−1
−2
Percent Expressed
25
50
75
B
Pericyte-like 2
Pericyte-like 1
Radial Glia 3
Dopaminergic Neurons
Dopaminergic Neuron Progenitors
Neural Progenitors 2
Neural Progenitors 1
Radial Glia 2
Radial Glia 1
S100A6
S100A10
S100A11
S100A13
ID1
ID2
ID3
HNRNPA2B1
Features
Average Expression
1
0
−1
−2
Percent Expressed
25
50
75

Supplemental Tables

Simplified identifier	Identifier	Patient	Gender	Age of sampling	Source
200	2.0.0.10.1.0	K7.1 WT/C4 WT	Female	81	Reinhardt et al., 2013
201	2.0.0.15.0.0	A13777	Female	Cord Blood	GIBCO/A13777

Table S1 related to experimental procedures. iPS cell lines used in this study.

Antibody	Host species	Source	Ref.-No.	Dilution
TH	Rabbit	Abcam	ab112	1:1000
TUJ1	Chicken	Millipore	AB9354	1:1000
Actin-β	Mouse	Cell signalling	3700	1:100000
CD31	Mouse	DAKO	M082301	1:200
TH	Rabbit	Abcam	ab112	1:1000
MAP2	Chicken	Abcam	ab5392	1:1000
Collagen IV	Rabbit	Abcam	ab6586	1:200
α-Smooth muscle actin	Rabbit	Abcam	ab5694	1:100
VE-Cadherin	Rabbit	Abcam	ab33168	1:300
Pimonidazole	Rabbit	Hypoxyprobe		
IBA1	Goat	Abcam	ab5076	1:250
PU1	Rabbit	Cell signalling	2258S	1:250
TRA-1-81	Mouse	Millipore	MAB4381	1:50
SOX2	Rabbit	Abcam	ab97959	1:100
TRA-1-60	Mouse	Millipore	MAB4360	1:50
Nanog	Rabbit	Millipore	AB5731	1:200
SSEA-4	Mouse	Millipore	MAB4304	1:50
Oct-4	Rabbit	Abcam	ab19857	1:400
Nestin	Mouse	Millipore	MAB5326	1:100
SOX2	Goat	R&D systems	AF2018	1:100
PAX6	Rabbit	Biolegend	901301	1:300
Alexa Fluor® 647 Anti-chicken	Donkey	Jackson Immuno	703-605-155	1:1000
Alexa Fluor® 488 anti-goat	Donkey	Invitrogen	A-11055	1:1000
Alexa Fluor® 568 anti-goat	Donkey	Thermo Fisher	a11057	1:1000
Alexa Fluor® 647 anti-goat	Donkey	Invitrogen	a21447	1:1000
Alexa Fluor® 488 anti-rabbit	Donkey	Thermo Fisher	a21206	1:1000
Alexa Fluor® 568 anti-rabbit	Donkey	Invitrogen	a10042	1:1000
Alexa Fluor® 647 anti-rabbit	Donkey	Invitrogen	a31573	1:1000
Alexa Fluor® 488 anti-mouse	Donkey	Invitrogen	a21202	1:1000
Alexa Fluor® 568 anti-mouse	Donkey	Invitrogen	a10037	1:1000
Hoechst 33342 Solution (20 mM)	-	Invitrogen	62249	1:10000

IgG H+L 800 anti-rabbit	Goat	Cell signalling	5151	1:10000
IgG H+L 680 anti-mouse	Goat	Cell signalling	5470	1:10000

Table°S2 related to experimental procedures. Antibodies used in this study.

CHAPTER 5

DISCUSSION AND PERSPECTIVES

Organoid systems have been developed over the last years to further increase the complexity of 2D cell culture models and closely represent the human body on a tissue and organ level. Interactions between multiple cell types can be studied in organoid systems, where cells communicate with each other in a 3D microenvironment. Besides, and thanks to the discovery of iPSC technology, patient-specific organoids have been developed to study human diseases from a personalized medicine perspective. iPSC-derived organoids have been applied to model human pathologies in different organs and tissues. Some examples are bronchial organoids to study lung cancer (Kim et al., 2019), colonic organoids to model colorectal cancer (Crespo et al., 2017) and pancreatic organoids to model dysplasia in cancer (Breunig et al., 2021). The brain is one of the most inaccessible areas of the human body; thus, obtaining human brain biopsies is a complex procedure that involves a high risk for the patient. Consequently, iPSC-derived brain organoids are of extremely high value for personalized medicine. Hence, scientists are nowadays able to obtain a recapitulation of the patient's brain and study the pathophysiology of multiple disorders with only the use of low invasive skin biopsies. Cerebral organoids have been developed to study human diseases such as microcephaly (Lancaster et al., 2013), glioblastoma (Linkous et al., 2019) and Alzheimer's disease (Zhao et al., 2020).

Midbrain organoids are tissue-specific 3D structures with heterogeneous cell composition and diversity (Monzel et al., 2017; Smits et al., 2019). Midbrain organoid systems have been used to study the effects of Zika virus infection in the developing midbrain (Qian et al., 2016). Thanks to their midbrain-specific identity and their high proportion of dopaminergic neurons, midbrain

organoids have been applied as a model to study genetic PD (Boussaad et al., 2020; Smits et al., 2019). While the complexity increase of organoid systems with respect to 2D cultures is clear, the question of how clinically relevant midbrain organoids are in respect to *in vivo* models remains unclear. In this thesis, we first focused on validating the accuracy of midbrain organoids in PD modelling and drug testing. Then, we explored in detail the cellular composition of the current system in order to identify and confirm its limitations. Finally, we improved the midbrain organoid model by integrating key missing compartments and therefore increasing its cellular complexity.

5.1. Midbrain organoids as a PD model

Most PD cases worldwide are idiopathic, where aging, environmental factors or combinations of multiple risk variants lead to the development of the disease. Interestingly, dopaminergic neuron toxicity has been induced in midbrain organoids via 6-OHDA treatment as a basis to develop a machine learning pipeline, predicting effects of neurotoxic compounds in organoids (Monzel et al., 2020). However, the high variability of the causative factors and phenotypes leading to idiopathic PD increase the difficulty to model such cases *in vitro*. Importantly, around 15% of the cases are genetic, where mutations in genes such as SNCA, PINK1, LRRK2 and DJ-1 lead to the development of the disease (Bhat et al., 2018; Inamdar et al., 2007). Genetic PD cases represent a lower complexity of genetic variants, and cellular and molecular phenotypes can be targeted more easily by focusing on pathways where a specific gene is involved. Moreover, patients known to carry causative mutations (e.g. with a family history of genetic PD) can be followed by physicians before the appearance of clinical symptoms, which allows to gather important clinical information about the different stages of disease progression. Genetic PD has been studied in midbrain organoid systems, where organoids carrying *LRRK2* (Smits et al., 2019) and *PARK7* (Boussaad et al., 2020) mutations were used.

Manuscript I represents a genetic PD modelling study focusing on PINK1 mutations. The work carried out displays the first efforts to study complex metabolic pathways such as autophagy and mitophagy in midbrain organoids. More importantly, the study shows that phenotypes and drug rescue experiments conducted in organoids are validated by mouse models. Indeed, an impairment in dopaminergic neuron differentiation was observed in 2D cultures and midbrain organoids carrying *PINK1* mutations, and similar results were observed in a MPTP-induced PD mouse model. Moreover, other studies confirmed the impairment of dopaminergic neuron differentiation in midbrain organoids and Zebrafish deficient for *PINK1* (Brown et al., 2021). In Manuscript I, 2D cultures of neurons carrying mutations in *PINK1* are used to target phenotypes in autophagy and mitophagy. Treatment of HP-β-CD, which modulates autophagy, led to an increase in autophagy and mitophagy in neurons and organoids carrying *PINK1*

mutations. For the first time, alterations in complex metabolic pathways such as autophagy were recapitulated and treated using midbrain organoids, in comparison with previous studies. In Smits et al., 2019, phenotyping focused on the amount and morphology of dopaminergic neurons. In Boussaad et al. 2020, drug treatment focused on rescuing dopaminergic neuron loss by restoring the expression of *PARK7*. Furthermore, in Manuscript I, dopaminergic neuron differentiation impairment and rescue after HP-β-CD treatment was validated with a PD-induced mouse model. In conclusion, we effectively demonstrated the translatability and clinical relevance of organoid phenotypes and drug testing approaches in comparison to *in vivo* systems.

5.2. Studying cellular heterogeneity in midbrain organoids

The cellular diversity in human tissue has been explored with single-cell transcriptomic technologies. These methods provide detailed gene expression information at the single cell resolution, thus allowing for the extensive study of cellular diversity and differences in gene expression in a single sample. In comparison with immunodetection assays, transcriptomic analysis brings a considerably higher amount of information using only a small amount of tissue sample. This technology has been applied to study the heterogeneous cellular composition of the human midbrain using adult *post-mortem* human substantia nigra, revealing the presence of astrocytes, oligodendrocytes, endothelial cells, microglia, oligodendrocyte precursor cells and neurons – including dopaminergic and GABAergic (Agarwal et al., 2020).

The cellular diversity in midbrain organoids has been extensively assessed via immunodetection assays (Monzel et al., 2017; Smits et al., 2019). However, detailed transcriptomic analysis identifying and characterizing cell clusters has not been done to date. Detailed information about gene expression in organoids would enable comparisons with embryonic human midbrain datasets, which would allow for a clear distinction of the embryonic age equivalent of organoids. Furthermore, since microglia and vasculature had not been detected previously in midbrain organoids, transcriptomics analysis is of high value to elucidate if non-detected cell types could develop within organoids.

In Manuscript II we identify and characterize cell populations in midbrain organoids via scRNA-Seq. Importantly, and since midbrain organoid systems recapitulate the human midbrain at embryonic age, the work developed in Manuscript II has later been used for comparisons with human embryonic midbrain datasets (Zagare et al., 2022). In that study, the transcriptomic identity of midbrain organoids matched the identity of the human embryonic midbrain between week 6 and 11 of development (Zagare et al., 2022). The results from Manuscript II show that, as expected, and considering the neuroectodermal patterning of the organoids' starting

population, no mesodermal cell types were identified. Interestingly, a mesenchymal cell cluster was observed, which was later named ‘fibroblasts’ because of the high expression of ECM-related genes. Single-cell transcriptomics analysis in a different midbrain organoid model derived from a neuroectodermal stem cell population showed similar results. Namely, a cluster named ‘vascular leptomeningeal cells’ was identified, which was characterized by the expression of ECM-related genes such as *COL1A1* and *COL1A2* (Fiorenzano et al., 2021). Mesenchymal cells in the human body normally have a mesodermal origin, although studies using animal models have also described the differentiation of mesenchymal cells from neural crest cells in the developing brain (also called the ‘ectomesenchyme’, Blentic et al., 2008). A recent study identified a cell cluster named ‘pericytes’ in midbrain organoid samples, characterized by the expression of ECM genes such as *CSPG4, MCAM* or *SPARC* (Zagare et al., 2022). Mesenchymal cells in the brain can give rise to meningeal fibroblasts and vascular leptomeningeal cells, which layers the meninges and thus participate in the isolation of cerebrospinal fluid from the BBB (Derk et al., 2021). Furthermore, evidence has demonstrated that pericytes can differentiate from neuroectoderm-derived precursor cells (Couly et al., 1992, 1993; Etchevers et al., 2001; Korn et al., 2002). Altogether, this indicates that all these cell types could refer to different stages of the brain ectomesenchyme, which can give rise to fibroblasts and vascular leptomeningeal cells such as pericytes.

The analysis performed in Manuscript II confirmed the expected lack of mesoderm-derived cell types such as microglia and endothelial cells. Consequently, we then focused to address these observed limitations in order to bring midbrain organoid systems closer to the complex cellular scenario in the human midbrain, and thus produce more advanced models.

5.3. From midbrain organoids to complex assembloids. Increasing the system complexity

Neurons in the brain are in constant communication with macroglia, microglia and vasculature. We speculate that the presence of microglia and a vasculature system in midbrain organoids would be beneficial by decreasing oxidative stress and hypoxia, and would optimise neuronal physiology and maturation. Furthermore, we hypothesize that a complete model containing both mesoderm-derived compartments would lead to interactions between endothelial cells and microglia, representing the neurovascular unit in 3D.

5.3.1. Microglia in midbrain organoids

Interactions between microglia have been studied *in vitro* via 2D co-culture. Studies where primary (Goshi et al., 2020) or iPSC-derived (Haenseler et al., 2017b; Lopez-Lengowski et al., 2021) cortical neurons were successfully co-cultured with microglia indicate that cortical neurons and microglia are technically compatible *in vitro* when cultured with the same culture medium. However, there are no studies showing successful co-culture between iPSC-derived microglia and dopaminergic neurons. Interestingly, co-culture of primary midbrain-specific neurons with primary microglia has been achieved in order to study neuroinflammation in PD (Tu et al., 2019). Moreover, an in-direct co-culture method of primary microglia with iPSC-derived neural precursors demonstrated the capacity of microglia to promote TH-positive cell differentiation (Schmidt et al., 2021). Nonetheless, no iPSC derived microglia were used in that study, but human and mouse primary cells. Thus, microglia were already in a differentiated state and were cultured in basal medium without small molecules that induce microglia differentiation. Furthermore, the contact between microglia and neurons was established through inserts and for a time period of 5 days (Schmidt et al., 2021). While that work is highly valuable to understand the effects of microglia in dopaminergic differentiation *in vitro*, it does not demonstrate the long-term viability and identity of microglia and dopaminergic neurons in co-culture. The lack of studies where iPSC-derived dopaminergic neurons are co-cultured with iPSC-derived microglia – which implies inducing differentiation of both cell types – could be due to the technical difficulties in engineering a culture medium that induces both dopaminergic neuron and microglia differentiation.

Furthermore, previous work has described an innate differentiation of microglia in human iPSC-derived cerebral organoids (Ormel et al., 2018) and optic vesicle organoids (Gabriel et al., 2021). The observed innate differentiation was most likely due to the fact that cerebral organoids undergo unguided differentiation, which leads to self-organization of cellular structures from different lineages. However, microglia differentiation does not always occur innately in iPSC-derived cerebral organoids. In multiple unguided differentiation approaches, microglia had to be incorporated since it did not develop innately (Abud et al., 2017; Muffat et al., 2016; Popova et al., 2021). Interestingly, the induction of an innate microglia differentiation within iPSC-derived brain organoids has been achieved via overexpression of the microglial transcription factor *PU1* (Cakir et al., 2022). In order to obtain region-specific organoids, the applied cell culture approach is a guided differentiation, where small molecules are applied at

specific concentrations and time exposures, leading to specificity and differentiation of the tissue. Guided cell culture differentiation often implies a pre-patterned initial cell population, specifically neuroepithelial stem cells in the case of midbrain organoids (Jacob et al., 2021). Recently, incorporation of microglia into human cortical spheroids has been achieved (Bejoy et al., 2019). However, no 3D studies showed microglial presence in midbrain-specific organoids until now. In Manuscript III, we successfully integrated microglia into midbrain organoids by co-culture with macrophage precursors using a specifically designed co-culture medium.

In this study, microglia phagocytosis ability was assessed in 2D via Zymosan assay, which showed successful engulfment and phagocytosis of particles by iPSC-microglia. The phagocytosis efficiency of microglia in 2D indicate that these cells could also be able to phagocyte within organoids. Importantly, when in a 3D environment, microglia in organoids expressed multiple cytokine and chemokine genes, as well as phagocytosis and inflammation-related genes. Hence, we decided to analyse the supernatant of microglia-containing organoid cultures. We were able to confirm the secretion of several cytokines and chemokines, which were not observed in medium from organoids without microglia. Amongst them, pro-inflammatory cytokines such as IL-6 and TNFα, and anti-inflammatory cytokines, such as IL-10 were produced by microglia in organoids, indicating that they could induce different types of responses in neural cells present in the system. These observations strongly demonstrate that microglia may be functional within organoids; however, further analysis assessing functional mechanisms of microglia in 3D would be of high value to confirm these observations. For example, molecular assays assessing cell viability and oxidative stress could be performed to validate that microglia phagocytose metabolic waste products and debris, reducing stress and increasing viability in organoids. Furthermore, assessing hypoxia in organoids with microglia would allow us to understand whether phagocytosis of cell debris and small organoid size leads to a better oxygen diffusion throughout the organoid tissue.

In line with our observations, studying synapse pruning in organoids containing microglia could be an additional way to explore microglia functionality in 3D. In the brain, microglia interact with neural cell types and affect synaptic functions as well as perform synapse pruning, (Tremblay et al., 2011; Wake et al., 2009). Apart from synapses, they also clear metabolic waste products and phagocyte apoptotic neurons (Witting et al., 2000). Further assays exploring synapse pruning in organoids would be highly important in order to confirm the downregulation of synapse genes observed in Manuscript III, as well as the lower levels of the pre-synaptic vesicle protein VAMP2.

An example would be a high-resolution microscopy approach to detect tagged synaptic proteins within microglia cell bodies. Treatment of microglia-containing organoids with fluorescently labelled synaptosomes would be another possible approach to assess synapse pruning in 3D. However, studying synapse pruning in 3D has not yet been achieved, while 2D co-culture systems of primary mouse microglia and neurons have been used to study synapse pruning and spine elimination *in vitro* (Cheadle et al., 2020; Scott-Hewitt et al., 2020). Considering that synapse pruning is associated to an efficient synaptic transmission and neuronal functionality, the observed improved electrophysiological properties in organoids with microglia could be linked to this phenomenon. Moreovoer, lower inter-spike interval and lower action potential threshold measurements were recorded, which can be a result of a more spontaneous action potential firing and, possibly, a higher neuronal maturation. Future efforts should focus on assessing neuronal maturation in organoids with microglia via specific marker expression and morphological features such as spine formation.

A limitation of the microglia-containing midbrain organoid system described in Manuscript III is the amoeboid-like microglia morphology within organoids. The fact that iPSC-derived microglia display an amoeboid morphology that resemble human microglia upon injury of disease has been previously discussed (Hasselmann and Blurton-Jones, 2020). The morphological complexity of 2D iPSC-derived microglia tends to increase in 3D systems, but it often needs molecular queues from the CNS upon transplantation into animal models to display a comparable morphology to the one seen *in vivo* (Hasselmann and Blurton-Jones, 2020). The innate differentiation of microglia within cerebral organoids seemed to display a more ramified morphology than in Manuscript III (Ormel et al., 2018). These observations could be explained by the high sensitivity to stress and the technical manipulations of isolated iPSC-derived microglia, which could induce morphology changes in the cells. This hypothesis is supported by a study where, shortly after isolation from the CNS, primary microglia lost their differentiated gene identity, which was restored upon re-transplantation into the mouse brain (Bohlen et al., 2017). Future efforts could focus on bringing microglia in midbrain organoids closer to the physiological state in the human brain by, for instance, reducing the levels of stress in the system. For this purpose, a possible option could be obtaining a less compact tissue and therefore enhance passive diffusion of oxygen and nutrients to the core. Organoid perfusion through tubular structures or scaffold could also be a suitable option to promote oxygen and nutrient flow throughout the organoid. A different approach could focus on supplementing the culture media with antioxidants to try to reduce oxidative stress in the system. We hypothesize that, in an environment

with lower stress levels, microglia would more accurately recapitulate their morphology in the human brain, and morphological differences upon neurodegeneration or infection could be more easily observed.

In conclusion, we were able to generate and characterize a midbrain organoid system containing microglia. Since one of the final goals of midbrain organoids is modelling PD, future experiments should focus on modelling neuroinflammation and reactive microgliosis using this optimized midbrain organoid model. Ultimately, the effects of immune system alterations in dopaminergic neuron degeneration could be studied using our proposed patient-derived midbrain organoids with microglia.

5.3.2. Vascularized midbrain organoids

The main cell compartment forming blood vessels are endothelial cells, which have a mesodermal origin. Because of the neuroepithelial starting cell population of midbrain organoids, endothelial cells – and therefore blood vessels - do not innately develop within organoids. The gene expression analysis and cell type clustering undertaken in Manuscript II, did not reveal an endothelial cell cluster. While endothelial cells are essential for blood vessel development and stability, they are not the only cell type in vasculature structures. Pericytes, which can derive from the mesoderm or neuroectoderm, surround and support endothelial cells, and communicate with them through molecular signalling (Tata et al., 2015). As discussed previously, the mesenchymal cell cluster identified in midbrain organoids in Manuscript II, could match the pericyte cluster identified later on in Zagare et al. 2022, and further confirms the neuroectodermal origin of pericytes in the brain.

In the past years, several approaches have been used to implement a blood vessel network into whole brain or region-specific organoids. One of the most successful techniques is transplantation into mice, which leads to angiogenesis and invasion of host vessels into the organoid structure (Mansour et al., 2018; Pham et al., 2018). However, animal models represent disadvantages such as reproducibility, time-efficiency and ethical concerns. Other approaches for the integration of vasculature into organoids include co-culture with mesoderm-derived cells (Bergmann et al., 2018; Wörsdörfer et al., 2020) and integration of pre-coated perfusable artificial scaffolds (Miller et al., 2012; Nashimoto et al., 2017).

Developing vasculature invades the brain following angiogenic signals from neural cells. We speculate that an interesting way to integrate vasculature into midbrain organoids would be by recapitulating angiogenesis in the developing neural tube from the perineural vascular plexus. From this point of view, we considered co-culture of midbrain organoids with vascular organoids (Wimmer et al., 2019) as a suitable option. In Manuscript IV, by fusing vascular organoids with midbrain organoids, we successfully integrated an endothelial network, where endothelial cells connected through adherens junctions forming tube-like structures. Pericyte markers and basal lamina structures were observed in the vascularised midbrain organoids. This technical approach had already been applied previously to fuse blood vessel organoids with cerebral organoids (Ahn et al., 2021). However, region specific brain organoids, particularly midbrain organoids, have not been successfully vascularized *in vitro* until now. The presence of organized vessel-like structures has been studied in brain organoids (Ahn et al., 2021; Cakir et al., 2019; Pham et al., 2018; Wörsdörfer et al.). The high-magnification immunofluorescence images in Manuscript IV suggest that endothelial structures may present a tubular shape. However, we did not show a full closure of vessel-like structures, suggesting that the system may still be immature, and perfusion would lead to diffusion through not fully closed areas. Previous work with iPSC-derived vasculature mimicking the BBB resulted in perfusable networks (Belair et al., 2015; Campisi et al., 2018; Palladino et al., 2019). Later efforts will focus on assessing tube closure in later culture time points via high-resolution microscopy and vessel perfusion using with a tagged dye such as Dextran. Apart from studying the morphology and closure of vessels, permeability should be assessed to explore whether the vessel network has BBB properties. In line with this perspective, some studies assessed the trans-endothelial electrical resistance to assess permeability in the model (Cakir et al., 2019). It would be of high interest studying the trans-endothelial electrical resistance in our vascularized assembloids in order to assess the functionality endothelial networks and to explore possible differences in PD.

A common issue in organoid systems is the ‘dead core’ phenomenon, where cells in the inner regions are closely packed, which leads to a perturbed diffusion gradient of nutrients and oxygen that do not reach the core, resulting in cell death (Beauchamp et al., 2015; Lancaster et al., 2013; Monzel et al., 2017; Ramachandran et al., 2015). By vascularizing midbrain organoids, we hypothesize that we could increase the oxygen supply, and therefore reduce cell death in the inner centre. Researchers in previous studies tried to assess cell death and hypoxia in vascularized organoids and observed lower cell death by TUNEL assay, and lower levels of the gene HIF-1α (Hypoxia-

inducible factor 1α, Cakir et al., 2019). However, these organoids were grafted into mice in order to promote angiogenesis and generate a vascular network. Likewise, previous efforts assessed the engineering of perfusable artificial scaffolds that work as a vascular network, and their integration into tissue-like structures have also been achieved (Miller et al., 2012; Nashimoto et al., 2017). Artificial perfusable networks have been proven to be closed perfusable systems, suitable for oxygenation of tissues (Miller et al., 2012; Nashimoto et al., 2017). However, they do not represent the entire blood vessel structure as they are missing pericytes, extracellular matrix and basal lamina. In Manuscript IV, we show for the first time lower levels of hypoxia and cell death in vascularized assembloids without the need for gene editing, artificial scaffolds or transplantation into animal models. Since we did not confirm that blood vessels are perfusable, we speculate that the culture medium flow inside blood vessels within assembloids is unlikely. Instead, these changes could be due to a higher passive diffusion of oxygen and nutrients in assembloids because of a less compact tissue, which should be confirmed by further experiments. We speculate that a closed perfusable vasculature system in organoids could further ameliorate oxygenation due to the low compactness observed in our assembloids.

5.3.3. On the way to highly complex midbrain organoid systems

Previous studies have focused on the cellular interactions between microglia and endothelial cells in the neurovascular unit. Some of them have used animal models to assess the spatial interactions and contacts between cells (Grossmann et al., 2002; Rymo et al., 2011) and cell signalling between the microglia and endothelium compartment (Li et al., 2019). This has been assessed in healthy conditions, but also in disease (Chen et al., 2019; Klement et al., 2019) and aging (Yousef et al., 2019). Apart from animal models, organ-on-chip technologies have been applied to mimic a neurovascular unit on-chip (Achyuta et al., 2013). Furthermore, alpha-synuclein spread has been studied in a substantia nigra-specific neurovascular unit on-chip (Pediaditakis et al., 2021). However, little is known about cellular and molecular interactions in the neurovascular unit in iPSC-derived human whole brain or region-specific organoids. The incorporation of microglia into vascularized assembloids represents a key factor to not only to study the human midbrain not only in physiological conditions, but also in neurodegeneration. In neurodegenerative diseases, neuroinflammation can accelerate neuronal damage and negatively affect the BBB functioning (Daneman et al., 2010; Liebner et al., 2018). Therefore, having complex midbrain-specific assembloid systems

with neural cell types, microglia and vasculature could help scientists to better understand cellular interactions and molecular microenvironments in PD.

The separate and simultaneous integration of microglia and vasculature in midbrain organoids represented an advancement of the midbrain organoid model. As shown in Manuscript IV, two mesoderm-derived cell compartments successfully co-inhabited with neural cells in the system, further increasing the complexity shown in Manuscript III and the vasculature part of Manuscript IV. Moreover, microglia, endothelial cells and neurons established connectiions in 3D, showing multi-cellular communication within organoids. Structures where the three cell compartments interact, ultimately mimic the neurovascular unit *in vitro*. In the human brain, the neurovascular unit is constituted by endothelial cells, pericytes, neurons, microglia and astrocytes, in contact with smooth muscle cells and extracellular matrix (McConnell et al., 2017). In vascularized assembloids, we did not observe astrocytic processes at the analysed time point. However the up-regulation of astrocyte differentiation-related genes could indicate that in longer culture durations, differences in the astrocyte numbers may appear in assembloids compared to midbrain organoids. Thus, further efforts should focus on comparing organoids and assembloids at later time points in order to assess whether higher numbers of astrocytes appear in assembloids. Studying the interaction of astrocyte feet with the complex formed by neurons, endothelial cells and microglia would be of high interest for future studies, since astrocytes are a major component of the neurovascular unit and in physiological conditions, astrocytes release angiogenic factors and support molecules for blood vessels (Liebner et al., 2018). Furthermore, a detailed characterization of the morphological features in microglia, endothelial cells and astrocytes in the system could be addressed. Comparison of these features with midbrain organoids where some of these compartments are missing would be of great value to understand the high importance of cellular interactions for cell type maturation in the midbrain. Finally, studies using PD patient-derived vascularized assembloids with microglia would be of extreme value to assess neuroinflammation, BBB disruption and instability of the neurovascular unit *in vitro.*

The presence of microglia in vascularized assembloids led to an increase in the length of endothelial cell protrusions. Microglia have been associated with angiogenesis *in vitro*, since they can produce factors that stimulate the migration and proliferation of endothelial cells via VEGF-A and PDGF-BB expression (Ding et al., 2018). VEGF-A produced by microglia has been associated with blood vessel sprouting *in vitro* (Rymo et al., 2011). Long endothelial projections have been associated to vessel development

and closure; therefore, elongated endothelial cells could be associated to a further development of blood vessels (Tsuji-Tamura and Ogawa, 2018). In line with the discussed limitation concerning vessel closure in vascularized assembloids, we speculate that microglia may promote vessel closure in the system. This hypothesis should be verified through additional experiments. As suggested for the astrocyte analysis, longer culture durations could help unravel the blood vessel formation and closure process in assembloids with and without microglia. Interestingly, longer ramifications of microglia were also observed in the presence of vasculature. This observation goes in line with the published evidence confirming the importance of complex CNS signalling – coming from multiple cell types – in microglia differentiation and morphological complexity (Bohlen et al., 2017; Hasselmann and Blurton-Jones, 2020). Amoeboid microglia morphologies and shorter processes are associated with pathological conditions and a pro-inflammatory state. We speculate that endothelial cells in assembloids could secrete factors that induce the ramification of microglia cells, corresponding with a resting state (Iadecola and Anrather, 2011; Liang et al., 2020; Perego et al., 2011). Analysis of cytokine and chemokine secretion from endothelial cells and microglia in assembloids could help to unravel the molecular signalling mechanisms underlying these morphological changes in the system.

The complexity of 3D culture systems has rapidly increased over the last years, and studies where organoid models are further advanced using co-culture systems, engineered devices and extracellular matrix compounds are quickly rising. These advancements represent a step forward in modelling human organs and tissues. Furthermore, connexions and interactions between organoids represent a step forward in the ‘body-on-chip’ concept. The result of this PhD thesis is a complex midbrain-assembloid system, containing ectodermal and mesodermal cell types in the human midbrain. It represent an open door to the study of midbrain-specific mechanisms in neurons, glia and vasculature in health – such as those during midbrain development - and disease – like those in PD. Finally, it expands the possible cellular targets for drug treatments, representing a higher relevance for clinical studies.

REFERENCES

Abud, E.M., Ramirez, R.N., Martinez, E.S., Healy, L.M., Nguyen, C.H.H., Newman, S.A., Yeromin, A. V., Scarfone, V.M., Marsh, S.E., Fimbres, C., et al. (2017). iPSC-Derived Human Microglia-like Cells to Study Neurological Diseases. Neuron *94*, 278-293.e9.

Achyuta, A.K.H., Conway, A.J., Crouse, R.B., Bannister, E.C., Lee, R.N., Katnik, C.P., Behensky, A.A., Cuevas, J., and Sundaram, S.S. (2013). A modular approach to create a neurovascular unit-on-a-chip. Lab Chip *13*, 542–553.

Agarwal, D., Sandor, C., Volpato, V., Caffrey, T.M., Monzón-Sandoval, J., Bowden, R., Alegre-Abarrategui, J., Wade-Martins, R., and Webber, C. (2020). A single-cell atlas of the human substantia nigra reveals cell-specific pathways associated with neurological disorders. Nat. Commun. 2020 111 *11*, 1–11.

Aguilar, C., Alves da Silva, M., Saraiva, M., Neyazi, M., Olsson, I.A.S., and Bartfeld, S. (2021). Organoids as host models for infection biology – a review of methods. Exp. Mol. Med. 2021 5310 *53*, 1471–1482.

Ahn, Y., An, J.H., Yang, H.J., Lee, D.G., Kim, J., Koh, H., Park, Y.H., Song, B.S., Sim, B.W., Lee, H.J., et al. (2021). Human blood vessel organoids penetrate human cerebral organoids and form a vessel-like system. Cells *10*.

Alcendor, D.J., Block, F.E., Cliffel, D.E., Daniels, J.S., Ellacott, K.L.J., Goodwin, C.R., Hofmeister, L.H., Li, D., Markov, D.A., May, J.C., et al. (2013). Neurovascular unit on a chip: implications for translational applications. Stem Cell Res. Ther. *4 Suppl 1*.

Andersson, E., Tryggvason, U., Deng, Q., Friling, S., Alekseenko, Z., Robert, B., Perlmann, T., and Ericson, J. (2006). Identification of intrinsic determinants of midbrain dopamine neurons. Cell *124*, 393–405.

Araque, A., Carmignoto, G., Haydon, P.G., Oliet, S.H.R., Robitaille, R., and Volterra, A. (2014). Gliotransmitters travel in time and space. Neuron *81*, 728–739.

Arenas, E. (2008). Foxa2: The Rise and Fall of Dopamine Neurons. Cell Stem Cell *2*, 110–112.

Arnò, B., Grassivaro, F., Rossi, C., Bergamaschi, A., Castiglioni, V., Furlan, R., Greter, M., Favaro, R., Comi, G., Becher, B., et al. (2014). Neural progenitor cells orchestrate microglia migration and positioning into the developing cortex. Nat. Commun. *5*.

Ashrafi, G., and Schwarz, T.L. (2012). The pathways of mitophagy for quality control and clearance of mitochondria. Cell Death Differ. 2013 201 *20*, 31–42.

Askew, K., Li, K., Olmos-Alonso, A., Garcia-Moreno, F., Liang, Y., Richardson, P., Tipton, T., Chapman, M.A., Riecken, K., Beccari, S., et al. (2017). Coupled Proliferation and Apoptosis Maintain the Rapid Turnover of Microglia in the Adult Brain. Cell Rep. *18*, 391–405.

Badanjak, K., Mulica, P., Smajic, S., Delcambre, S., Tranchevent, L.C., Diederich, N., Rauen, T., Schwamborn, J.C., Glaab, E., Cowley, S.A., et al. (2021). iPSC-Derived Microglia as a Model to Study Inflammation in Idiopathic Parkinson's Disease. Front. Cell Dev. Biol. *9*.

Bagley, J.A., Reumann, D., Bian, S., Lévi-Strauss, J., and Knoblich, J.A. (2017). Fused cerebral organoids model interactions between brain regions. Nat. Methods 2017 147 *14*, 743–751.

Ball, W.S., Byars, A.W., Schapiro, M., Bommer, W., Carr, A., German, A., Dunn, S., Rivkin, M.J., Waber, D., Mulkern, R., et al. (2012). Total and Regional Brain Volumes in a Population-Based Normative Sample from 4 to 18 Years: The NIH MRI Study of Normal Brain Development. Cereb. Cortex *22*, 1–12.

Bautch, V.L., and James, J.M. (2009a). Neurovascular development: The beginning of a beautiful friendship. Cell Adh. Migr. *3*, 199.

Bautch, V.L., and James, J.M. (2009b). Neurovascular development: The beginning of a beautiful friendship. Cell Adhes. Migr. *3*, 199–204.

Beauchamp, P., Moritz, W., Kelm, J.M., Ullrich, N.D., Agarkova, I., Anson, B.D., Suter, T.M., and Zuppinger, C. (2015). Development and Characterization of a Scaffold-Free 3D Spheroid Model of Induced Pluripotent Stem Cell-Derived Human Cardiomyocytes. Tissue Eng. Part C. Methods *21*, 852–861.

Bejoy, J., Yuan, X., Song, L., Hua, T., Jeske, R., Sart, S., Sang, Q.X.A., and Li, Y. (2019). Genomics Analysis of Metabolic Pathways of Human Stem Cell-Derived Microglia-Like Cells and the Integrated Cortical Spheroids. Stem Cells Int. *2019*.

Belair, D.G., Whisler, J.A., Valdez, J., Velazquez, J., Molenda, J.A., Vickerman, V., Lewis, R., Daigh, C., Hansen, T.D., Mann, D.A., et al. (2015). Human vascular tissue models formed from human induced pluripotent stem cell derived endothelial cells. Stem Cell Rev. *11*, 511.

Bennett, M.L., Bennett, F.C., Liddelow, S.A., Ajami, B., Zamanian, J.L., Fernhoff, N.B., Mulinyawe, S.B., Bohlen, C.J., Adil, A., Tucker, A., et al. (2016). New tools for studying microglia in the mouse and human CNS. Proc. Natl. Acad. Sci. U. S. A. *113*, E1738–E1746.

Bergles, D.E., and Richardson, W.D. (2016). Oligodendrocyte Development and Plasticity. Cold Spring Harb. Perspect. Biol. *8*.

Bergmann, S., Lawler, S.E., Qu, Y., Fadzen, C.M., Wolfe, J.M., Regan, M.S., Pentelute, B.L., Agar, N.Y.R., and Cho, C.F. (2018). Blood-brain-barrier organoids for investigating the permeability of CNS therapeutics. Nat. Protoc. *13*, 2827–2843.

Bhat, S., Acharya, U.R., Hagiwara, Y., Dadmehr, N., and Adeli, H. (2018). Parkinson's disease: Cause factors, measurable indicators, and early diagnosis. Comput. Biol. Med. *102*, 234–241.

Birey, F., Andersen, J., Makinson, C.D., Islam, S., Wei, W., Huber, N., Fan, H.C., Metzler, K.R.C., Panagiotakos, G., Thom, N., et al. (2017). Assembly of functionally integrated human forebrain spheroids. Nature *545*, 54–59.

Blauwendraat, C., Reed, X., Krohn, L., Heilbron, K., Bandres-Ciga, S., Tan, M., Gibbs, J.R., Hernandez, D.G., Kumaran, R., Langston, R., et al. (2020). Genetic modifiers of risk and age at onset in GBA associated Parkinson's disease and Lewy body dementia. Brain *143*, 234.

Blentic, A., Tandon, P., Payton, S., Walshe, J., Carney, T., Kelsh, R.N., Mason, I., and Graham, A. (2008). The emergence of ectomesenchyme. Dev. Dyn. *237*, 592.

Block, M.L., Zecca, L., and Hong, J.-S. (2007). Microglia-mediated neurotoxicity: uncovering the molecular mechanisms. Nat. Rev. Neurosci. *8*, 57–69.

Bohlen, C.J., Bennett, F.C., Tucker, A.F., Collins, H.Y., Mulinyawe, S.B., and Barres, B.A. (2017). Diverse requirements for microglial survival, specification, and function revealed by defined-medium cultures. Neuron *94*, 759.

Boullerne, A.I., and Feinstein, D.L. (2020). History of Neuroscience I. Pío del Río-Hortega (1882–1945): The Discoverer of Microglia and Oligodendroglia. ASN Neuro *12*.

Boussaad, I., Obermaier, C.D., Hanss, Z., Bobbili, D.R., Bolognin, S., Glaab, E., Wolynska, K., Weisschuh, N., De Conti, L., May, C., et al. (2020). A patient-based model of RNA mis-splicing uncovers treatment targets in Parkinson's disease. Sci. Transl. Med. *12*.

Braak, H., De Vos, R.A.I., Bohl, J., and Del Tredici, K. (2006). Gastric α-synuclein immunoreactive inclusions in Meissner's and Auerbach's plexuses in cases staged for Parkinson's disease-related brain pathology. Neurosci. Lett. *396*, 67–72.

Brás, J., Guerreiro, R., and Hardy, J. (2015). SnapShot: Genetics of Parkinson's disease. Cell *160*, 570-570.e1.

Breunig, M., Merkle, J., Wagner, M., Melzer, M.K., Barth, T.F.E., Engleitner, T., Krumm, J., Wiedenmann, S., Cohrs, C.M., Perkhofer, L., et al. (2021). Modeling plasticity and dysplasia of pancreatic ductal organoids derived from human pluripotent stem cells. Cell Stem Cell *28*, 1105-1124.e19.

Brown, S.J., Boussaad, I., Jarazo, J., Fitzgerald, J.C., Antony, P., Keatinge, M., Blechman, J., Schwamborn, J.C., Krüger, R., Placzek, M., et al. (2021). PINK1 deficiency impairs adult neurogenesis of dopaminergic neurons. Sci. Reports 2021 111 *11*, 1–14.

Caddeo, S., Boffito, M., and Sartori, S. (2017). Tissue Engineering Approaches in the Design of Healthy and Pathological In Vitro Tissue Models. Front. Bioeng. Biotechnol. *5*.

Cakir, B., Xiang, Y., Tanaka, Y., Kural, M.H., Parent, M., Kang, Y.J., Chapeton, K., Patterson, B., Yuan, Y., He, C.S., et al. (2019). Engineering of human brain organoids with a functional vascular-like system. Nat. Methods *16*, 1169–1175.

Cakir, B., Tanaka, Y., Kiral, F.R., Xiang, Y., Dagliyan, O., Wang, J., Lee, M., Greaney, A.M., Yang, W.S., duBoulay, C., et al. (2022). Expression of the transcription factor PU.1 induces the generation of microglia-like cells in human cortical organoids. Nat. Commun. *13*.

Campisi, M., Shin, Y., Osaki, T., Hajal, C., Chiono, V., and Kamm, R.D. (2018). 3D Self-Organized Microvascular Model of the Human Blood-Brain Barrier with Endothelial Cells, Pericytes and Astrocytes. Biomaterials *180*, 117.

Castaño, A., Herrera, A.J., Cano, J., and Machado, A. (1998). Lipopolysaccharide intranigral injection induces inflammatory reaction and damage in nigrostriatal dopaminergic system. J. Neurochem. *70*, 1584–1592.

Chan, W.Y., Kohsaka, S., and Rezaie, P. (2007). The origin and cell lineage of microglia—New concepts. Brain Res. Rev. *53*, 344–354.

Cheadle, L., Rivera, S.A., Phelps, J.S., Ennis, K.A., Stevens, B., Burkly, L.C., Lee, W.C.A., and Greenberg, M.E. (2020). Sensory experience engages microglia to shape neural connectivity through a non-phagocytic mechanism. Neuron *108*, 451.

Chen, A.Q., Fang, Z., Chen, X.L., Yang, S., Zhou, Y.F., Mao, L., Xia, Y.P., Jin, H.J., Li, Y.N., You, M.F., et al. (2019). Microglia-derived TNF-α mediates endothelial necroptosis aggravating blood brain–barrier disruption after ischemic stroke. Cell Death Dis. *10*.

Chinta, S.J., and Andersen, J.K. (2005). Dopaminergic neurons. Int. J. Biochem. Cell Biol. *37*, 942–946.

Couch, Y., Alvarez-Erviti, L., Sibson, N.R., Wood, M.J.A., and Anthony, D.C. (2011). The acute inflammatory response to intranigral α-synuclein differs significantly from intranigral lipopolysaccharide and is exacerbated by peripheral inflammation. J. Neuroinflammation *8*, 1–14.

Couly, G.F., Coltey, P.M., and Le Douarin, N.M. (1992). The developmental fate of the cephalic mesoderm in quail-chick chimeras. Development *114*, 1–15.

Couly, G.F., Coltey, P.M., and Le Douarin, N.M. (1993). The triple origin of skull in higher vertebrates: a study in quail-chick chimeras. Development *117*, 409–429.

Crespo, M., Vilar, E., Tsai, S.Y., Chang, K., Amin, S., Srinivasan, T., Zhang, T., Pipalia, N.H., Chen, H.J., Witherspoon, M., et al. (2017). Colonic organoids derived from human induced pluripotent stem cells for modeling colorectal cancer and drug testing. Nat. Med. *23*, 878–884.

Cserép, C., Pósfai, B., Lénárt, N., Fekete, R., László, Z.I., Lele, Z., Orsolits, B., Molnár, G., Heindl, S., Schwarcz, A.D., et al. (2020). Microglia monitor and protect neuronal function through specialized somatic purinergic junctions. Science *367*, 528–237.

Czepiel, M., Balasubramaniyan, V., Schaafsma, W., Stancic, M., Mikkers, H., Huisman, C., Boddeke, E., and Copray, S. (2011). Differentiation of induced pluripotent stem cells into functional oligodendrocytes. Glia *59*, 882–892.

Członkowska, A., Kohutnicka, M., Kurkowska-Jastrzębska, I., and Członkowski, A. (1996). Microglial reaction in MPTP (1-methyl-4-phenyl-1,2,3,6-tetrahydropyridine) induced Parkinson's disease mice model. Neurodegeneration *5*, 137–143.

Daneman, R., Zhou, L., Kebede, A.A., and Barres, B.A. (2010). Pericytes are required for blood-brain barrier integrity during embryogenesis. Nature *468*, 562–566.

Derk, J., Jones, H.E., Como, C., Pawlikowski, B., and Siegenthaler, J.A. (2021). Living on the Edge of the CNS: Meninges Cell Diversity in Health and Disease. Front. Cell. Neurosci. *15*, 245.

Diaz-Aparicio, I., Paris, I., Sierra-Torre, V., Plaza-Zabala, A., Rodríguez-Iglesias, N., Márquez-Ropero, M., Beccari, S., Huguet, P., Abiega, O., Alberdi, E., et al. (2020). Microglia actively remodel adult hippocampal neurogenesis through the phagocytosis secretome. J. Neurosci. *40*, 1453–1482.

Ding, X., Gu, R., Zhang, M., Ren, H., Shu, Q., Xu, G., and Wu, H. (2018). Microglia enhanced the angiogenesis, migration and proliferation of co-cultured RMECs. BMC Ophthalmol. *18*.

Djelloul, M., Holmqvist, S., Boza-Serrano, A., Azevedo, C., Yeung, M.S., Goldwurm, S., Frisén, J., Deierborg, T., and Roybon, L. (2015). Alpha-Synuclein Expression in the Oligodendrocyte Lineage: an In Vitro and In Vivo Study Using Rodent and Human Models. Stem Cell Reports *5*, 174–184.

Dohgu, S., Takata, F., Matsumoto, J., Kimura, I., Yamauchi, A., and Kataoka, Y. (2019). Monomeric α-synuclein induces blood–brain barrier dysfunction through activated brain pericytes releasing inflammatory mediators in vitro. Microvasc. Res. *124*, 61–66.

di Domenico, A., Carola, G., Calatayud, C., Pons-Espinal, M., Muñoz, J.P., Richaud-Patin, Y., Fernandez-Carasa, I., Gut, M., Faella, A., Parameswaran, J., et al. (2019). Patient-Specific iPSC-Derived Astrocytes Contribute to Non-Cell-Autonomous Neurodegeneration in Parkinson's Disease. Stem Cell Reports *12*, 213.

Dong, T., Li, M., Gao, F., Wei, P., and Wang, J. (2022). Construction and imaging of a neurovascular unit model. Neural Regen. Res. *17*, 0.

Dugger, B.N., and Dickson, D.W. (2017). Pathology of Neurodegenerative Diseases. Cold Spring Harb. Perspect. Biol. *9*.

Duncan, G.J., Simkins, T.J., and Emery, B. (2021). Neuron-Oligodendrocyte Interactions in the Structure and Integrity of Axons. Front. Cell Dev. Biol. *9*.

Durkee, C.A., and Araque, A. (2019). DIVERSITY AND SPECIFICITY OF ASTROCYTE-NEURON COMMUNICATION. Neuroscience 73–78.

Erkkinen, M.G., Kim, M.O., and Geschwind, M.D. (2018). Clinical Neurology and Epidemiology of the Major Neurodegenerative Diseases. Cold Spring Harb. Perspect. Biol. *10*.

Etchevers, H.C., Vincent, C., Le Douarin, N.M., and Couly, G.F. (2001). The cephalic neural crest provides pericytes and smooth muscle cells to all blood vessels of the face and forebrain. Development *128*, 1059–1068.

Eyo, U.B., Mo, M., Yi, M.H., Murugan, M., Liu, J., Yarlagadda, R., Margolis, D.J., Xu, P., and Wu, L.J. (2018). P2Y12R-Dependent Translocation Mechanisms Gate the Changing Microglial Landscape. Cell Rep. *23*, 959–966.

Fiorenzano, A., Sozzi, E., Birtele, M., Kajtez, J., Giacomoni, J., Nilsson, F., Bruzelius, A., Sharma, Y., Zhang, Y., Mattsson, B., et al. (2021). Single-cell transcriptomics captures features of human midbrain development and dopamine neuron diversity in brain organoids. Nat. Commun. 2021 121 *12*, 1–19.

Gabriel, E., Albanna, W., Pasquini, G., Ramani, A., Josipovic, N., Mariappan, A., Schinzel, F., Karch, C.M., Bao, G., Gottardo, M., et al. (2021). Human brain organoids assemble functionally integrated bilateral optic vesicles. Cell Stem Cell.

Gammill, L.S., and Bronner-Fraser, M. (2003). Neural crest specification: Migrating into genomics. Nat. Rev. Neurosci. *4*, 795–805.

Ghosh, S.K. (2020). Camillo Golgi (1843–1926): Scientist Extraordinaire and Pioneer Figure of Modern Neurology. Anat. Cell Biol. *53*, 385–392.

Gibb, W.R.G., and Lees, A.J. (1988). The relevance of the Lewy body to the pathogenesis of idiopathic Parkinson's disease. J. Neurol. Neurosurg. Psychiatry *51*, 745–752.

Gilbert, S.F. (2000). Paraxial Mesoderm: The Somites and Their Derivatives.

Gilbert, S.F., and Barresi, M.J.F. (2017). DEVELOPMENTAL BIOLOGY, 11TH EDITION 2016. Am. J. Med. Genet. Part A *173*, 1430–1430.

Ginhoux, F., Greter, M., Leboeuf, M., Nandi, S., See, P., Gokhan, S., Mehler, M.F., Conway, S.J., Ng, L.G., Stanley, E.R., et al. (2010). Fate mapping analysis reveals that adult microglia derive from primitive macrophages. Science (80-.). *330*, 841–845.

Ginhoux, F., Lim, S., Hoeffel, G., Low, D., and Huber, T. (2013). Origin and differentiation of microglia. Front. Cell. Neurosci. *7*, 1–14.

Gjorevski, N., Ranga, A., and Lutolf, M.P. (2014). Bioengineering approaches to guide stem cell-based organogenesis. Development *141*, 1794–1804.

Goshi, N., Morgan, R.K., Lein, P.J., and Seker, E. (2020). A primary neural cell culture model to study neuron, astrocyte, and microglia interactions in neuroinflammation. J. Neuroinflammation *17*, 1–16.

Gray, M.T., and Woulfe, J.M. (2015). Striatal blood-brain barrier permeability in Parkinson's disease. J. Cereb. Blood Flow Metab. *35*, 747–750.

Grebenyuk, S., and Ranga, A. (2019). Engineering Organoid Vascularization. Front. Bioeng. Biotechnol. *7*.

Grossmann, R., Stence, N., Carr, J., Fuller, L., Waite, M., and Dailey, M.E. (2002). Juxtavascular Microglia Migrate Along Brain Microvessels Following Activation During Early Postnatal Development.

Haenseler, W., Sansom, S.N., Buchrieser, J., Newey, S.E., Moore, C.S., Nicholls, F.J., Chintawar, S., Schnell, C., Antel, J.P., Allen, N.D., et al. (2017a). A Highly Efficient Human Pluripotent Stem Cell Microglia Model Displays a Neuronal-Co-culture-Specific Expression Profile and Inflammatory Response. Stem Cell Reports *8*, 1727–1742.

Haigh, J.J., Morelli, P.I., Gerhardt, H., Haigh, K., Tsien, J., Damert, A., Miquerol, L., Muhlner, U., Klein, R., Ferrara, N., et al. (2003). Cortical and retinal defects caused by dosage-dependent reductions in VEGF-A paracrine signaling. Dev. Biol. *262*, 225–241.

Harpaz, D., Koh, B., Seet, R.C.S., Abdulhalim, I., and Tok, A.I.Y. (2020). Functionalized silicon dioxide self-referenced plasmonic chip as point-of-care biosensor for stroke biomarkers NT-proBNP and S100β. Talanta *212*.

Hasselmann, J., and Blurton-Jones, M. (2020). Human iPSC-derived microglia: A growing toolset to study the brain's innate immune cells. Glia *68*, 721.

Hirsch, E.C., and Hunot, S. (2009). Neuroinflammation in Parkinson's disease: a target for neuroprotection? Lancet. Neurol. *8*, 382–397.

Hogan, K.A., Ambler, C.A., Chapman, D.L., and Bautch, V.L. (2004). The neural tube patterns vessels developmentally using the VEGF signaling pathway. Development *131*, 1503–1513.

Hollmann, E.K., Bailey, A.K., Potharazu, A. V., Neely, M.D., Bowman, A.B., and Lippmann, E.S. (2017). Accelerated differentiation of human induced pluripotent stem cells to blood-brain barrier endothelial cells. Fluids Barriers CNS *14*.

Holmqvist, S., Chutna, O., Bousset, L., Aldrin-Kirk, P., Li, W., Björklund, T., Wang, Z.Y., Roybon, L., Melki, R., and Li, J.Y. (2014). Direct evidence of Parkinson pathology spread from the gastrointestinal tract to the brain in rats. Acta Neuropathol. 2014 1286 *128*, 805–820.

Hughes, A.N., and Appel, B. (2019). Oligodendrocytes express synaptic proteins that modulate myelin sheath formation. Nat. Commun. 2019 101 *10*, 1–15.

Huntley, G.W., and Benson, D.L. (2020). Origins of Parkinson's Disease in Brain Development: Insights From Early and Persistent Effects of LRRK2-G2019S on Striatal Circuits. Front. Neurosci. *14*, 265.

Hynes, M., Poulsen, K., Tessier-Lavigne, M., and Rosenthal, A. (1995a). Control of neuronal diversity by the floor plate: Contact-mediated induction of midbrain dopaminergic neurons. Cell *80*, 95–101.

Hynes, M., Porter, J.A., Chiang, C., Chang, D., Tessier-Lavigne, M., Beachy, P.A., and Rosenthal, A. (1995b). Induction of midbrain dopaminergic neurons by Sonic hedgehog. Neuron *15*, 35–44.

Iadecola, C. (2017). The Neurovascular Unit Coming of Age: A Journey through Neurovascular Coupling in Health and Disease. Neuron *96*, 17–42.

Iadecola, C., and Anrather, J. (2011). The immunology of stroke: from mechanisms to translation. Nat. Med. *17*, 796.

Inamdar, N., Arulmozhi, D., Tandon, A., and Bodhankar, S. (2007). Parkinson's Disease: Genetics and Beyond. Curr. Neuropharmacol. *5*, 99.

Jacob, F., Schnoll, J.G., Song, H., and Ming, G. li (2021). Building the brain from scratch: Engineering region-specific brain organoids from human stem cells to study neural development and disease. Curr. Top. Dev. Biol. *142*, 477.

Jacobson, S., and Marcus, E.M. (2008). Neuroanatomy for the Neuroscientist.

Jagmag, S.A., Tripathi, N., Shukla, S.D., Maiti, S., and Khurana, S. (2015). Evaluation of Models of Parkinson's Disease. Front. Neurosci. *9*, 503.

Jamieson, J.J., Linville, R.M., Ding, Y.Y., Gerecht, S., and Searson, P.C. (2019). Role of iPSC-derived pericytes on barrier function of iPSC-derived brain microvascular endothelial cells in 2D and 3D. Fluids Barriers CNS *16*.

Jarazo, J., Barmpa, K., Modamio, J., Saraiva, C., Sabaté-Soler, S., Rosety, I., Griesbeck, A., Skwirblies, F., Zaffaroni, G., Smits, L.M., et al. (2021). Parkinson's Disease Phenotypes in Patient Neuronal Cultures and Brain Organoids Improved by 2-Hydroxypropyl-β-Cyclodextrin Treatment. Mov. Disord. 1–16.

Jo, J., Xiao, Y., Sun, A.X., Cukuroglu, E., Tran, H.-D., Göke, J., Tan, Z.Y., Saw, T.Y., Tan, C.-P., Lokman, H., et al. (2016). Midbrain-like organoids from human pluripotent stem cells contain functional dopaminergic and neuromelanin producing neurons. Cell Stem Cell *19*, 248.

Ju, F., Ran, Y., Zhu, L., Cheng, X., Gao, H., Xi, X., Yang, Z., and Zhang, S. (2018). Increased BBB permeability enhances activation of microglia and exacerbates loss of dendritic spines after transient global cerebral ischemia. Front. Cell. Neurosci. *12*, 236.

Kang, S.H., Li, Y., Fukaya, M., Lorenzini, I., Cleveland, D.W., Ostrow, L.W., Rothstein, J.D., and Bergles, D.E. (2013). Degeneration and impaired regeneration of gray matter oligodendrocytes in amyotrophic lateral sclerosis. Nat. Neurosci. 2013 165 *16*, 571–579.

Kassmann, C.M., Lappe-Siefke, C., Baes, M., Brügger, B., Mildner, A., Werner, H.B., Natt, O., Michaelis, T., Prinz, M., Frahm, J., et al. (2007). Axonal loss and neuroinflammation caused by peroxisome-deficient oligodendrocytes. Nat. Genet. 2007 398 *39*, 969–976.

Kele, J., Simplicio, N., Ferri, A.L.M., Mira, H., Guillemot, F., Arenas, E., and Ang, S.L. (2006). Neurogenin 2 is required for the development of ventral midbrain dopaminergic neurons. Development *133*, 495–505.

Kilic, O., Pamies, D., Lavell, E., Schiapparelli, P., Feng, Y., Hartung, T., Bal-Price, A., Hogberg, H.T., Quinones-Hinojosa, A., Guerrero-Cazares, H., et al. (2016). Brain-on-a-chip model enables analysis of human neuronal differentiation and chemotaxis. Lab Chip *16*, 4152–4162.

Kim, M., Mun, H., Sung, C.O., Cho, E.J., Jeon, H.J., Chun, S.M., Jung, D.J., Shin, T.H., Jeong, G.S., Kim, D.K., et al. (2019). Patient-derived lung cancer organoids as in vitro cancer models for therapeutic screening. Nat. Commun. *10*.

Kinoshita, K., Iwase, M., Yamada, M., Yajima, Y., and Seki, M. (2016). Fabrication of multilayered vascular tissues using microfluidic agarose hydrogel platforms. Biotechnol. J. *11*, 1415–1423.

Klement, W., Blaquiere, M., Zub, E., deBock, F., Boux, F., Barbier, E., Audinat, E., Lerner-Natoli, M., and Marchi, N. (2019). A pericyte-glia scarring develops at the leaky capillaries in the hippocampus during seizure activity. Epilepsia *60*, 1399–1411.

Klucken, J., Poehler, A.M., Ebrahimi-Fakhari, D., Schneider, J., Nuber, S., Rockenstein, E., Schlötzer-Schrehardt, U., Hyman, B.T., McLean, P.J., Masliah, E., et al. (2012). Alpha-synuclein aggregation involves a bafilomycin A1-sensitive autophagy pathway. Autophagy *8*, 754.

Korn, J., Christ, B., and Kurz, H. (2002). Neuroectodermal origin of brain pericytes and vascular smooth muscle cells. J. Comp. Neurol. *442*, 78–88.

Kuan, W.L., Bennett, N., He, X., Skepper, J.N., Martynyuk, N., Wijeyekoon, R., Moghe, P. V., Williams-Gray, C.H., and Barker, R.A. (2016). α-Synuclein pre-formed fibrils impair tight junction protein expression without affecting cerebral endothelial cell function. Exp. Neurol. *285*, 72–81.

Kuhn, H.G., Dickinson-Anson, H., and Gage, F.H. (1996). Neurogenesis in the dentate gyrus of the adult rat: age-related decrease of neuronal progenitor proliferation. J. Neurosci. *16*, 2027–2033.

Lacaud, G., and Kouskoff, V. (2017). Hemangioblast, hemogenic endothelium, and primitive versus definitive hematopoiesis. Exp. Hematol. *49*, 19–24.

Lancaster, M.A., and Knoblich, J.A. (2014). Organogenesis in a dish: modeling development and disease using organoid technologies. Science *345*.

Lancaster, M.A., Renner, M., Martin, C.A., Wenzel, D., Bicknell, L.S., Hurles, M.E., Homfray, T., Penninger, J.M., Jackson, A.P., and Knoblich, J.A. (2013). Cerebral organoids model human brain development and microcephaly. Nature *501*, 373–379.

Lang, C., Campbell, K.R., Ryan, B.J., Carling, P., Attar, M., Vowles, J., Perestenko, O. V., Bowden, R., Baig, F., Kasten, M., et al. (2019). Single-Cell Sequencing of iPSC-Dopamine Neurons Reconstructs Disease Progression and Identifies HDAC4 as a Regulator of Parkinson Cell Phenotypes. Cell Stem Cell *24*, 93-106.e6.

Lee, S.W.L., Rogosic, R., Venturi, C., Raimondi, M.T., Pavesi, A., and Adriani, G. (2022). A Human Neurovascular Unit On-a-Chip. Methods Mol. Biol. *2373*, 107–119.

Leventoux, N., Morimoto, S., Imaizumi, K., Sato, Y., Takahashi, S., Mashima, K., Ishikawa, M., Sonn, I., Kondo, T., Watanabe, H., et al. (2020). Human Astrocytes Model Derived from Induced Pluripotent Stem Cells. Cells *9*.

Li, J., Khankan, R.R., Caneda, C., Godoy, M.I., Haney, M.S., Krawczyk, M.C., Bassik, M.C., Sloan, S.A., and Zhang, Y. (2019). Astrocyte-to-astrocyte contact and a positive feedback loop of growth factor signaling regulate astrocyte maturation. Glia *67*, 1571.

Liang, J., Gu, S., Mao, X., Tan, Y., Wang, H., Li, S., and Zhou, Y. (2020). Endothelial Cell Morphology Regulates Inflammatory Cells Through MicroRNA Transferred by Extracellular Vesicles. Front. Bioeng. Biotechnol. *8*, 369.

Liebner, S., Dijkhuizen, R.M., Reiss, Y., Plate, K.H., Agalliu, D., and Constantin, G. (2018). Functional morphology of the blood-brain barrier in health and disease HHS Public Access. Acta Neuropathol *135*, 311–336.

Lin, Y.T., Seo, J., Gao, F., Feldman, H.M., Wen, H.L., Penney, J., Cam, H.P., Gjoneska, E., Raja, W.K., Cheng, J., et al. (2018). APOE4 Causes Widespread Molecular and Cellular Alterations Associated with Alzheimer's Disease Phenotypes in Human iPSC-Derived Brain Cell Types. Neuron *98*, 1141-1154.e7.

Lindborg, B.A., Brekke, J.H., Vegoe, A.L., Ulrich, C.B., Haider, K.T., Subramaniam, S., Venhuizen, S.L., Eide, C.R., Orchard, P.J., Chen, W., et al. (2016). Rapid Induction of Cerebral Organoids From Human Induced Pluripotent Stem Cells Using a Chemically Defined Hydrogel and Defined Cell Culture Medium. Stem Cells Transl. Med. *5*, 970–979.

Linkous, A., Balamatsias, D., Snuderl, M., Edwards, L., Miyaguchi, K., Milner, T., Reich, B., Cohen-Gould, L., Storaska, A., Nakayama, Y., et al. (2019). Modeling Patient-Derived Glioblastoma with Cerebral Organoids. Cell Rep. *26*, 3203-3211.e5.

Von Linstow, C.U., Delano-Taylor, M., Kordower, J.H., and Brundin, P. (2020). Does Developmental Variability in the Number of Midbrain Dopamine Neurons Affect Individual Risk for Sporadic Parkinson's Disease? J. Parkinsons. Dis. *10*, 405–411.

Livesey, M.R., Magnani, D., Cleary, E.M., Vasistha, N.A., James, O.T., Selvaraj, B.T., Burr, K., Story, D., Shaw, C.E., Kind, P.C., et al. (2016). Maturation and electrophysiological properties of human pluripotent stem cell-derived oligodendrocytes. Stem Cells *34*, 1040–1053.

Lopez-Lengowski, K., Kathuria, A., Gerlovin, K., and Karmacharya, R. (2021). Co-Culturing Microglia and Cortical Neurons Differentiated from Human Induced Pluripotent Stem Cells. J. Vis. Exp. *2021*.

Loughlin, S.E., and Fallon, J.H. (1984). Substantia nigra and ventral tegmental area projections to cortex: Topography and collateralization. Neuroscience *11*, 425–435.

Lovinger, D.M. (2008). Communication Networks in the Brain Neurons, Receptors, Neurotransmitters, and Alcohol. Alcohol Res. Heal. *31*, 196–214.

Lyu, Z., Park, J., Kim, K.M., Jin, H.J., Wu, H., Rajadas, J., Kim, D.H., Steinberg, G.K., and Lee, W. (2021). A neurovascular-unit-on-a-chip for the evaluation of the restorative potential of stem cell therapies for ischaemic stroke. Nat. Biomed. Eng. *5*, 847–863.

Ma, D.K., Bonaguidi, M.A., Ming, G.L., and Song, H. (2009). Adult neural stem cells in the mammalian central nervous system. Cell Res. *19*, 672.

Magistretti, P.J., and Allaman, I. (2015). A Cellular Perspective on Brain Energy Metabolism and Functional Imaging. Neuron *86*, 883–901.

La Manno, G., Gyllborg, D., Codeluppi, S., Nishimura, K., Salto, C., Zeisel, A., Borm, L.E., Stott, S.R.W., Toledo, E.M., Villaescusa, J.C., et al. (2016). Molecular Diversity of Midbrain Development in Mouse, Human, and Stem Cells. Cell *167*, 566.

Mansour, A.A., Gonçalves, J.T., Bloyd, C.W., Li, H., Fernandes, S., Quang, D., Johnston, S., Parylak, S.L., Jin, X., and Gage, F.H. (2018). An in vivo model of functional and vascularized human brain organoids. Nat. Biotechnol. *36*, 432–441.

Matsui, T.K., Tsuru, Y., Hasegawa, K., and Kuwako, K. ichiro (2021). Vascularization of human brain organoids. Stem Cells *39*, 1017–1024.

McConnell, H.L., Kersch, C.N., Woltjer, R.L., and Neuwelt, E.A. (2017). The translational significance of the neurovascular unit. J. Biol. Chem. *292*, 762–770.

McGeer, P.L., Itagaki, S., Boyes, B.E., and McGeer, E.G. (1988). Reactive microglia are positive for HLA-DR in the substantia nigra of Parkinson's and Alzheimer's disease brains. Neurology *38*, 1285–1291.

Van Der Meer, A.D., and Van Den Berg, A. (2012). Organs-on-chips: breaking the in vitro impasse. Integr. Biol. *4*, 461–470.

Menassa, D.A., and Gomez-Nicola, D. (2018). Microglial dynamics during human brain development. Front. Immunol. *9*, 1014.

Mensch, S., Baraban, M., Almeida, R., Czopka, T., Ausborn, J., El Manira, A., and Lyons, D.A. (2015). Synaptic vesicle release regulates myelin sheath number of individual oligodendrocytes in vivo. Nat. Neurosci. 2015 185 *18*, 628–630.

Miller, J.S., Stevens, K.R., Yang, M.T., Baker, B.M., Nguyen, D.H.T., Cohen, D.M., Toro, E., Chen, A.A., Galie, P.A., Yu, X., et al. (2012). Rapid casting of patterned vascular networks for perfusable engineered three-dimensional tissues. Nat. Mater. *11*, 768–774.

Min, R., and Nevian, T. (2012). Astrocyte signaling controls spike timing-dependent depression at neocortical synapses. Nat. Neurosci. *15*, 746–753.

Mittelbronn, M., Dietz, K., Schluesener, H.J., and Meyermann, R. (2001). Local distribution of microglia in the normal adult human central nervous system differs by up to one order of magnitude. Acta Neuropathol. *101*, 249–255.

Monzel, A.S., Smits, L.M., Hemmer, K., Hachi, S., Moreno, E.L., van Wuellen, T., Jarazo, J., Walter, J., Brüggemann, I., Boussaad, I., et al. (2017). Derivation of Human Midbrain-Specific Organoids from Neuroepithelial Stem Cells. Stem Cell Reports *8*, 1144–1154.

Monzel, A.S., Hemmer, K., Kaoma, T., Smits, L.M., Bolognin, S., Lucarelli, P., Rosety, I., Zagare, A., Antony, P., Nickels, S.L., et al. (2020). Machine learning-assisted neurotoxicity prediction in human midbrain organoids. Parkinsonism Relat. Disord. *75*, 105–109.

Moysidou, C.M., and Owens, R.M. (2021). Advances in modelling the human microbiome–gut–brain axis in vitro. Biochem. Soc. Trans. *49*, 187.

Muffat, J., Li, Y., Yuan, B., Mitalipova, M., Omer, A., Corcoran, S., Bakiasi, G., Tsai, L.H., Aubourg, P., Ransohoff, R.M., et al. (2016). Efficient derivation of microglia-like cells from human pluripotent stem cells. Nat. Med. *22*, 1358–1367.

Musafargani, S., Mishra, S., Gulyás, M., Mahalakshmi, P., Archunan, G., Padmanabhan, P., and Gulyás, B. (2020). Blood brain barrier: A tissue engineered microfluidic chip. J. Neurosci. Methods *331*.

Nalls, M.A., Blauwendraat, C., Vallerga, C.L., Heilbron, K., Bandres-Ciga, S., Chang, D., Tan, M., Kia, D.A., Noyce, A.J., Xue, A., et al. (2019). Identification of novel risk loci, causal insights, and heritable risk for Parkinson's disease: a meta-analysis of genome-wide association studies. Lancet. Neurol. *18*, 1091–1102.

Nashimoto, Y., Hayashi, T., Kunita, I., Nakamasu, A., Torisawa, Y.S., Nakayama, M., Takigawa-Imamura, H., Kotera, H., Nishiyama, K., Miura, T., et al. (2017). Integrating perfusable vascular networks with a three-dimensional tissue in a microfluidic device. Integr. Biol. (United Kingdom) *9*, 506–518.

Nickels, S.L., Modamio, J., Mendes-Pinheiro, B., Monzel, A.S., Betsou, F., and Schwamborn, J.C. (2020). Reproducible generation of human midbrain organoids for in vitro modeling of Parkinson's disease. Stem Cell Res. *46*.

Nimmerjahn, A., Kirchhoff, F., and Helmchen, F. (2005). Resting microglial cells are highly dynamic surveillants of brain parenchyma in vivo. Neuroforum *11*, 95–96.

Nishioku, T., Matsumoto, J., Dohgu, S., Sumi, N., Miyao, K., Takata, F., Shuto, H., Yamauchi, A., and Kataoka, Y. (2010). Tumor Necrosis Factor-α Mediates the Blood–Brain Barrier Dysfunction Induced by Activated Microglia in Mouse Brain Microvascular Endothelial Cells. J. Pharmacol. Sci. *112*, 251–254.

Nybø, C.J., Gustavsson, E.K., Farrer, M.J., and Aasly, J.O. (2020). Neuropathological findings in PINK1-associated Parkinson's disease. Parkinsonism Relat. Disord. *78*, 105–108.

Ormel, P.R., Vieira de Sá, R., van Bodegraven, E.J., Karst, H., Harschnitz, O., Sneeboer, M.A.M., Johansen, L.E., van Dijk, R.E., Scheefhals, N., Berdenis van Berlekom, A., et al. (2018). Microglia innately develop within cerebral organoids. Nat. Commun. *9*.

Outeiro, T.F., Putcha, P., Tetzlaff, J.E., Spoelgen, R., Koker, M., Carvalho, F., Hyman, B.T., and McLean, P.J. (2008). Formation of Toxic Oligomeric α-Synuclein Species in Living Cells. PLoS One *3*.

Palladino, A., Mavaro, I., Pizzoleo, C., De Felice, E., Lucini, C., de Girolamo, P., Netti, P.A., and Attanasio, C. (2019). Induced Pluripotent Stem Cells as Vasculature Forming Entities. J. Clin. Med. *8*.

Palmer, T.D., Ray, J., and Gage, F.H. (1995). FGF-2-responsive neuronal progenitors reside in proliferative and quiescent regions of the adult rodent brain. Mol. Cell. Neurosci. *6*, 474–486.

Panagiotakopoulou, V., Ivanyuk, D., De Cicco, S., Haq, W., Arsić, A., Yu, C., Messelodi, D., Oldrati, M., Schöndorf, D.C., Perez, M.J., et al. (2020). Interferon-γ signaling synergizes with LRRK2 in neurons and microglia derived from human induced pluripotent stem cells. Nat. Commun. *11*.

Parent, A., and Carpenter, M.B. (1996). Carpenter's human neuroanatomy (Baltimore : Williams & Wilkins,).

Park, T.E., Mustafaoglu, N., Herland, A., Hasselkus, R., Mannix, R., FitzGerald, E.A., Prantil-Baun, R., Watters, A., Henry, O., Benz, M., et al. (2019). Hypoxia-enhanced Blood-Brain Barrier Chip recapitulates human barrier function and shuttling of drugs and antibodies. Nat. Commun. *10*.

Pasca, S.P. (2018). The rise of three-dimensional human brain cultures. Nature *553*, 437–445.

Pasca, S.P. (2019). Assembling human brain organoids. Science (80-.). *363*, 126–127.

Pediaditakis, I., Kodella, K.R., Manatakis, D. V., Le, C.Y., Hinojosa, C.D., Tien-Street, W., Manolakos, E.S., Vekrellis, K., Hamilton, G.A., Ewart, L., et al. (2021). Modeling alpha-synuclein pathology in a human brain-chip to assess blood-brain barrier disruption. Nat. Commun. *12*.

Peguera, B., Segarra, M., and Acker-Palmer, A. (2021). Neurovascular crosstalk coordinates the central nervous system development. Curr. Opin. Neurobiol. *69*, 202–213.

Pereda, A.E. (2014). Electrical synapses and their functional interactions with chemical synapses. Nat. Rev. Neurosci. 2014 154 *15*, 250–263.

Perego, C., Fumagalli, S., and De Simoni, M.-G. (2011). Temporal pattern of expression and colocalization of microglia/macrophage phenotype markers following brain ischemic injury in mice. J. Neuroinflammation *8*, 174.

Pham, M.T., Pollock, K.M., Rose, M.D., Cary, W.A., Stewart, H.R., Zhou, P., Nolta, J.A., and Waldau, B. (2018). Generation of human vascularized brain organoids. Neuroreport *29*, 588–593.

Popova, G., Soliman, S.S., Kim, C.N., Keefe, M.G., Hennick, K.M., Jain, S., Li, T., Tejera, D., Shin, D., Chhun, B.B., et al. (2021). Human microglia states are conserved across experimental models and regulate neural stem cell responses in chimeric organoids. Cell Stem Cell *28*, 2153-2166.e6.

Qian, X., Nguyen, H.N., Song, M.M., Hadiono, C., Ogden, S.C., Hammack, C., Yao, B., Hamersky, G.R., Jacob, F., Zhong, C., et al. (2016). Brain-Region-Specific Organoids Using Mini-bioreactors for Modeling ZIKV Exposure. Cell *165*, 1238–1254.

Ramachandran, S.D., Schirmer, K., Münst, B., Heinz, S., Ghafoory, S., Wölfl, S., Simon-Keller, K., Marx, A., Oie, C.I., Ebert, M.P., et al. (2015). In Vitro Generation of Functional Liver Organoid-Like Structures Using Adult Human Cells. PLoS One *10*.

Ramesh, T., Nagula, S. V, Tardieu, G.G., Saker, E., Shoja, M., Loukas, M., Oskouian, R.J., and Tubbs, R.S. (2017). Update on the Notochord Including its Embryology, Molecular Development, and Pathology: A Primer for the Clinician. Cureus *9*.

Reemst, K., Noctor, S.C., Lucassen, P.J., and Hol, E.M. (2016). The indispensable roles of microglia and astrocytes during brain development. Front. Hum. Neurosci. *10*, 566.

Reiner, O., Sapir, T., and Parichha, A. (2020). Using multi-organ culture systems to study Parkinson's disease. Mol. Psychiatry 2020 263 *26*, 725–735.

Réu, P., Khosravi, A., Bernard, S., Mold, J.E., Salehpour, M., Alkass, K., Perl, S., Tisdale, J., Possnert, G., Druid, H., et al. (2017). The Lifespan and Turnover of Microglia in the Human Brain. Cell Rep. *20*, 779–784.

Roodveldt, C., Labrador-Garrido, A., Gonzalez-Rey, E., Fernandez-Montesinos, R., Caro, M., Lachaud, C.C., Waudby, C.A., Delgado, M., Dobson, C.M., and Pozo, D. (2010). Glial Innate Immunity Generated by Non-Aggregated Alpha-Synuclein in Mouse: Differences between Wild-type and Parkinson's Disease-Linked Mutants. PLoS One *5*, e13481.

Roudsari, L.C., Jeffs, S.E., Witt, A.S., Gill, B.J., and West, J.L. (2016). A 3D Poly(ethylene glycol)-based Tumor Angiogenesis Model to Study the Influence of Vascular Cells on Lung Tumor Cell Behavior. Sci. Rep. *6*.

Russo, F.B., Freitas, B.C., Pignatari, G.C., Fernandes, I.R., Sebat, J., Muotri, A.R., and Beltrão-Braga, P.C.B. (2018). Modeling the Interplay Between Neurons and Astrocytes in Autism Using Human Induced Pluripotent Stem Cells. Biol. Psychiatry *83*, 569–578.

Rymo, S.F., Gerhardt, H., Sand, F.W., Lang, R., Uv, A., and Betsholtz, C. (2011). A Two-Way Communication between Microglial Cells and Angiogenic Sprouts Regulates Angiogenesis in Aortic Ring Cultures. PLoS One *6*.

Schmidt, S.I., Bogetofte, H., Ritter, L., Agergaard, J.B., Hammerich, D., Kabiljagic, A.A., Wlodarczyk, A., Lopez, S.G., Sørensen, M.D., Jørgensen, M.L., et al. (2021). Microglia-Secreted Factors Enhance Dopaminergic Differentiation of Tissue- and iPSC-Derived Human Neural Stem Cells. Stem Cell Reports *16*, 281.

Schmitt, F.A., Davis, D.G., Wekstein, D.R., Smith, C.D., Ashford, J.W., and Markesbery, W.R. (2000). "Preclinical" AD revisited: Neuropathology of cognitively normal older adults. Neurology *55*, 370–376.

Schwamborn, J.C. (2018). Is Parkinson's Disease a Neurodevelopmental Disorder and Will Brain Organoids Help Us to Understand It? Stem Cells Dev. *27*, 968–975.

Schweitzer, J.S., Song, B., Herrington, T.M., Park, T.-Y., Lee, N., Ko, S., Jeon, J., Cha, Y., Kim, K., Li, Q., et al. (2020). Personalized iPSC-Derived Dopamine Progenitor Cells for Parkinson's Disease. N. Engl. J. Med. *382*, 1926–1932.

Scott-Hewitt, N., Perrucci, F., Morini, R., Erreni, M., Mahoney, M., Witkowska, A., Carey, A., Faggiani, E., Schuetz, L.T., Mason, S., et al. (2020). Local externalization of phosphatidylserine mediates developmental synaptic pruning by microglia. EMBO J. *39*.

Sekar, A., Bialas, A.R., De Rivera, H., Davis, A., Hammond, T.R., Kamitaki, N., Tooley, K., Presumey, J., Baum, M., Van Doren, V., et al. (2016). Schizophrenia risk from complex variation of complement component 4. Nat. 2016 5307589 *530*, 177–183.

Skoff, R.P. (1990). Gliogenesis in rat optic nerve: Astrocytes are generated in a single wave before oligodendrocytes. Dev. Biol. *139*, 149–168.

Smits, L.M., Reinhardt, L., Reinhardt, P., Glatza, M., Monzel, A.S., Stanslowsky, N., Rosato-Siri, M.D., Zanon, A., Antony, P.M., Bellmann, J., et al. (2019). Modeling Parkinson's disease in midbrain-like organoids. Npj Park. Dis. 2019 51 *5*, 1–8.

Sonntag, F., Schilling, N., Mader, K., Gruchow, M., Klotzbach, U., Lindner, G., Horland, R., Wagner, I., Lauster, R., Howitz, S., et al. (2010). Design and prototyping of a chip-based multi-micro-organoid culture system for substance testing, predictive to human (substance) exposure. J. Biotechnol. *148*, 70–75.

Stiles, J., and Jernigan, T.L. (2010). The basics of brain development. Neuropsychol. Rev. *20*, 327–348.

Sung, J.H., and Shuler, M.L. (2009). A micro cell culture analog (microCCA) with 3-D hydrogel culture of multiple cell lines to assess metabolism-dependent cytotoxicity of anti-cancer drugs. Lab Chip *9*, 1385–1394.

Takahashi, K., and Yamanaka, S. (2006). Induction of pluripotent stem cells from mouse embryonic and adult fibroblast cultures by defined factors. Cell *126*, 663–676.

Takata, F., Nakagawa, S., Matsumoto, J., and Dohgu, S. (2021). Blood-Brain Barrier Dysfunction Amplifies the Development of Neuroinflammation: Understanding of Cellular Events in Brain Microvascular Endothelial Cells for Prevention and Treatment of BBB Dysfunction. Front. Cell. Neurosci. *15*, 344.

Tansey, M.G., and Goldberg, M.S. (2010). Neuroinflammation in Parkinson's disease: its role in neuronal death and implications for therapeutic intervention. Neurobiol. Dis. *37*, 510.

Tata, M., Ruhrberg, C., and Fantin, A. (2015). Vascularisation of the central nervous system. Mech. Dev. *138*, 26–36.

Tavian, M., and Péault, B. (2005). Embryonic development of the human hematopoietic system. Int. J. Dev. Biol. *49*, 243–250.

Tiwari, N., Pataskar, A., Pé, S., Ló Pez-Mascaraque, L., Tiwari, V.K., and Correspondence, B.B. (2018). Stage-Specific Transcription Factors Drive Astrogliogenesis by Remodeling Gene Regulatory Landscapes. Cell Stem Cell *23*, 557–571.

Tremblay, M.È., Stevens, B., Sierra, A., Wake, H., Bessis, A., and Nimmerjahn, A. (2011). The role of microglia in the healthy brain. J. Neurosci. *31*, 16064–16069.

Troncoso-Escudero, P., Parra, A., Nassif, M., and Vidal, R.L. (2018). Outside in: Unraveling the role of neuroinflammation in the progression of Parkinson's disease. Front. Neurol. *9*, 860.

Tsuji-Tamura, K., and Ogawa, M. (2018). Morphology regulation in vascular endothelial cells. Inflamm. Regen. 2018 381 *38*, 1–13.

Tsunemi, T., Ishiguro, Y., Yoroisaka, A., Valdez, C., Miyamoto, K., Ishikawa, K., Saiki, S., Akamatsu, W., Hattori, N., and Krainc, D. (2020). Astrocytes Protect Human Dopaminergic Neurons from α-Synuclein Accumulation and Propagation. J. Neurosci. *40*, 8618–8628.

Tu, D., Gao, Y., Yang, R., Guan, T., Hong, J.S., and Gao, H.M. (2019). The pentose phosphate pathway regulates chronic neuroinflammation and dopaminergic neurodegeneration. J. Neuroinflammation *16*.

Ueno, M., Fujita, Y., Tanaka, T., Nakamura, Y., Kikuta, J., Ishii, M., and Yamashita, T. (2013). Layer v cortical neurons require microglial support for survival during postnatal development. Nat. Neurosci. *16*, 543–551.

Unagolla, J.M., and Jayasuriya, A.C. (2020). Hydrogel-based 3D bioprinting: A comprehensive review on cell-laden hydrogels, bioink formulations, and future perspectives. Appl. Mater. Today *18*, 100479.

Vatine, G.D., Barrile, R., Workman, M.J., Sances, S., Barriga, B.K., Rahnama, M., Barthakur, S., Kasendra, M., Lucchesi, C., Kerns, J., et al. (2019). Human iPSC-Derived Blood-Brain Barrier Chips Enable Disease Modeling and Personalized Medicine Applications. Cell Stem Cell *24*, 995-1005.e6.

Vijayanathan, Y., Lim, S.M., Tan, M.P., Lim, F.T., Majeed, A.B.A., and Ramasamy, K. (2021). Adult Endogenous Dopaminergic Neuroregeneration Against Parkinson's Disease: Ideal Animal Models? Neurotox. Res. *39*, 504–532.

Wake, H., Moorhouse, A.J., Jinno, S., Kohsaka, S., and Nabekura, J. (2009). Resting microglia directly monitor the functional state of synapses in vivo and determine the fate of ischemic terminals. J. Neurosci. *29*, 3974–3980.

Weiss, N., Miller, F., Cazaubon, S., and Couraud, P.O. (2009). The blood-brain barrier in brain homeostasis and neurological diseases. Biochim. Biophys. Acta - Biomembr. *1788*, 842–857.

Williamson, A., Singh, S., Fernekorn, U., and Schober, A. (2013). The future of the patient-specific Body-on-a-chip. Lab Chip *13*, 3471–3480.

Wimmer, R.A., Leopoldi, A., Aichinger, M., Wick, N., Hantusch, B., Novatchkova, M., Taubenschmid, J., Hämmerle, M., Esk, C., Bagley, J.A., et al. (2019). Human blood vessel organoids as a model of diabetic vasculopathy. Nature *565*, 505–510.

Witting, A., Müller, P., Herrmann, A., Kettenmann, H., and Nolte, C. (2000). Phagocytic clearance of apoptotic neurons by microglia/brain macrophages in vitro: Involvement of lectin-, integrin-, and phosphatidylserine-mediated recognition. J. Neurochem. *75*, 1060–1070.

Workman, M.J., Mahe, M.M., Trisno, S., Poling, H.M., Watson, C.L., Sundaram, N., Chang, C.F., Schiesser, J., Aubert, P., Stanley, E.G., et al. (2017). Engineered human pluripotent-stem-cell-derived intestinal tissues with a functional enteric nervous system. Nat. Med. *23*, 49–59.

Wörsdörfer, philipp, Dalda, nahide, Kern, A., Krüger, S., Wagner, nicole, Keong Kwok, chee, Henke, erik, and ergün, S. Generation of complex human organoid models including vascular networks by incorporation of mesodermal progenitor cells.

Wörsdörfer, P., Rockel, A., Alt, Y., Kern, A., and Ergün, S. (2020). Generation of Vascularized Neural Organoids by Co-culturing with Mesodermal Progenitor Cells. STAR Protoc. *1*, 100041.

Wu, Q., Liu, J., Wang, X., Feng, L., Wu, J., Zhu, X., Wen, W., and Gong, X. (2020). Organ-on-a-chip: recent breakthroughs and future prospects. Biomed. Eng. OnLine 2020 191 *19*, 1–19.

Xiang, Y., Tanaka, Y., Patterson, B., Kang, Y.J., Govindaiah, G., Roselaar, N., Cakir, B., Kim, K.Y., Lombroso, A.P., Hwang, S.M., et al. (2017). Fusion of Regionally Specified hPSC-Derived Organoids Models Human Brain Development and Interneuron Migration. Cell Stem Cell *21*, 383-398.e7.

Xicoy, H., Wieringa, B., and Martens, G.J.M. (2017). The SH-SY5Y cell line in Parkinson's disease research: a systematic review. Mol. Neurodegener. *12*, 1–11.

Xu, C., Chai, W., Huang, Y., and Markwald, R.R. (2012). Scaffold-free inkjet printing of three-dimensional zigzag cellular tubes. Biotechnol. Bioeng. *109*, 3152–3160.

Yamamoto, S., Muramatsu, M., Azuma, E., Ikutani, M., Nagai, Y., Sagara, H., Koo, B.N., Kita, S., O'Donnell, E., Osawa, T., et al. (2017). A subset of cerebrovascular pericytes originates from mature macrophages in the very early phase of vascular development in CNS. Sci. Reports 2017 71 *7*, 1–16.

Ye, W., Shimamura, K., Rubenstein, J.L.R., Hynes, M.A., and Rosenthal, A. (1998). FGF and Shh signals control dopaminergic and serotonergic cell fate in the anterior neural plate. Cell *93*, 755–766.

Young, C.B., Reddy, V., and Sonne, J. (2021). Neuroanatomy, Basal Ganglia. StatPearls.

Yousef, H., Czupalla, C.J., Lee, D., Chen, M.B., Burke, A.N., Zera, K.A., Zandstra, J., Berber, E., Lehallier, B., Mathur, V., et al. (2019). Aged blood impairs hippocampal neural precursor activity and activates microglia via brain endothelial cell VCAM1. Nat. Med. *25*, 988.

Zagare, A., Barmpa, K., Smajic, S., Smits, L.M., Grzyb, K., Gruenewald, A., Skupin, A., Nickels, S.L., and Schwamborn, J. (2022). Midbrain organoids represent a physiologically relevant model that recapitulates a LRRK2-G2019S-associated gene expression signature during early neurodevelopment. Am. J. Hum. Genet.

Zhang, Y.S., Arneri, A., Bersini, S., Shin, S.R., Zhu, K., Goli-Malekabadi, Z., Aleman, J., Colosi, C., Busignani, F., Dell'Erba, V., et al. (2016). Bioprinting 3D microfibrous scaffolds for engineering endothelialized myocardium and heart-on-a-chip. Biomaterials *110*, 45–59.

Zhao, J., Fu, Y., Yamazaki, Y., Ren, Y., Davis, M.D., Liu, C.C., Lu, W., Wang, X., Chen, K., Cherukuri, Y., et al. (2020). APOE4 exacerbates synapse loss and neurodegeneration in Alzheimer's disease patient iPSC-derived cerebral organoids. Nat. Commun. *11*.

APPENDIX. PATENT

The work developed in this thesis led to the Luxembourg patent application No. LU500789 filed on 26-Oct-2021 in the name of Université du Luxembourg, "Means and methods for generating immunocompetent midbrain assembloid", inventors: Sònia Sabaté Soler, Jens Schwamborn, Sally Cowley.